THE UNIVERSITY
of EDINBURGH

Substituent Effects on Non-Covalent Interactions

Rebecca Jayne Burns

Thesis presented for the degree of

Doctor of Philosophy

The University of Edinburgh

2020

Declaration

I declare that this thesis has been composed entirely by myself.

I confirm that a substantial volume of the research presented herein has been performed by myself, and any contributions from other researchers have been outlined at the beginning of each chapter and indicated in relevant figure captions.

I declare that this work has not been submitted for any other degree or professional qualification.

Signature: Date: 20th July 2020

Rebecca Jayne Burns

Table of Contents

Declaration ..... **ii**

Table of Contents ..... **iii**

Acknowledgements ..... **vi**

Abstract ..... **viii**

Lay Summary ..... **x**

Abbreviations ..... **xi**

Publications ..... **xiii**

1.1 Introduction **2**

1.2 Historical Empirical Quantification of Substituent Effects **4**

1.2.1 Substituent Constants *4*

1.2.2 Empirical models to predict and quantify substituent effects *11*

1.3 Modern Approaches to Substituent Effect Quantification **16**

1.4 Through-Space *vs.* Through-Bond Substituent Effects **31**

1.4.1 Substituent Effects in π-Interactions: Investigating the Local, Direct Interaction Model *31*

1.4.2 Through-Space Effects on Reactivity *45*

1.4.3 Through-Space Effects on Ionisation Constants *46*

1.5 Field Effects in Nature and Synthesis **50**

1.6 Conclusions and Remarks **55**

1.7 Thesis Aims and Outlook **56**

1.8 References **57**

2.1 Introduction **70**

2.2 Aims of the Project **71**

2.3 Molecular Balances **72**

2.3.1 Molecular Balance Design ... *76*

2.3.2 Molecular Balance Synthesis ... *80*

2.4 Results and Discussion ... **83**

2.4.1 Determination of Equilibrium Constants ... *83*

2.4.2 Determination of Substituent Constants ... *88*

2.4.3 Analysis of Experimentally Determined Substituent Constants ... *92*

2.4.4 Computational Analysis ... *97*

2.5 Solvent Effects on Through-Space Substituent Effects ... **109**

2.5.1 Dissecting Solvent Effects ... *112*

2.6 Conclusions and Outlook ... **114**

2.7 References ... **116**

3.1 Introduction ... **125**

3.2 Aims of the Project ... **126**

3.3 Through-Space Effects on Chemical Reactivity ... **126**

3.3.1 Model Reaction and System Design ... *126*

3.3.2 Pyridine Derivative Synthesis ... *130*

3.3.3 Measurement of Rate Constants ... *135*

3.3.4 Quantification of Substituent Effects on Reactivity ... *139*

3.3.5 Computational Analysis ... *144*

3.3.6 Conclusions on Through-Space Effects on Reactivity ... *152*

3.5 Transferability of Through-Space Substituent Effects ... **153**

3.6 Conclusions and Remarks ... **155**

3.7 References ... **157**

4.1 Introduction ... **164**

4.1.1 Hydrogen Bonds ... *164*

4.1.2 Organofluorine and Other Halides as Hydrogen Bond Acceptors ... *168*

4.1.3 Other Functional Groups as Hydrogen Bond Acceptors 173

4.2 Project Background 175

4.3 Aims of the Project 178

4.4 Molecular Balance Synthesis 178

4.5 Results and Discussion 180

4.5.1 Computational and Experimental Results 180

4.5.2 Hammett Analysis 184

4.5.3 SAPT Analysis 188

4.6 Conclusions and Remarks 195

4.7 References 196

Acknowledgements

I would like to thank my supervisor, Prof. Scott L. Cockroft, for allowing me to join his group and giving me the opportunity to work on stimulating projects. Throughout my PhD, he has been very supportive both academically and personally. He has always been willing to spend hours discussing projects together and his support during my surgery in 2016 was extremely helpful. Overall, being mentored by Scott has helped me grow as a person as well as a scientist and I am a more confident individual now than I was when I started my PhD.

I would also like to thank the Cockroft group, past and present for providing a fun, relaxed and supportive working environment. Our daily trips to the campus shop (together with its own song) and countless cups of tea accompanied by conversation topics as varied as synthetic chemistry to the pros and cons of Yorkshire tea (mostly cons) are memories I will cherish forever. Specifically, I would like to thank Karina Krogstrup and Dr Nicole Meredith to whom I am always grateful for the fumehood-side conversations I shared with each that brightened up my days and through which I learned a lot about life. I would like to thank Dr Marius Haugland for his support both personally and academically and always being understanding. Thank you to Alex Elmi for always being patient and helpful in the arena of computational chemistry. I thank Andrew Mark London West for his wisdom and for always being able to make me laugh with his dead-pan, left-field observational comedy. Thank you to Dr Stefan Borsley for helping me grow as a scientist and showing me how to be critical of my work in a way that is productive. Thanks to Dr Dominic Pascoe for helping me settle in when I first started my PhD.

I would like to give a huge and heartfelt thank you to Dominic Cairns-Gibson. He has provided continuous and unwavering support not only during my write-up but throughout the years we have known each other. He always grounds me and helps me to see the bigger picture in situations where I find it difficult to do so. I cannot express how much I appreciate his friendship; all I can say is thank you.

Of course, my write-up and PhD have been greatly supported by my friends and loved ones outside of the lab who have always been there for me and provided fun external to my studies for which I am very thankful.

It is most important that I thank my parents, Andrena and Ralph, who are always in my corner and without whom I wouldn't be the person I am today. I love them with all my heart. I would like to also thank my Grandad and Grandma Burns for always supporting and encouraging my scientific endeavours.

I thank various others within the University of Edinburgh, School of Chemistry. The Lusby group, past and present, for being kind and friendly faces that brighten up my day when I see them. The School technical staff: Dr Lorna Murray and Mr. Juraj Bella in NMR and Mr Alan Taylor in mass spec. Thanks extend to the stores team: Simon Cummings, Tim Calder, Mark Forrest and John Kenmure. I also thank the Organic Teaching Laboratory team: Dr Peter Kirsop, Ms Kirsty Bain and Ms Jennifer Anderson.

I thank The University of Edinburgh and the Leverhulme Trust for funding.

Abstract

Non-covalent interactions play a vital role in biological and chemical systems, underpinning important processes such as ligand–receptor binding and protein structure. Substituent effects on these non-covalent interactions are often used to influence the system and are generally predicted based upon empirically defined constants.

Chapter 1 of this thesis provides a literature review covering the quantification of substituent effects from Hammett's seminal constants to their present-day treatment. The contributions to the overall influence of a substituent on a chemical system *via* through-bond and through-space effects is explored, culminating in the most recent studies pointing towards the often overseen importance of the latter.

Chapter 2 utilises a combined computational and experimental approach to explore the influence of through-space substituent effects on chemical equilibria. Synthetic molecular torsion balances were employed for the experimental measurements of the conformational equilibrium constants from which a new set of substituent constants were derived. Computational modelling to obtain Electrostatic Potential (ESP) surfaces and slices uncovered the origin of the experimental findings to be a through-space effect. In addition, this analysis provided evidence for the geometrical sensitivity of through-space effects resulting in the demonstration of the tune-ability of such substituent effects. Through-space substituent effects were shown to be sensitive to solvent effects *via* a mathematical model applied to the experimental data obtained in a range of solvents. The through-space substituent effects were greatly attenuated by competitive solvents, due to the intrinsic electrostatic nature of through-space effects with electrostatic effects being sensitive to changes in solvent.

Chapter 3 is a detailed examination of the transferability of the substituent constants derived in **Chapter 2** by comparing the constants to experimental reaction rates. Through-space substituent effects on reactivity was not well predicted by the constants derived in **Chapter 2**, showing the sensitivity of field effects to geometrical influences

in the transition state. Ultimately, this analysis showed that through-space substituent effects are best understood *via* simple computational modelling.

Chapter 4 provides a detailed analysis into the nature of weak hydrogen bonding interactions using molecular balances and Energetic Decomposition Analysis (EDA). Substituents that are known to be weak hydrogen bond acceptors were observed to perturb the hydrogen bonding interaction between an *ortho* hydroxyl group with a carbonyl group *via* conformational free energies. The surprising competitive nature of these substituents was investigated through EDA, which showed that the apparent competitive hydrogen bonds to the adjacent substituents were instead driven by repulsive interactions (e.g. between lone pairs of electrons). It is proposed that such contacts are instead best described as "pseudo-hydrogen bonds", which lack the attractive characteristic of true hydrogen bonds.

Lay Summary

To influence the reactivity of an organic molecule, chemists often use substituents which are small molecules one adds to an existing molecule to change its chemical and physical properties. They are helpful as they allow the chemist to tune interactions between atoms that are not bonded to one another; these interactions are termed "non-covalent". Processes as important as catalysis in synthetic chemistry, which has vital applications in a variety of industries, are governed by such interactions. Thus, it follows that by understanding and being able to predict the change to a system induced by a particular substituent, chemists will be able to exploit these interactions to enable more efficient processes.

Substituent effects are most often predicted by constants which were derived some eighty years ago by experimental means. Over this timeframe, the inability of these constants to describe and predict substituent effects in a number of situations has led to much research regarding the origin of these effects. Generally, chemists think of these effects as being manifested through the bonds connecting the substituent and the part of the molecule that takes part in a reaction. However, growing evidence that the effect of substituents through-space is just as important as through-bond influences has cast doubt on this long-held view. The first three chapters of this thesis focus on these through-space effects, moving from a literature review in **Chapter 1** to the quantification of their effects in **Chapters 2** and **3**. Computational and experimental means were used to probe the importance of through-space interactions, showing that they were important in non-covalent interactions (**Chapter 2**) and to reaction rates (**Chapter 3**). The utility of the quantification performed in **Chapter 2** was assessed, showing ultimately that computational means of predicting through-space effects were more transferrable than experimentally derived parameters.

The same combined approach was employed in **Chapter 4** to the study of hydrogen bonds, one of the most important non-covalent interactions. In particular, weak hydrogen bonds, which are difficult to investigate, were probed. The experimental and computational analysis performed showed that the nature of hydrogen bonding is not always attractive, as it has always been thought to be.

Abbreviations

1D	1-Dimensional
2D	2-Dimensional
Ar	Aromatic
B3LYP	Beke, three-parameter, Lee-Yang-Parr functional
CSD	Cambridge Structural Database
COSY	Correlation SpectroscopY (NMR spectrscopy)
d	Doublet (in NMR analysis)
DBA	Dibenzylideneacetone
DCM	Dichloromethane
dd	Doublet of doublets (in NMR analysis)
DFT	Density Functional Theory
DME	1,2-Dimethoxyethane
DMEDA	1,2-Dimethylethylenediamine
DMF	*N,N*-Dimethylformamide
DMSO	Dimethylsulfoxide
DNA	Deoxyribonucleic acid
DPPF	1,1'-Bis(diphenylphosphino)ferrocene
dt	Doublet of triplets (in NMR analysis)
EDA	Energy Decomposition Analysis
EDG	Electron-Donating Group
EI	Electrospray Ionisation
ESP	Electrostatic Potential

Ether	Unless otherwise specified refers to diethyl ether
Et	Ethyl
EWG	Electron-Withdrawing Group
FISAPT	Functional group Intramolecular Symmetry Adapted Perturbation Theory
(FT)IR	(Fourier transform) Infrared spectroscopy
h	Hours
HF	Hartree Fock
HMBC	Heteronuclear Multiple Bond Correlation (NMR spectroscopy)
HRMS	High Resolution Mass Spectrometry
HSQC	Heteronuclear Single Quantum Coherence (NMR spectrscopy)
m	Multiplet (in NMR analysis)
m-	*meta*
m.p.	Melting point
Me	Methyl
MS	Molecular Sieves
n-Hex	*n*-Hexane
IE	Ionisation Energy
NBO	Natural Bond Orbital
NMR	Nuclear Magnetic Resonance Spectroscopy
NOE	Nuclear Overhauser Effect (in NMR spectroscopy)
NOESY	Nuclear Overhauser Effect SpectroscopY (NMR spectroscopy)
o-	*ortho*
OAc	Acetate

p-	*para*
PCy_3	Tricyclohexylphosphine
PDB	Protein Data Bank
Ph	Phenyl
pK_a	Acid dissociation constant
ppm	Parts Per Million
q	Quartet (in NMR analysis)
r.t.	Room temperature (25 °C)
s	Singlet (in NMR analysis)
SAPT	Symmetry Adapted Perturbation Theory
S.D.	Standard deviation
SPhos	2-Dicyclohexylphosphino-2',6'-dimethoxybiphenyl
t	Triplet (in NMR analysis)
t-Bu	*tert*-Butyl
THF	Tetrahydrofuran
TLC	Thin-layer chromatography

Publications

Quantifying Through-Space Substituent Effects, *submitted*. (**Chapters 2** and **3**)

Chapter 1

Quantifying Electronic Substituent Effects

Abstract

Electronic substituent effects can influence non-covalent interactions, meaning they are able to tune the molecular recognition events that these interactions underpin. This chapter will review the quantification of substituent effects from Hammett's seminal constants to their present-day treatment and the utility of this quantification to the understanding of chemical and biological processes. The nature of substituent effects are also discussed and the many studies performed with the aim to dissect these effects into their constituent parts are overviewed. Thus, the contributions to the overall influence of a substituent *via* through-bond and through-space effects is explored, culminating in the most recent studies pointing towards the often-overlooked significance of the latter.

Contributions: This chapter is a literature review compiled by Rebecca Jayne Burns (RJB).

1.1 Introduction

The electronic effects of substituents play a key role in governing the non-covalent interactions that are a fundamental force in many chemical phenomena. They are central to molecular recognition and as such are the driving force behind ligand-receptor binding, the mechanics of molecular machines, the structure of supramolecular complexes and control the stereo- and regio-chemical outcomes of reactions.[1-5] Systematic variation of substituents is often exploited as a means of tuning such chemical behaviour. Studying the effects of systematic substituent variation on the strength and selectivity of non-covalent interactions is a tool that chemists often use to gain insight into the interaction at hand. Through understanding the principles of non-covalent interactions, a core understanding of the chemical processes to which they are key could be achieved. Insight into the fundamental mechanics behind non-covalent interactions would also provide the chemist with the power to rationally tune them; opening the door to more considered syntheses of pharmaceuticals, materials and the more rational design of organocatalysts.[6] In addition, understanding substituent effects and their effect on non-covalent interactions would improve predictive powers of reaction rates and chemical equilibria.

Electronic substituent effects on the properties, interactions and reactivity of organic molecules are well documented. However, there is a lack of a unifying theory on the way in which substituent effects are mediated.[7] These effects can be considered as through-bond (induction and resonance) and through-space (field) effects (**Figure 1.1**).[8]

Through-bond effects reflect the ability of a substituent to withdraw or donate electrons from a nearby reactive centre, through σ bonds (induction) or π bonds (resonance) (**Figure 1.1**, left-hand side). Inductive effects are the result of bond polarisation caused by a substituent, with the magnitude of the effect being dependent upon the nature and number of bonds between the substituent and reactive centre. It was noted as early as 1911 that the strength of the inductive effect falls off with the number of carbon atoms between the substituent and reactive centre.[9-12] Resonance

effects occur within delocalised systems containing unsaturated bonds where the electron density is distributed through the molecule *via* π bonds.[13]

Through-space interactions, also termed "field effects", between a substituent and remote reaction centre occur due to the changes in the local electric field imposed by the substituent and are therefore electrostatic by nature (**Figure 1.1**, right-hand side).[14] By virtue of being mediated through space, the magnitude of through-space effects is dependent upon the geometry of the interacting pairs which can be either inter- or intramolecular.[9] Within this review, the terms through-space and field will be used interchangeably; terminology that speaks to the mode of transmission and the origin of the effect respectively.

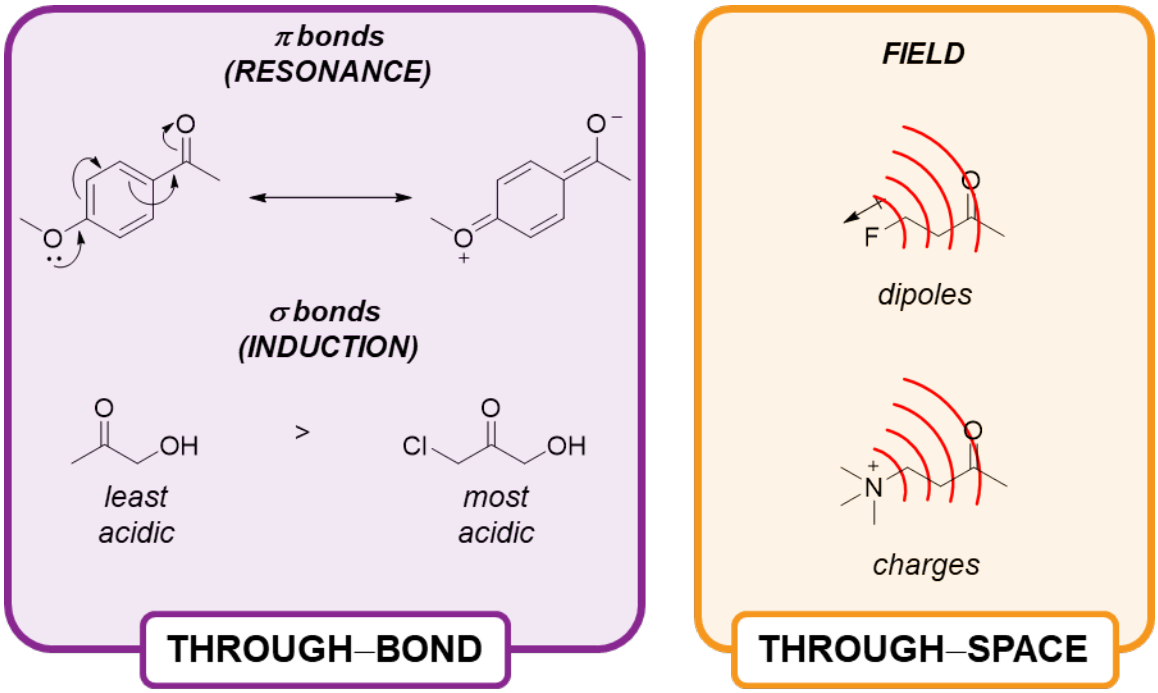

Figure 1.1: Resonance effects (purple box, top) are depicted by the delocalisation of the oxygen lone pair of electrons through the π system. Inductive effects (purple box, bottom) are shown by the effect of an "electron-withdrawing" substituent, chlorine, on the acidity of a nearby functional group. Field effects (orange box) are shown as red lines for a dipole (C–F bond) and a formal charge (N^+). [8]

1.2 Historical Empirical Quantification of Substituent Effects

Electronic substituent effects can have a large influence on the properties of a chemical system, and as such, much effort has been put into classifying and quantifying their behaviour. Chemists often rationalise substituent effects through consideration of the relative electronegativities of adjacent atoms, empirically derived substituent constants or mathematical models.[7]

1.2.1 Substituent Constants

The first to quantify substituent effects was Hammett, who aimed to rank their effects on the equilibria and reaction rates of organic molecules. To do this, the change in the acidity of *meta* and *para* substituted benzoic acids relative to the unsubstituted acid was measured (**Figure 1.2**), defining the σ_m and σ_p constants respectively using **Equation 1.1**.[7, 15-17] *Ortho* substituent constants were not defined by this relation due to being complicated by multiple effects (see later).[7]

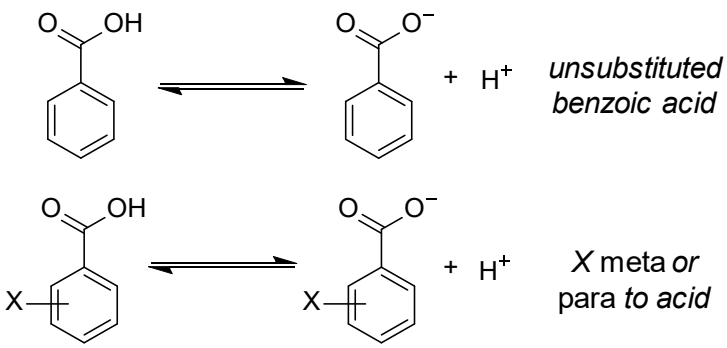

Figure 1.2: The ionisation of benzoic acid, used by Hammett to quantify substituent effects in the *meta* and *para* positions of aromatic systems.[7, 15-17]

$$\sigma_X = log\left(\frac{K_X}{K_H}\right) \qquad \textbf{Equation 1.1}$$

Where K_H is the ionisation constant for benzoic acid and K_X is the ionisation constant for substituted benzoic acid measured in water at 25 °C.

Interpretation of the resulting substituent constants was based upon the sign of the constant, with the magnitude showing the strength of the effect relative to a proton substituent, which thereby defines zero on the Hammett scale. Negative σ_m or σ_p values mean that the substituted benzoic acid is less acidic than the unsubstituted acid and the substituent would make a nearby reaction centre more electron rich. Such substituents are said to be "electron-donating". Conversely, a positive σ_m or σ_p value means that the substituent would make a nearby reaction centre less electron rich and these are referred to as "electron-withdrawing".[7-8, 13, 15-18]

Such rationalisation of substituent effects has been instrumental in the study of organic reaction mechanisms through utilisation of Hammett plots. These plots are Linear Free Energy Relationships (LFERs) that give information on the nature of the rate determining step and thus the mechanism of the reaction. In general, LFERs correlate experimental free energies or (logged) reaction rates against a parameter that describes the changes in electronic substituent effects. For Hammett plots, the parameter used is the Hammett σ_m or σ_p constant. The gradient of these plots, termed the "reaction constant" with the symbol ρ, is related to the experimental equilibrium or rate constant and the Hammett constant *via* **Equation 1.2**.[7-8, 13, 15-18]

$$\rho\sigma_X + \gamma = log\left(\frac{K_x}{K_H}\right) \qquad \textbf{Equation 1.2}$$

Where $K_{X/H}$ can also be rate constants, $k_{X/H}$ and γ is the intercept of such plots.

The magnitude of ρ indicates how sensitive the reaction is to electronic substituent effects relative to that of the ionization of benzoic acid as a result of the dependence of **Equation 1.2** on Hammett substituent constants. For those reactions where the magnitude of ρ is greater than 1, the reaction is more sensitive to electronic substituent effects than benzoic acid. The sign of ρ indicates the sign of the charge built up in the rate determining step transition state as shown in **Figure 1.3**.[8, 13, 15-16, 18]

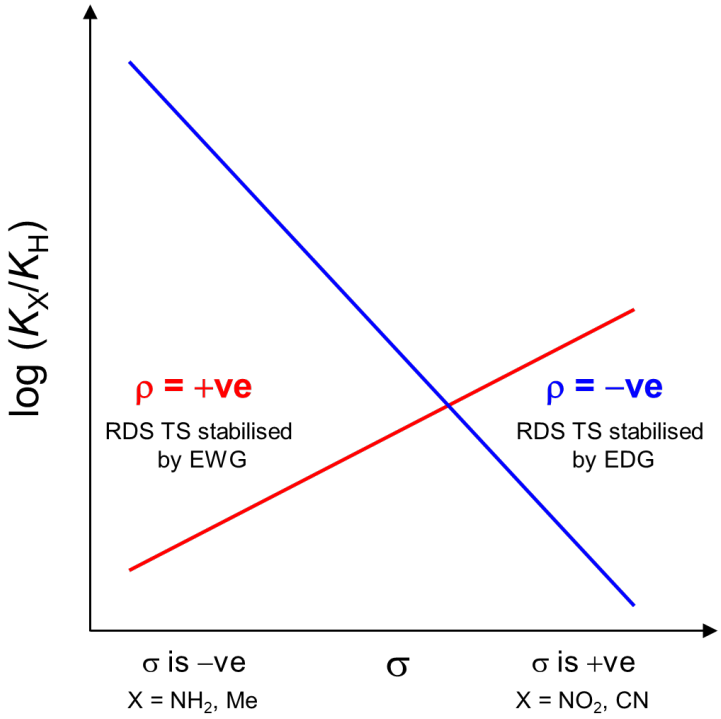

Figure 1.3: A Hammett plot schematic showing reaction constants, ρ, that are positive (red) and negative (blue) and how this relates to the electron withdrawing or donating nature of the substituent as defined through Hammett constants, σ_m and σ_p.

Stabilisation of the rate determining step transition state will reduce its energy and lead to an increase in reaction rate. For a Hammett plot, stabilisation of a build-up of charge in the transition state is by electronic substituent effects. When ρ is positive, this indicates that there is an increase in electron density, e.g. negative charge, which is stabilised by electron-withdrawing substituents. Thus, the rate of such reactions are increased with substituents with positive Hammett constants. Conversely, negative ρ values indicate a decrease in electron density that is stabilised by electron-donating substituents. Armed with this knowledge of the transition state of the rate determining step, the chemist can rationalise a mechanistic pathway that satisfies the results of the Hammett plot analysis.[8, 13, 18]

The relation used in Hammett plots (**Equation 1.2**) also allows prediction of rate/equilibrium constants through knowledge of ρ for a particular reaction and use of the appropriate Hammett constant.[13] Tables of collated ρ values for many different

types of reaction are available meaning that this LFER can have useful predictive power for reaction rates and equilibrium constants.[19] However, it should be kept in mind that ρ changes depending on the experimental conditions, e.g. temperature or solvent.

Deviations from linearity in Hammett plots can also aid in mechanistic elucidation by providing information on how the transition state structure or mechanism of the reaction changes as the electronic properties of the substituent is changed. These results are brought about by a change in preference of rate determining step or mechanistic pathway that result from varying the electronic effect of the substituent, i.e. σ_m or σ_p. The insight afforded by Hammett analyses of reactions has been useful in elucidating mechanisms in processes as varied as catalytic antibody action and substituent elimination within iron complexes.[20-21]

Despite successful applications of Hammett substituent constants, their scope is limited by being unable to appropriately describe substituent effects in a variety of situations. As such, various studies have been performed on new substrates in an analogous fashion to Hammett's empirical approach, or have employed mathematical models involving different combinations of previously derived substituent constants (**Figure 1.4**).[7]

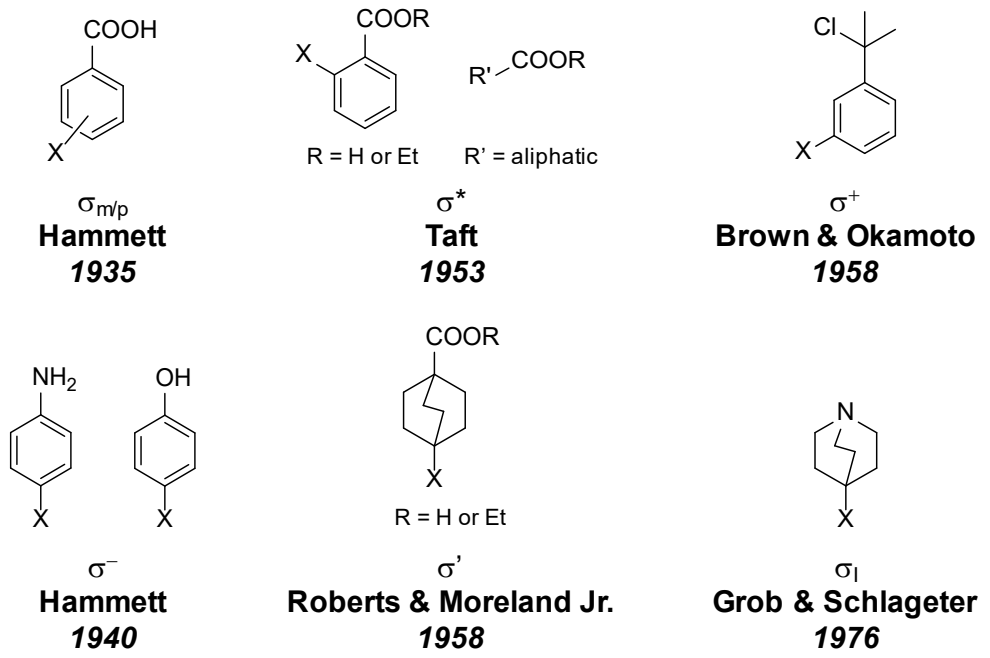

Figure 1.4: Alternative empirical substituent effect scales. X substituents are varied and numerous, encompassing a large range of electron withdrawing and donating substituents. Mathematical relations to obtain, for example, F and R have not been included but are given in the main text.[7, 9, 22-29]

A significant limitation to σ_m and σ_p was the absence of a "σ_o" parameter which was the result of Hammett being unable to capture the effects of *ortho* substituted benzoic acids or aliphatic systems. The complicated behaviour observed in these situations relative to the *meta* and *para* substituted cases was attributed to the "steric pressure" of substituents in the *ortho* position.[7, 30-33] To describe substituent effects in these systems a new constant, σ*, was coined by Taft and co-workers through the esterification and hydrolysis rates of various *ortho* substituted benzoate groups and aliphatic esters (**Figure 1.4**).[23-25] This constant was used to define a steric effect constant, E_s which was expanded upon by Charton with his constant Q_X during his studies into σ_I and σ_R.[22, 24]

Another limitation of σ_m and σ_p is that they encode the overall electronic effect of a substituent, meaning that they are the sum of through-bond and through-space influences. Thus, the origin of substituent effects are not taken into account when rationalising their influence on chemical systems, meaning these constants were unable to capture nuanced behaviour arising due to differences in the relative

importance of different factors in different contexts (e.g. beyond aromatic systems). To better understand the origin of substituent effects on organic compounds, much work was performed to dissect Hammett σ constants into their constituent components; resonance and induction/field.

Resonant substituent effects are dominant within systems that include delocalisation and are therefore more easily dissected than the separation of induction from field effects.[7, 9, 16] To take account of resonant substituent effects, the constants σ^+ and σ^- were defined using experimental data from *meta*-substituted *tert*-cumyl chloride derivatives and aniline/phenols respectively (**Figure 1.4**).[7, 19, 26] These new constants describe the ability of a substituent to stabilise positive (σ^+) and negative (σ^-) charges and were used by Leo and co-workers to obtain "resonance constants" R^- and R^+ using the general relation shown in **Equation 1.3**.[7] Further constants, σ_R (using **Equation 1.4**) and R (using **Equation 1.3**), were coined in the following years in a bid to quantify the resonant component of substituent effects.[7, 31, 34]

$$\sigma = \alpha F + R \qquad \textbf{Equation 1.3}$$

Where σ is a constant obtained from empirical quantification, α is a weighting factor, F is the field component and R the resonant component of a given substituents behaviour.[7, 34]

Historically, inductive and field effects have been treated together due to the difficulty in separating the two effects in experimental systems.[9] Inductive effects are the result of σ bond polarisation and as such are dependent only upon the nature of the bonds in a compound.[13] Field effects, on the other hand, are dependent upon the geometry of the molecule meaning that their effects can be different even if the nature of the bonds in the two systems is identical.[9, 13] As such, despite substituent constants being defined that separate out resonance effects, the further separation of induction and field effects is not fulfilled by σ_R, R or $\sigma^{+/-}$.

An early step towards disentangling inductive and field effects was Roberts and Moreland Jr.'s 1953 study wherein reaction rates and acid dissociation constants of

bicyclo[2.2.2]octane-1-carboxylic acid derivatives and their parent ethyl esters were used to obtain a substituent constant, σ′ (**Figure 1.4**) As there is no conjugation between the substituent and the reactive site, resonant effects are minimal and any substituent effect observed is due to a combination of inductive and field influences.[9, 22] The experimental reactivities of the compounds studied correlated with the Kirkwood-Westheimer electrostatic model (see ***Section 1.2.2***), showing that field effects were important to the constant σ'.[12, 35-36] Strikingly, the σ′ values correlated well with σ_p constants, despite the bicyclo[2.2.2]octane-1-carboxylic acid derivatives having no resonant contribution from the substituent. Such a result shows that σ_p substituent constants determined by Hammett are not dominated by resonance effects. Therefore, this is an early, experimental example of the potential dominance of through-space substituent effects on ionisation and rate constants.[9]

While σ′ encoded only the inductive and field components of substituent effects, further decomposition such that induction was the sole substituent effect parameterised was attempted by Taft and co-workers who used their previously established σ* values to coin a new constant, σ_I.[37] This constant was intended to describe only the inductive contribution to the overall substituent effect, but likely includes contributions from through-space substituent effects due to the difficulty in separating these two processes. Taft's σ_I is related to σ_R by Hammett's σ_p constant *via* **Equation 1.4** , meaning σ_I can also be calculated from σ_R values.[7]

$$\sigma_p = \sigma_I + \sigma_R \qquad \textbf{Equation 1.4}$$

In 1976, Grob and Schlageter used the ionisation of protonated quinuclidines (**Figure 1.4**) to obtain σ_I through direct empirical observation, in contrast to the mathematical approach employed by Taft to obtain the same constant.[27] These quinuclidine (or 1-aza-bicyclo[2.2.2]-octane) derivatives are more sensitive to the X substituents than Roberts and Moreland Jr.'s bicyclo[2.2.2]octane-1-carboxylic acid derivatives due to the experimental reporter being part of the ring.[7, 22] Much like Taft's version of σ_I, Grob and Schlageter's σ_I also describes the combined local substituent effect.

Therefore, while these studies aimed to dissect induction from the overall electronic substituent effects, they ultimately only took account for the rest of the substituent effect that was not parametrised by σ_R.

Numerous studies were performed to dissect the various contributions to the overall electronic substituent effect on organic molecules meaning that by the 1970s there were at least twenty different constants that each aimed to complement Hammett's seminal σ_m and σ_p constants.[22, 34] Swain and co-workers theorised that the underlying assumption made in defining these constants was flawed and realised the importance of understanding the origin of the substituent effect to be able to provide universal quantification.[34] It was noted that the relative importance of through-bond and through-space electronic effects of a substituent was not a fixed quantity and was dependent upon the distance of a substituent from the reaction centre and that in some cases through-space effects dominated over through-bond influences.[34] Indeed, Leo and Taft note in their comprehensive 1991 review that field effects dominate for distant substituents.[7] With the aim of dissecting the field and resonance components of electrostatic substituent effects, Swain and co-workers brought together myriad aforementioned constants to dissect out F constants that encode through-space field effects (**Equation 1.3**).[31, 34] Charton performed a similar analysis of the available experimental data, aiming to obtain a localised (that is the inductive and field effects combined) substituent effect constant.[22]

1.2.2 Empirical models to predict and quantify substituent effects

Despite numerous, intensive studies, viable dissections of substituent effects was not achieved. Moving into the 1970s, attention turned towards seeking understanding of the relative importance of inductive and field effects by applying empirical models to system design and analysis.

Substituent effects in the inductive model depend upon the number and nature of the bonds as well as the number of paths between the substituent and reaction centre.[12, 38] Thus, there is a "fall-off" in the effect of the substituent with increasing bond distances.[12, 39] This idea was first proposed by Derick in 1911 who proposed a "rule of

thirds" upon observing the change in pK_a's of carboxylic acids to be related to the number of carbon atoms between the substituent and carbonyl group.[10-11, 40-42] This idea was put into a quantitative relation by Branch and Calvin in the 1940s and expanded by Exner and Fielder, leading to **Equation 1.5**.[38, 43] Taft and McGowan used the inductive model outlined in **Equation 1.5** in investigations regarding substituent effects in both aliphatic and aromatic systems, with "fall-off" factors ranging from 2 to 3.[38, 43-44] It should be noted, however, that this model does not take into account for any solvent effects or the angular dependence of substituent effects.[38]

$$log\left(\frac{K_X}{K_H}\right) \propto \sum \epsilon^n \qquad \textbf{Equation 1.5}$$

Where ϵ is the transmission coefficient and n is the number of bonds between the substituent and reaction centre.

The field effect of substituents is most often modelled using the Kirkwood-Westheimer electrostatic cavity model where the effect is the result of bond dipole moments. Within this model, the molecule is placed in a cavity of low dielectric constant, D_i, that is within a solvent continuum, D (**Figure 1.5**).[11-12, 35-36, 38]

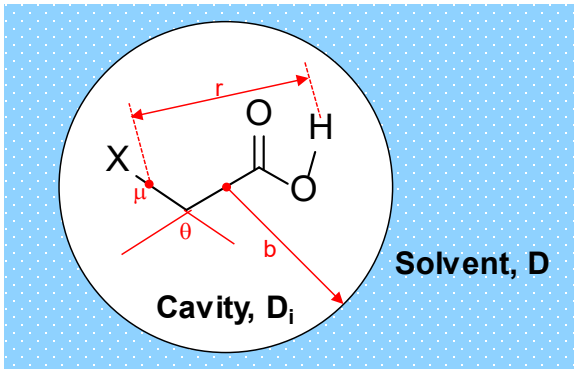

Figure 1.5: The Kirkwood-Westheimer model. The molecule is placed in a cavity of radius, b, and dielectric constant, D_i. The cavity is within a solvent continuum of dielectric constant, D. The distance between the dipole moments of the substituent and the reactive site is defined by "r" and this and the angle "θ" are dependent upon the geometry of the substituent and the reactive site. The bond dipole moment is μ and thus θ is the angle between this and r.[12, 35-36]

The solvent cavity within which the molecule is placed has a low dielectric constant to allow the field effect of the substituent be transmitted effectively through space.[36] The mathematical relation derived in this model estimates the Gibb's free energy of the deprotonation of an acid in the presence of a dipolar substituent. Importantly, this model predicts a spatial dependence of the substituent effects whereas the traditional inductive model does not.[12, 35-36]

A number of studies were performed in the 1970s and 80s that aimed to understand the relative importance of field and inductive effects through clever design of structures that investigate various aspects of each model.[12]

The dissociation constants of 4-substituted bicyclo[2.2.2]octane-1-carboxylic acids were again used by Wilcox and Leung, but this time to assess the relative importance of field and inductive substituent effects.[11] To do this, a series of analogous 4-substituted bicyclo[2.2.1]heptane-1-carboxylic acids were studied (**Figure 1.6**).

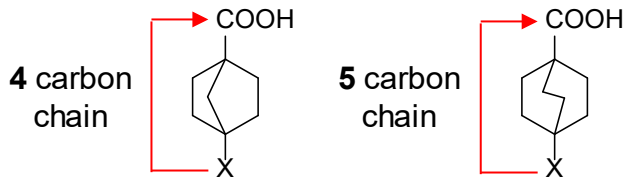

Figure 1.6: Bicyclo[2.2.1]heptane-1-carboxylic acid and bicyclo[2.2.2]octane-1-carboxylic acid derivatives used by Wilcox and Leung to dissect inductive and field effects from one another.[11] The length of the carbon chain between the X substituent and carboxylic acid are indicated.

According to the Kirkwood-Westheimer electrostatic model, the field effects of the two systems should be comparable. However, inductive models suggest that the bicyclo[2.2.1]heptane-1-carboxylic acid derivatives will encode more of the inductive effect due to the smaller carbon chain linking the substituent and reactive centre. Thus, the two models suggest a different linear relation between the pK_a's of the two systems and ultimately, the experimental results are in line with that predicted by the Kirkwood-Westheimer model and are different to those predicted by the inductive

model. These results suggest that through-space effects dominated the overall substituent effect on the pK_a values of the acids studied and the authors note that their study shows the "essential" role that through-space effects may play in substituent effects.[11]

In 1971, Grubbs *et. al.* used bridged anthracene derivatives as rigid models to understand the relationship between the effect of a substituent on dissociation constants and reaction rates with the geometry of the molecule (**Figure 1.7**).[45]

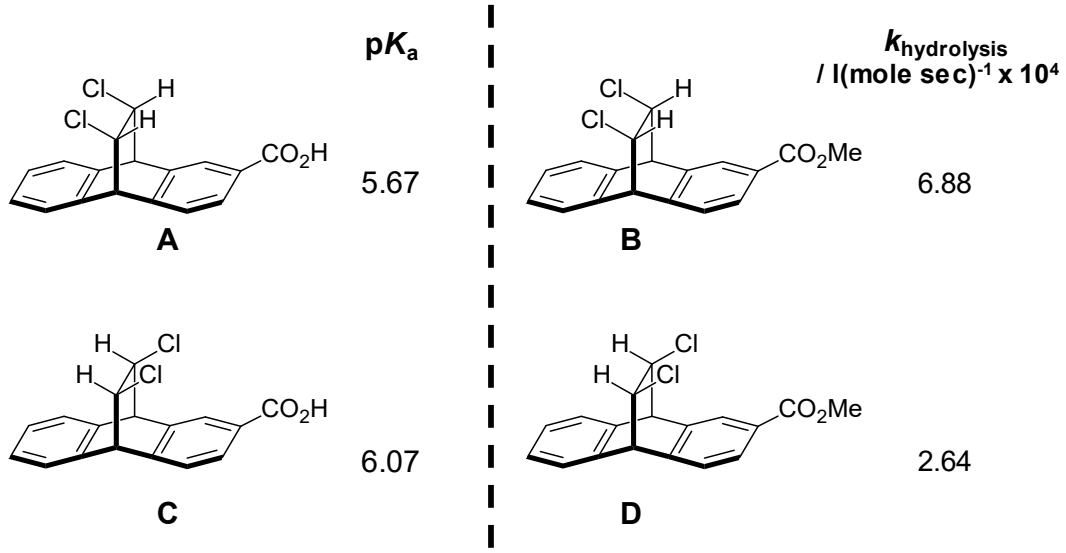

Figure 1.7: Ethano-bridged anthracene derivatives used by Grubbs *et. al.* to study the geometric dependence of the effects of a substituent (in this case, chlorine) on the pK_a of a carboxylic acid (left) and the rate of hydrolysis of an ester (right).[45]

As compounds **A** and **C** (**Figure 1.7**) share the same types of bonds, the inductive effect of the chlorine substituents on the acidity of the carboxylic acid is the same. The difference between them is that they have different geometries which has an impact on the ability of the chlorine substituents to affect the pK_a of the acid group *via* field effects. In compound **C**, the chlorine substituents are on the same side of the ethano-bridge as the carboxylic acid whereas in compound **A**, they are on the opposite side of the bridge to the acid (**Figure 1.7**). Therefore, the field effect of the chlorine substituents is geometrically allowed in **C** but not in **A** (**Figure 1.7**). The pK_a values of these compounds show that there is indeed a difference in the influence of the

chlorine substituents on the acidity of the carboxylic acid. In compound **A**, where field effects of the chlorine substituents are weak, the pK_a is lower than that of compound **C** (**Figure 1.7**). A similar observation is found with the ester derivatives, **B** and **D**, wherein the rate of hydrolysis is reduced when the chlorine substituent is on the same side of the bridge as the ester (**Figure 1.7**).[45]

Stock and Golden used 8-substituted 9,10-ethanoanthracene-1-carboxylic acids in their investigation to discern the relative importance of inductive and field substituent effects (**Figure 1.8**).[46]

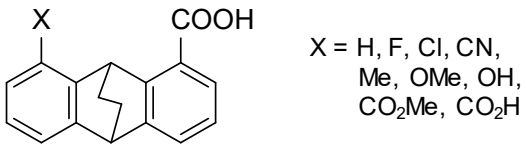

Figure 1.8: 8-Substituted 9,10-ethanoanthracene-1-carboxylic acids studied by Stock and Golden.[46]

Through analysis of the dissociation constants of the 8-substituted 9,10-ethanoanthracene-1-carboxylic acids, a reversal of behaviour according to that predicted by inductive effects was observed. The experimental data was in line with the estimation of behaviour through use of the Kirkwood-Westheimer model, pointing to the dominance of through-space effects to the overall substituent effect in these compounds.[46]

Another example of the dominance of through-space over inductive effects aided by the predictive power of their relative models was provided by Liotta and co-workers. Predicted behaviour of various 6-substituted spiro[3.3]heptane-2-carboxylic acids as set out by the Kirkwood-Westheimer model correlated well with the experimental dissociation constants.[44]

These studies show the utility of predictive models in understanding of the mode of transmission of substituent effects through the use of comparable compounds. Analysis *via* these models show the predominance of field effects within the localised effect of a substituent (i.e. those in the absence of resonance effects). However,

separate quantification of inductive and field contributions is not obtained through the use of these models, only the indication that one model explains the experimental findings better than the other. Thus, the separation of these effects into their own, distinct, constants was not achieved and there remains a lack of substituent constant or mathematical formula that is able to universally predict and explain the behaviour of a system given a certain substitution.

1.3 Modern Approaches to Substituent Effect Quantification

Computational chemistry has become an invaluable tool in the study of substituent effects on various systems and has provided a means of side-stepping the intricacies of the simplified empirical models historically applied to substituent effect quantification. Density functional theory (DFT) methods provide a means of directly probing the electrostatic potential at any point in space around a molecule.[47-49] Such direct measurements afforded by computational calculations have emerged since the 1980s and were not accessible to Hammett *et. al.* during the early days of substituent effect quantification.

The first to use computational means to investigate electronic substituent effects was Topsom in his 1981 study to assess the relative importance of inductive and field effects.[50] This investigation was conducted *in silico* to overcome the challenges associated with the ability to compare different, fixed geometries of model compounds experimentally. Computational analysis also allows the use of an isolated molecule model, where the effect of a substituent on a reactive centre is assessed by analysing the effect between two discrete entities; one with the probe and another with the substituent. In this model, the substituent is not covalently linked to the molecule with the probe on it and is instead held in space where it would be if it were linked. Therefore, the isolated molecule method of analysis can dissect through-bond substituent effects and allows the assessment of the field effect of the substituent in the absence of through-bond effects. This type of analysis is powerful in understanding the relative importance of through-bond and through-space substituent effects as it eliminates the former to allow focus on the latter and is another reason why

computational studies are crucial to the study of substituent effects as this procedure cannot be performed empirically. In Topsoms study, computationally derived proton affinities of substituted alkylamines (**Figure 1.9A**) were in good agreement with those of the isolated molecules (**Figure 1.9B**) demonstrating that the behaviour of the substituent can be emulated in systems where no through-bond effects can operate. In addition, the proton affinities of the alkylamines were in agreement with predictions based on the electrostatic model, showing the importance of through-space substituent effects on these systems.[50]

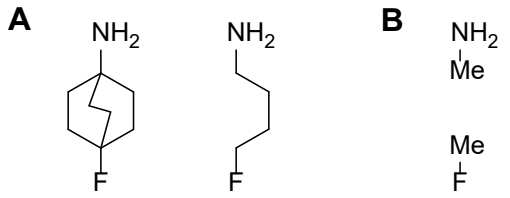

Figure 1.9: Systems used by Topsom *et. al.* in their computational analysis of the field and inductive effects. **(A)** ω-Substituted alkylamines for which proton affinities were calculated. **(B)** Isolated molecules for calculation of the substituent effect in the absence of through-bond influence.[50]

In 1984, Topsom and Marriott used *ab initio* calculations to define a theoretical scale of field substituent effects to overcome the solvent sensitivity of σ_F and the difficulties in choosing the appropriate value of σ_F from the multiple available for a given substituent.[14] The interaction energies, $\Delta E°$, between hydrogen-capped amines and hydrogen-capped X substituents gave a high correlation with σ_F and from this correlation a relationship was defined to allow calculation of a field parameter (again denoted as σ_F) from computationally derived $\Delta E°$ values (**Figure 1.10** and **Equation 1.6**).

Figure 1.10: Hydrogen-capped interacting pairs used to obtain $\Delta E°$ values used in Topsom and Marriotts 1984 study. These values were then used in **Equation 1.6**.[14]

$$\sigma_F = -0.074\Delta E° \qquad \textbf{Equation 1.6}$$

The authors note that a universally applicable scale of field effect constants is not possible due to the lack of uniformity in the geometric relationship between the reaction probe and substituent between systems.[14]

More recently, in 2016 Sigman and co-workers performed an elegant combined approach to substituent effect quantification, bringing empirical and DFT methods together to understand *ortho* substituent effects within aryl systems.[33] To test the utility of computationally derived parameters, Natural Bond Orbital (NBO) charges were calculated for the carbonyl oxygen atom of forty seven *para*-substituted benzoic acids and were correlated with σ_p Hammett constants. An excellent correlation was found, showing that one could apply NBO charges as substitutes for σ_p. For *ortho*-substituted systems, Sigman *et. al.* used multivariate linear regression analysis of site selectivity within Heck reactions of alkenols and β-aryl elimination of triphenylmethanols to obtain mathematical models containing computationally derived and experimentally obtained parameters (**Figure 1.11**). A subset of the substituents for which NBO charges of the *para*-substituted benzoic acids were calculated were used as the substituents in these *ortho*-substituted model reactions. Thus, for a substitution where X is a methoxy group, the NBO charge and IR stretching frequency of the 4-methoxybenzoic acid carbonyl group was used in the multivariate linear regression analysis of the model reactions.

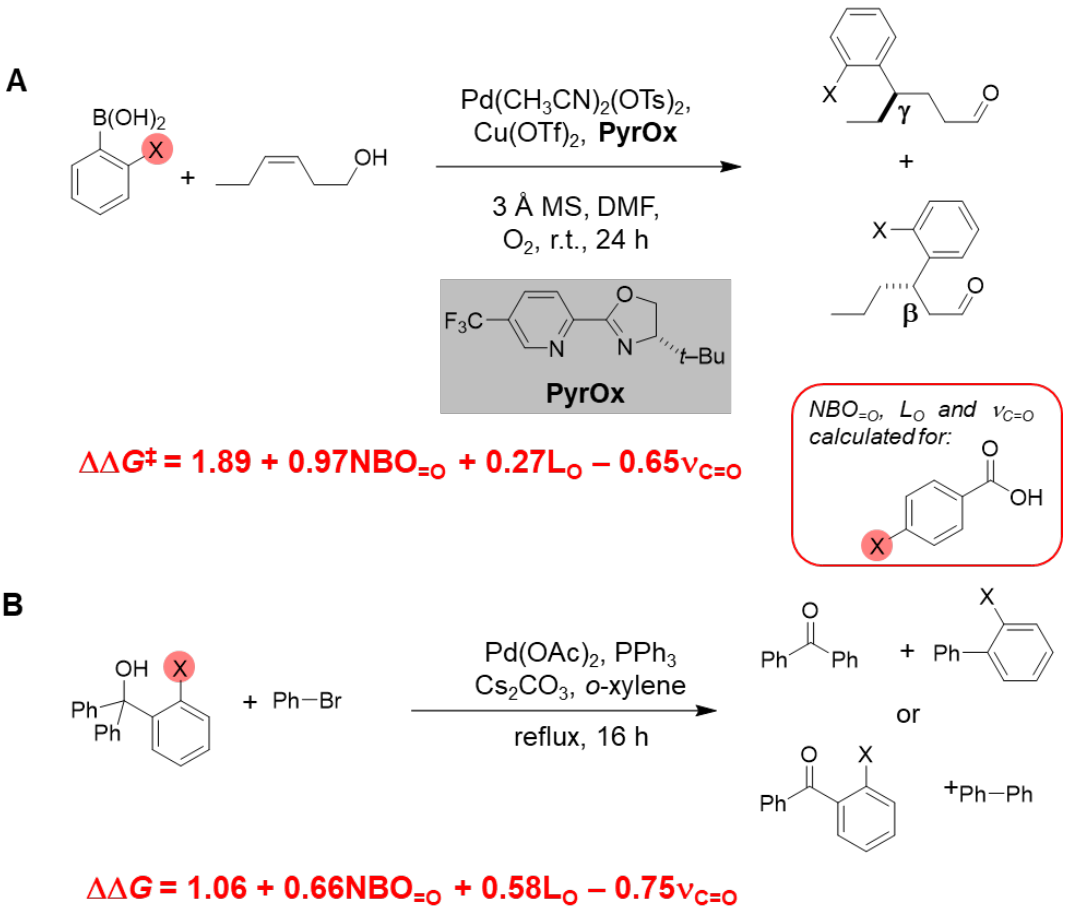

Figure 1.11: Case studies used by Sigman and co-workers to develop an *ortho* substituent parameter together with the mathematical model derived for each reaction. $NBO_{=O}$ is the NBO charge of the carbonyl oxygen atom, L_O is the Sterimol parameter that describes the length along the bond between the substituent and the rest of the molecule and $\nu_{C=O}$ is the IR stretching frequency of the C=O bond in the same X substituted benzoic acid derivative. **(A)** Heck reaction between *ortho*-substituted arylboronic acids and alkenols. **(B)** Pd mediated β-aryl elimination of triphenylmethanols bearing an *ortho* substituted aryl group.[33]

The experimental data of both the Heck and β-elimination reactions produced excellent correlations against a mathematical model that included experimental IR carbonyl stretching frequencies and NBO charges of the carbonyl oxygen atom, meaning that the *ortho* effect of the substituent in these case studies was taken into account using a combination of computational and empirical parameters.[33]

Akin to how Sigman *et. al.* used computationally derived NBO charges as substitutes for Hammett σ values, a number of purely computational studies have sought to quantify substituent effects using computationally derived molecular electrostatic potentials (ESPs). The majority of these modern, purely computational approaches to

quantification have focussed on aromatic interactions, ranging from ion–π to π–π stacking interactions.

Suresh has used ESP minima (V_{min}) to encode substituent effects in a number of systems. In 1998, this parameter was used to quantify substituent effects in doubly substituted benzene derivatives.[51] Three constants were calculated *via* V_{min} where the relation between the two substituents was either *ortho*, *meta* or *para* (D_o, D_m and D_p respectively). These constants were found to correlate well with empirical σ_m and σ_p Hammett constants and were able to predict the computational behaviour of triply substituted benzenes with fair results. The same group subsequently used V_{min} as a means of quantifying substituent effects in singly substituted benzene rings.[49] V_{min} values of fourteen differently substituted benzene derivatives were obtained and formed a linear correlation with σ_p values with an R^2 of 0.99. This high correlation with constants routinely used in the analysis of substituent effects points to the utility of ESPs in modern quantification as the V_{min} values have an equal ability to measure substituent effects as σ_p.[49]

Following from the successful application of V_{min} to the quantification of substituent effects in aromatic systems, Suresh and co-workers used this approach to evaluate the inductive effect.[30] V_{min} values of 4-substituted bicyclo[2.2.2]octane carboxylic acids and quinuclidines were correlated with σ_I. Although a good correlation between V_{min} and σ_I was obtained, the V_{min} values did not drop when the substituent was moved from the 2 to 4 positions on the ring relative to quinuclidine nitrogen atom as anticipated by σ_I. The authors attribute this observation to through-space interactions within the quinuclidine cage.[30]

Suresh and co-workers turned their attention to the resonant component of substituent effects and applied their V_{min} analysis to it. Using the V_{min} values of substituted benzenes, σ_R^V was calculated with the aim to establish a scale of substituent resonant effects.[32] Validation of the σ_R^V values came from comparison with the difference in reaction energies between three isodesmic reactions (**Figure 1.12**). These correlations pointed to this constant being an easily obtainable parameter with which to evaluate

resonant substituent effects, with the authors suggesting the utility of such a constant in QSAR studies.[32]

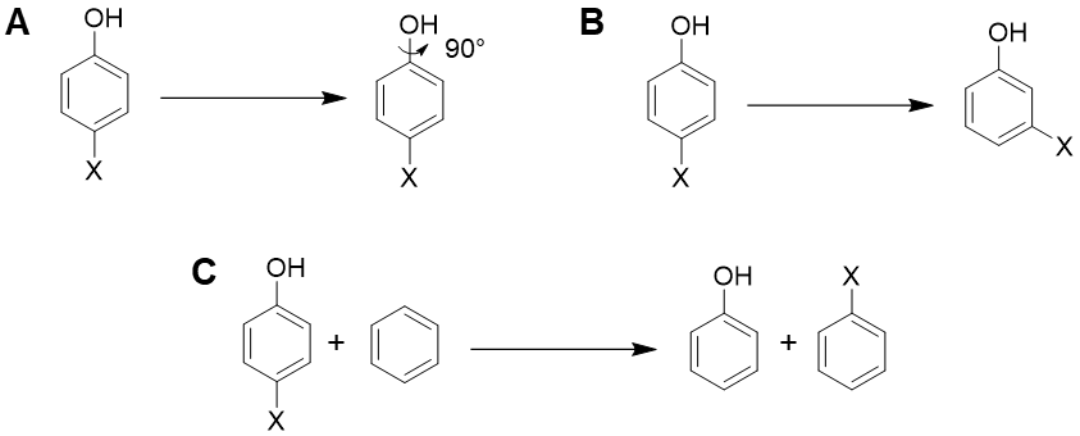

Figure 1.12: Isodesmic reactions used by Suresh and co-workers to test their σ_R^V constants.[32]

Galabov *et. al.* used ESPs of substituted benzenes to obtain a parameter, ΔV_i, to encode the change to the ESP values of the ring carbons as a result of substitution. As such, ΔV_i was calculated from the subtraction of the ESP of unsubstituted benzene (V(benzene)) from that of the substituted benzene derivative (V_i(R)) according to **Equation 1.7**.[47]

$$\Delta V_i = V_i(R) - V(benzene) \qquad \textbf{Equation 1.7}$$

Correlation of these values with Hammett constants were excellent, meaning ESP values were able to encode and quantify substituent effects; providing extra evidence to the findings of Suresh and co-workers .[32, 47]

In a 2016 study, Suresh and Remya used ESPs of substituted benzenes to quantify substituent effects and obtain a constant from which substituent classification and ranking was achieved.[52] The constant, ΔV_c, was the difference in the ESP values of the carbon atom *para* to the substituent and that of a carbon atom in the unsubstituted case, i.e. benzene. For this parameter, electron-donating substituents have negative ΔV_c

values and *vice versa* for electron-withdrawing groups. Within these classes defined by their sign, the magnitude of ΔV_c indicated the relative strengths of these effects within the same class. These ΔV_c values did not correlate well with σ_p Hammett constants, which the authors linked to the limited number of substituents used to calculate σ_p values. This study thus highlighted a benefit that measuring substituent effects *in silico* affords; efficient parameterisation of a large number of substituents with only one computational measurement in comparison to numerous, time-expensive experimental measurements.[52]

In addition to providing numerical assistance in the analysis of substituent effects, ESPs have become an invaluable, qualitative, visual tool for analysing non-covalent interactions.[53] The interpretation of ESPs is often incorrect due to the assumption that substituent induced changes in the ESP of an organic molecule correlate to changes in the local electron density. In 2009, Wheeler and Houk investigated substituent effects on the ESPs of aromatic systems.[53-56] They showed that the changes in the ESP upon substitution could be recreated by simply summing the ESPs of the hydrogen-capped substituent and unsubstituted benzene (**Figure 1.13**). Thus, substituent-induced changes in the ESPs of substituted benzene derivatives could be reproduced without any changes in electron density of the aryl π system *via* through-bond effects.

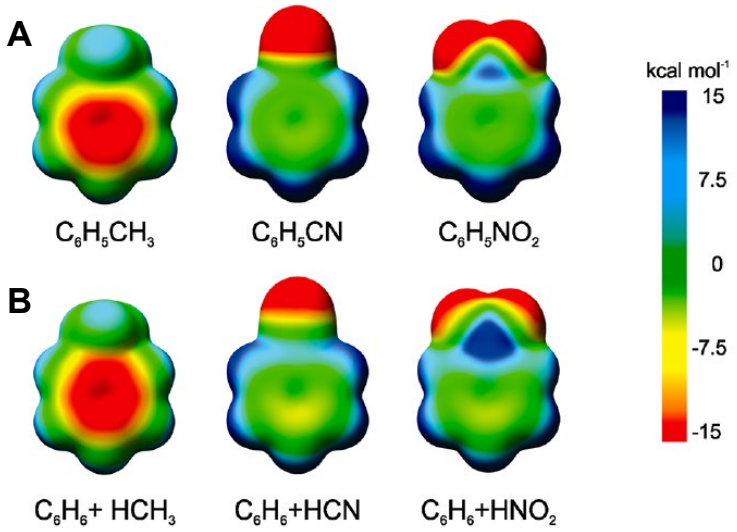

Figure 1.13: Substituent effects on the ESP of substituted aryl systems can be recreated by an additive model of unsubstituted benzene and the hydrogen-capped substituent, showing the importance of through-space effects on the ESP of the substituted system. **(A)** Substituted benzene ESP and **(B)** the ESP sum of benzene and the hydrogen-capped substituent.[53-54] Image taken from the 2014 *J. Phys. Chem. A* Feature Article by Wheeler and Bloom.[54]

Wheeler and Houk concluded that aryl π electron resonance have little impact on the changes in the ESP that occurs upon substitution, meaning that the through-space electrostatic effect of the substituent was more important.[4, 53-54]

Further to this, Wheeler and Houk analysed two-dimensional slices through the ESPs of the sum of unsubstituted benzene (C_6H_6) and hydrogen cyanide (HCN) *versus* benzonitrile (C_6H_5CN) (**Figure 1.14**).

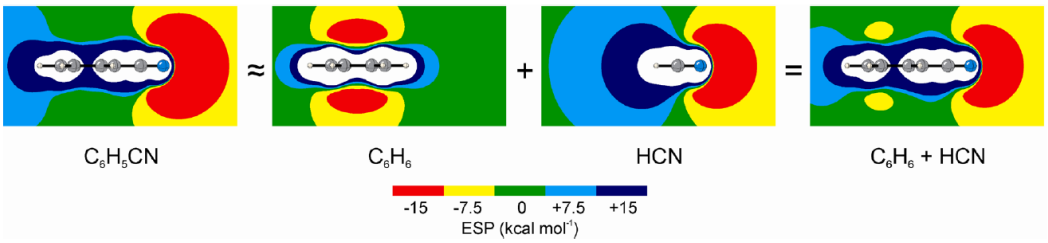

Figure 1.14: Two dimensional slices through the ESPs of benzonitrile (C_6H_5CN), unsubstituted benzene (C_6H_6), hydrogen cyanide (HCN) and the sum of benzene and hydrogen cyanide (C_6H_6 + HCN) showing the through-space effect of the nitrile group on the electrostatic potential above the ring centroid of benzonitrile.[4, 53] Image taken from the 2013 *Acc. Chem. Res.* Article by Wheeler.[4]

Analysis of these two-dimensional plots shows that the polarisation of the hydrogen cyanide bond (HCN) has a through-space effect on the additive benzene and hydrogen cyanide system (C_6H_6 + HCN), making the centre of the benzene ring more positive than the unsubstituted ring (C_6H_6). It was concluded that the through-space effect of the local hydrogen cyanide dipole overwhelmed the negative ESP associated with the aryl π system.[4, 53-54]

In 2010, Suresh and co-workers used their V_{min} approach to investigate the relative importance of through-space and through-bond effects of a variety of substituents in saturated and unsaturated systems (**Figure 1.15**).[57]

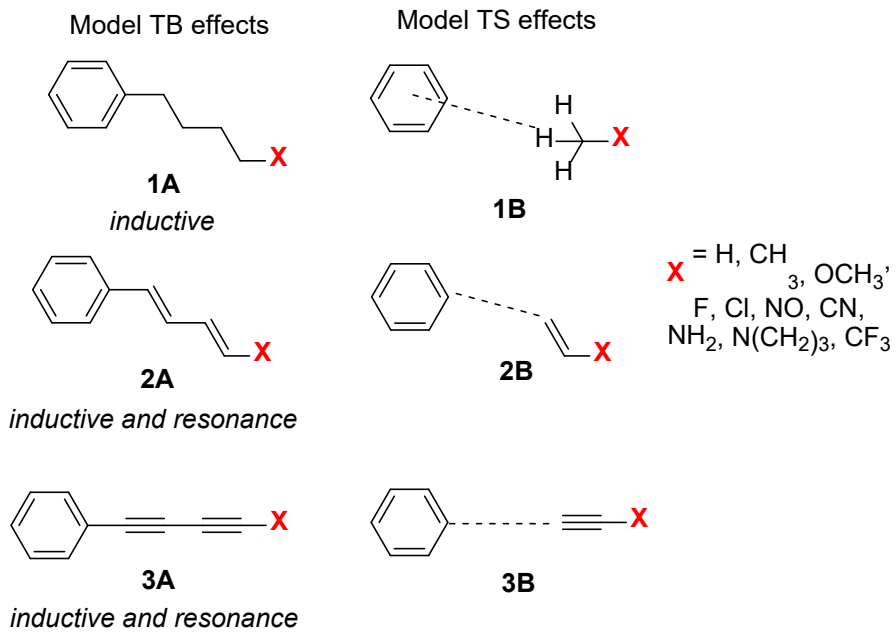

Figure 1.15: Model compounds used by Suresh and co-workers, the ESPs of which were used to assess the relative contributions of through-space and through-bond substituent effects.[57]

The difference in V_{min} between the systems in which through-bond effects were possible (**Figure 1.15**, **1A**, **2A** and **3A**) and the analogous systems where only through-space effects could exist (**Figure 1.15**, **1B**, **2B** and **3B**) was calculated using the ESP value of the benzene ring of each system. This analysis allowed separation of the relative importance of the through-bond and through-space effects of the substituent, a task known to be very difficult *via* empirical methods.[9, 57]

It was seen that in the saturated system (**Figure 1.15**, **1A** and **1B**), the through-space component dominated and accounted for 79.6% of the total electronic substituent effect. However, for the unsaturated analogues (**Figure 1.15**, **2A** and **B**, **3A** and **B**), the through-space effect accounted for only around 45% of the total substituent effect, being slightly exceeded by through-bond effects.[57]

Substituent effects on ion–π interactions have also been the subject of computational studies.[4, 6, 54, 58-59] It was previously assumed that these interactions are the result of polarisation of the aryl π system. In this traditional model, electron-donating substituents lead to a "π-electron rich" aryl system and electron-withdrawing substituents give rise to "π-electron deficient" aryl systems. Therefore, it is assumed that aryl systems bearing electron-donating substituents bind to cations and those with electron-withdrawing substituents bind anions. Wheeler, Houk and Suresh have investigated cation-π interactions using computational methods (**Figure 1.16** and **1.17** respectively).[4, 54, 58-59] While Hunter *et. al.* showed that the electronic effects of substituents has a bearing on cation-π interactions,[60] whether this substituent effect is due primarily to through-bond or through-space interactions had not been extensively investigated prior to these studies.

Wheeler and Houk used an additive model to approximate the cation-π interaction energy where there could be no through-bond effects of the substituent on the aryl π system, meaning any substituent effect is a product of through-space interactions between the substituent and the cation (Na^+) (**Figure 1.16**).[4, 54, 59]

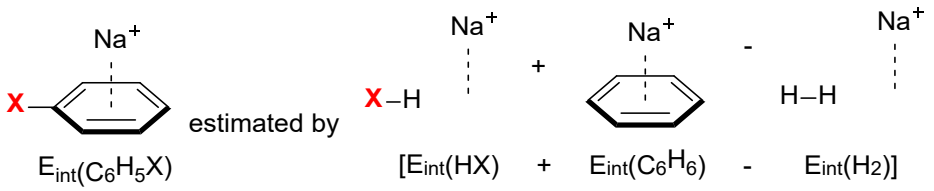

Figure 1.16: Model computations used by Wheeler and Houk to investigate the nature of the non-covalent interactions between cations and substituted π systems. $E_{int}(C_6H_5X)$ was calculated and compared to an estimate of this energy from the interaction energies (E_{int}) for HX, C_6H_6 and H_2 with a sodium cation.[4, 54, 59]

The estimated energy was then compared to the computed value of the intact substituted benzene and a high correlation was achieved. This high correlation, with outliers the result of strong π resonance acceptors and donors, allowed the conclusion that through-space interactions between the substituent and the cation are more important to binding than substituent-induced polarisation of the aryl π system.[4, 54, 59]

The relative importance of through-bond and through-space substituent effects on cation-π interactions was probed by Suresh and co-workers who utilised a similar additive approach to that used by Wheeler and Houk (**Figure 1.17**).[58]

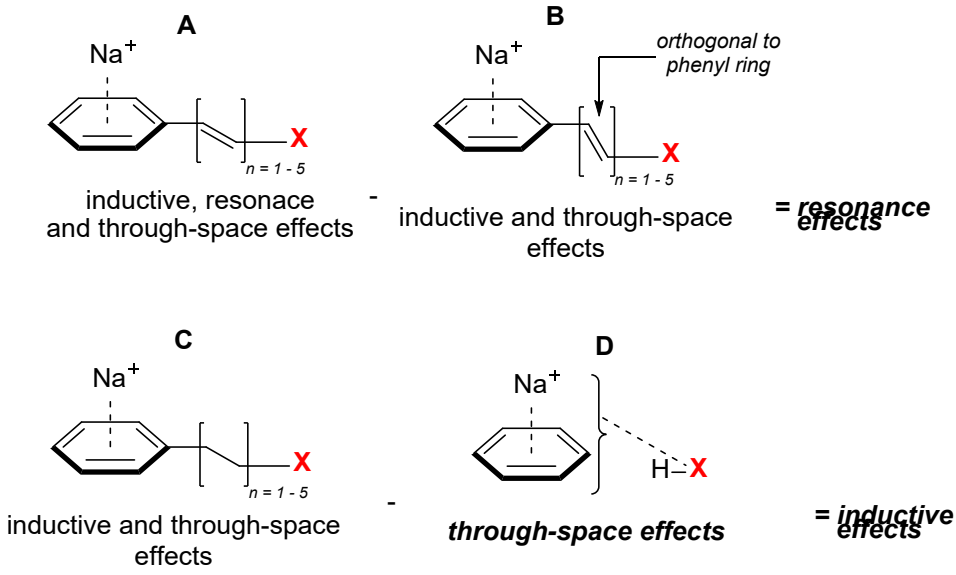

Figure 1.17: Model compounds used by Suresh *et. al.* to determine the relative importance of through space and through bond effects of substituents on cation-π interactions. Through subtraction of the energy of **(B)** from **(A)**, the contribution of resonance to the substituent effects can be determined. Similarly, subtracting the energy of **(D)** from that of **(C)** will give the inductive contribution to the total electrostatic substituent effect.[58]

Through clever design of their model compounds used in computations, Suresh *et. al.* were able to dissect the contributions of through-bond and through-space substituent effects on cation-π binding. While concluding that the effect of a substituent on this binding was a combination of both through-bond and through-space substituent effects, it was noted that through-space effects were dominant for electron-withdrawing substituents, while resonance dominated the effects of electron-donating

substituents.[58] This finding is largely in step with that of Wheeler and Houk, with the nuanced behaviour in the difference between electron-withdrawing and donating substituents in Suresh and co-workers study likely due to the more proximal relationship of the substituent to the aryl ring relative to Wheeler and Houks model of direct aryl ring substitution. In 2012, the same group used these findings to help them devise a means of predicting substituent effects on cation-π interactions for a diverse series of aromatic systems.[61]

The effects of substituents on anion-π interactions were investigated computationally by Wheeler and Houk using an additive model designed to assess the relative importance of through-space and through-bond resonance substituent effects on anion-π interactions (**Figure 1.18**).[4, 6, 54]

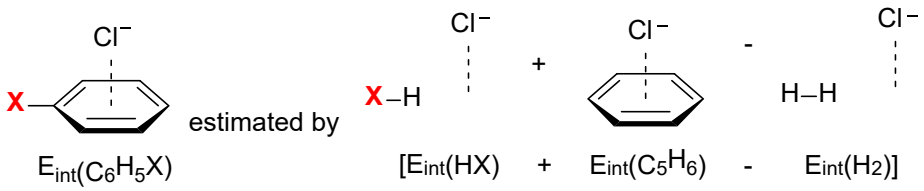

Figure 1.18: Model compounds used by Wheeler and Houk to investigate the nature of the non-covalent interactions between anions and substituted π systems. $E_{int}(C_6H_5X)$ was calculated and compared to an estimate of this energy from the interaction energies (E_{int}) for HX, C_6H_6 and H_2 with a chloride anion.[4, 6, 54]

Through comparison of the energy of the additive model with that of the intact substituted benzene system, the relative importance of the polarisation of the aryl π-system by the substituent and the through-space effects of the substituent was deduced. As there is no polarisation of the π-system possible in the additive model, the strong correlation between the energies of the two systems shows that the substituent effects are not due to polarisation of the π-system. As such, it was concluded by Houk and Wheeler that the dominant substituent effects at play in anion-π interactions were through-space effects.[4, 6, 54]

In 2008, Wheeler and Houk computationally investigated substituent effects in π-π stacking and found that the through-space effects of the substituents dominated over

the through-bond effects. It was found that substituent effects in the Ph–X···Ph dimers were strongly correlated with the energies of the hydrogen-capped substituent, HX and benzene dimers. This result was attributed to a direct, through-space interaction between the substituent and the unsubstituted ring.[4, 54, 62] Further studies by Wheeler and Houk in 2011 revealed that these through-space interactions occur between the local dipole associated with the substituent and the nearby C–H local dipole of the other ring. This was termed the local, direct interaction model (**Figure 1.19**).[3-4, 54]

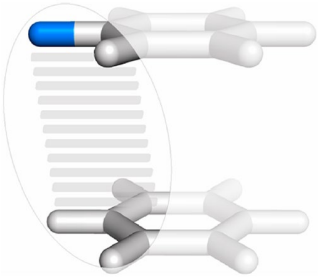

Figure 1.19: Local, direct interaction model postulated by Wheeler and Houk to account for the stacking interactions between a substituted aryl ring and an unsubstituted ring. Through-space effects of the substituents dominate, with the interaction taking place between the local dipole induced by the substituent and the C–H local dipole of the unsubstituted ring. Changes to areas of either molecule shaded in grey will therefore have no net impact on the substituent effect.[3-4, 54] Image taken from the 2013 *Acc. Chem. Res.* Article by Wheeler.[4]

Sherrill and Parrish performed an energetic decomposition analysis (EDA) *via* Functional group Symmetry Adapted Perturbation Theory (FSAPT) calculations as a means of evaluating Wheeler and Houk's local, direct interaction model.[63] This study focussed on the π-π stacking interactions that were central to Wheeler and Houk's studies and performs EDA with the partitions shown in **Figure 1.20** to obtain interaction energies as a function of the aryl ring and substituent of the substituted benzene partner of the dimer. To achieve this, the interaction energy difference between the Ph–X···Ph and Ph–H···Ph dimers is calculated first according to **Equation 1.8**.

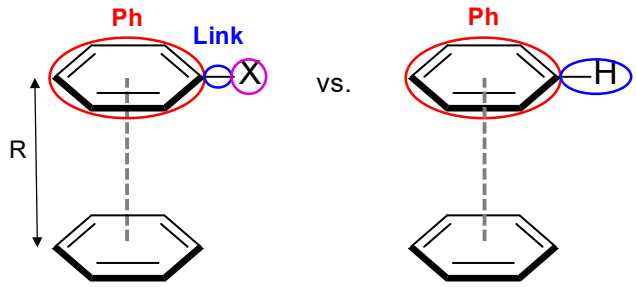

Figure 1.20: FSAPT partitions of Ph–X and Ph–H performed by Sherrill and Parrish to analyse the local, direct interaction model. The dimers are separated by distance R.[63]

$$\Delta E_{int} = E_{int}(Ph - X) - E_{int}(Ph - H) \qquad \textbf{Equation 1.8}$$

The overall, Ph–X···Ph interaction energy is then broken down into the contributions from Ph (of Ph–X), X and Link fragments as exemplified in **Equations 1.9** for the Ph fragment.[63]

$$\Delta E_{int}^{Ph} = \Delta E_{int}^{Ph}(Ph - X) - \Delta E_{int}^{Ph}(Ph - H) \qquad \textbf{Equation 1.9}$$

ΔE_{int}^{Ph} is the difference in interaction energy between Ph–X···Ph and Ph–H···Ph due to the substituent-induced polarisation of the Ph fragment; this is encoding the traditional model of aryl ring polarisation and thus its contribution to the overall ΔE_{int}. The local, direct interaction model contribution to ΔE_{int} is therefore given directly by ΔE_{int}^{X} and indirectly by ΔE_{int}^{Link}. For all substituents examined, the traditional model contributes to the overall difference in interaction energy, but it was the direct, interaction model contributions that dominated the overall interaction energy difference. This was displayed visually by difference ESP surfaces showing the contributions of each component to the overall ΔE_{int} ESP surface (**Figure 1.21**).[63]

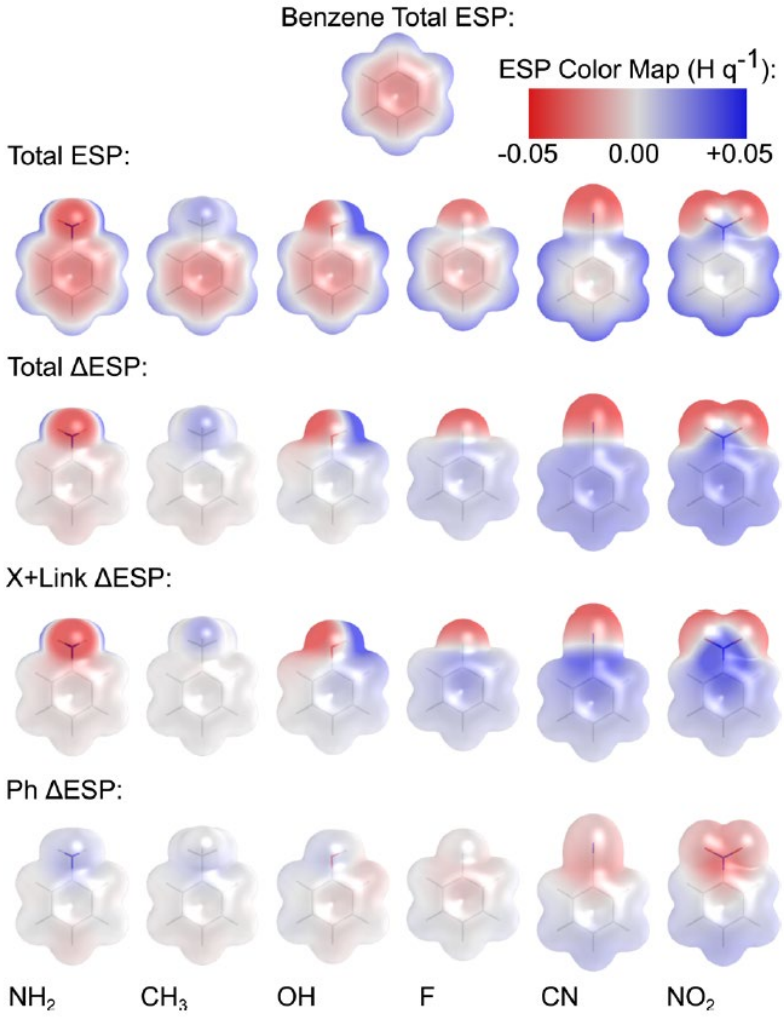

Figure 1.21: ESP analysis showing the difference between the substituted and unsubstituted benzene rings in Sherrill and Parish's study. Image taken from the 2014 *J. Am. Chem. Soc.* Article by Parrish and Sherrill.[63]

Interestingly, these plots show that the substituent and link form very localised and strong electric fields. Therefore, the FSAPT and ESP analysis of these dimers provided support for Wheeler and Houk's local, direct interaction model.[63]

The range of interactions probed *via* computational methods for understanding and quantifying substituent effects demonstrates the utility of DFT calculations in this arena. Computational approaches facilitate dissection of substituent effects by removal of functional groups or other energy partitioning methods. Thus, they have allowed the separation of inductive and field effects and provided evidence of the dominance of through-space substituent effects in non-covalent interactions as varied as anion-π and

π-π interactions. However, such theoretical manipulations often do not have an experimentally viable equivalent, for example hydrogen-capped substituents, meaning that it remains challenging to effectively separate through-bond and through-space influences *via* empirical measurements.[9, 14, 64-65]

1.4 Through-Space *vs.* Through-Bond Substituent Effects

The growing number of computational examples that show the dominance of through-space substituent effects has led to numerous experimental and *in silico* studies that investigate the relative importance of through-bond and through-space effects including ionisation energies and reactivity. In particular, the local, direct interaction model posed by Wheeler and Houk has sparked a debate within the literature over whether it or the Hunter-Sanders model describes substituent effects in π-π stacking interactions.

1.4.1 Substituent Effects in π-Interactions: Investigating the Local, Direct Interaction Model

Traditionally, non-covalent interactions involving aromatic rings were considered to be dominated by electrostatic interactions with substituent effects arising from polarisation of the π-system.[56, 65-67] The Hunter-Sanders model is based on such a simple qualitative model.[66] According to this model, electron-withdrawing substituents are supposed to reduce electrostatic repulsion between a substituted and unsubstituted benzene heterodimer through withdrawal of π-electron density, thus promoting aromatic stacking with respect to the unsubstituted case. Conversely, electron-donating substituents enhance electrostatic repulsion through donation of π-electron density thereby weakening aromatic stacking compared to an unsubstituted benzene homodimer.[66] This model was called into question with a number of computational studies, even prior to Wheeler and Houk's work, which showed

substituted benzene dimers had stronger binding energies than the unsubstituted dimer, irrespective of whether the substituent was electron-withdrawing or donating.[68-71]

In 2003, Sherrill and Sinnokrot provided the first computational study to dispute the Hunter-Sanders model.[68] Modelling substituent effects on π-π stacking binding energies over various levels of theory showed that, regardless of whether the substituent was electron-donating or withdrawing, all substituents led to stronger binding energies than the unsubstituted benzene homodimer case. Through-space interactions, now enveloped by the local, direct interaction model, were not implicated in this observation so EDA analysis *via* SAPT was performed on the dimers to investigate the initial finding of the study.[68-69] From this analysis, the electrostatic component of binding was stabilising for all of the substituents examined, including electron-donating and withdrawing substituents. However, the dispersion and exchange-repulsion components contributed more to the total SAPT energy and were thus more important to the overall binding energy than the electrostatic component. The relative lack of importance of the electrostatic component of binding was confirmed *via* predictions of binding energies based upon the Hunter-Sanders model and that observed by ESP analysis which were not in line with one another. Thus, the EDA and ESP analysis both ran in direct contrast to the Hunter-Sanders model.[69] Sherrill and Sinnokrot confirmed these findings with high-level, benchmark-quality *ab initio* methods.[70] However, it should be cautioned that energetic effects such as repulsion and dispersion are cancelled in equilibrated experimental systems in solution.

Kim and co-workers performed high-level computational calculations to obtain arene-arene binding energies and also observed a stronger binding for substituted benzene dimers than for unsubstituted benzene dimers, regardless of the through-bond nature of the substituent.[71] They also found that dispersion was the most important component of the overall binding energy. However, these calculations showed that the relative importance of the components comprising the overall binding energy was dependent upon the relative geometry of the interacting pair as well as the relative energy of the pair and thus is governed by electrostatics. This is in line with the Kirkwood-Westheimer electrostatic model which predicts geometrical sensitivity of

through-space substituent effects.[11-12, 35-36, 38] Kim *et. al.* thus note that the dominance of electrostatics in π-π stacking interactions would imply that polar solvents would perturb such an interaction.[71]

The computational studies conducted by the groups of Sherrill and Kim have shown that stronger binding, with respect to the unsubstituted benzene homodimer, occurs upon substitution regardless of its through-bond nature, i.e. electron-donating or withdrawing.[68-71] This is the opposite of that predicted by the Hunter-Sanders polarisation model.[66] Empirical examination including molecular balances and regiochemical reaction outcomes have also contradicted this facet of the Hunter-Sanders model. Wheeler and Houk themselves performed an experimental investigation regarding substituent effects following their 2008 computational study that showed the lack of importance of substituent-induced π-polarisation of aryl rings in π-π stacking interactions.[62, 72] To test this hypothesis, stereo-selective Diels-Alder reactions were probed where stereo-selectivity was governed by π-π stacking interactions (**Figure 1.22**).[72]

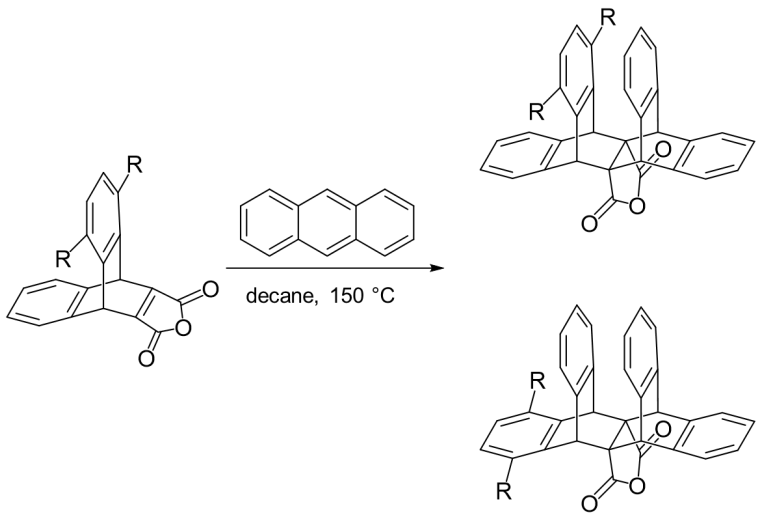

Figure 1.22: Stereo-selective Diels-Alder reaction investigated by Wheeler and Houk *et. al.*.[72]

π-Stacking interaction free energies were calculated using the distribution of products and provided high correlations with Hammett's σ_m constant. As σ_m is dominated by inductive substituent effects and not resonance, these free energies provide an

experimental confirmation of the lack of importance of changes to the π-system upon substitution causing changes to π-π stacking interactions.[66, 72]

Shimizu *et. al.* used *N*-phenylimidine molecular balances to test the experimental validity of the local, direct interaction model (**Figure 1.23**).[64, 73] Through the use of control compounds, the relative contributions to the overall folding energy of balance **A** could be dissected.

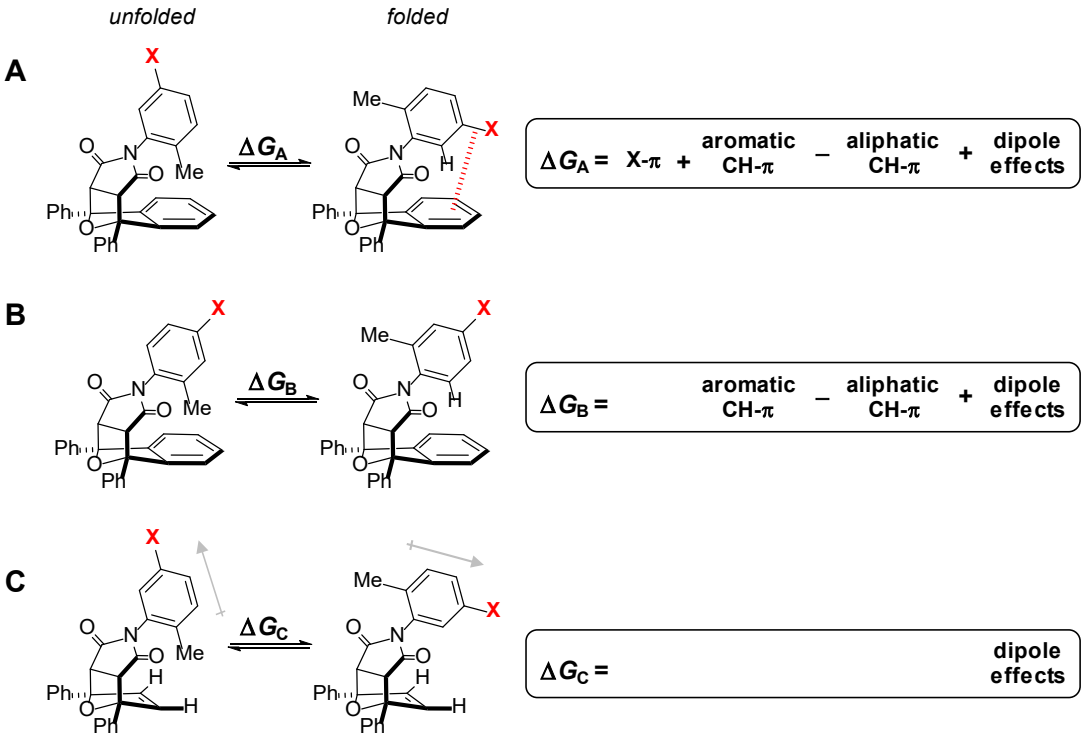

Figure 1.23: The series of molecular balances used by Shimizu and co-workers to dissect the contributions of **(A)** substituent-π, **(B)** CH-π (aromatic and aliphatic) and **(C)** dipole effects to the overall folding energy of molecular balance **A**.[64]

These components included the substituent-π (local, direct interaction model), aromatic CH-π and aliphatic CH-π interactions and dipole effects. In the folded conformer of the **A** balances, there are through-space interactions between the aromatic shelf of the *N*-phenylimidine molecular balances and the substituents. The folding free energies, as measured by ^{1}H NMR, for substituted balances **A** were all more negative compared to the X = H balance, meaning that they preferred the folded

conformer. Plotting the folding free energies against σ_m Hammett constants showed the importance of the relative interaction components in balances **A**. The determined energies correlated well with the electrostatic parameter, σ_m, and also showed great variance with it, indicated by the ρ gradient of –0.26 kcal mol^{-1}. However, balances **C** had a ρ gradient of +0.03 kcal mol^{-1} and this lack of variance over the eight substituents analysed means that the dipole effects, taken account of by this series of balances, had little effect on the folding free energy of balances **A**. Balances **B** also showed little variance with σ_m, with a gradient of ρ –0.02 kcal mol^{-1}, meaning that the CH-π interactions did not contribute significantly to the folding free energy of balances **A**. With the folding free energy shown to be dominated by substituent-π interactions, whether dispersion/polarisability was important was determined through correlation of ΔG_A with substituent molar refractivity (MR). This plot was a scatter, showing the lack of importance of dispersion/polarisability which was bolstered by computational modelling of the balances to obtain space-filling models that showed no direct contact between the substituents and aromatic shelf. Therefore, this study provided experimental support for Wheeler and Houk's local, direct interaction model of substituent-π interactions.[3-4, 54, 64]

Diederich and co-workers used Trögers base derived molecular balances to investigate substituent effects in edge-to-face aromatic interactions (**Figure 1.24**).[74]

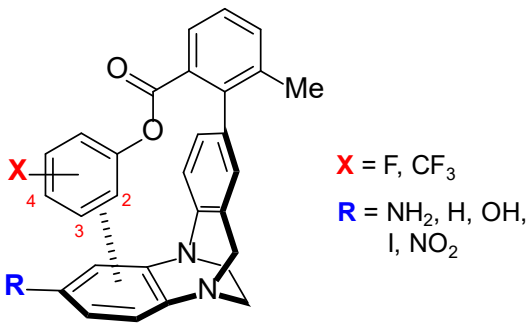

Figure 1.24: Diederich *et. al.*'s Trögers base derived molecular torsion balances where the X substituent is in the 4, 3 or 2 position. For each position of X, there is a series of R substitutions.[74]

The X substituent was in the 2, 3 or 4 position, giving rise to three subsets of

compounds for each X substituent. For each subset, there were five R substituents investigated. The slope of the best fit lines for the correlation between the folding free energies, ΔG_{fold}, of each balance subset against the σ_m Hammett constants of the R groups was steepest for both X = F and CF_3 in the 4 position. Thus, the folding free energy of these balances was more sensitive to the electronic properties of the arene. The slope also indicated that the folded conformer, where the X···arene interaction present, becomes more favourable as the R substituent becomes more electron donating. This is in line with that predicted by the local, direct interaction model.[3-4, 54, 74]

The thermodynamics of the folding of these balances was probed by van't Hoff analysis *via* variable-temperature NMR (VT-NMR) spectroscopy. For the 4-position X-substituted balances, the folding enthalpy was more favourable for electron- donating substituents while the entropy became more unfavourable. Thus, the overall result is a small energetic contribution to the overall ΔG_{fold}. In contrast, the folding enthalpy and entropies for the balances bearing X in the 2 or 3 position were not sensitive to the electronic properties of the arene. This result supports the assessment that the balance with the X-substituent in the 4 position was the result of a local, direct interaction between the substituent and arene as postulated by Wheeler and Houk.[3-4, 54, 74]

Diederich *et. al.* investigated distance dependence of substituent effects in parallel displaced π-π dimers by employing a host-guest system with a 2,6-di(isobutryamido)pyridine ligand and Rebek imide type receptor (**Figure 1.25**).[67, 75]

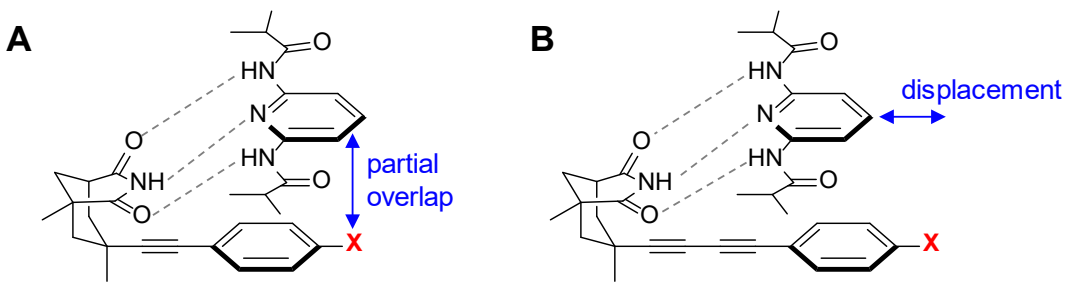

Figure 1.25: Host-guest system used by Diederich *et. al.* to investigate distance dependence of substituent effects in parallel displaced π-π stacked dimers. **(A)** Complex with a partial

overlap between the *para* substituent of the aryl ring of the receptor and the pyridine ligand.[75] **(B)** The same complex as in **A** but with an increased displacement between the pyridine ligand and *para* substituent due to elongation of the acetylene linker by one unit.[67, 75]

The *para* substituents of the phenyl ring linked *via* acetylene to the Rebek-imide receptor partially overlap the 2,6-di(isobutryamido)pyridine ligand with a distance of 3.3 Å between them when complexed together (**Figure 1.25A**). The binding constants, K_a, of these complexes were independent of the electronic nature of the X substituent as shown by the lack of correlation with σ_p. Thus, X-substitution led to more stable complexes than the X = H complex regardless of whether X was electron-donating or withdrawing. This finding is concurrent with that predicted by Wheeler and Houk's local, direct interaction model.[3-4, 54, 67, 75]

To understand the distance dependence of the local, direct interaction observed for the complex in **Figure 1.25A**, the linker between the Rebek-imide body and X-substituted phenyl ring was lengthened by one acetylene unit (**Figure 1.25B**).[67] This resulted in an elongation of the displacement between 2,6-di(isobutryamido)pyridine and the phenyl unit of the Rebek-imide receptor. Crystal structure analysis showed that the distance between the X substituent and the phenyl ring was 3.6 Å which is too long for a local, direct interaction between the X substituent and pyridine ring. Thus, a strong correlation was observed between the binding constant, K_a, and the Hammett σ_p constant meaning that it was the polarisation of the phenyl ring that dictated the binding strength of these complexes and the Hunter-Sanders model prevails.[66-67] Thus, these two complexes show that the distance between the stacking pair changes the dominant model of substituent effects in π-π stacking.[67, 75] This experimental finding is in line with experimental predictions on substituent effects on parallel displaced dimers by Sherrill and co-workers.[67, 76]

Another aspect of the Hunter-Sanders model and the local, direct interaction model that run concurrent to one another is the influence of multiple substituents on the overall substituent effects in aryl dimers. The Hunter-Sanders, π-polarisation model predicts that the largest substituent effect on stacking interactions occurs upon initial substitution, with successive substituents having a minimal and in equal influence on binding energies. This is due to the build-up of charge on the aromatic ring caused by

multiple substitution resulting in the aromatic ring becoming more difficult to polarise.[77] In contrast, the local, direct interaction model predicts an additivity of substituent effects. Experimental and computational studies showed substituent effects on π–π stacking interactions to be additive.[3, 70, 77-79]

Siegel, Cozzi and co-workers assessed the incremental change to the interaction energy of aryl dimers upon addition of fluorine to one of the interacting arenes, with the other remaining unsubstituted and thus relatively electron rich.[70] The model system for this study was 1,8-diarylnaphthalene derivatives, where the π-π stacking between the aryl groups is enforced due to the geometry of the compound but where the rings are able to rotate (**Figure 1.26**). Thus, the interaction energy strength between the two rings is indirectly measured from the rotational barrier as determined by ^{1}H and ^{19}F NMR spectroscopy.[79]

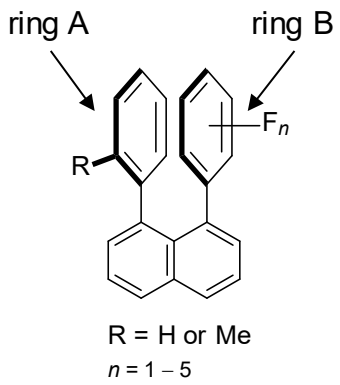

Figure 1.26: The 1,8-diarylnaphthalene derivatives that showed additivity of the effect of the fluorine substituent to the rotational barrier and thus the interaction energy between the two aryl rings.[79]

The rotational barrier was found to decrease upon the successive addition of fluorine to ring B (**Figure 1.26**). This means that the electrostatic repulsion between the aryl rings is decreased as the number of fluorines on ring B is increased; a finding in line with what would be expected based upon the through-bond electron-withdrawing nature of fluorine. The decrease in the rotational barrier was additive, with a decrease of roughly 0.5 kcal mol^{-1} per fluorine atom.[79] This is in contrast to that predicted by the π–polarisation, Hunter-Sanders model.[77]

The additivity of the substituent effects on π-π stacking interactions shown by Siegel, Cozzi and co-workers study of 1,8-diarylnaphthalene derivatives was probed by Shimizu *et. al.* using a molecular balance system.[56, 65, 70, 77, 80] The bicyclic *N*-arylimide molecular balances contained parallel displaced dimers where the stacking interaction was only present in the folded conformation (**Figure 1.27**).[77]

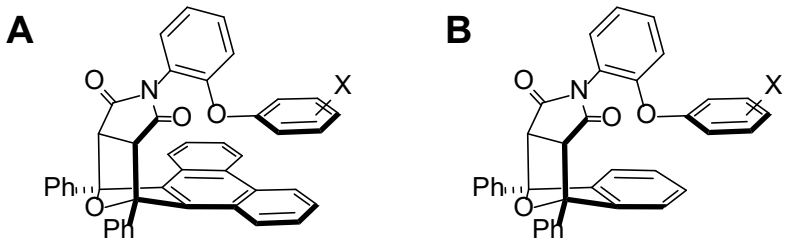

$$SE_{exp} = (\Delta G_{A,X} - \Delta G_{B,X}) - (\Delta G_{A,X=H} - \Delta G_{B,X=H})$$

Figure 1.27: The *N*-arylimide molecular balances studied by Shimizu *et. al.* to assess additivity of substituent effects in π-π interactions. **(A)** The balance series where an interaction between the X substituent and an arene is possible. **(B)** Control balance series where this interaction is not possible. The folded conformation of each balance is shown.[77]

The folding free energy, Δ*G*, of the molecular balances was obtained through ^{1}H NMR and the π-π interaction energies could be ascertained through comparison of the Δ*G* values of series A (**Figure 1.27A**) and control series B (**Figure 1.27B**) *via* the relation shown in **Figure 1.27** to give the substituent effect (SE) parameter, SE_{exp}. The SE_{exp} values of the mono-substituted balances were used to predict the substituent effect for the multi-substituted balances studied, SE_{pred}, *via* an additive model. These SE_{pred} values were shown to have good predictive power when compared to the SE_{exp} values of the multi-substituted balances across a spectrum of electron-donating and electron-withdrawing substituents. For example, the SE_{pred} value for X = Me was –0.37 compared to the experimentally observed value of SE_{exp} = –0.35. The ability to predict the experimental interaction energies of multi-substituted balances *via* an additive model based on the mono-substituted derivatives shows that the substituent effects in the parallel displaced π-π stacking interactions were additive.[77]

Further to this rather simplistic model, Shimizu and co-workers derived a predictive parameter based on a more involved consideration of the experimental data. The SE_{model} parameter was assigned to each of the nine substituents investigated and was obtained from experimental data of both the mono- and multi-substituted balances through multi-variant analysis. The correlation between SE_{model} and SE_{exp} was excellent, with the R^2 and gradient of best fit value being > 0.98. This high quality correlation confirms the additivity of substituent effects observed in the prior, more simple, model and shows that this analysis allows for the prediction of substituent effects of a mono-substituted balance with substituents that were not part of the original nine of this study.[77]

While this result seems to overturn the Hunter-Sanders π-polarisation model, Shimizu *et. al.* sought to test the relative importance of this model and the local, direct interaction model through ESP analysis. The ESP values of substituted benzene derivatives with the number of substituents ranging from zero to six and including both electron-donating and withdrawing substituents were compared with those predicted by an additive model. The computed ESP values of each set of derivatives initially were in line with those predicted by the additive model, but increasingly deviated from the predicted value as the number of substituents increased beyond three. The maximum number of substituents in the experimental study was three, meaning it was within the range where the Hunter-Sanders model could explain the experimental results of substituent effect additivity. However, the authors note that even though the local, direct interaction model was developed in relation to parallel benzene dimers, instances of the applicability of this model to parallel displaced dimers exist.[67, 75] Additionally, the *meta* mono-substituted balances, where the substituent is closer to the aromatic shelf with which there is a stacking interaction, had larger substituent effects on the folding free energies compared to their *para* mono-substituted counterparts. This positional dependence of the magnitude of the substituent effect is in line with a direct, through-space interaction between the substituent and interacting partner as predicted by the local, direct interaction model.[3-4, 54, 77]

Sinnokrot and Sherrill computed interaction energies of parallel heterodimers between unsubstituted benzene and increasingly multiply substituted benzene derivatives.[70, 78]

A range of substituents were examined, from electron-donating to electron-withdrawing and the interaction energies of all substituted heterodimers were stronger than that of the unsubstituted homodimers (irrespective of whether the substituents were EDGs or EWGs), in line with Sherrill and co-workers previous observations.[68-69] Further, the interaction energy upon successive substitution increased by the same amount as that of the first substitution from unsubstituted benzene and this additivity persisted to the hexa-substituted heterodimers. The gradient of the best fit line of the plot between the number of substituents and interaction energy gives the average change to the interaction energy per single substitution.[70, 78] Interestingly, this value for fluorine was very close to that determined experimentally by Siegel and co-workers at 0.6 kcal mol^{-1} compared to 0.5 kcal mol^{-1}.[70, 78-79] This study was the purely computational counterpart to Shimizu and co-workers experimental study and came to the same conclusion; that substituent effects in π-π stacking interactions were additive.[70, 77-78] In a 2011 study by Wheeler and Houk, the additivity of substituent effects in π–π stacking interactions came to the same conclusion as the study Sherrill and co-workers but at a higher level of theory.[3, 78]

Thus, there is a compelling wealth of computational and experimental analyses that point to the additivity of substituent effects in π-π stacking interactions, contradicting the Hunter-Sanders model and providing evidence of the local, direct interaction model.[64, 66-72, 74-75, 77-79]

Outside of the competing models for substituent effects on π-π interactions by Hunter-Sanders and Wheeler-Houk, the experimental dominance of through-space effects in π-π stacking interactions was shown as early as 1992. This seminal empirical study, performed by Siegel and co-workers, focussed on the rotational barrier, $\Delta G^{\ddagger}$, of the aryl groups in 1,8-diarylnaphthalenes measured by ^{1}H NMR (**Figure 1.28**).[81]

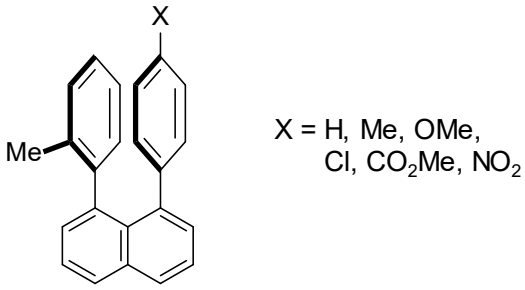

Figure 1.28: 1,8-Diarylnaphthalenes with through-space "polar-π" interactions between the stacked arenes studied by Siegel and co-workers.[81]

The rotational barrier free energies, $\Delta G^{\ddagger}$, gave a linear correlation with σ_p Hammett constants. This correlation showed that the barrier increased on substitution from electron-withdrawing to electron-donating substituents. This contradicts the predictions of behaviour based on resonance or charge-transfer being responsible for the effect of the substituents on the barrier to rotation. Conjugation effects would lead to substitution, regardless whether electron-withdrawing (nitro) or donating (methoxy) in nature, causing lower rotational barriers than the unsubstituted case due to the enhancement in conjugation between the two rings by these substituents (nitro and methoxy) relative to hydrogen. Charge-transfer, on the other hand, predicts the unsubstituted case would have a higher rotational barrier than both nitro and methoxy substituted derivatives. The through-space prediction, based on a dominance of electrostatic interactions for such an interaction, fits the experimental observations where electron-deficient arenes (those bearing electron-withdrawing substituents) would reduce repulsion between the stacked arenes and thus lower the barrier to rotation. Thus, Siegel and co-workers termed this as a through-space "polar-π" effect.[81]

In 1993, Siegel sought to further understand the nature of the interaction between the enforced stacked arene dimers of their 1,8-diarylnaphthalenes, this time with both arenes substituted in the *para*-position (**Figure 1.29**).[82]

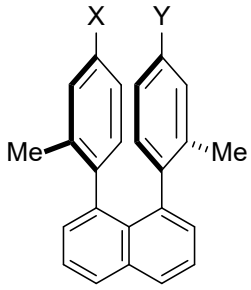

Figure 1.29: 1,8-Diarylnaphthalenes with substitution on both arenes to investigate the through-space "polar-π" effect uncovered in Siegel and co-workers 1992 study.[82]

Both arenes being substituted allowed assessment of the competition between charge-transfer and the through-space "polar-π" interactions. Electrostatic, through-space polar-π interactions would result in stronger binding between stacked dimers of arenes that are both electron deficient due to the reduction in Columbic repulsion and therefore weaker binding between two electron-rich arenes. However, if charge-transfer interactions are dominant, then the strongest binding would be observed between arenes of opposite polarity, i.e. one was substituted with an electron-donating and the other with and electron-withdrawing substituent.[82]

The binding strength was assessed indirectly through NMR measurements to give a rotational barrier, $\Delta G^{\ddagger}$. This gave a strong correlation with the sum of the Hammett σ_p constants meaning that the highest rotational barrier, and thus the strongest binding energy, was between two electron-deficient arenes. Thus, it was through-space polar-π interactions that dominated the stacking interaction, confirming the findings of the 1992 study.[81-82] Additionally, this finding overturns another prediction of the Hunter-Sanders model wherein substituent effects on binding energies between monosubstituted aryl homodimers (i.e. $C_6H_5X\cdots C_6H_5X$) should repel one another whereas monosubstituted aryl heterodimers (i.e. $C_6H_5X\cdots C_6H_5Y$) should have strong binding interactions.[3]

Further to their study into parallel stacked dimers, Siegel and co-workers investigated the importance of through-space polar-π interactions on parallel displaced dimers (**Figure 1.30A**) using the model compound shown in **Figure 1.30B**/**C**.[83]

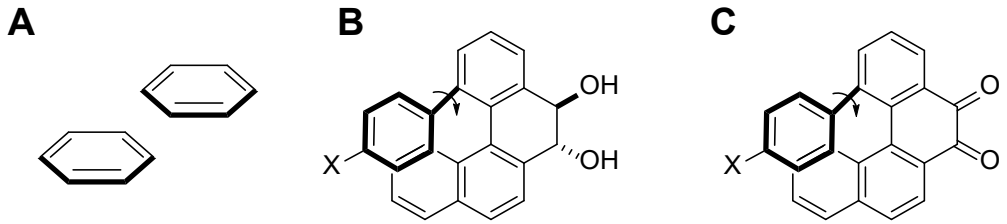

Figure 1.30: Model compound used to assess the nature of the interaction between parallel displaced arene dimers by Siegel and co-workers. The barrier to rotation is measured around the bond indicated.[83]

The free energy of rotation, $\Delta G^{\ddagger}$, around the aryl-aryl bond highlighted in **Figure 1.30B** and **C** was calculated by VT-NMR and resulted in a strong, linear relationship with the Hammett σ_p constant. As this was the same relationship between the binding energy, indirectly probed by $\Delta G^{\ddagger}$, for the parallel stacked dimers of the 1992 and 1993 studies, it was concluded that the same through-space polar-π interaction governed the binding between parallel displaced dimers. As a result of their studies into the through-space polar-π effect on arene dimers, Siegel *et. al.* conclude that this through-space effect is how these substituent effects interactions should be understood and predicted.[83]

Substituent effects on π-π interactions have been the subject of extensive experimental and computational studies, with two competing models to describe their behaviour being debated. The main facets of the Hunter-Sanders model, dominated by through-bond substituent effects have been experimentally and computationally countered and instead given evidence to support the local, direct interaction model which are based on dominant through-space substituent effects. Thus, these studies point to through-space substituent effects governing π-π interactions, in addition to their predicted dominance in π-ion interactions based on computational analyses.[4, 6, 15, 54, 58-59] It is worth noting that the studies by Diederich and Shimizu showed a distance dependence to the predominant model that describes substituent effects on π-π interactions.[67, 75, 77] This is unsurprising owing to the intrinsic geometrical dependence of through-space substituent effects.[11-12, 35-36, 38] However, based on the studies discussed in this section, that substituent effects on π-π interactions can broadly be understood using through-space effects in all examples.

1.4.2 Through-Space Effects on Reactivity

Lectka and co-workers performed two studies where through-space effects were able to override through-bond substituent effects on reactivity.[84-85] Through-space OH···arene interactions were shown to activate electron-deficient rings towards electrophilic aromatic substitution in the presence of comparatively electron-rich rings (**Figure 1.31**).[84]

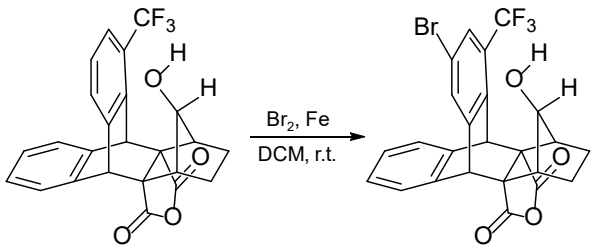

Figure 1.31: Switchable through-space OH···arene/HO···arene activation shown to govern reactivity and selectivity in electrophilic aromatic substitution reactions.[84]

The hydroxyl group allowed switching of its through-space effect on the reactivity and selectivity of electrophilic aromatic substitutions. OH···arene interactions deactivate the arene rings making them less susceptible to electrophilic aromatic substitution and *vice versa* for HO···arene interactions. It was found that OH···arene interactions were switched to HO···arene when the arene was substituted with electron-withdrawing substituents and it is this through-space interaction that led to subsequent activation of this deactivated ring. HO···arene interactions with an arene furnished with a trifluoromethyl substituent in the presence of an unsubstituted ring resulted in the deactivated arene preferentially undergoing mono-bromination under electrophilic aromatic substitution conditions.[84]

Electrophilic aromatic substitution reactions were at the centre of another study which showed arene activation by through-space F···arene interactions (**Figure 1.32**).[85]

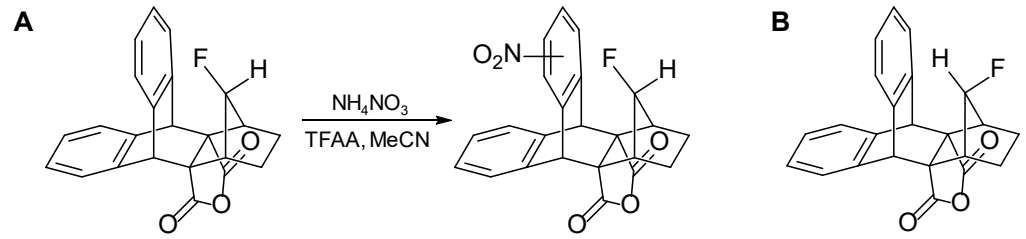

Figure 1.32: Arene activation towards electrophilic aromatic substitution reactions by through-space fluorine interactions. **(A)** Nitration exclusively upon the ring involved in a F···arene through-space interaction. **(B)** Control compound with no F···arene interaction possible.[85]

Fluorine substituents result in deactivation of the benzene ring due to its electron-withdrawing through-bond nature. However, the through-space effect of fluorine results in activation of the ring towards electrophilic aromatic substitution with a rate a factor of 1500 times faster than that of a control compound where an F···arene interaction is not possible (**Figure 1.32B**). As well as activation, this through-space interaction also served to direct the regiochemistry of electrophilic aromatic substitution, with nitration occurring exclusively upon the arene ring involved in the F···arene through-space interaction (**Figure 1.32A**). Thus, this study shows that the through-space interaction compliments the through-bond nature of fluorine and through-space interactions can govern chemical reactivity.[85]

1.4.3 Through-Space Effects on Ionisation Constants

Siegel sought to determine whether through-space effects of substituents have a significant effect on the behaviour of functional groups in molecular recognition processes. As such, a group of 2,6-*bis*(*p*-X-phenyl)benzoic acids was devised and the substituents varied to assess how the field effect of the substituent can affect the ionisation constant of a carboxylic acid (**Figure 1.33**).[86]

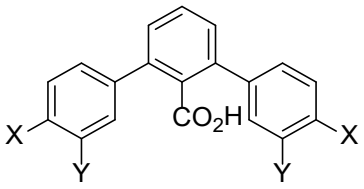

Figure 1.33: 2,6-*bis*(*p*-X-phenyl)benzoic acid derivatives used to assess whether the field effect of the substituents in the X position can affect the behaviour of the central functional group by measuring the pK_a of the carboxylic acid.[86]

The effect of the substituents on the properties of the carboxylic acid was measured by charting the change in the pK_a of the acid as the substituents are varied. Substituents in the Y position yielded the same effect on the pK_a values are those in the X position. Thus, as well as the X-substituted compounds correlating well in a plot of pK_a against σ_p, the pK_a values of the Y-substituted derivatives were correlated with σ_p. Interestingly, despite the ability of σ_p to describe the experimental findings, resonance substituent effects were ruled out due to the lack of conjugation between the flanking rings and the central, acid substituted ring. These two findings are consistent with the substituent effects on the acidity of the carboxylic acid being through-space in nature.[86]

More recently, Mecinović and co-workers investigated through-space substituent effects by measuring the ionisations constants of a number of substituted 2,6-diaryl systems (**Figure 1.34**) akin to that used by Siegel (**Figure 1.33**).[87]

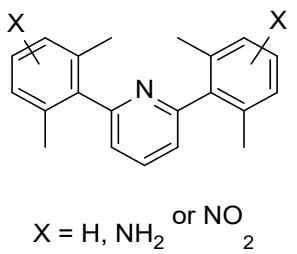

Figure 1.34: System used to investigate through-space effects of substituents in a 2,6-diaryl system used by Mecinović and co-workers (**18**).[87]

Mecinović and co-workers investigated the through-space polar-π interactions between the pyridine moiety and the 2,6-diaryl rings of substituted 2,6-diarylpyridine compounds by measuring the change in pK_a value as the substituent is varied. It was

found that the pK_a of both *meta* and *para* methoxy substituted diaryl systems were almost identical, despite the difference in the σ values of the methoxy substituent in the *meta* and *para* positions. Importantly, it was found that electron rich π systems (those with electron donating substituents, X = NH_2) led to an increase in the basicity of the pyridine with respect to the electron poor π systems (those with electron withdrawing substituents, X = NO_2). This effect was attributed to through-space polar-π interactions between the pyridine reaction centre and the substituted aryl rings.[87]

A similar study was performed on 2,6-diarylphenols (**Figure 1.35**) where the pK_a of phenol was monitored as the nature of its through-space OH···arene / HO···arene interaction was changed through substitution of the flanking arenes.[88] Being of the same structural design as the systems at the heart of Siegel and Mecinović, resonance effects in the present are minimal.[86-87]

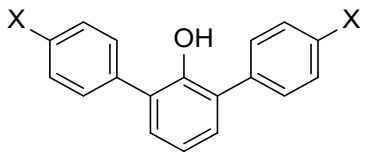

X = H, OMe, Me, F, CF_3

Figure 1.35: 2,6-Diarylphenols used to assess the through-space effect of the flanking arenes to the phenol pK_a.[88]

A strong linear correlation between the experimental pK_a values and σ_p Hammett constants indicated that the electron-rich rings (those with electron-donating groups) led to a higher pK_a due to the stability afforded to the hydroxyl group by through-space interactions with the substituted arenes and *vice versa* for electron-withdrawing X-substituents. Further to this experimental display of through-space stabilisation of the phenolic anion, computationally derived proton affinity energies (ΔE^{PA}) were investigated. These values also produced excellent correlations with σ_p Hammett constants showing the through-space influence on the pK_a's of the 2,6-diarylphenols. Thus, the through-space polar-π interactions between the hydroxyl group and *para*

substituted flanking arenes influence the pK_a of the hydroxyl groups of 2,6-diarylphenols.[88]

Given that through-space interactions dominated the pK_a's of 2,6-diarylphenols and pyridines, Mecinović *et. al.* analysed the through-space interactions using the same skeleton but turned their attention to the ionisation energies of amine groups (**Figure 1.36**).[89]

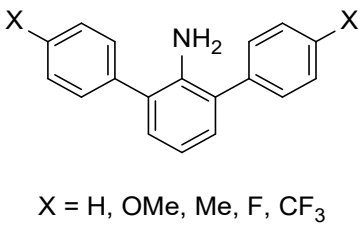

Figure 1.36: 2,6-Diarylanilines with the flanking arenes substituted in the *para* position.[89]

The pK_a of the aniline group was affected by substitution upon the flanking arene groups and formed a strong linear correlation with Hammett σ_p constants. As observed with this scaffold in prior studies, the arene rings are not planar, meaning that resonant effects from the X-substituent are not able to confer an electronic substituent effect to the aniline *via* through-bond effects.[86-88] Thus, Mecinović attributed this correlation to through-space stabilisation of the ammonium cation formed upon protonation by electron-rich arenes and *vice versa* with electron-deficient arenes. Computational EDA gave further evidence of this through-space interaction by showing that it is indeed an electrostatic interaction between the arene and aniline and not an orbital interaction between the interacting pair.[89]

Experimental ionisation constants of three different functional groups were shown to be primarily influenced by through-space substituent effects, with computational analysis providing extra evidence to these findings. This facet of the properties of organic molecules is important in biological systems as well as in synthetic organic chemistry. Mecinović and co-workers highlight, for each of their studies, that the through-space interactions are between groups that are biologically relevant; cation-π and OH-π are present in protein interactions and pyridines are found in drug

molecules.[87-89] Thus, it could be that these interactions in biology are supported by through-space interactions.

1.5 Field Effects in Nature and Synthesis

Through-space substituent effects, arising from substituent induced changes in the local field, have been suggested to be of importance in nature due to the long-range electrostatic communication they afford. In particular, these effects have been implicated in enzyme function. Warshel and co-workers suggest that the predominant effect in the catalytic function of enzymes is the electrostatic, i.e. through-space, effect of substituents organising substrates in protein enzymatic pockets and stabilising transitions state structures within the active site.[90-92] For example, it is theorised that the polar N–H bonds within the Gln360, Gly359 and Leu358 residues in the P450 enzyme exert an electrostatic field mediated influence on the enzyme substrate to control the specificity of the active site.[91] Experimental evidence of such electrostatic dominance in enzymatic action was provided in the form of Stark spectrometry. These experiments measure the electric field experienced by a substrate when bound within an enzyme active site by applying an external electric field to the immobilised species of interest. Stark spectrometric measurements of the ketosteroid isomerase active site showed that 72% of the total rate acceleration was attributed to electric field catalysis.[93]

As well as allowing the measurement of electrostatic fields *via* the Stark effect, externally applied electric fields (EEFs) have been shown to influence chemical reactivity, giving access to control over the regiochemical outcome of Diels-Alder reactions taking place on immobilised substrates and activity in anion-π catalysis.[92, 94-95]

Shaik and co-workers have shown that externally applied electric fields can aid in bond breakage when they are orientated along bond axes by stabilising an ionic form of a covalent bond (**Figure 1.37**). The ionic structure that is stabilised is the structure which

opposes the polarity of the EEF, allowing selectivity in the direction of the dipole formed upon application of an EEF.[92, 94]

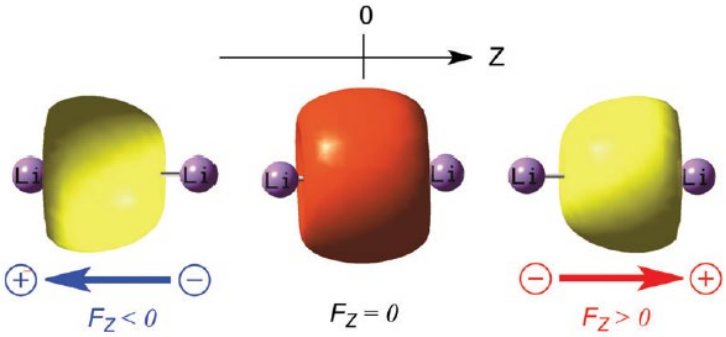

Figure 1.37: Effect of an orientated EEF (F_Z) on the charge distribution and dipole moments of an Li-Li bond. Image taken from the 2018 *Chem. Soc. Rev.* Tutorial Review by Shaik and co-workers.[92, 94]

Catalysis occurs when the EEF is orientated along the axis in the transition state where product bonds are formed, and reactant bonds are broken (this is also termed the "reaction axis"). On the flip side, one may inhibit a reaction by applying the opposite polarity to the reaction axis. Such regiochemical control is illustrated by the theoretical use of an orientated EEF to control whether hydroxylation or epoxidation occurs between propene and an active species of the enzyme P450 (**Figure 1.38**).[92, 94, 96]

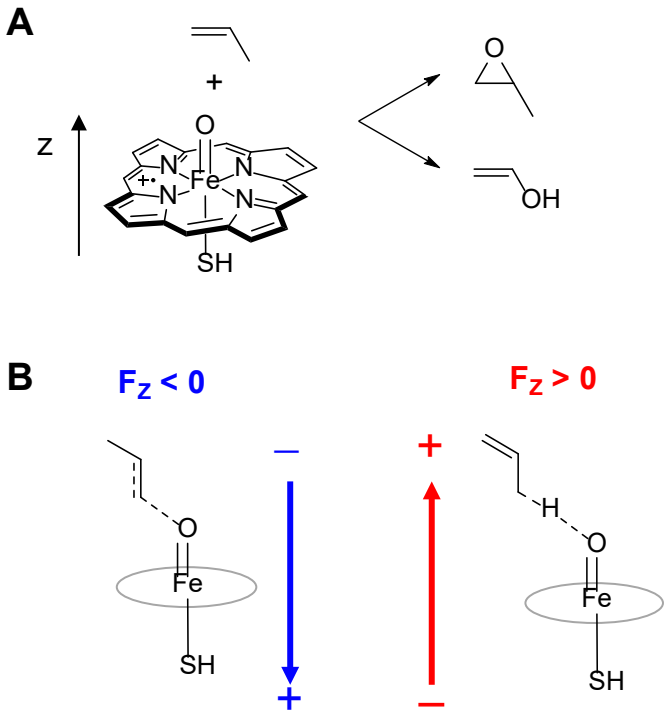

Figure 1.38: The effect of an EEF orientated along the z axis (F_Z) on the regiochemical outcome of the reaction between propene and a P450 active species. **(A)** Propene and an iron-oxo Por radical cation which acts as a model for the enzyme active species in P450. **(B)** The preferred mechanism when the applied EEF (F_Z) is negative and positive. In particular, F_Z is the EEF orientated along the z axis. Note, the dipole moment effected by F_Z will oppose its direction.[92, 94, 96]

As shown in **Figure 1.38**, regiochemical control is obtained by applying the orientated EEF along the O–Fe–S bond axis where negative EEFs prefer epoxidation but positive EEFs result in hydroxylation.[92, 94, 96]

The ability of orientated EEFs to catalyse chemical transformations has been evaluated through empirical single molecule cycloadditions between immobilised substrates and have shown the power of orientated EEFs in catalysing such transformations in a selective manner, thus serving as a proof of principle.[97-98] In addition, Matile and co-workers have shown enhanced anion-π catalysis through the use of an EEF, with the rate of enolate addition increasing 100-fold.[95] Such empirical confirmation of the theoretical predictions of the utility of EEFs in catalysis points to an exciting new era of catalysis in organic synthesis and how influential field effects can be on chemical reactivity. However, the challenge of making this process accessible to the general

chemist remains due to the requirement of orientation of the EEF with respect to the substrate which enforces substrate immobilisation.[92]

Further, stereo-selectivity can be achieved with EEFs through removal of forbidden-orbital mixing, which is performed by positioning the EEF off the reaction axis. This is exemplified by the theoretical display of orientated EEF *endo/exo* selectivity within Diels-Alder reactions. Computational studies by Shaik *et. al.* have pointed to the ability of orientated EEFs to confer *endo*/*exo* selectivity in the Diels-Alder cycloaddition between cyclopentadiene and maleic anhydride.[92, 94, 99] These examples show that the EEF method of controlling the electronic properties of a molecule to exert control over chemical transformations offers an elegant and more predictable approach to the traditional use of substituents.

Recently, Cockroft and co-workers have shown the effects of EEFs on molecular recognition events at the single-molecule level through nanopore analysis.[100] For all of the six supramolecular cages investigated (**Figure 1.39**), the association kinetics between the analyte and protein nanopore were governed by the EEF and thus were uniform across the data set. However, the dissociation kinetics were governed either by applied or local electrostatic forces meaning that it was different for each cage.

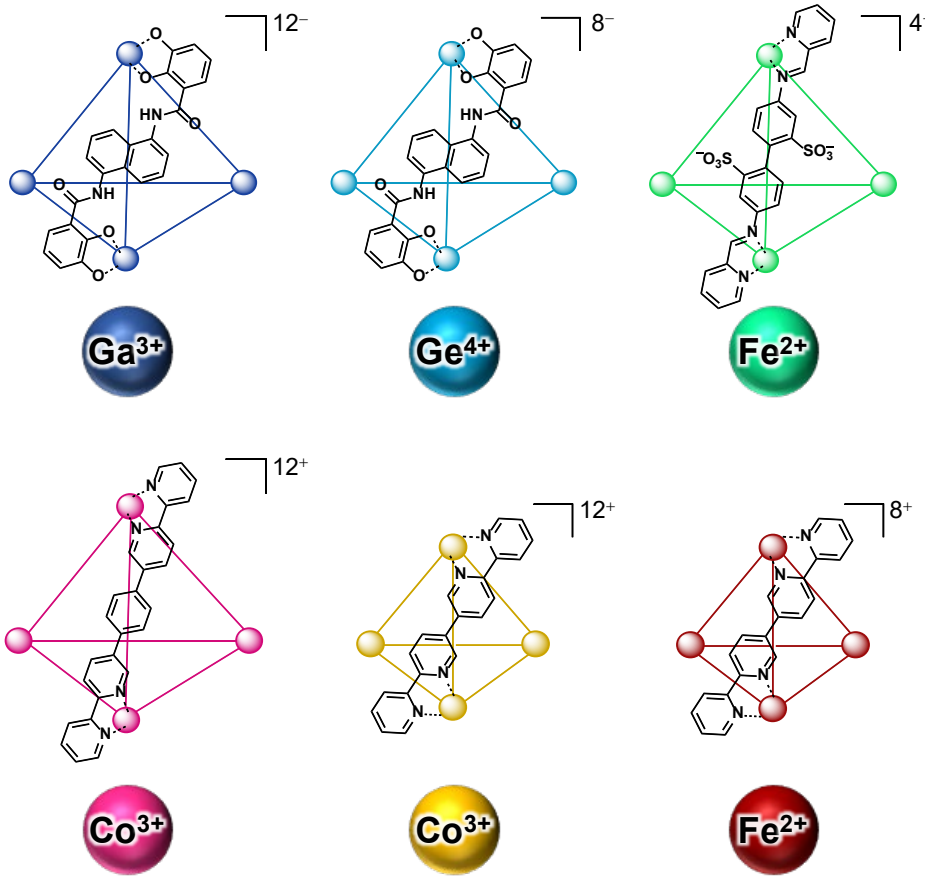

Figure 1.39: The six cages investigated by Cockroft *et. al. via* protein nanopore analysis. Image slightly modified from that in the 2019 *Chem.* Article.[100]

Exploiting the difference in behaviour induced by the EEF, Cockroft *et. al.* were able to select a specific cage to bind with the nanopore in the presence of a large excess of another cage through modulation of the EEF voltage. This result points to the possibility of control over molecular recognition events using EEFs.[100]

The emerging work on EEFs highlight the utility of fully understanding the origin of the electronic effect on chemical reactivity. EEFs are not complicated by the mixture of through-bond and through-space effects which are difficult to rationalise and predict for substituents. Thus, greater understanding of through-space substituent effects would allow finer tuning of the phenomena to which they are key.

1.6 Conclusions and Remarks

Numerous empirical and theoretical studies over the past 90 years have focussed on understanding and quantifying substituent effects on organic molecules. Despite the wealth of such studies, there remains a lack of a unified theory on the transmission of substituent effects. The empirical challenges associated separating inductive and field substituent effects have limited the ability of synthetic chemists to understand the relative importance of the contributions of these facets to substituent effects. Thus, a solid and consistent framework for the interpretation and prediction of substituent effects remains unfulfilled. That there has been such extensive effort afforded to obtaining a universally applicable substituent constant demonstrates how challenging, but ultimately important such quantification is.

In seeking a universal quantification of substituent effects, the dominance of through-space over through-bond effects emerged. Through-space effects have dominated substituent effects on π-π and π-ion non-covalent interactions, ionisation constants, empirical regiochemistry and reaction rates. However, a solid predictive theoretical framework for how through-space substituent effects modulate chemical reactivity and interaction energies is yet to be determined.

Since the 1980s, computational techniques, including the isolated molecule and additive models as well as energetic decomposition analysis, have been employed to fill the void in our understanding left by the difficulties faced in dissecting through-bond and through-space effects experimentally. A handful of these studies have enabled substituent effect quantification through the use of both ESP values and computed interaction energies.

The prevailing view of most organic chemists is that through-bond substituent effects dominate chemical reactivity. However, the literature presented within this review highlights the overlooked importance of the through-space component of substituent effects. It follows that understanding the modes of transmission of substituent effects on organic molecules could help improve the applicability and universality of their quantification and thus, studies aiming to provide a constant to understand and predict

substituent effects should incorporate both through-bond and through-space effects in their analyses.

1.7 Thesis Aims and Outlook

This review has demonstrated the importance of substituent effect quantification to the chemists seeking to understand and predict reaction rates and interaction strengths. While there is a tendency to assume that substituent effects are dominated by through-bond effects, there exists a wealth of examples where through-space substituent effects dominate experimental and computational observables. The work presented in this thesis seeks to study substituent effects on chemical equilibria, reaction rates and hydrogen bonding strength using combined experimental and computational analysis. To achieve this, model systems were designed to probe a specific aspect of substituent effects on organic molecules.

Quantification of through-space substituent effects is probed in **Chapter 2** using molecular balances to measure such effects on chemical equilibria, and to transpose these effects onto the familiar Hammett substituent effect scale. A major limitation of substituent effect quantification to date has been the lack of appreciation for through-space substituent effects which is aimed to be remedied in **Chapter 2** through the combined experimental and computational approach that permeates the work in this thesis. The through-space substituent effects observed in **Chapter 2** are further assessed *via* a solvation model applied to experimental data obtained in a range of solvents.

For a substituent constant to be useful, it must aid in the prediction of substituent effects in other systems. Thus, the transferability of the constants derived in **Chapter 2** will be tested against the reaction rates of an orthogonal set of pyridine compounds in **Chapter 3**. The same experimental and theoretical analysis employed in **Chapters 2** and **3** is applied to the assessment of the nature of weak hydrogen bonding interactions.

As non-covalent interactions, and the processes they govern, are of key importance to many biological and chemical processes, a deeper understanding of both the underlying mechanisms by which substituent effects operate and the "hydrogen bonding" interaction with non-classical acceptors is of interest to the wider academic, agrochemical and pharmaceutical industrial communities.

1.8 References

1. Mati, I. K.; Cockroft, S. L., Molecular balances for quantifying non-covalent interactions. *Chem. Soc. Rev.* **2010,** *39*, 4195 - 4205.

2. Mati, I. K.; Adam, C.; Cockroft, S. L., Seeing through solvent effects using molecular balances. *Chem. Sci.* **2013,** *4*, 3965 - 3972.

3. Wheeler, S. E., Local Nature of Substituent Effects in Stacking Interactions. *J. Am. Chem. Soc.* **2011,** *133*, 10262 - 10274.

4. Wheeler, S. E., Understanding Substituent Effects in Noncovalent Interactions Involving Aromatic Rings. *Acc. Chem. Res.* **2013,** *46* (4), 1029 - 1038.

5. Hunter, C. A., Quantifying Intermolecular Interactions: Guidelines for the Molecular Recognition Toolbox. *Angew. Chem. Int. Ed.* **2004,** *43* (40), 5310 - 5324.

6. Wheeler, S. E.; Houk, K. N., Are Anion/Pi Interactions Actually a Case of Simple Charge-Dipole Interactions? *J. Phys. Chem.* **2010,** *114* (33), 8658 - 8664.

7. Hansch, C.; Leo, A.; Taft, R. W., A survey of Hammett substituent constants and resonance and field parameters. *Chem. Rev.* **1991,** *91* (2), 165-95.

8. Ansyln, E. V.; Dougherty, D. A., *Modern Physical Organic Chemistry*. University Science Books: United States of America, 2006.

9. Roberts, J. D.; Moreland Jr, W. T., Electrical Effects of Substituent Groups in Saturated Systems. Reactivities of 2-substituted Bicyclo[2.2.2]octane-1-carboxylic Acids. *J. Am. Chem. Soc.* **1953,** *75* (9), 2167 - 2173.

10. Derick, C. G., Application of Polarity Measured in Terms of a Logarithmic Function of the Ionization Constant. III. Correlation of Chemical Structure with Ionization. *J. Am. Chem. Soc.* **1911,** *33* (7), 1181-1189.

11. Wilcox, C. F.; Leung, C., Transmission of substituent effects. Dominance of field effects. *J. Am. Chem. Soc.* **1968,** *90* (2), 336-341.

12. Stock, L. M., The origin of the inductive effect. *J. Chem. Ed* **1972,** *49* (6), 400.

13. Smith, M. B.; March, J., *March's Advanced Organic Chemistry: Reactions, Mechanisms, and Structure*. 6th ed.; John Wiley & Sons, Inc.: United States of America, 2007.

14. Marriott, S.; Topsom, R. D., A Theoretical Scale of Substituent Field Parameters. *J. Am. Chem. Soc.* **1984,** *106* (1), 7 - 10.

15. Hammett, L. P., Some Relations Between Reaction Rates and Equilibrium Constants. *Chem. Rev.* **1935,** *16* (2), 125 - 136.

16. Hammett, L. P., The Effect of Structure upon the Reactions of Organic Compounds. Benzene Derivatives. *J. Am. Chem. Soc.* **1937,** *59* (1), 96 - 103.

17. Hammett, L. P., Linear free energy relationships in rate and equilibrium phenomena. *Transactions of the Faraday Society* **1938,** *34* (0), 156-165.

18. Clayden, J.; Greeves, N.; Warren, S.; Wothers, P., *Organic Chemistry*. Oxford University Press: United Kingdom, 2001.

19. Jaffé, H. H., A Reëxamination of the Hammett Equation. *Chem. Rev.* **1953,** *53* (2), 191-261.

20. Wentworth, P.; Datta, A.; Smith, S.; Marshall, A.; Partridge, L. J.; Blackburn, G. M., Antibody Catalysis of BAc2 Aryl Carbamate Ester Hydrolysis: A Highly Disfavored Chemical Process. *J. Am. Chem. Soc.* **1997,** *119* (9), 2315-2316.

21. Pulukkody, R.; Kyran, S. J.; Drummond, M. J.; Hsieh, C.-H.; Darensbourg, D. J.; Darensbourg, M. Y., Hammett correlations as test of mechanism of CO-induced disulfide elimination from dinitrosyl iron complexes. *Chem. Sci.* **2014,** *5* (10), 3795-3802.

22. Charton, M., Electrical Effect Substituent Constants for Correlation Analysis. In *Progress in Physical Organic Chemistry*, Taft, R. W., Ed. John Wiley & Sons: 1981; Vol. 13, pp 119-251.

23. Taft Jr., R. W., The General Nature of the Proportionality of Polar Effects of Substituent Groups in Organic Chemistry. *J. Am. Chem. Soc.* **1953,** *75* (17), 4231 - 4238.

24. Taft Jr, R. W., Polar and Steric Substituent Constants for Aliphatic and *o*-Benzoate Groups from Rates of Esterification and Hydrolysis of Esters. *J. Am. Chem. Soc.* **1952,** *74* (12), 3120 - 3128.

25. Taft Jr, R. W., Linear Free Energy Relationships from Rate of Esterification and Hydrolysis of Aliphatic and Ortho-substituted Benzoate Esters. *J. Am. Chem. Soc.* **1952,** *74* (11), 2729 - 2732.

26. Brown, H. C.; Okamoto, Y., Electrophilic Substituent Constants. *J. Am. Chem. Soc.* **1958,** *80* (18), 4979-4987.

27. Grob, C. A.; Schlageter, M. G., The Derivation of Inductive Substituent Constants from pKa Values of 4-Substituted Quinuclidines. Polar effects. Part I. *Helv. Chim. Acta.* **1976,** *59* (1), 264-276.

28. Exner, O.; Charton, M.; Galkin, V., The inductive effect – the present position. *J. Phys. Org. Chem.* **1999,** *12* (4), 289-289.

29. Exner, O., The inductive effect: theory and quantitative assessment. *J. Phys. Org. Chem.* **1999,** *12* (4), 265-274.

30. Suresh, C. H.; Alexander, P.; Vijayalakshmi, K. P.; Saj, Use of molecular electrostatic potential for quantitative assessment of inductive effect. *Phys. Chem. Chem. Phys.* **2008,** *10* (43), 6492 - 6499.

31. Swain, C. G.; Unger, S. H.; Rosenquist, N. R.; Swain, M. S., Substituent Effects on Chemical Reactivity. Improved Evaluation of Field and Resonance Components. *J. Am. Chem. Soc.* **1983,** *105* (3), 492 - 502.

32. Sayyed, F. B.; Suresh, C. H., An electrostatic scale of substituent resonance effect. *Tetrahedron Lett.* **2009,** *50* (52), 7351 - 7354.

33. Santiago, C. B.; Milo, A.; Sigman, M. S., Developing a Modern Approach To Account for Steric Effects in Hammett-Type Correlations. *J. Am. Chem. Soc.* **2016,** *138* (40), 13424-13430.

34. Swain, C. G.; Lupton Jr, E. C., Field and Resonance Components of Substituent Effects. *J. Am. Chem. Soc.* **1968,** *90* (16), 4328 - 4337.

35. Westheimer, F. H.; Kirkwood, J. G., The Electrostatic Influence of Substituents on the Dissociation Constants of Organic Acids. II. *J. Chem. Phys.* **1938,** *6* (9), 513-517.

36. Kirkwood, J. G.; Westheimer, F. H., The Electrostatic Influence of Substituents on the Dissociation Constants of Organic Acids. I. *J. Chem. Phys.* **1938,** *6* (9), 506-512.

37. Taft, R. W.; Lewis, I. C., The General Applicability of a Fixed Scale of Inductive Effects. II. Inductive Effects of Dipolar Substituents in the Reactivities of m- and p-Substituted Derivatives of Benzene1,2. *J. Am. Chem. Soc.* **1958,** *80* (10), 2436-2443.

38. Bowden, K.; Grubbs, E. J., Through-bond and Through-space Models for Interpreting Chemical Reactivity in Organic Reactions. *Chem. Soc. Rev.* **1996,** *25* (3), 171 - 177.

39. Ehrenson, S., *Theoretical Interpretations of the Hammett and Derivative Structure-Reactivity Relationships*. 1964.

40. Derick, C. G., Polarity of Elements and Radicals Measured in Terms of a Logarithimic Function of the Ionization Constant. *J. Am. Chem. Soc.* **1911,** *33* (7), 1152-1162.

41. Derick, C. G., Application of Polarity Measured in Terms of a Logarithmic Function of the Ionization Constant. I. The Use of Polarity in the Explanation of the Reactions of Aldehydes and Ketones. *J. Am. Chem. Soc.* **1911,** *33* (7), 1162-1167.

42. Derick, C. G., Application of Polarity Measured in Terms of a Logarithmic Function of the Ionization Constant. II. Scale of Combined Influence of Substitution in Organic Compounds. *J. Am. Chem. Soc.* **1911,** *33* (7), 1167-1181.

43. Exner, O.; Friedl, Z., *Transmission of Substituent Effects: The Through-Space and Through-Bond Models and their Experimental Verification*. 1993; Vol. 19.

44. Liotta, C. L.; Fisher, W. F.; Greene, G. H.; Joyner, B. L., Mechanism of transmission of nonconjugative substituent effects. IV. Analysis of the dissociation

constants of 6-substituted spiro[3.3]heptane-2-carboxylic acids. *J. Am. Chem. Soc.* **1972,** *94* (14), 4891-4897.

45. Grubbs, E. J.; Fitzgerald, R.; Phillips, R. E.; Petty, R., The transmission of substituent effects in isomeric dichloroethano-bridged anthracene derivatives. *Tetrahedron* **1971,** *27* (5), 935-944.

46. Golden, R.; Stock, L. M., Dissociation constants of 8-substituted 9,10-ethanoanthracene-1-carboxylic acids and related compounds. Evidence for the field model for the polar effect. *J. Am. Chem. Soc.* **1972,** *94* (9), 3080-3088.

47. Galabov, B.; Nikolova, V.; Ilieva, S., Does the Molecular Electrostatic Potential Reflect the Effects of Substituents in Aromatic Systems? *Chem. Eur. J.* **2013,** *19* (16), 5149-5155.

48. Galabov, B.; Ilieva, S.; Schaefer III, H. F., An Efficient Computational Approach for the Evaluation of Substituent Constants. *J. Org. Chem.* **2006,** *71* (17), 6382 - 6387.

49. Suresh, C. H.; Gadre, S. R., Electrostatic Potential Minimum of the Aromatic Ring as a Measure of Substituent Constant. *J. Phys. Chem. A.* **2007,** *111* (4), 710-714.

50. Topsom, R. D., The isolated molecule approach. Theoretical studies of the inductive effect. *J. Am. Chem. Soc.* **1981,** *103* (1), 39-44.

51. Suresh, C. H.; Gadre, S. R., A Novel Electrostatic Approach to Substituent Constants: Doubly Substituted Benzenes. *J. Am. Chem. Soc.* **1998,** *120* (28), 7049 - 7055.

52. Remya, G. S.; Suresh, C. H., Quantification and classification of substituent effects in organic chemistry: a theoretical molecular electrostatic potential study. *Phys. Chem. Chem. Phys.* **2016,** *18* (30), 20615-20626.

53. Wheeler, S. E.; Houk, K. N., Through-Space Effects of Substituents Dominate Molecular Electrostatic Potentials of Substituted Arenes. *J. Chem. Theory Comput.* **2009,** *5* (9), 2301 - 2312.

54. Wheeler, S. E.; Bloom, J. W. G., Toward a More Complete Understanding of Noncovalent Interactions Involving Aromatic Rings. *J. Phys. Chem. A* **2014,** *118* (32), 6133 - 6147.

55. Wheeler, S. E.; Houk, K. N., Origin of substituent effects in edge-to-face aryl–aryl interactions. *Mol. Phys.* **2009,** *107* (8-12), 749-760.

56. Neel, A. J.; Hilton, M. J.; Sigman, M. S.; Toste, F. D., Exploiting non-covalent π interactions for catalyst design. *Nature* **2017,** *543*, 637.

57. Sayyed, F. B.; Suresh, C. H.; R., G. S., Appraisal of Through-Bond and Through-Space Substituent Effects via Molecular Electrostatic Potential Topography. *J. Phys. Chem. A* **2010,** *114* (42), 12330 - 12333.

58. Sayyed, F. B.; Suresh, C. H., Substituent Effects in Cation-Pi Interactions: A Unified View from Inductive, Resonance, and Through-Space Effects. *J. Phys. Chem. A* **2011,** *115* (22), 5660 - 5664.

59. Wheeler, S. E.; Houk, K. N., Substituent Effects in Cation/Pi Interactions and Electrostatic Potentials above the Center of Substituted Benzenes Are Due Primarily to through-Space Effects of the Substitents. *J. Am. Chem. Soc.* **2009,** *131* (9), 3129 - 3127.

60. Hunter, C. A.; Low, C. M. R.; Vinter, J. G.; Zonta, C., Quantification of Functional Group Interactions in Transition States. *J. Am. Chem. Soc* **2003,** *125*, 9936 - 9937.

61. Sayyed, F. B.; Suresh, C. H., Accurate Prediction of Cation−π Interaction Energy Using Substituent Effects. *J. Phys. Chem. A.* **2012,** *116* (23), 5723-5732.

62. Wheeler, S. E.; Houk, K. N., Substituent Effects in the Benzene Dimer are Due to Direction Interactions of the Substituents with the Unsubstituted Benzene. *J. Am. Chem. Soc.* **2008,** *130* (33), 10854 - 10855.

63. Parrish, R. M.; Sherrill, C. D., Quantum-Mechanical Evaluation of π–π versus Substituent−π Interactions in π Stacking: Direct Evidence for the Wheeler–Houk Picture. *J. Am. Chem. Soc.* **2014,** *136* (50), 17386-17389.

64. Hwang, J.; Li, P.; Vik, E. C.; Karki, I.; Shimizu, K. D., Study of Through-Space Substituent-π Interactions Using N-Phenylimide Molecular Balances. *Organic Chemistry Frontiers* **2019**.

65. Hwang, J. w.; Li, P.; Shimizu, K. D., Synergy between experimental and computational studies of aromatic stacking interactions. *Org. Biomol. Chem.* **2017,** *15* (7), 1554-1564.

66. Hunter, C. A.; Sanders, J. K. M., The nature of .pi.-.pi. interactions. *J. Am. Chem. Soc.* **1990,** *112* (14), 5525-5534.

67. Riwar, L.-J.; Trapp, N.; Kuhn, B.; Diederich, F., Substituent Effects in Parallel-Displaced π–π Stacking Interactions: Distance Matters. *Angew. Chem. Int. Ed.* **2017,** *56* (37), 11252-11257.

68. Sinnokrot, M. O.; Sherrill, C. D., Unexpected Substituent Effects in Face-to-Face π-Stacking Interactions. *J. Phys. Chem. A.* **2003,** *107* (41), 8377-8379.

69. Sinnokrot, M. O.; Sherrill, C. D., Substituent Effects in π−π Interactions: Sandwich and T-Shaped Configurations. *J. Am. Chem. Soc.* **2004,** *126* (24), 7690-7697.

70. Sinnokrot, M. O.; Sherrill, C. D., High-Accuracy Quantum Mechanical Studies of π−π Interactions in Benzene Dimers. *J. Phys. Chem. A.* **2006,** *110* (37), 10656-10668.

71. Lee, E. C.; Kim, D.; Jurečka, P.; Tarakeshwar, P.; Hobza, P.; Kim, K. S., Understanding of Assembly Phenomena by Aromatic−Aromatic Interactions: Benzene Dimer and the Substituted Systems. *J. Phys. Chem. A.* **2007,** *111* (18), 3446-3457.

72. Wheeler, S. E.; McNeil, A. J.; Müller, P.; Swager, T. M.; Houk, K. N., Probing Substituent Effects in Aryl−Aryl Interactions Using Stereoselective Diels−Alder Cycloadditions. *J. Am. Chem. Soc.* **2010,** *132* (10), 3304-3311.

73. Shimizu, K. D.; Carroll, W. R.; Zhao, C.; Smith, M. D.; Pellechia, P. J., A Molecular Balance for Measuring Aliphatic CH-Pi Interactions. *Org. Lett.* **2011,** *13* (16), 4320 - 4323.

74. Gardarsson, H.; Schweizer, W. B.; Trapp, N.; Diederich, F., Structures and Properties of Molecular Torsion Balances to Decipher the Nature of Substituent Effects on the Aromatic Edge-to-Face Interaction. *Chem. Eur. J.* **2014,** *20* (16), 4608-4616.

75. Harder, M.; Carnero Corrales, M. A.; Trapp, N.; Kuhn, B.; Diederich, F., Rebek Imide Platforms as Model Systems for the Investigation of Weak Intermolecular Interactions. *Chem. Eur. J.* **2015,** *21* (23), 8455-8463.

76. Arnstein, S. A.; Sherrill, C. D., Substituent effects in parallel-displaced π–π interactions. *Phys. Chem. Chem. Phys.* **2008,** *10* (19), 2646-2655.

77. Hwang, J.; Li, P.; Carroll, W. R.; Smith, M. D.; Pellechia, P. J.; Shimizu, K. D., Additivity of Substituent Effects in Aromatic Stacking Interactions. *J. Am. Chem. Soc.* **2014,** *136* (40), 14060-14067.

78. Ringer, A. L.; Sinnokrot, M. O.; Lively, R. P.; Sherrill, C. D., The Effect of Multiple Substituents on Sandwich and T-Shaped π–π Interactions. *Chem. Eur. J.* **2006,** *12* (14), 3821-3828.

79. Cozzi, F.; Ponzini, F.; Annunziata, R.; Cinquini, M.; Siegel, J. S., Polar Interactions between Stacked π Systems in Fluorinated 1,8-Diarylnaphthalenes: Importance of Quadrupole Moments in Molecular Recognition. *Angew. Chem. Int. Ed. in English* **1995,** *34* (9), 1019-1020.

80. Shimizu, K. D.; Li, P.; Hwang, J., CHAPTER 5 Solution-Phase Measurements of Aromatic Interactions. In *Aromatic Interactions: Frontiers in Knowledge and Application*, The Royal Society of Chemistry: 2017; pp 124-171.

81. Cozzi, F.; Cinquini, M.; Annunziata, R.; Dwyer, T.; Siegel, J. S., Polar/.pi. interactions between stacked aryls in 1,8-diarylnaphthalenes. *J. Am. Chem. Soc.* **1992,** *114* (14), 5729-5733.

82. Cozzi, F.; Cinquini, M.; Annuziata, R.; Siegel, J. S., Dominance of polar/.pi. over charge-transfer effects in stacked phenyl interactions. *J. Am. Chem. Soc.* **1993,** *115* (12), 5330-5331.

83. Cozzi, F.; Annunziata, R.; Benaglia, M.; Cinquini, M.; Raimondi, L.; Baldridge, K. K.; Siegel, J. S., Through-space interactions between face-to-face, center-to-edge oriented arenes: importance of polar–π effects. *Org. Biomol. Chem.* **2003,** *1* (1), 157-162.

84. Guan, L.; Holl, M. G.; Pitts, C. R.; Struble, M. D.; Siegler, M. A.; Lectka, T., Through-Space Activation Can Override Substituent Effects in Electrophilic Aromatic Substitution. *J. Am. Chem. Soc.* **2017**.

85. Holl, M. G.; Struble, M. D.; Singal, P.; Siegler, M. A.; Lectka, T., Positioning a Carbon-Fluorine Bond over the Pi Cloud of an Aromatic Ring: A Different Type of Arene Activation. *Angew. Chem. Int. Ed.* **2016,** *55* (29), 8266 - 8269.

86. Chen, C.-T.; Siegel, J. S., Through-Space Polar-.pi. Effects on the Acidity and Hydrogen-Bonding Capacity of Carboxylic Acids. *J. Am. Chem. Soc.* **1994,** *116* (13), 5959-5960.

87. Padial, J. S.; de Gelder, R.; Fonseca Guerra, C.; Bickelhaupt, F. M.; Mecinović, J., Stabilisation of 2,6-Diarylpyridinium Cation by Through-Space Polar–π Interactions. *Chem. Eur. J.* **2014,** *20* (21), 6268-6271.

88. Bosmans, V.; Poater, J.; Hammink, R.; Tinnemans, P.; Bickelhaupt, F. M.; Mecinović, J., Probing Through-Space Polar−π Interactions in 2,6-Diarylphenols. *The Journal of Organic Chemistry* **2019,** *84* (6), 3632-3637.

89. Simó Padial, J.; Poater, J.; Nguyen, D. T.; Tinnemans, P.; Bickelhaupt, F. M.; Mecinović, J., Stabilization of 2,6-Diarylanilinum Cation by Through-Space Cation−π Interactions. *The Journal of Organic Chemistry* **2017,** *82* (18), 9418-9424.

90. Warshel, A., Electrostatic basis of structure-function correlation in proteins. *Acc. Chem. Res.***1981,** *14* (9), 284-290.

91. Warshel, A.; Sharma, P. K.; Kato, M.; Xiang, Electrostatic Basis for Enzyme Catalysis. *Chem. Rev.* **2006,** *106* (8), 3210 - 3235.

92. Shaik, S.; Mandal, D.; Ramanan, R., Oriented electric fields as future smart reagents in chemistry. *Nature Chemistry* **2016,** *8*, 1091.

93. Fried, S. D.; Boxer, S. G., Electric Fields and Enzyme Catalysis. *Annual Review of Biochemistry* **2017,** *86* (1), 387-415.

94. Shaik, S.; Ramanan, R.; Danovich, D.; Mandal, D., Structure and reactivity/selectivity control by oriented-external electric fields. *Chem. Soc. Rev.* **2018,** *47* (14), 5125-5145.

95. Zhao, Y.; Cotelle, Y.; Liu, L.; López-Andarias, J.; Bornhof, A.-B.; Akamatsu, M.; Sakai, N.; Matile, S., The Emergence of Anion−π Catalysis. *Acc. Chem. Res.***2018,** *51* (9), 2255-2263.

96. Shaik, S.; de Visser, S. P.; Kumar, D., External Electric Field Will Control the Selectivity of Enzymatic-Like Bond Activations. *J. Am. Chem. Soc.* **2004,** *126* (37), 11746-11749.

97. Huang, X.; Tang, C.; Li, J.; Chen, L.-C.; Zheng, J.; Zhang, P.; Le, J.; Li, R.; Li, X.; Liu, J.; Yang, Y.; Shi, J.; Chen, Z.; Bai, M.; Zhang, H.-L.; Xia, H.; Cheng, J.; Tian, Z.-Q.; Hong, W., Electric field–induced selective catalysis of single-molecule reaction. *Science Advances* **2019,** *5* (6), eaaw3072.

98. Aragonès, A. C.; Haworth, N. L.; Darwish, N.; Ciampi, S.; Bloomfield, N. J.; Wallace, G. G.; Diez-Perez, I.; Coote, M. L., Electrostatic catalysis of a Diels–Alder reaction. *Nature* **2016,** *531*, 88.

99. van der Lubbe, S. C. C.; Zaccaria, F.; Sun, X.; Fonseca Guerra, C., Secondary Electrostatic Interaction Model Revised: Prediction Comes Mainly from Measuring Charge Accumulation in Hydrogen-Bonded Monomers. *J. Am. Chem. Soc.* **2019,** *141* (12), 4878-4885.

100. Borsley, S.; Haugland, M. M.; Oldknow, S.; Cooper, J. A.; Burke, M. J.; Scott, A.; Grantham, W.; Vallejo, J.; Brechin, E. K.; Lusby, P. J.; Cockroft, S. L., Electrostatic Forces in Field-Perturbed Equilibria: Nanopore Analysis of Cage Complexes. *Chem* **2019,** *5* (5), 1275-1292.

Chapter 2

Measuring Through-Space Substituent Effects using Molecular Balances

Abstract

The rationalisation of substituent effects in organic molecules tends to be dominated by through-bond effects. Computational and empirical studies have shown the importance of the overlooked through-space substituent effects that are at the heart of the present study. Here, twenty-four specially designed molecular balances are used to assess through-space substituent effects in conformational chemical equilibria. Empirically derived conformational equilibrium constants are subjected to a Hammett analysis to obtain a new set of substituent constants in contexts where through-space effects are dominant. Computationally derived electrostatic potential (ESP) values, surfaces and slices showed the importance of field effects on the experimental and computational observables; highlighting the importance of through-space effects on chemical equilibria and confirming that the constants derived in this study describe situations in which through-space substituent effects dominate. The utility of the constants quantified were evaluated *via* the application of a mathematical solvation model. Ultimately, the field effects were shown to be sensitive to solvent properties.

Supplementary details are given in Appendix A.

Contributions: All experimental and computational results of the **1–X** group of compounds described in this chapter were obtained by RJB with the exception of compounds **1–a** to **1–h** inclusive which were obtained by Dr Ioulia K. Mati[1] as described in the caption of **Figure 2.4**. Computational results and experimental free energies of the **1'–Y** series were previously reported,[2-3] with a few exceptions. All data for **1'–Me** was obtained by RJB. Benzene, acetone, acetonitrile, ethyl acetate, THF and ethanol data for **1'–CF_3** were obtained by RJB and required synthesis of this compound by RJB. Acetone, acetonitrile, ethyl acetate, THF and DMSO data for **1'–COMe** was obtained by RJB and required synthesis of this compound by RJB. Solvent dissection and transferability analysis was performed by RJB.

2.1 Introduction

It is within the lexicon of all organic chemists to classify substituents as either electron-withdrawing or electron-donating based on the rationalisation of their effects *via* through-bond phenomena. Linear free energy relationships that are regularly utilised to elucidate mechanisms and predict reaction rates rely on substituent constants, most commonly σ_m and σ_p, that were founded upon the assumption that these effects are dominated by the through-bond nature of the substituent. However, several empirical and computational studies have pointed towards the overlooked importance of through-space substituent effects (**Chapter 1**). Thus, it is possible that this is the underlying cause of substituent effects that are unexplainable by through-bond phenomena.

The assumption that substituent effects are driven by through-bond phenomena can cause difficulties in their interpretation as exemplified by a 1966 study by Byron in which the ionisation of a series of 2'-, 3'- and 4'-substituted biphenyl-4-carboxylic acids was measured (**Figure 2.1**).[4]

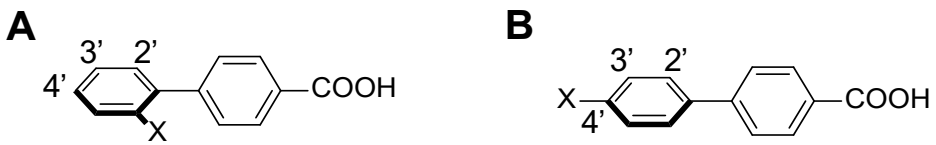

Figure 2.1: 2'- and 4'-substituted biphenyl-4-carboxylic acids investigated by Byron.[4]

It was found that the 2'-substituted carboxylic acids (**Figure 2.1A**) were generally less acidic than their 4'-substituted counterparts (**Figure 2.1B**). This experimental observation could not be explained in terms of traditional through-bond substituent effects and as such, it was theorised that the "steric pressure" of the substituent in the 2'-position caused a deformation of the π-system, pushing π-electrons towards the carboxylic acid and leading to the decrease in acidity of these systems with respect to the 4-substituted carboxylic acids. This study was conducted in the 1960s before quantum mechanical modelling was widely available. Therefore, it could be that the

effect of the 2'-subtituent on the acidity of the carboxylic acid could actually be the result of a through-space interaction between the substituent and the reaction centre rather than "steric pressure".[4] The example highlights the potential importance of quantifying through-space substituent effects.

2.2 Aims of the Project

With a growing number of experimental and computational studies displaying the importance of through-space effects on the properties of organic molecules, it could be the ignorance of these effects that has led to the difficulties in obtaining a universally applicable constant to describe and predict substituent effects on organic molecules.

The overarching aim of this project was to quantify substituent effects in contexts where through-space influences were most likely to dominate. To do this, it was important to design a robust experimental system that allowed the assessment of through-space substituent effects with minimal input from through-bond effects. Quantification *via* empirical methods was performed with the mathematical relation used by Hammett to obtain σ_m and σ_p constants, $-\log_{10}(K_X/K_H)$, which was applied to the equilibrium constants of a series of molecular balances. The values of $-\log_{10}(K_X/K_H)$ for a control series of molecular balances were transposed onto the Hammett scale by plotting them against σ_p. Using the equation of the straight line of this plot, the value of ρ was determined, alongside that of a constant, γ. These values were used to calculate a new substituent constant, $\sigma_{p(conf)}$ according to a rearrangement of the equation of the straight line of the calibration plot (**Equation 2.3**). This constant represents the experimental data obtained for the molecular balances at the heart of this study set in the context of Hammett's σ constants.

Computational analysis *via* ESP surfaces, which have been successful in the study of through-space substituent effects in prior studies, were used in the present study to understand the experimental results. In addition, as through-space substituent effects are electrostatic in nature, the modulation of these effects by the surrounding solvent

is evaluated *via* a mathematical solvation model. Thus, the conformational equilibrium constants of the molecular balances at the heart of this study were measured in eleven solvents of ranging polarity. Overall, a combined computational and experimental approach was taken to meet the aim of this project.

2.3 Molecular Balances

Molecular torsion balances can be used for the experimental quantification of weak non-covalent interactions.[5] Most commonly, molecular balances are designed to exchange slowly between two distinct conformational states *via* rotation about a restricted bond (**Figure 2.2A**).

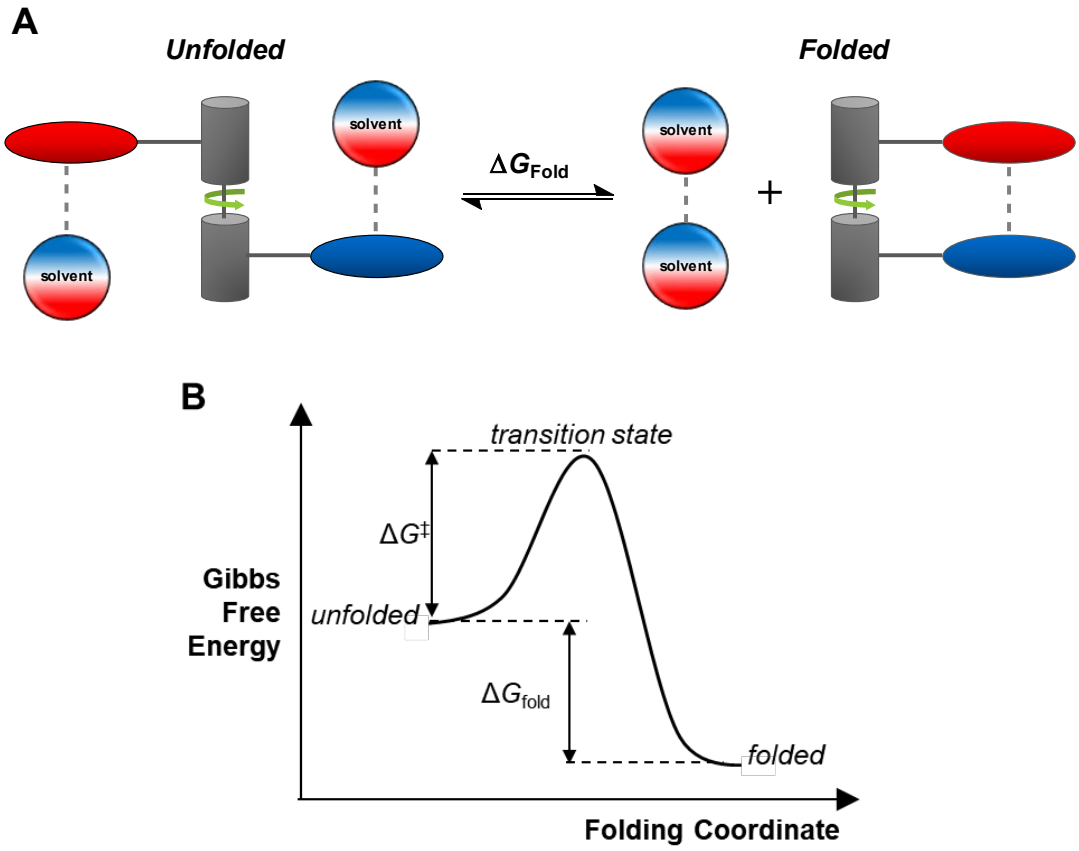

Figure 2.2: (A) The conformational equilibrium of a simplified molecular balance with two ground state conformations. **(B)** The free energy of the barrier of rotation ($\Delta G^{\ddagger}$) and of the free energy of folding the molecule (ΔG_{fold}) are shown on an energy profile corresponding to the free energy of the system as the molecule is folded. Figure adapted from the *Chem. Soc. Rev.* Tutorial Review by Mati and Cockroft.[5]

The position of the equilibrium between these states is governed by the solvent and intramolecular non-covalent interactions present in one conformation that are not present in the other. Measurement of the energy difference between these two states through spectroscopic means quantifies the strength of the non-covalent interaction of interest and any associated solvent effects. In the most ideal designs, molecular balances that are highly symmetrical minimise secondary effects to ensure that the position of the conformational equilibrium is governed mostly by an interaction of interest. However, it is still possible to obtain the energetics of the interaction of interest from a less ideal balance through the use of control compounds and/or double mutant cycles.[5]

Molecular balances that possess two well-defined ground-state conformations give rise to two free energy terms that may be used to assess the strength of an interaction (**Figure 2.2B**); the energy of the barrier to rotation ($\Delta G^{\ddagger}$) and the free energy of folding the molecule (ΔG_{fold}).[5]

The barrier to rotation, $\Delta G^{\ddagger}$, is the difference in free energy between the ground-state energy of conformer and the transition-state maxima as the balance moves between the folded and unfolded conformers. However, the interpretation of such barriers to rotation is challenging since the barrier is determined by energetic influences in both the ground state conformer and a highly strained, non-equilibrium transition state. Instead, the more easily interpreted free energy difference of folding, ΔG_{fold}, which corresponds to the energy difference between the major ground state conformations is most widely probed experimentally.[3, 5]

The free energy of folding can be determined experimentally using NMR spectroscopy. This is most easily attained when the conformational interconversion is slow enough on the NMR timescale to allow both conformers to be observed at room temperature. Such molecular balances include a restricted bond with a barrier to rotation, $\Delta G^{\ddagger}$, greater than 65 kJ mol^{-1}.[5] As the two conformers give distinct signals at room temperature, the relative population of each conformer can be determined by integration of the NMR signals corresponding to each conformer which gives a measure of the equilibrium constant, K_{fold}. This experimental value of K_{fold} can then be used to determine the free energy difference between the two conformers (ΔG_{fold}).[3, 5-

[6] However, it should be noted that equilibrium can be difficult to reach for compounds with very high rotational barriers and in these instances, distinct atropisomers are observed.

Molecular balances have provided insight into solvent effects and strengths of a wealth of non-covalent interactions (**Figure 2.3**), starting with the first molecular balances by Ōki in 1990.[5, 7] These were based on 1,9-disubstituted triptycene derivatives, where substituent-induced restricted rotation around the C–C bond indicated in **Figure 2.3A** allowed two conformational states to be observed *via* NMR spectroscopy at low temperatures. Ōki *et. al.* used these balances to study various C–H···O, C–H···arene and O/halogen···arene interactions and they were later adapted by Gung and co-workers in their investigations into O···arene interactions (**Figure 2.3A**).[7-9]

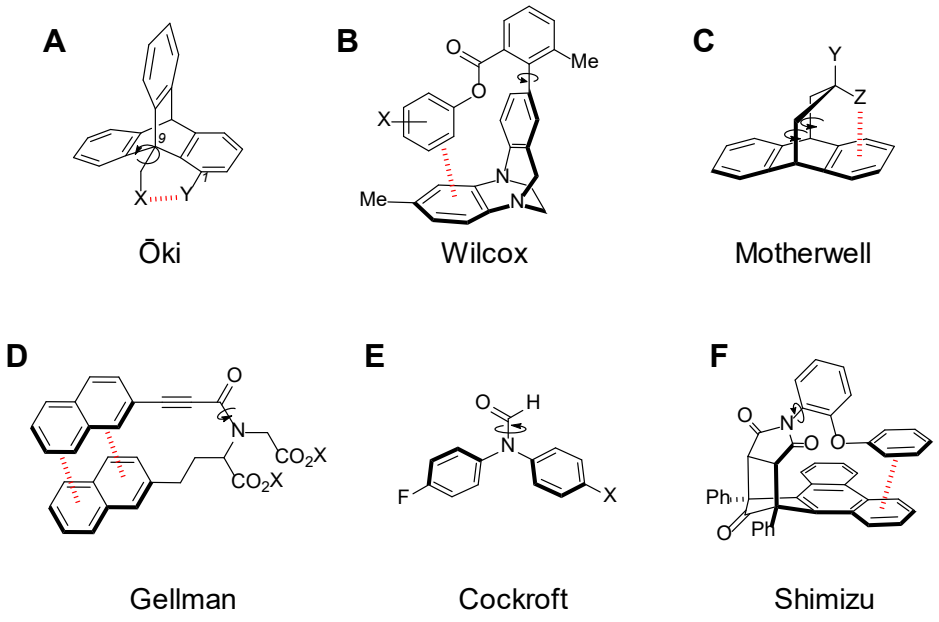

Figure 2.3: (A) The basic 1,9-substituted tryptcene derivatives used by Ōki and Gung.[7] **(B)** The Tröger's base based molecular balance framework, often referred to as the "Wilcox balance".[10] **(C)** Dibenzo-bicyclo[3.2.2]-nonane based molecular balances developed by Motherwell and co-workers.[11] **(D)** Gellman *et. al.*'s molecular balance used in the study of aromatic stacking interactions.[12-13] **(E)** The Cockroft balance based on the slow rotation of the amide C–N bond.[2-3] **(F)** Molecular balance designed by Shimizu and co-workers.[14]

Another highly successful molecular balance framework was developed by Wilcox in 1994 and was based on Tröger's base (**Figure 2.3B**).[10] Wilcox was the first to coin the

phrase "molecular torsion balance" and investigated functional group···arene and aromatic edge-to-face interactions using this balance. The Wilcox balance has since been adapted by other researchers to study C=O···C=O and C–F···C=O interactions.[6, 10, 15-17] More recently, Motherwell and co-workers have used rigid dibenzo-biyclo[3.2.2]-nonane based molecular balances (**Figure 2.3C**) in the study of solvation effects on functional groups and functional group···arene interactions.[11]

Gellman and Cockroft have utilised the restricted rotation of the C–N bond of amides to build molecular torsion balances where the former has investigated aryl-aryl stacking interactions (**Figure 2.3D**) and the latter has probed interactions such as hydrogen bonding as well as solvent effects on non-covalent interactions (**Figure 2.3E**).[2-3, 12-13, 18]

Shimizu and co-workers have used their *N*-phenylimide molecular torsion balance design in the study of numerous arene based non-covalent interactions including arene···arene stacking, C–H···arene, C=O···arene, O···arene, O–H···arene, F···arene, S···arene and even silver···arene interactions (**Figure 2.3F**).[14, 19-26] In particular, Shimizu *et. al.* have utilised this molecular balance scaffold to probe the Wheeler and Houk's 'direct interaction model', as discussed in **Chapter 1**.[27]

The large range of non-covalent interactions that have been analysed using molecular balances, including Shimizu's study of through-space effects, showcases the utility of molecular balances in aiding the understanding of non-covalent interactions. Thus, it stands to reason that molecular torsion balances are useful systems to study through-space substituent effects. The wealth of literature regarding through-space substituent effects has been largely computational,[28-37] notably including the pioneering work by Wheeler and Houk.[38-43] While computational methods are extremely useful in gaining insight into non-covalent interactions, they sometimes model situations that are difficult, or even impossible to probe experimentally (e.g. functional groups held in specific spatial orientations, or functional group dissections that do not exist). For example, artificially positioned hydrogen-capped substituents were used by Wheeler and Houk in their computational determination of the minimal role of electron density changes on the electrostatic potentials of aryl π–systems.[38-40] Moreover, modelling solvent effects is both theoretically challenging and computationally expensive. In

contrast, molecular balances provide an extremely sensitive experimental measurement of folding free energies with an accuracy down to ~0.12 kJ mol^{-1} allowing the examination of weak non-covalent interactions.[5]

2.3.1 Molecular Balance Design

In the present study, a range of molecular balances (**Figure 2.4A**) were employed based on an established design that previously been used to probe substituent and solvent effects on various intramolecular interactions (**Figure 2.4B**).[2-3, 18, 44] By measuring substituent-induced changes in the relative positions of the conformational equilibria, compounds in the **1–X** series enable quantification of the through-space influence of substituents placed in the *ortho*-position to the biphenyl bond (**Figure 2.4**).

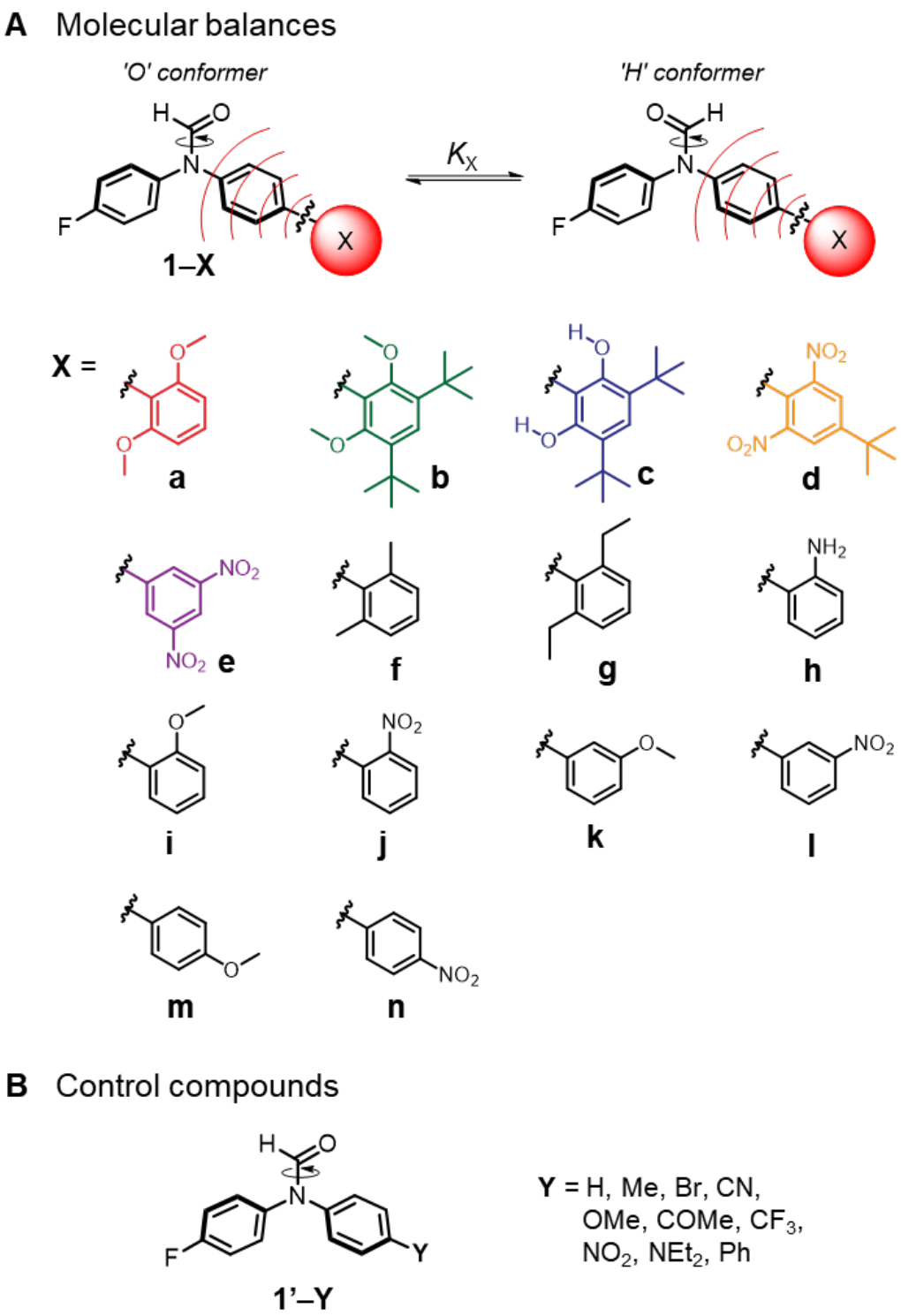

Figure 2.4: Molecular torsion balances used in this study. **(A)** Biphenyl derivatives of the Cockroft balance wherein substitution of the **X** ring allows assessment of through-space substituent effects as represented by red lines. Balances **1–i** to **1–m** inclusive were synthesised and characterised by RJB and the rest by Dr Ioulia K. Mati.[1] **(B)** Molecular balances previously established[2-3] and used in the present study as control compounds. All

molecular balances were previously reported,[2-3] with the exception of **1'–Me** and the **1'–CF_3** data in benzene which were obtained by RJB.

Such balances have a number of characteristics that allow the facile study of non-covalent interactions. The C–N bond of the amide possesses restricted rotation due to partial double-bond character arising from conjugation between the nitrogen lone pair and carbonyl oxygen (**Figure 2.5**). The partial double bond character of the formamide C–N bond results in slow rotation on the NMR timescale and in turn, distinct ^{19}F NMR signals of each conformer at room temperature; one where the formamide oxygen points over the Y-substituted ring of those in **Figure 2.4B** which will be referred to as the 'O' conformer and correspondingly, the conformer where the formamide oxygen points over the F-substituted ring is denoted as the 'H' conformer.

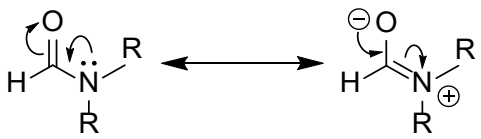

Figure 2.5: Delocalisation of nitrogen lone pair of the amide group resulting in the restricted rotation of the C–N bond, giving rise to two distinct conformers observable on NMR spectra.

The use of a ^{19}F tag allows the use of a wide range of non-deuterated solvents in NMR spectroscopy experiments, sidestepping the requirement of often expensive deuterated solvents. In addition, ^{19}F spectra are not complicated by solvent peaks, unless the solvent contains fluorine. In addition, the natural abundance of ^{19}F is 100% and ^{19}F NMR conformer peaks are often well separated, making determination of conformation equilibrium constants both simple and accurate.[45] Through integration of the ^{19}F NMR signals corresponding to each conformer, the experimental conformational equilibrium constant, K_X, is easily accessed, and will enable a Hammett-type analysis of substituent effects (see ***Section 2.4.2***).

It is known that the separation of through-bond and through-space substituent effects is known to be challenging (**Chapter 1**).[46] The biphenyl system at the heart of Byron's 1966 work (**Figure 2.1**) provided useful inspiration for the design of our balances

(**Figure 2.4A**) as the through-bond effects of the substituents placed on the X-substituted ring are minimised.[4] Resonant substituent effects involve lone pair, p or π orbitals and thus require appropriate orbital alignment for effective resonant communication.[47] For a biphenyl system, this requires the two rings to be planar to one another. However, computational modelling shows that the rings are not in the same plane in the equilibrium geometry (**Figure 2.6A** and **B**), thus limiting resonant substituent effects on the X-substituted ring, particularly in di-*ortho*-substituted examples such as that shown in **Figure 2.6B**. Computationally derived barriers to rotation of the biaryl unit present in series **1–X** (see **Appendix A**, ***Section A.1.2***) were also calculated. However, as the amide nitrogen to phenyl bond of this molecular balance design is freely rotating, this barrier to rotation will not impact the experimental measurement of through-space effects.

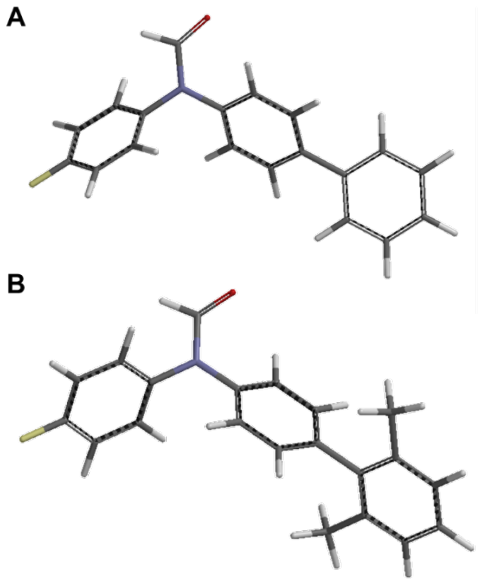

Figure 2.6: Computational models of **(A) 1'–Ph** and **(B) 1–f** showing that the biphenyl rings, even for the unsubstituted **1'–Ph**, are not planar. Structures were minimised using DFT/B3LYP/6–31G* in Spartan '14.

The chosen biphenyl systems also position the X-substituents far from the formamide conformational reporter such that steric interference is avoided. In addition, all of the proposed molecular balances are overall neutral in charge, meaning there are no

complications from changes in solvent structure or counter ions that would complicate our experimental observables.

2.3.2 Molecular Balance Synthesis

The molecular balances of the **1'–Y** series, except **1'–Me** and **1'–Ph**, were prepared according to the general copper-mediated coupling routes shown in **Figure 2.7** (full details of all syntheses are given in **Appendix A**).[2-3]

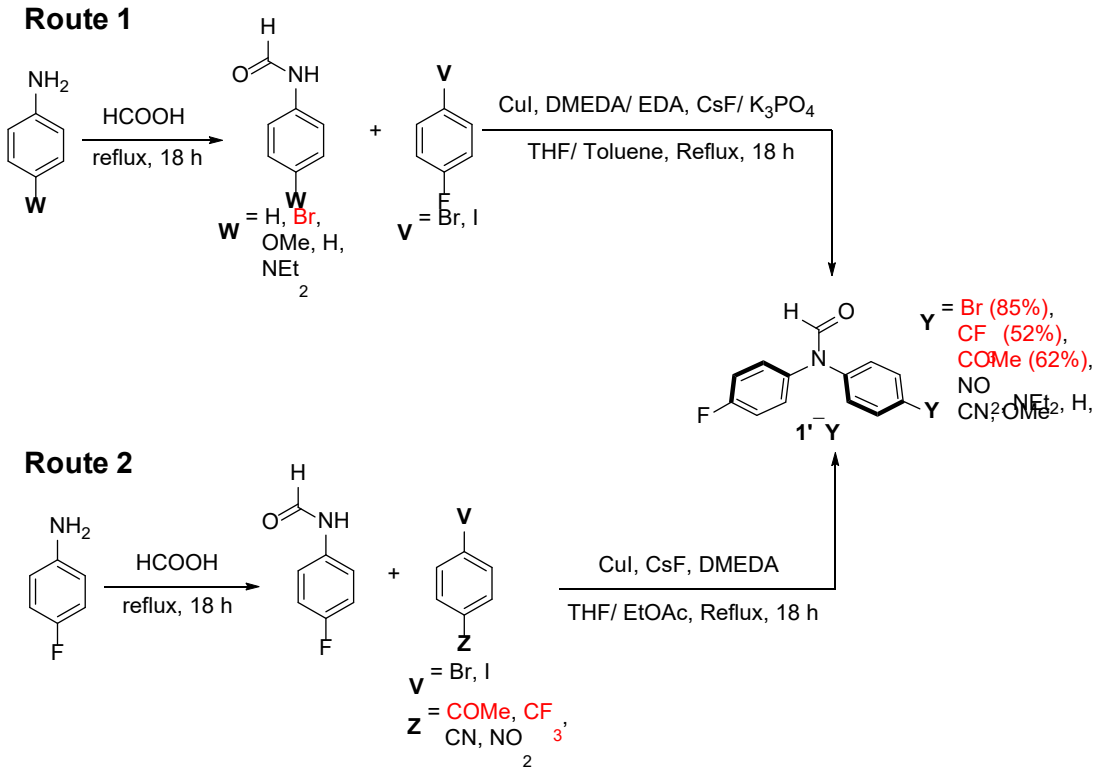

Figure 2.7: General procedure for copper-mediated coupling of halo-aromatics to aryl-amides in the preparation of molecular balances **1'–Y** (except where **Y**= Me and Ph). All compounds were previously reported [2-3] except three balances (highlighted in red) which were resynthesised by RJB. **1'–CF$_3$** was resynthesised by RJB (**Y** = CF_3, 52 %) to obtain data for this compound in benzene-d_6 and **1'–Br** was resynthesised by RJB (**Y** = Br, 85 %) to enable synthesis of **1–X** compounds. Compound **1'–COMe** was resynthesized by RJB (**Y** = COMe, 62 %) to obtain this data in various solvents. Yields marked in red are those obtained by RJB. Full details are given in Appendix A.

Both synthetic **Routes 1** and **2** begin with a high-yielding formylation of a

commercially available 4-substituted aniline derivative. The product formamides were then used in Cu(I)-catalysed Goldberg-Ullmann couplings with the appropriate 4-substituted bromo- or iodobenzene derivatives to furnish the final molecular balances in only two steps in generally good yields (52% to 85%).[2-3]

Synthesis of **1'–Me** was also straightforward (**Figure 2.8**), beginning with the facile Buchwald-Hartwig amination of 4-methylaniline and 4-fluoroiodobenzene, which were both commercially available. Formylation of the resulting amine by refluxing in neat formic acid overnight gave **1'–Me** from just two steps.

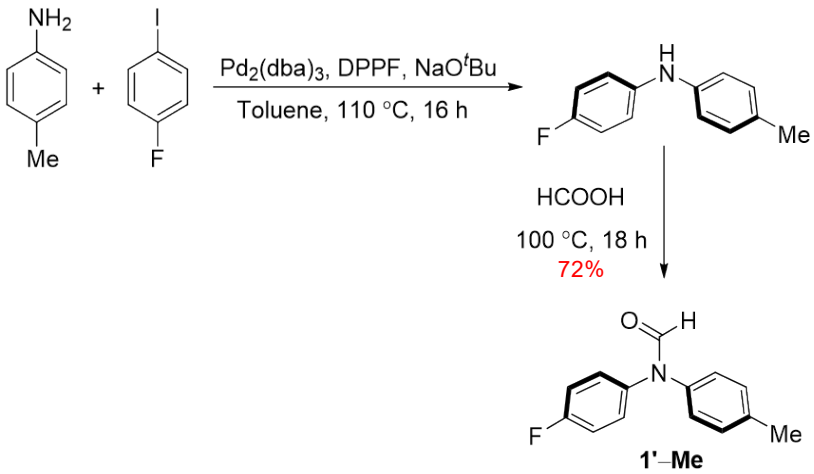

Figure 2.8: Preparation of **1'–Me**, synthesised by RJB.

The **1–X** series, except **1–d** and **1–e**, and **1'–Ph** were all prepared from **1'–Br** and the same general palladium-mediated coupling procedure (**Figure 2.9**).[1]

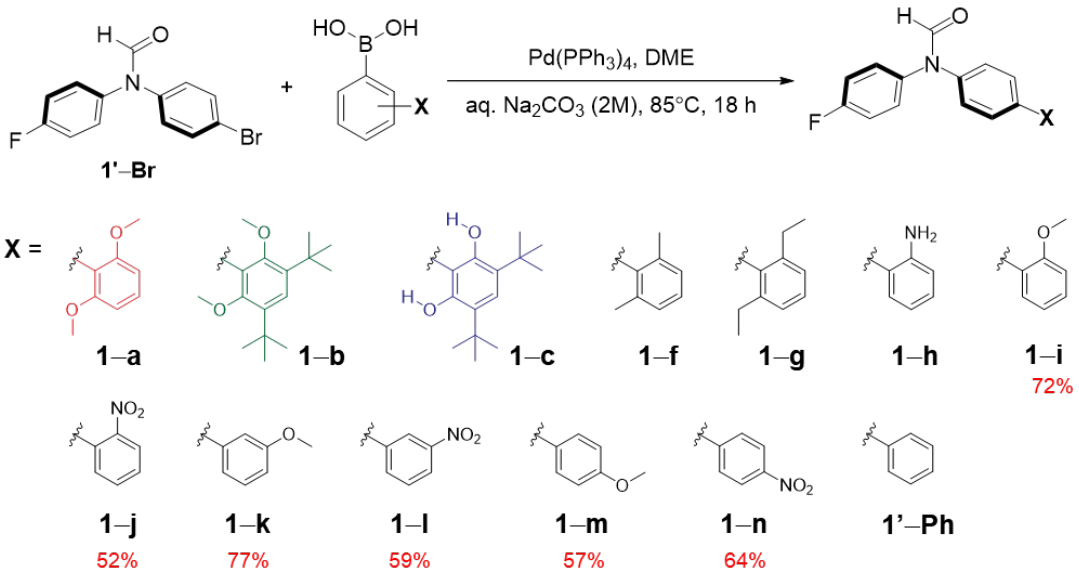

Figure 2.9: Preparation of **1–X** compounds (except **1–d** and **1–e**) from **1'–Br** and of **1'–Ph**. Molecular balance **1'–Ph** was previously reported.[2-3] Compounds **1–a** to **1–h** inclusive were synthesised by Dr Ioulia K. Mati[1] and **1–l** to **1–n** inclusive were synthesised by RJB. Yields of the compounds obtained by RJB are given in red below the compound number.

This generalised tetrakis(triphenylphospine)palladium(0)-mediated Suzuki-Miyaura procedure tolerated a good range of substituents, allowing for the synthesis of **1'–Ph** and all but two of the **1–X** series, all in good yields (52% to 77%).

Palladium-catalysed cross-coupling is a well-established means of synthesising 4-phenyl substituted benzene compounds [48] and provide a flexible route to such systems, allowing the synthesis of the **1–X** molecular balances and **1'–Ph** from the **1'–Br** balance and the appropriate boronic acid.[2]

The synthesis of balances **1–d** and **1–e** differed from others in the **1–X** series in that the Suzuki-Miyaura coupling to form the biphenyl preceded *via* formylation of the amine group (**Figure 2.10**). These compounds were obtained in good yields.[1]

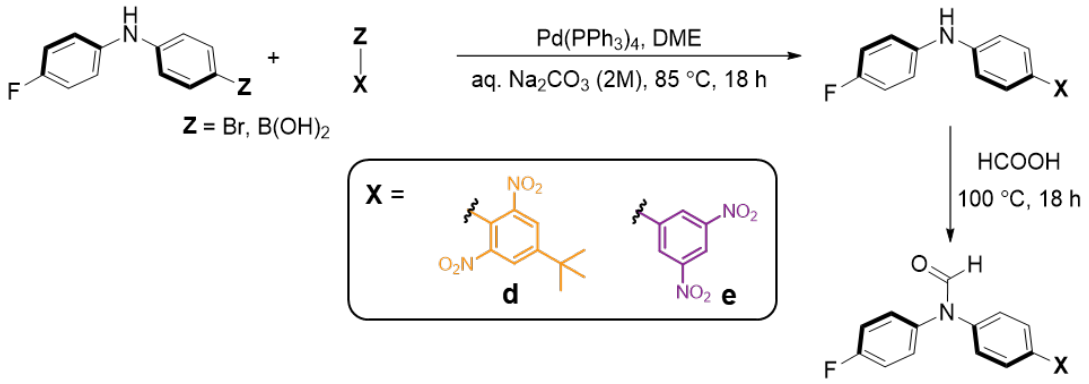

Figure 2.10: The synthesis of compounds **1–d** and **1–e** from the appropriate *N*,*N*-diphenyl amine derivative and subsequent Suzuki-Miyaura coupling and amine formylation. These compounds were synthesised by Dr Ioulia K. Mati.[1]

2.4 Results and Discussion

2.4.1 Determination of Equilibrium Constants

With the molecular balances in hand, conformational equilibrium constants, K_X were determined as defined in **Figure 2.11**.

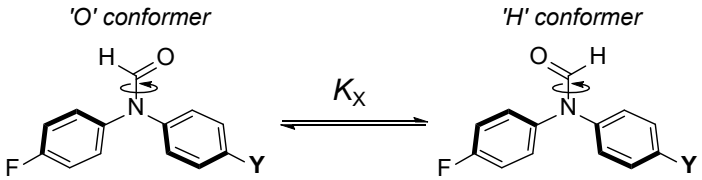

Figure 2.11: Definition of the equilibrium between the 'O' conformer and the 'H' conformer to allow calculation of K_X.

The relative population of the 'H' and the 'O' conformers for each balance was determined through integration of the discreet ^{19}F NMR peaks of the two conformers **(Figure 2.12)** and **Equation 2.1** was used to obtain the equilibrium constant.

$$K_X = \frac{H\ conformer}{O\ conformer} \qquad \textbf{Equation 2.1}$$

Where "H conformer" is the ^{19}F integral of the H conformer and "O conformer" is that of the O conformer.

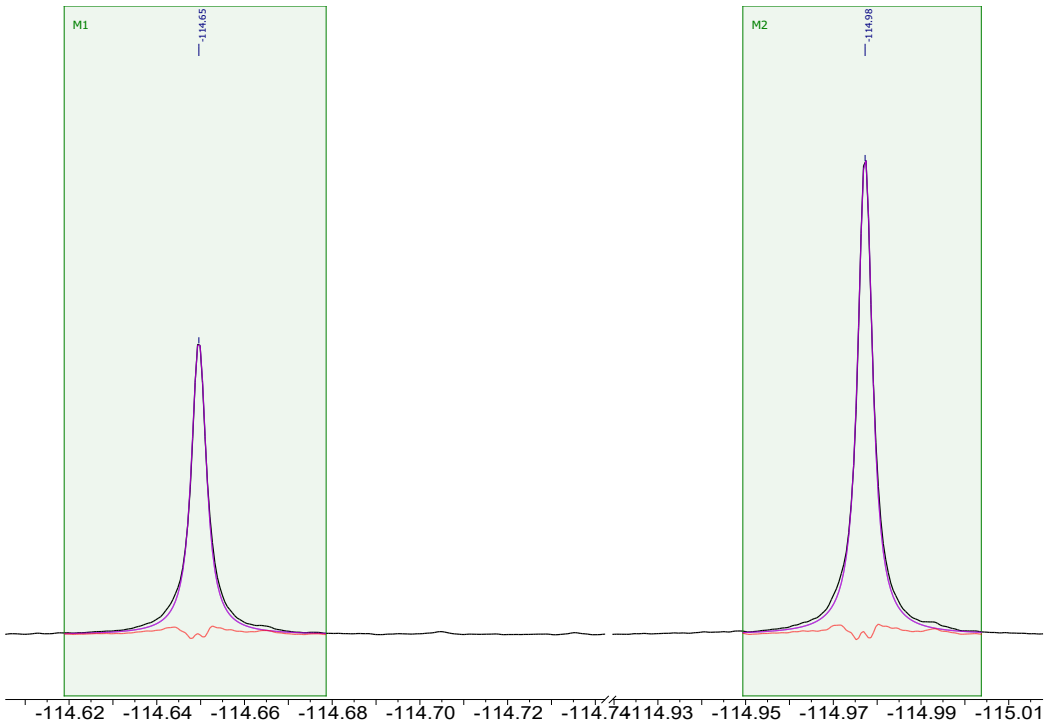

Figure 2.12: Portion of the $^{19}F\{^{1}H\}$ NMR spectrum of molecular balance **1'–Me** showing the fluorine tag peaks of the two conformers observed at room temperature (chloroform-*d*, 376.5 MHz, 298 K). The line fitting used to obtain the relative proportions of each conformer is shown as a green box, with the fitted line being a purple overlay of the black peak trace and the residuals shown as a red line. Data obtained and analysed by RJB.

Thus, to enable correct assignment of K_X, it is important to know which peak on the ^{19}F NMR spectrum belongs to the O conformer and which belongs to the H conformer. To uncover the identity of the peaks of the ^{19}F NMR spectrum, 2D NMR spectroscopy was utilised. The closeness in space between the proton of the amide group and the phenyl protons *ortho* to the amide group as shown in **Figure 2.13** mean that Nuclear Overhauser Effect SpectroscopY (NOESY) can facilitate the assignment of ^{19}F NMR peaks to a particular conformer.

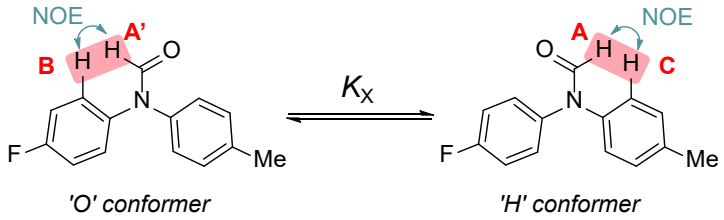

Figure 2.13: Molecular balance **1'–Me** with the NOE interactions in each conformer highlighted.

A cross peak between the amide proton **A'** and the proton assigned to the F-substituted ring, **B**, (**Figure 2.14**) means that the amide proton of this conformer is close in space to the F-substituted ring and therefore peak **A'** corresponds to the O conformer. It follows that peak **A** is that of the H conformer.

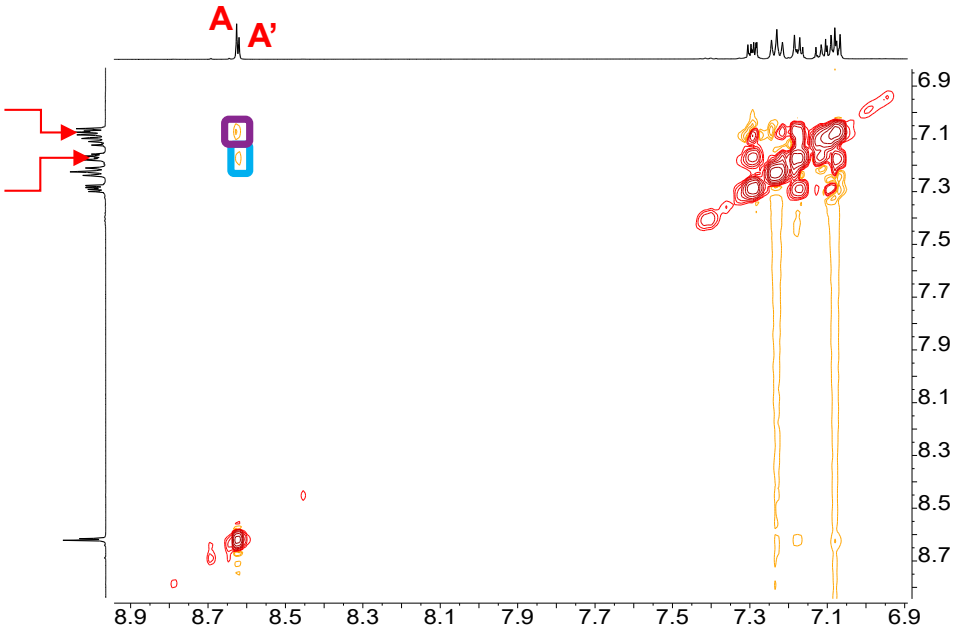

Figure 2.14: Portion of the ^{1}H-^{1}H NOESY spectrum (chloroform-*d*, 500.1 MHz, mixing time = 400 ms, 298 K) of balance **1–Me**. The cross peak between protons **A** and **C** is highlighted with a purple box whereas coupling between **A'** and **B** is highlighted with a blue box. Data obtained and analysed by RJB.

This assignment can be confirmed by ^{13}C-^{1}H Heteronuclear Multiple Bond Correlation (HMBC) NMR spectroscopy. The 'W-effect', as shown in **Figure 2.15**, is a phenomenon wherein a planar 'W' shape exhibits long-range cross-coupling between atoms that are *trans* to each other in the 'W' shape.[49] For the molecular balances

studied, the ^{13}C-^{1}H HMBC cross peaks occur between the amide proton and the carbon atoms bonded to the amide nitrogen atom on the appropriate phenyl ring.

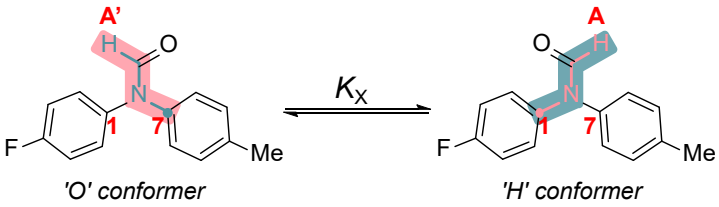

Figure 2.15: The 'W' coupling between the formamide proton and the carbon atom *trans* to it as highlighted for molecular balance **1'–Me**.

The cross peak between proton **A** and carbon **1** and that between proton **A'** and carbon **7** confirms the identity of **A** as the H conformer and **A'** as the O conformer (**Figure 2.16**) in the example of **1'–Me**.

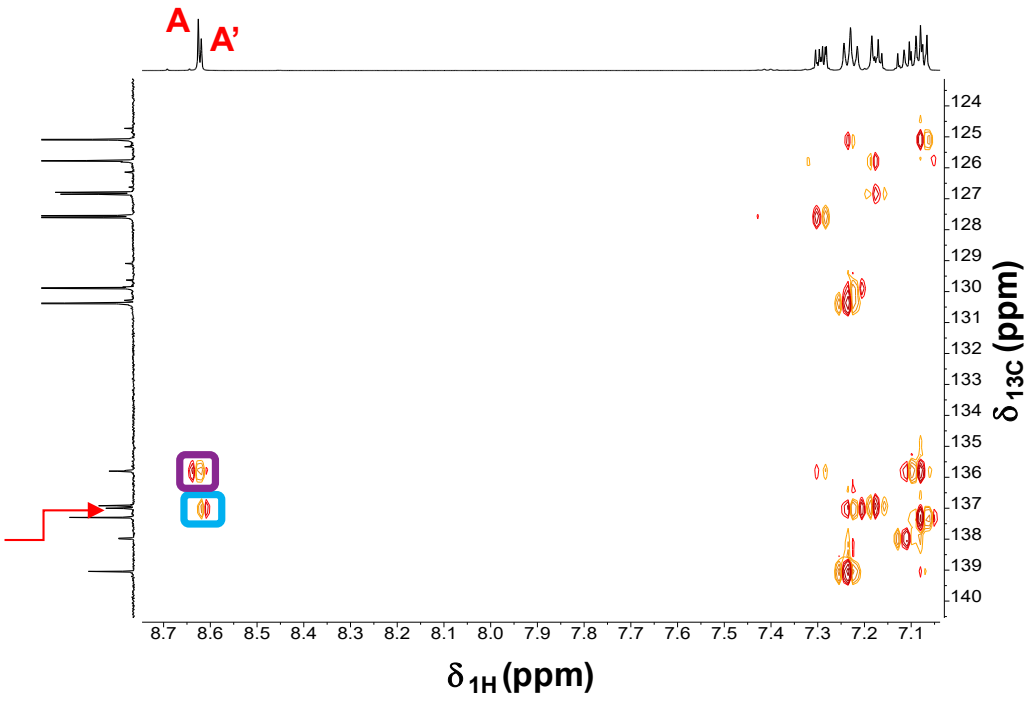

Figure 2.16: HMBC spectrum (chloroform-*d*, 500.1 MHz, 298 K) of **1'–Me**, with the cross peaks between the formamide proton of the 'H' conformer, "**A**" and carbon **1** highlighted with

a purple box. The cross peak between the formamide proton of the 'O' conformer, "**A'**" and carbon **7** highlighted with a green box. Data obtained and analysed by RJB.

The conformer assignment of all molecular balances studied was performed in this way using both 2D NMR techniques in chloroform-*d*. The difference in the ^{19}F NMR chemical shifts between the H and O conformers in benzene-d_6 were compared to that in chloroform-*d*. Outliers of this plot would mean the conformer assignment had swapped in benzene-d_6 relative to chloroform-*d* and in these cases, a full NMR analysis in benzene-d_6 was performed. For the majority of the balances studied, there did not appear to be any outliers so it was assumed the conformer assignment in chloroform-*d* was conserved in benzene-d_6. Therefore, assignment of the conformers in benzene-d_6 could be made based on the relative integrals of the observed ^{19}F NMR resonances.

Conformational equilibria were found to be independent of concentration (**Figure 2.17**) meaning that secondary intermolecular interactions did not influence the conformational equilibrium in the concentration range studied (~ 3 mM).

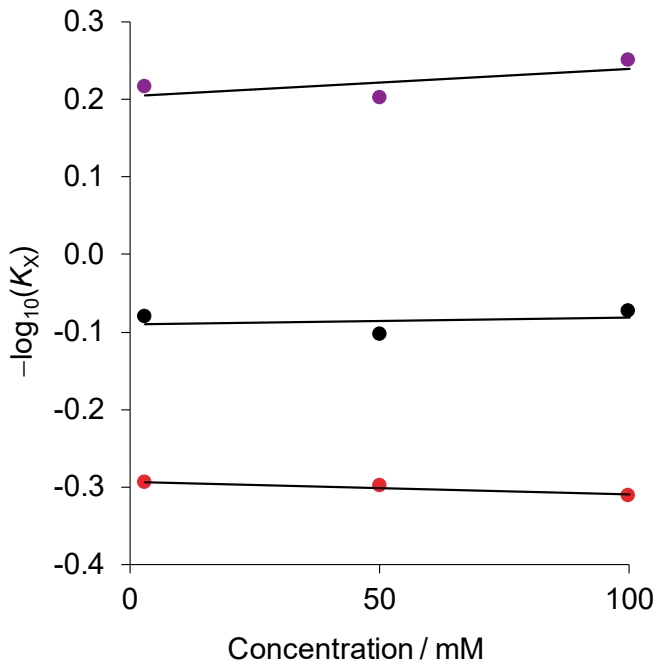

Figure 2.17: Concentration dependence of molecular balances **1–a** (red), **1–e** (purple) and **1'–Ph** (black) over 100 mM range measured by ^{19}F{^{1}H} NMR spectroscopy (376.5 MHz at 298 K) in benzene-d_6. Experimental data of all balances at each concentration were obtained by RJB, except at 3 mM which were obtained by Dr Ioulia K. Mati.[1] Errors were calculated as described in Appendix A and are omitted for clarity. A version of this figure with error bars is given in Appendix A.

2.4.2 Determination of Substituent Constants

It is known that the positions of the conformational equilibria in molecular balances **1'–Y** (**Figure 2.4B**) are governed by substituent-induced changes in the electrostatics of the Y-substituted ring.[3] Substituents that reduce the electrostatic potential of the Y-substituted ring favour the O conformer and those that increase the electrostatic potential favour the H conformer. Thus, classically electron-withdrawing substituents (Br, CN, NO_2, CF_3) favour the O conformer, while classically electron-donating substituents (OMe, Me and NEt_2) favour the H conformer.

The Hammett-style relationship $-\log_{10}(K_X/K_H)$ is used to quantify the effects of substitution on the conformational equilibrium of both molecular balance series **1–X** and **1–Y**, where K_X is the equilibrium constant of substituent X and K_H is the equilibrium constant when X = H, *i.e.* that of balance **1'–H**.[50] Importantly, since classic σ_p Hammett substituent constants are known for all of the Y substituents[50-51] then it is possible to transpose experimentally determined conformational equilibrium constants onto the already established Hammett substituent scale using a calibration plot (**Figure 2.18**).

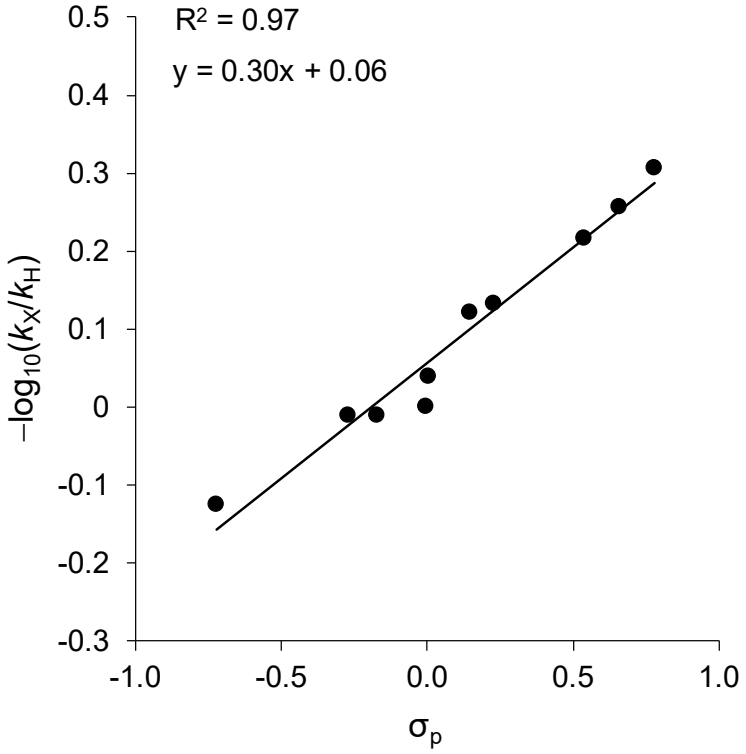

Figure 2.18: Correlation between σ_p Hammett substituent constants values and conformational equilibrium constants of compounds **1'–Y** to transpose experimentally determined conformational equilibrium constants onto to the classic Hammett scale of substituent effects.[50-51] $K_{X/H}$ values measured in benzene-d_6 (376.5 MHz, 298 K).

The strong correlation of the calibration plot shows that conformational equilibrium constants, K_X, encode the transferrable substituent effects previously established by Hammett.[50] Using the equation of a straight line ($y = mx + c$), the following equations (**2.2** and **2.3**) can be defined:

$$\sigma_{p(conf)}\rho + \gamma = -log_{10}\left(\frac{K_X}{K_H}\right) \qquad \textbf{Equation 2.2}$$

$$\sigma_{p(conf)} = \frac{\left(-log_{10}\left(\frac{K_X}{K_H}\right)\right) - \gamma}{\rho} \qquad \textbf{Equation 2.3}$$

Where $\sigma_{p(conf)}$ are substituent constants scaled onto the classic Hammett scale and ρ is the Hammett reaction constant defining the proportionality between the log of the conformational equilibrium constants, K_X, and $\sigma_{p(conf)}$. The value of ρ is obtained from the gradient of the best fit line of **Figure 2.18** and is thus 0.3. The final term, γ, corrects for non-ideal behaviour and is the intercept of the best fit line of **Figure 2.18** and is 0.06. $K_{X/H}$ are the equilibrium constants of substituent X and of compound **1'–H** respectively.

The experimental equilibrium constants of the molecular balances in both series **1–X** and **1'–Y** (**Figure 2.4**) were measured in benzene-d_6 at 298 K and the relationship in **Figure 2.18** was used to derive $\sigma_{p(conf)}$ Hammett substituent constants (**Table 2.1**).[50,52-54]

Table 2.1: $-\log_{10}(K_X/K_H)$ values of all molecular balances studied from the experimental equilibrium constants (K_X) measured in benzene-d_6 (376.5 MHz, 298 K) and substituent constants, $\sigma_{p(conf)}$, obtained from **Equation 2.3**. Values of K_X for **1–I** to **1–n** inclusive and **1'–Me** obtained by RJB, all other **1'–Y** K_X values calculated by RJB from previously reported ΔG values[2-3] and all other **1–X** K_X values calculated by RJB from ΔG values obtained by Dr Ioulia K. Mati.[1] Analysis of all compounds to obtain $-\log_{10}(K_X/K_H)$ and $\sigma_{p(conf)}$ by RJB. Error analysis details can be found in Appendix A.

Compound	K_X	$-\log_{10}(K_X/K_H)$	$\sigma_{p(conf)}$[a]
1'–H	1.32	0.00	–0.21 (0.00)
1'–OMe	1.35	–0.01	–0.25 (-0.27)
1'–NEt_2	1.75	–0.12	–0.66 (-0.72)
1'–Me	1.20	+0.04	–0.07 (-0.17)
1'–Ph	1.20	+0.04	–0.07 (+0.01)
1'–CN	0.73	+0.26	+0.72 (+0.66)
1'–NO_2	0.65	+0.31	+0.90 (+0.78)
1'–CF_3	0.85	+0.19	+0.44 (+0.54)
1'–$COCH_3$	0.89	+0.17	+0.37 (+0.50)
1'–Br	0.97	+0.13	+0.25 (+0.23)
1'–F	1.00	+0.12	+0.22 (+0.15)
1–a	1.97	–0.18	–0.85
1–b	1.13	+0.07	+0.03
1–c	0.82	+0.21	+0.54
1–d	1.28	+0.01	–0.17
1–e	0.61	+0.34	+1.00
1–f	1.30	+0.01	–0.19
1–g	1.33	0.00	–0.23
1–h	1.08	+0.09	+0.10
1–i	1.45	–0.04	–0.37
1–j	1.23	+0.03	–0.11
1–k	1.40	–0.03	–0.31
1–l	0.82	+0.20	+0.53
1–m	1.27	+0.02	–0.15
1–n	0.73	+0.26	+0.72

[a] Hammett σ_p constant values quoted in brackets for the **1'–Y** series.[50-51]

2.4.3 Analysis of Experimentally Determined Substituent Constants

The first subset of compounds within the **1–X** series that display unusual experimental behaviour is comprised of compounds **1–a**, **1–b** and **1–c** (**Figure 2.19**).

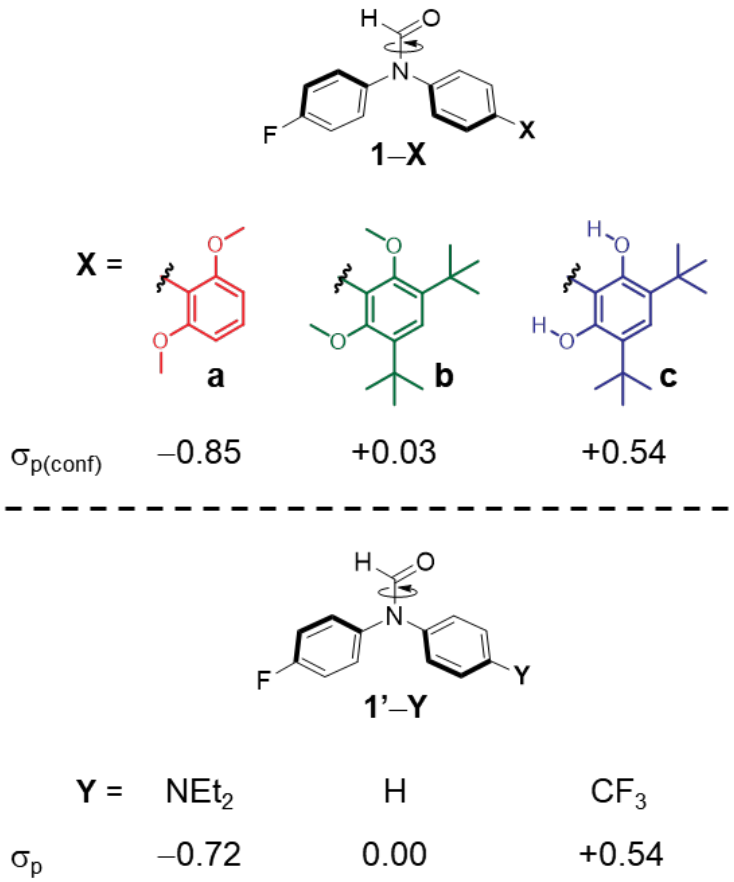

Figure 2.19: Subset of compounds that exhibit experimental behaviour unexpected from rationalisation by through-bond substituent effects, shown with **1'–Y** compounds that have similar $\sigma_{p(conf)}$ values as **1–a**, **1–b** and **1–c**.

The **1'–Y** series can provide useful benchmarks for the characterisation of the behaviour of the **1–X** series. Thus, through comparison with the **1'–Y** balances, the X substituent in molecular balance **1–a** can be described as an electron-donating group, whereas **1–b** would be considered electronically neutral and **1–c** would be described as an electron-withdrawing group. Strikingly, the dimethoxyphenyl substituent in **1–a** ($\sigma_{p(conf)} = -0.80$) would be classically described as being substantially more "electron-

donating" than an NEt_2 group (σ_p = –0.72 and control compound **1'–NEt$_2$**).[50] In contrast, **1–b** contains an electronically neutral substituent ($\sigma_{p(conf)}$ = +0.03). Part of the difference in $\sigma_{p(conf)}$ can be attributed to the addition of two *tert*-butyl groups, but these are known to be only weakly electron-donating (σ_m = –0.10 per *tert*-butyl group),[50] relative to a total change in $\sigma_{p(conf)}$ of –0.88 between **1–a** and **1–b**.

Another striking observation is the $\sigma_{p(conf)}$ value of **1–c** which is +0.54 that means it would be classically described as a strong "electron-withdrawing" substituent, similar in electronic influence as a trifluoromethyl group (σ_p = +0.54 and control compound **1'–CF$_3$**).[50] This observation contrasts with expectations based on traditional through-bond consideration of substituent effects; since hydroxy groups are stronger electron-donors than methoxy groups (σ_p = –0.37 vs. –0.27, respectively),[50] then it might instead be anticipated that the dihydroxylated phenyl substituent in **1–c** would be more electron-donating in nature than the dimethoxy equivalent in **1–b**. Clearly, such differences can only be rationalised on the basis of through-space electrostatic field effects.

The rationalisation of the experimental behaviour of compounds **1–a**, **1–b** and **1–c** through their $\sigma_{p(conf)}$ values is emboldened through analysis of the ^{1}H NMR spectra of these compounds. Chemical shifts in NMR spectroscopy are known to give access to useful experimental inference of the electronic nature of aromatic rings.[55] Thus, the ^{1}H NMR resonances of the protons of the Y-substituted rings of both the **1'–Y** and **1–X** series provide an additional assessment of substituent effects. The lower the electric field (or in classic, but perhaps imprecise terms, the lower the electron density), the higher the chemical shift of the protons (**Table 2.2**). In particular, comparison of the *ortho* and *meta* protons on the Y-substituted rings relative to the formamide of the 'H' and 'O' conformers is useful (**Figure 2.20**). This phenomenon is exemplified through the comparison of the chemical shifts of **1'–OMe** and **1'–NO$_2$**.

Table 2.2: ^{1}H chemical shifts of the Y-substituted ring for balances **1'–Y** and **1–X** in chloroform-*d* (500.1 MHz, 298 K). Values for compounds **1'–Y** previously reported[2-3] except that of **1'–Me** which was obtained by RJB. Values for compounds **1**–**a** to **1**–**h** inclusive obtained by Dr Ioulia K. Mati and those of **1–l** to **1–n** inclusive obtained by RJB.

	Chemical shift (ppm) of *ortho* proton in $CDCl_3$		**Chemical shift (ppm) of *meta* proton in $CDCl_3$**	
Compound	**'H' conformer**	**'O' conformer**	**'H' conformer**	**'O' conformer**
1'–H	7.16	7.29	7.42	7.40
1'–OMe	7.11	7.19	6.94	6.91
1'–NEt_2	7.01	7.05	6.66	6.64
1'–Me	7.07	7.18	7.24	7.22
1'–Ph	7.23	7.35	7.63	7.60
1'–CN	7.20	7.44	7.68	7.63
1'–NO_2	7.29	7.54	8.29	8.25
1'–CF_3	7.24	7.46	7.70	7.66
1'–$COCH_3$	7.22	7.44	8.02	7.99
1'–Br	7.03	7.18	7.54	7.51
1–a	7.17	7.31	7.41	7.39
1–b	7.23	7.37	7.59	7.55
1–c	7.37	7.54	7.51	7.48
1–d	7.18	7.40	7.40	7.25
1–e	7.34	7.52	7.74	7.70
1–f	7.21	7.36	7.21	7.10
1–g	7.21	7.37	7.23	7.19
1–h	7.25	7.37	7.52	7.50
1–i	7.20	7.36	7.61	7.57
1–j	7.24	7.38	7.38	7.36
1–k	7.21	7.60	7.62	7.35
1–l	7.60	7.72	7.46	7.33
1–m	7.22	7.35	7.60	7.57
1–n	7.23	7.34	7.57	7.61

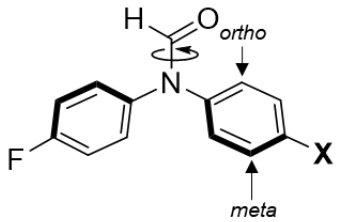

Figure 2.20: Position of "*ortho*" and "*meta*" referred to in **Table 2.2** and in the accompanying discussion regarding ^{1}H NMR chemical shifts. Nomenclature is application to both series **1'–Y** and **1–X**.

The chemical shifts of the aromatic protons of the "electron-rich" **1'–OMe** are lower than those of **1'–NO$_2$** for both the protons *ortho* but particularly those *meta* to the amide group, the latter of which are closest to the substituent. Comparing the chemical shifts of the Y-substituted rings of **1–a**, **1–b** and **1–c** shows that the trend in experimental behaviour that is described by $\sigma_{p(conf)}$ is held in the ^{1}H NMR spectra analysis of these compounds. According to $\sigma_{p(conf)}$, moving from **1–a** to **1–c** results in increasing "electron-withdrawing" behaviour, which would classically be attributed to a "less electron-rich" Y-substituted ring. This is mirrored in the ^{1}H NMR chemical resonances of the Y-substituted ring of these compounds that become more downfield in progressing from compound **1–a** to **1–c** (**Table 2.2**).

Another subset of compounds within the **1–X** series that show unusual experimental behaviour are **1–d** and **1–e** where moving the NO_2 groups around the X-substituted ring results in large differences in $\sigma_{p(conf)}$ (**Figure 2.21**).

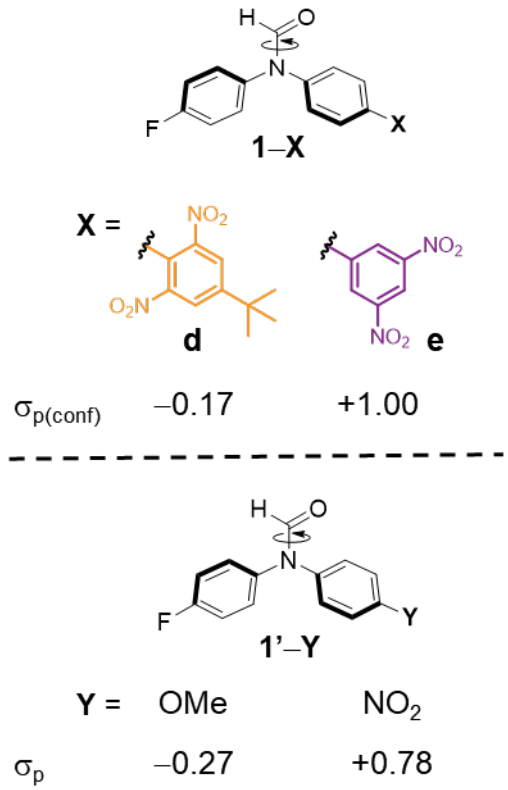

Figure 2.21: Compounds that exhibit experimental behaviour unexpected from rationalisation by through-bond substituent effects, shown with **1'–Y** compounds that have similar $\sigma_{p(conf)}$ values as **1–d** and **1–e**.

In compound **1–e** where the nitro groups are *meta* to the biphenyl bond, the $\sigma_{p(conf)}$ value is +1.00, which would classically be described as even more "electron-withdrawing" than the directly connected nitro substituent in compound **1'–NO₂** (σ_p = +0.78).[50] This result is unsurprising given the conjugated phenyl substituent contains two nitro groups. However, comparison of the $\sigma_{p(conf)}$ values reveals the experimental behaviour of compound **1–d**, where the nitro group is *ortho* to the biphenyl bond ($\sigma_{p(conf)}$ = –0.17), to be akin to that of a methoxy group (σ_p = –0.27 and compound **1'–OMe**).[50] Thus, the substituent in compound **1–d**, which contains traditionally electron-withdrawing nitro groups, is acting like a strongly electron-donating group. One may be tempted, again, to explain this striking reversal of the expected behaviour of **1–d** being the result of the *tert*-butyl group present, but the strength of the apparent "electron-donating" behaviour of this compound cannot be accounted for from the weak electron-donating nature of *tert*-butyl groups.

The disparity in experimental behaviour between compounds **1–d** and **1–e** is further displayed in the comparison of their aromatic ^{1}H NMR chemical shifts (**Table 2.2**). The chemical shifts in **1–d** more shielded than those of **1–e**, providing additional experimental evidence that **1–d** acts like an electron-donating group and **1–e** as an electron-withdrawing group, running in accordance with the evaluation of these compounds using $\sigma_{p(conf)}$.

2.4.4 Computational Analysis

To gain further insight into the interesting experimental results highlighted by their $\sigma_{p(conf)}$ values, the molecular balances studied were subject to computational modelling. As discussed in **Chapter 1**, electrostatic potential (ESP) surfaces are useful tools in the visualisation of non-covalent interactions and have been instrumental in studies of through-space substituent effects.[38-40, 43] Therefore, it was hoped that analysis of the molecular balances in this study would be aided through visualisation of their substituent effects *via* ESP surfaces and slices.

The equilibrium geometries of simple biphenyl fragments of the molecular balances were obtained at the DFT/B3LYP/6–31G* level of theory using Spartan '14. The minimised ESP surfaces and slices of these geometries were calculated and ESP values taken *ipso* to where the fragment would bond to the amide group of the full molecular balance (ESP_{ipso}) and *ortho* to this position (ESP_{ortho}). It was found that ESP_{ipso} gave the best correlation between with $\sigma_{p(conf)}$, with an R^2 of 0.91 (**Figure 2.22**).

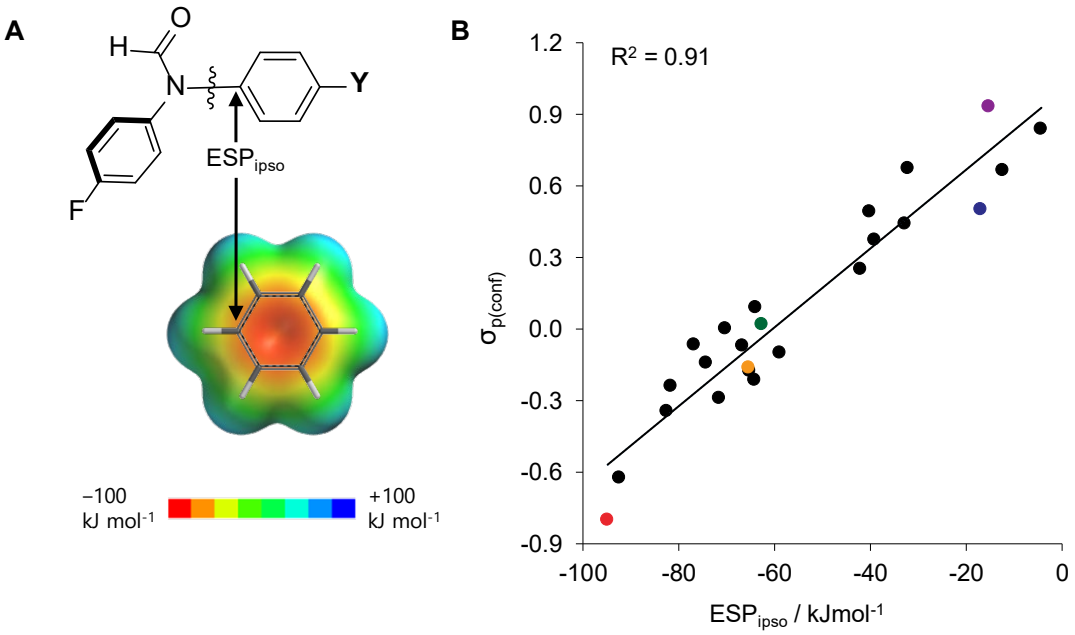

Figure 2.22: Relationship between calculated ESP_{ipso} values and experimentally determined substituent constants. **(A)** Position of ESP_{ipso} value measurement on as shown on the ChemDraw render of the molecular balances studied, with fragmentation taking place as indicated by the wavy line (**TOP**) and on the ESP surface of the fragment for molecular balance **1'–H** (**BOTTOM**). **(B)** Plot of ESP_{ipso} against $\sigma_{p(conf)}$ for all balances with the interesting examples discussed in ***Section 2.4.3*** highlighted according to their colour in **Figure 2.4**. All errors were less than ±0.12 kJ mol^{-1} and discussed in Appendix A. Errors bars are omitted for clarity but a version with their inclusion is given in Appendix A. The values for **1'–Y** balances (except **1'–Me**) were previously reported[2-3] and values for compounds **1–a** to **1–h** inclusive obtained by Dr Ioulia K. Mati and those of **1–l** to **1–n** inclusive obtained by RJB. Structures and surfaces were minimised using DFT/B3LYP/6–31G* in Spartan '14. The ESP values over the *ipso* position were taken at the 0.002 electron/Bohr^3 isosurface as indicated.

The strong correlation between the experimentally obtained $\sigma_{p(conf)}$ values for all of the molecular balances studied and their ESP_{ipso} values (**Table 2.3**) indicates that electrostatic interactions are important to the experimental equilibrium constants, K_X. In addition, this strong correlation shows that the experimentally measured substituent effects of the molecular balances studied can be assessed and explained through their ESP values, surfaces and slices.

Table 2.3: ESP_{ipso} values of all compounds within the **1'–Y** and **1–X** series of molecular balances. All structures and surfaces (from which ESP_{ipso} values were calculated) were minimised and calculated using DFT/B3LYP/6–31G* in Spartan '14. Full details on ESP_{ipso} calculation and error analysis given in Appendix A.

Compound	ESP_{ipso} / kJ mol^{-1}
1'–H	–70.4
1'–OMe	–81.8
1'–NEt_2	–92.5
1'–Me	–76.9
1'–Ph	–66.8
1'–CN	–12.5
1'–NO_2	–4.4
1'–CF_3	–32.9
1'–$COCH_3$	–39.3
1'–Br	–42.2
1–a	–95.0
1–b	–62.8
1–c	–17.2
1–d	–65.6
1–e	–15.6
1–f	–65.5
1–g	–64.3
1–h	–64.1
1–i	–82.7
1–j	–59.0
1–k	–71.7
1–l	–40.2
1–m	–74.4
1–n	–32.3

ESPs provide a visual and numerical measure of how much the local electron density shields the nuclear charge at a given position in space. More precisely, the ESP equates to the energy of the interaction between a hypothetical point positive charge and the

combined electric field (arising from the sum of nuclear and electronic charges) at a given position. Negative electrostatic potentials are shown as red on the ESP surfaces and slices presented in this thesis and indicate regions where the electronic charge is greater than the nuclear charge. Positive potentials are blue in colour and indicate regions where the electron density is insufficient to shield the nearby positive nuclear charges. Comparison of the ESP surfaces of **1'–OMe** and **1'–NO_2** (**Figure 2.23**) show that the ESP_{ipso} of the former is more negative than that of **1'–H**, which is indicated by a more intense red colour at this position. In contrast, the ESP_{ipso} of **1'–NO_2** is less negative than that of **1'–H** and the colour at this position on the ESP surface is accordingly more blue coloured. ESP slices (see ***Section A.1***) show the same phenomenon and simply map the same data plotted through-space rather than on an electron density isosurface.

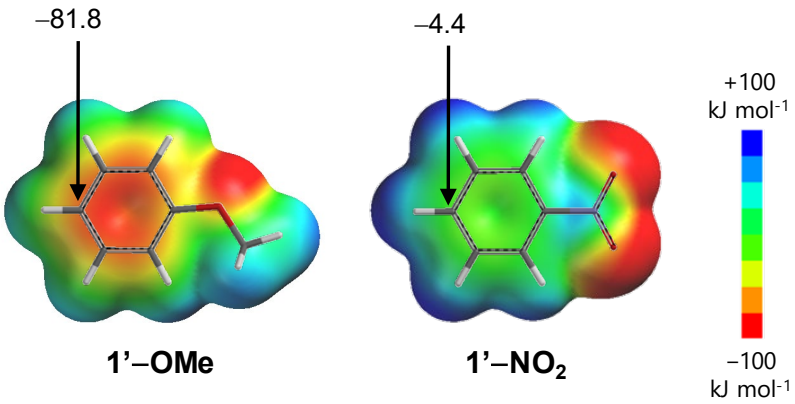

Figure 2.23: ESP surfaces of **1'–OMe** and **1'–NO_2** with ESP_{ipso} values given in kJ mol^{-1}. Structures and surfaces were minimised using DFT/B3LYP/6–31G* in Spartan '14. The ESP values over the *ipso* position were taken at the 0.002 electron/$Bohr^3$ isosurface as indicated. All surfaces were scaled from –100 to +100 kJ mol^{-1}.

To investigate the interesting experimental results highlighted in ***Section 2.4.3***, the ESP surfaces and slices of the substituents of interest are presented alongside the $\sigma_{p(conf)}$ values of these compounds and their experimentally similar **1'–Y** control substituted phenyl rings. The computational and experimental results of these compounds are distributed along a scale of $\sigma_{p(conf)}$ to facilitate the comparison between the experimental behaviour of these compounds and their computationally derived

ESP surfaces and slices (**Figure 2.24**). All surfaces and slices were scaled from −100 kJ mol^{-1} (red) to +100 kJ mol^{-1} (blue) to enable straightforward comparison between compounds.

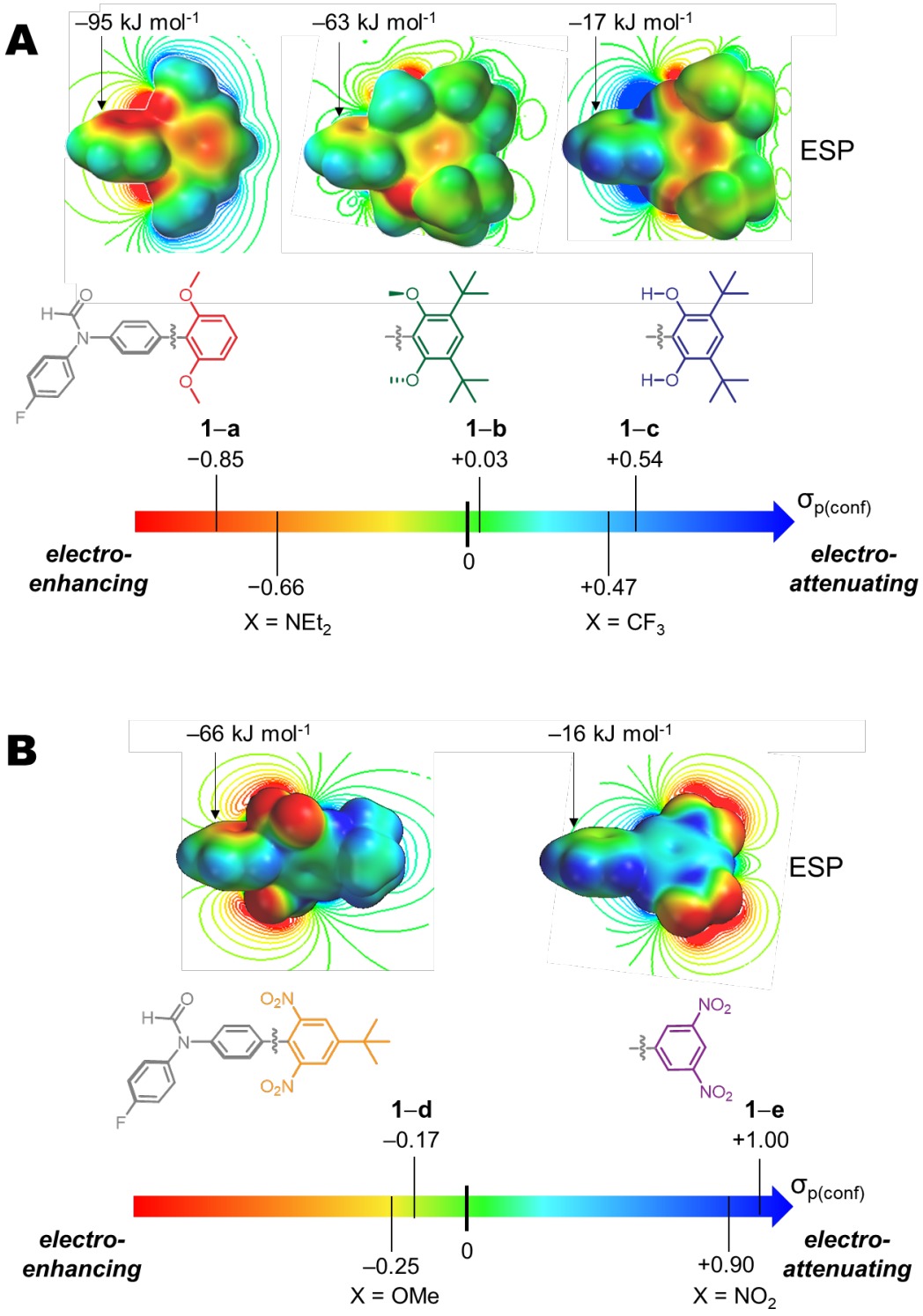

Figure 2.24: (A) The ESP surfaces and slices (**TOP**) of molecular balances **1–a**, **1–b** and **1–c** (ESP values quoted in kJ mol^{-1}) and the $\sigma_{p(conf)}$ values of these compounds and **1'–NEt$_2$**, **1'–H** and **1'–CF$_3$** which are distributed along a scale of $\sigma_{p(conf)}$ (**BOTTOM**). **(B)** The ESP surfaces and slices (**TOP**) for compounds **1–d** and **1–e** (ESP values quoted in kJ mol^{-1}) with the $\sigma_{p(conf)}$ values of **1'–OMe** and **1'–NO$_2$** (**BOTTOM**). All structures and surfaces were minimised and calculated using DFT/B3LYP/6–31G* in Spartan '14. The ESP surfaces and slices of all compounds in both the **1'–Y** and **1–X** series are in Appendix A.

The computational and experimental results of the substituents in compound **1–a**, **1–b** and **1–c** are shown in **Figure 2.24A**. The methoxy oxygen atoms in compound **1–a** are orientated such that they influence the electrostatics of the Y-substituted ring by perturbing the local electrostatic field over the Y-substituted ring. This effect is mirrored in the strong red colour of the Y-substituted ring in the ESP surface of compound **1–a** and the correspondingly highly negative ESP_{ipso} value of −95.0 kJ mol^{-1}. In contrast, the electron-rich lone pairs of the methoxy oxygen atoms in **1–b** are twisted away from the Y-substituted ring, due to the steric bulk of the flanking *tert*-butyl groups. The resulting change in the through-space substituent effects is reflected in the ESPs; the ESP_{ipso} in **1–b** is only −62.8 kJ mol^{-1} and the ESP slice indicates that the electron density of the lone pairs instead point away from the Y-substituted ring.

The Kirkwood-Westheimer electrostatic model predicts such spatial dependence on through-space field substituent effects.[56-60] Thus, through consideration of the ESP slices of **1–a** and **1–b**, it can be seen that the large difference in the experimental behaviour of these two compounds is manifested through the conformationally tuneable through-space effect of the methoxy groups, and not to through-bond substituent effects on the aryl π-system of the Y-substituted ring. Such a finding is in accord with Wheeler and Houk who found that the influence of substituents on aromatic stacking is dominated by through-space effects rather than through-bond electronic polarisation of the aryl π-system.[38, 40, 61] The observation in Wheeler and Houk's study was entirely computational in nature,[61] whereas this work is a combines computational and empirical evidence to confirm the experimental significance of through-space substituent effects.

The twisting of the methoxy groups due to steric bulk in **1–b** as shown by the computationally derived structures of the biphenyl fragments of **1–a** and **1–b** is supported by ^{1}H NMR resonances of the Y-substituted ring as these resonances contain conformational information of these compounds. In particular, the ^{1}H resonances of the methoxy groups sheds light on their respective orientations with respect to the Y-substituted ring. For compound **1–a**, the chemical shift of the methyl protons is 3.13 ppm, whereas for **1–b** it is 3.76 ppm (**Table 2.2**). The difference in environment

between these compounds is due to their differing conformations which change the spatial relation of the methyl group to the Y-substituted ring. When the methoxy groups point away from this ring, as in **1–a**, the methyl chemical shift is mainly influenced by the external magnetic field of the spectrometer. However, when the methyl protons reside close in space to the Y-substituted ring, the induced magnetic field of this ring is in the opposite direction to the externally applied field and causes these protons to resonate at a higher chemical shift.[62] Thus, the proposal that the through-space influence of the methoxy group is switched off on going from compound **1-a** to **1–b** by a sterically induced change in conformation is confirmed by the ^{1}H NMR spectroscopic evidence.

Given that the substituent effects in **1–a** and **1–b** are dominated by through-space effects, the use of classic descriptors such as "electron-donating" and "electron-withdrawing" are somewhat misleading. Such terminology speaks to the underlying assumption of the these effects being dominated by through-bond substituent effects. As such, a new set of terms are proposed from the outcomes of the present study that do not assume the origin of the substituent effect on the system; these are "electro-attenuating" and "electro-enhancing". These new terms focus instead on the overall effect of the substituent and for those that enhance the negative electrostatics of the system, the term is "electro-enhancing" and likewise those that attenuate the negative electrostatics of the system, these are termed "electro-attenuating". An example of this new terminology is given in **Figure 2.25** for nitrobenzene, with the negative side of the nitro group being termed as being "electro-enhanced" whereas the aryl ring bonded to the nitro group is described as being "electro-attenuated".

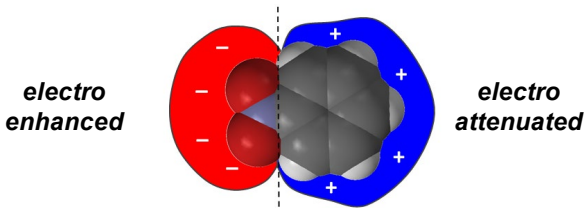

Figure 2.25: An example of the terms "electro attenuation" and " electro enhancement" for nitrobenzene.

Another example of the importance of the geometry of the field perturbation in relation to the Y-substituted ring is in compound **1–c**. In comparison to **1–b**, the behaviour of **1–c** is akin to that of the traditionally electron-withdrawing trifluoromethyl group of **1'–CF$_3$**. Comparison of their ESP slices unveils the cause of such disparity in their experimental behaviour (**Figure 2.24A**). The oxygen lone pairs of the hydroxyl groups in both **1–b** and **1–c** are orientated away from the Y-substituted ring, but the positively charged protons in the dihydroxyl compound point towards the **1–c** ring, reducing the electrostatic potential over the Y-substituted ring. Thus, the Y-substituted ring in **1–c** has the least negative ESP$_{ipso}$ (−17.2 kJ mol^{-1}) in this series of compounds. Since this effect is manifested by through-space field effects, describing the behaviour of the substituent in **1–c** as "electron-withdrawing" is incorrect; "electro-attenuating" instead provides a more accurate description.

For the nitro-containing molecular balances **1–d** and **1–e**, the ESP slices are again useful to examine the differences between these compounds (**Figure 2.24B**). The striking disparity in behaviour between these compounds as a result of changing the position of the nitro groups is also accompanied by a difference in the position of the through-space influence of the nitro groups. The positioning of the nitro groups in **1–d** electro-enhance the Y-substituted ring, whereas the *meta*-positioned nitro groups in **1–e** have an electro-attenuating influence. This difference is accompanied by a difference in the ESP$_{ipso}$ values of 50.5 kJ mol^{-1}, reflected in the increased red colour of the Y-substituted ring on the ESP surface for **1–d** than **1–e** (**Figure 2.24B**). Thus, the through-space electro-enhancing behaviour of the nitro groups in **1–d**, runs in contrast to its well-established through-bond behaviour.[50] This orthogonality of the through-space and through-bond effects of the nitro group is similar to that observed by Lectka *et. al.* for fluorine which acts as an activating group to electrophilic aromatic substitution *via* through-space effects, but is deactivating through its through-bond behaviour.[63] In addition, such reversal of experimental behaviour between the through-bond and through-space nature of a substituent was observed in Stock and Golden's study of dissociation constants for 8-substituted 9,10-ethanoanthracene-1-carboxylic acids.[64]

The electrostatic analysis presented above also sheds light on the behaviour of other subsets of compounds within the **1–X** series. Compounds **1–i**, **1–k** and **1–m**, where the methoxy group moves from being *ortho* to the biphenyl bond in **1–i** to being *para* to it in **1–m** have decreasingly electro-enhancing experimental behaviour, as encoded by $\sigma_{p(conf)}$ (**Table 2.1**). This is explained by an electro-enhancing through-space transmission of methoxy group substituent effects in compound **1–i** which is minimal for compound **1–k** and not present for **1–m** as seen in their ESP slices (**Figure 2.26**) and mirrored in their generally increasingly less negative ESP_{ipso} values (**Table 2.3**). The remains for both rotamers of **1–k**, *via* rotation around the C–O bond. The ΔESP_{ipso} between these rotamers is 3.9 kJ mol^{-1} which is a small difference in ESP_{ipso} values compared to those between **1–i** and either **1–k** or **1–m**.

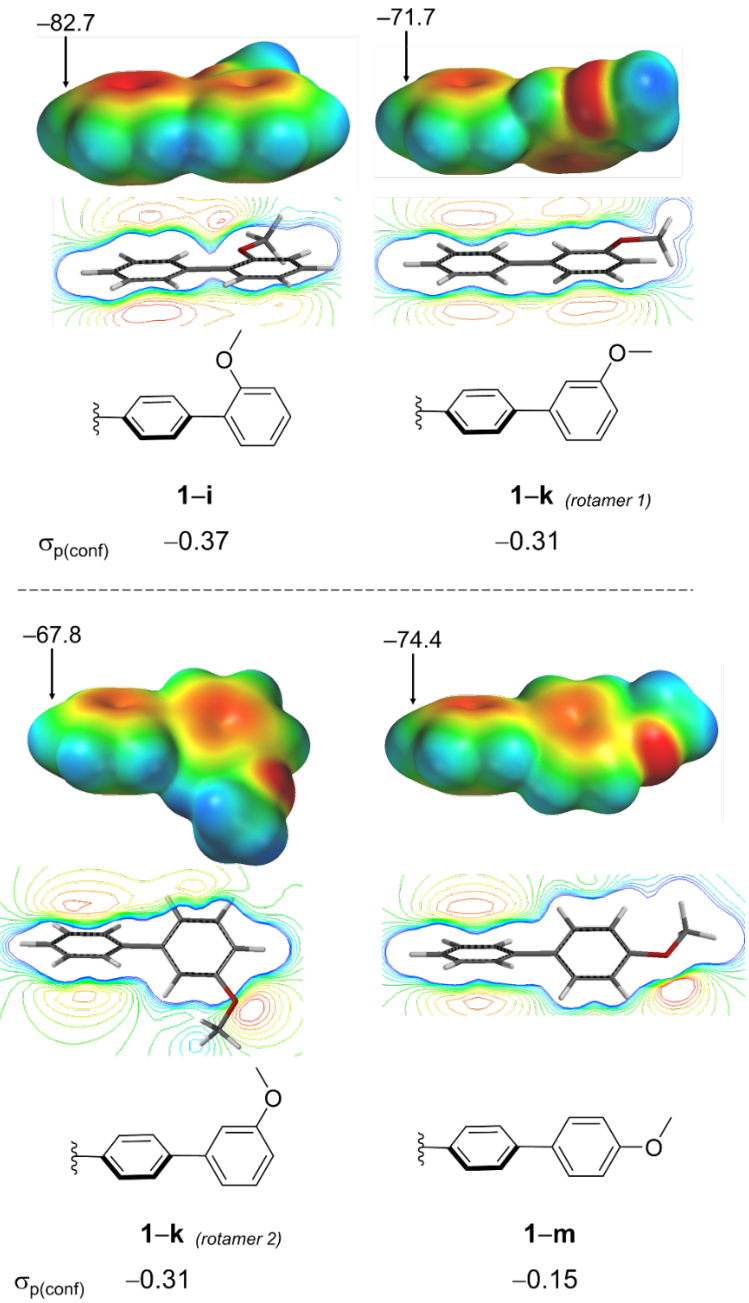

Figure 2.26: The ESP surfaces (**TOP**) and slices (**MIDDLE**) of molecular balances **1–i**, **1–k** (both rotamers) and **1–m** (ESP values quoted in kJ mol^{-1}). All structures and surfaces were minimised and calculated using DFT/B3LYP/6–31G* in Spartan '14. The ESP surfaces and slices of all compounds in both the **1'–Y** and **1–X** series are in Appendix A. ESP surfaces and slices scaled from –100 kJ mol^{-1} to +100 kJ mol^{-1}.

A similar trend is seen for compounds **1–j**, **1–l** and **1–n**. When the nitro group is *ortho* to the biphenyl bond, as in **1–j**, the experimental behaviour is akin to that of **1'–H** whereas when the nitro group is in the *meta* or *para* positions, the $\sigma_{p(conf)}$ values indicate strongly electro-attenuating behaviour (**Table 2.1**). The ESP slices of these

compounds (**Figure 2.27**) again show that through-space substituent effects of the nitro group in the *ortho* position to the biphenyl bond are in operation and influence the electrostatics, causing behaviour that is the opposite to what is expected by its through-bond behaviour.

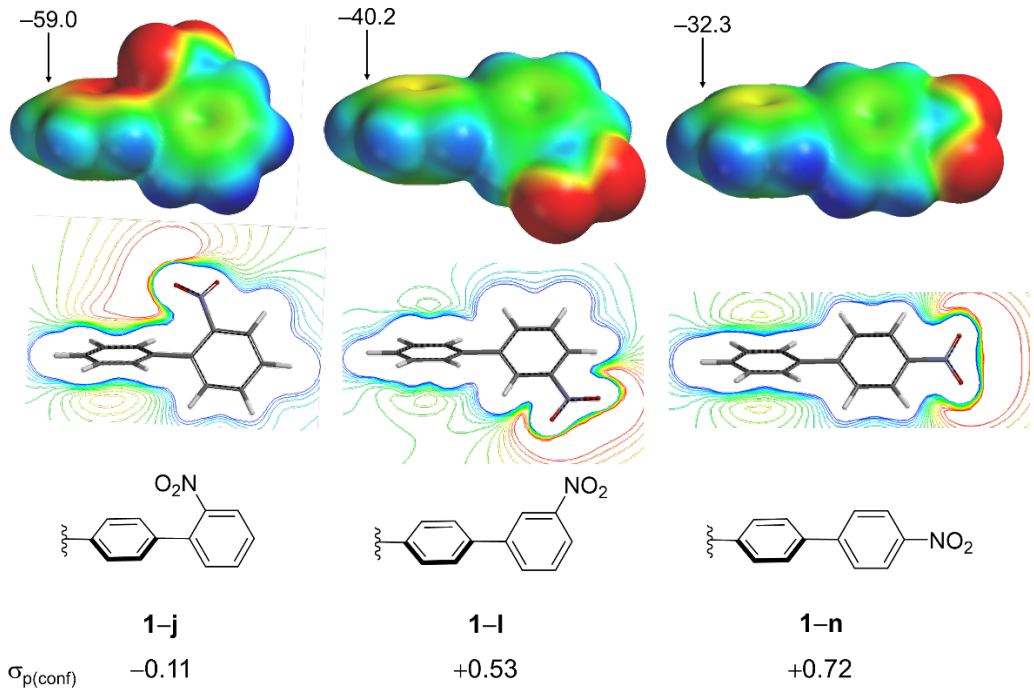

Figure 2.27: The ESP surfaces (**TOP**) and slices (**MIDDLE**) of molecular balances **1–j**, **1–l** and **1–n** (ESP values quoted in kJ mol^{-1}). All structures and surfaces were minimised and calculated using DFT/B3LYP/6–31G* in Spartan '14. The ESP surfaces and slices of all compounds in both the **1'–Y** and **1–X** series are in Appendix A. ESP surfaces and slices scaled from –100 kJ mol^{-1} to +100 kJ mol^{-1}.

As well as showing the importance of through-space effects in the experimental behaviour of molecular balances **1–a** to **1–e** inclusive, ESP values show that the electronic influence of the *tert*-butyl groups in compounds **1–b** and **1–d** are negligible (**Figure 2.28**).

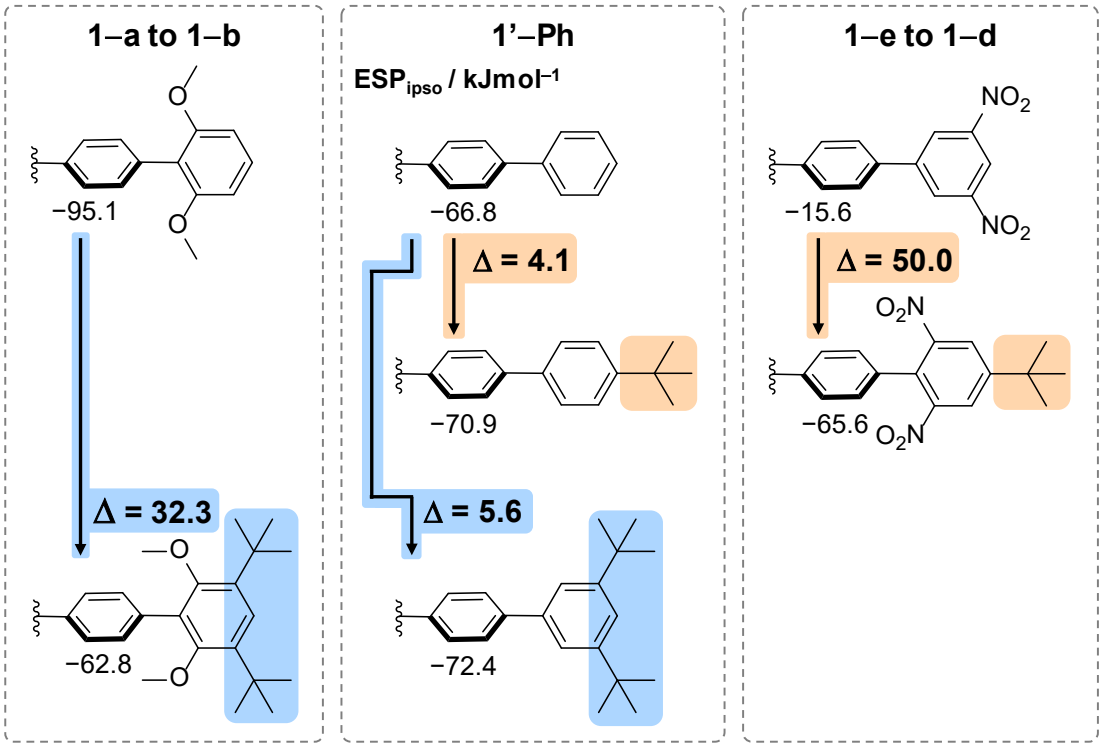

Figure 2.28: The effect of *tert*-butyl groups to the ESP_{ipso} values of compounds **1–b** and **1–d** through comparison with the ESP_{ipso} values of *para* and di-*meta* *tert*-butyl substituted biphenyls. All structures and surfaces (from which ESP_{ipso} values were calculated) were minimised and calculated using DFT/B3LYP/6–31G* in Spartan '14.

The change in the ESP_{ipso} value of the simple biphenyl with the addition of *tert*-butyl groups in the same positions as compounds **1–b** and **1–d** is, at most, 6 kJ mol^{-1}. The significant values of ΔESP_{ipso} between **1–a**/**1–b** and **1–d**/**1–e** cannot be accounted for by the presence of *tert*-butyl groups in **1–b** and **1–d**.

2.5 Solvent Effects on Through-Space Substituent Effects

An important step in quantifying through-space substituent effects and assessing the transferability of the substituent constant derived in ***Section 2.4.2*** is to understand how much the surrounding solvent modulates through-space substituent effects. It was proposed by Kim *et. al.* that the electrostatic nature of through-space substituent effects means that polar solvents are likely to perturb their influence on the properties of organic molecules.[37]

The equilibrium constants used to determine $\sigma_{p(conf)}$ were measured exclusively in benzene-d_6 (***Section 2.4.2***). Assessment of solvent effects on substituent effects in molecular balance series **1'–Y** and **1–X** was performed through measurement of the equilibrium constants in a diverse range of solvents: acetone-d_6, acetonitrile-d_3, chloroform-d, DCM-d_2, diethyl ether, DMSO-d_6, ethanol, ethyl acetate, methanol-d_4 and THF-d_8. The balance concentration in each solvent was 3 mM, where the equilibrium constants were previously established to be independent of concentration (***Section 2.4.1***). The substituent effects in each solvent were quantified by the same method as for benzene-d_6 (***Section 2.4.2***) and the experimental results in each solvent, $-\log_{10}(K_X/K_H)$, were plotted against the ESP_{ipso} values (**Figure 2.29**).

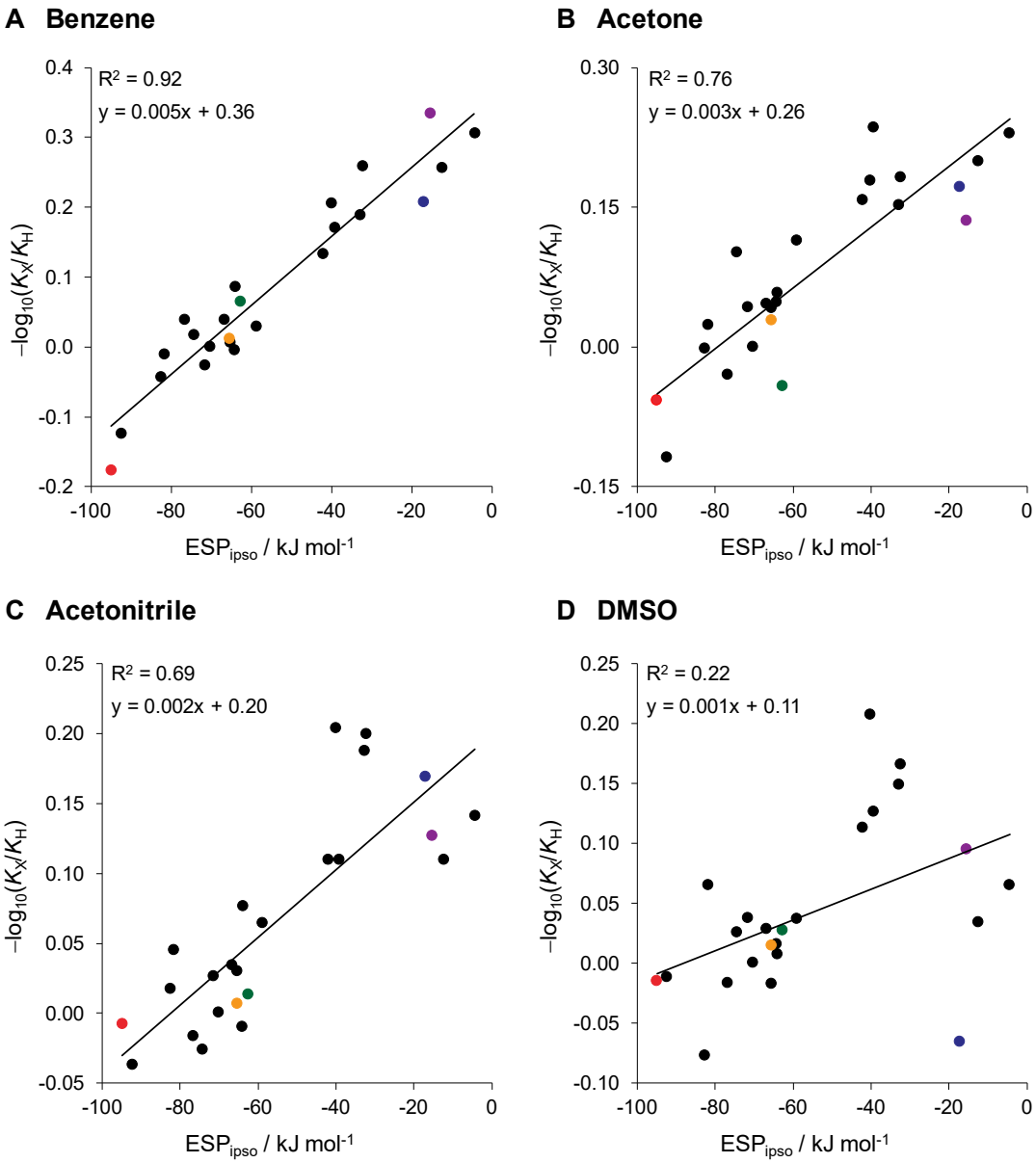

Figure 2.29: Plots of ESP_{ipso} values against $-\log_{10}(K_X/K_H)$ values for all balances obtained in **(A)** benzene-d_6, **(B)** acetone-d_6, **(C)** acetonitrile-d_3 and **(D)** DMSO-d_6. The interesting examples discussed in ***Section 2.4*** are highlighted according to their colour in **Figure 2.4**. Error analysis is given in Appendix A. Structures and surfaces were minimised using DFT/B3LYP/6–31G*. Plots of ESP_{ipso} against all of the other solvents investigated are in Appendix A. Tables with K_X and $-\log(K_X/K_H)$ data of all balances in each solvent are given in Appendix A.

The quality of correlations between ESP_{ipso} and the experimentally derived $-\log_{10}(K_X/K_H)$ values varies over the range of solvents studied. The correlations drop from an R^2 of 0.92 in benzene-d_6 to 0.22 in DMSO-d_6, in line with the increasing polarity of the solvent. Thus, as the solvents polarity increases, so does the solvents

ability to form intermolecular interactions with the molecular balances strong enough to perturb intramolecular interactions. Such competitive solvents also result in shallower best fit line gradients, showing that the solvent effects are leading to a dampening of the intramolecular interactions on the conformational equilibrium. This finding is unsurprising as the conformational equilibrium of these balances are known to be governed by the electrostatics of the Y-substituted ring of these balances[3] and through-space effects are electrostatic in nature.[37, 55-58]

2.5.1 Dissecting Solvent Effects

Solvent effects have been previously dissected from the Cockroft balance to unveil the pseudo gas phase behaviour of a subset of the molecular balances in series **1'–Y**.[2] To do this, a modification of Hunter's solvation model[65] was used and this was applied to the experimental equilibrium constants of series **1'–Y** and **1–X** in the present study (**Figure 2.30**).

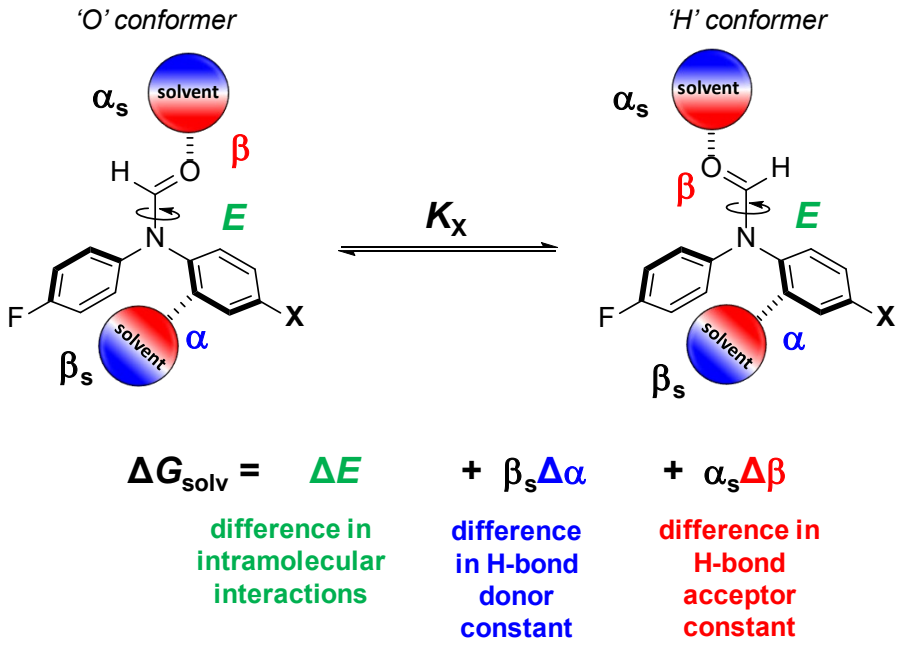

Figure 2.30: Modification[2] of Hunters solvation model[65] used to dissect solvent effects on the molecular balances of series **1'–Y** and **1–X**. The equation is that used in the multilinear regression analysis of the experimental data

As molecular balances are small, solvent-solvent interaction contributions to the equilibrium are negligible and thus, the solvophobic term was omitted from Hunter *et. al.*'s initial solvation model.[2, 65] The polarity of the solvent is described by the hydrogen bond donor and acceptor constants of the solvent, α_s and β_s respectively. The parameters ΔE, $\Delta\beta$ and $\Delta\alpha$ pertain to the properties of the molecular balances and give insight into individual interactions contributing to experimental free energy values. ΔE is a solvent independent term that encodes the difference in the intramolecular steric, dispersion and electrostatic interaction between the 'H' and 'O' conformers. The difference in the hydrogen bond donor and acceptor abilities of each conformer are $\Delta\alpha$ and $\Delta\beta$ respectively. While **Figure 2.30** shows only two possible solvation sites on the molecular balances, $\Delta\alpha$ and $\Delta\beta$ are the result of the Boltzmann average of all possible sites of solvation for each conformer.[2]

To perform this dissection to give insight into solvent effects on the through-space effects of substituents, the conformational free energies, ΔG_{exp}, of each balance are required. With the equilibrium constants, K_X, in hand from previous analysis to obtain $\sigma_{p(conf)}$, experimental conformational free energies of all balances, ΔG_{exp}, in each of the eleven solvents was obtained through **Equation 2.4** where R is the gas constant and T is the temperature.

$$\Delta G_{exp} = -RTlnK_X \qquad \textbf{Equation 2.4}$$

The ΔE, $\Delta\beta$ and $\Delta\alpha$ values of each balance were then obtained through multilinear regression fitting of the experimental data in each solvent with the modified Hunter solvation model in **Figure 2.30**. A strong correlation between the solvent independent term ΔE and the ESP_{ipso} values was found, with an R^2 of 0.92, (**Figure 2.31**) confirming that the conformational preference of the molecular balances was dependent upon the electrostatics of Y-substituted ring, and therefore influenced by through-space effects.

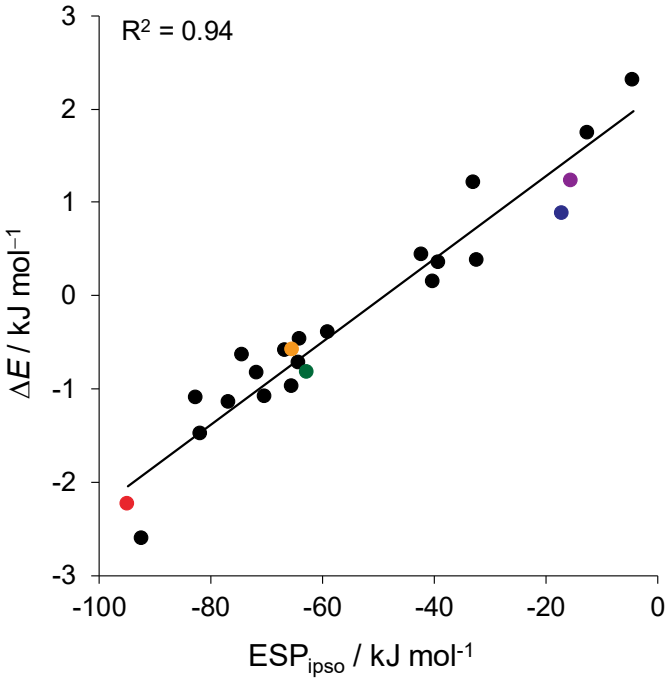

Figure 2.31: Plot of ΔE against ESP_{ipso} with the interesting compounds discussed in Chapter 2 highlighted according to their colour in **Figure 2.4**. The values of ΔG_{solv} are listed in Appendix A, alongside the ΔG_{exp} values of all balances in all solvents and the $\Delta\alpha$ and $\Delta\beta$ values. Solvent dissection performed by RJB and experimental and computational data performed by RJB, Dr Ioulia K. Mati and previously reported as described in **Figure 2.4**.[1-3]

2.6 Conclusions and Outlook

Through a combined computational and experimental study, a quantitative analysis of the importance of through-space effects on conformational equilibria has been performed. A Hammett analysis of experimentally determined conformational equilibrium constants in synthetic molecular balances enabled substituent constants $\sigma_{p(conf)}$ to be defined and quantified. These compounds yielded surprising results; compounds **1–d** and **1–e** showed the nitro group acts as an "electron-donating" group *via* through-space effects from the oxygen atoms. Moreover, the strikingly different behaviour of **1–a** and **1–b**, confirmed the through-space origin the effect, since a sterically imposed conformational flip of methoxy group orientation was shown to nullify the through-space effect of the oxygen lone pairs. Computed ESP surfaces and slices were employed to help understand the origin of these experimental results which unveiled electro-enhancing through-space substituent effects in both **1–a** and **1–d** that

were absent in **1−b** and **1−e**, respectively. These conclusions were supported by experimental NMR chemical shift analysis.

Overall, the computational and experimental analysis of the molecular balances in this study showed that not only can through-space effects override the traditional, through-bond nature of a substituent, but they can also overturn this behaviour. In addition, through-space effects were shown to also be susceptible to tuning using steric bulk to control the orientation of substituents, and thus, their local field effects.

Solvent effects on through-space substituent effects was performed by measuring the equilibrium constants of the balances studied in eleven solvents. The quality of the correlation between the experimental data and ESP_{ipso} values was sensitive to solvent, with the worst correlations found in competitive and polar solvents. Thus, this study has provided the first experimental evidence that the influence of through-space substituent effects can be perturbed or enhanced by the choice of solvent. However, the lack of uniformity in the quantification of through-space effects across the solvents studies points to an uncertainty in the ability to provide a universally applicable constant that describes these effects.

Thus, this study has provided experimental and computational confirmation of the findings of Wheeler and Houk, and quantified the influence of through-space effects on the familiar Hammett substituent constant scale. Thus, the aim of quantifying substituent effects in which through-space influences dominate was achieved. These results also point to the dominance of through-space effects on the pK_a values of Byrons 2'-substituted biphenyl-4-carboxylic acids as they share the biphenyl motif at the heart of the present study (**Figure 2.1**).[4] The transferability and predictive utility of Hammett substituent constants encoding through-space substituent effects will be further assessed in **Chapter 3**.

2.7 References

1. Mati, I. K. Molecular torsion balances for quantifying non-covalent interactions. The University of Edinburgh, 2013.

2. Mati, I. K.; Adam, C.; Cockroft, S. L., Seeing through solvent effects using molecular balances. *Chem. Sci.* **2013,** *4*, 3965 - 3972.

3. Muchowska, K. B.; Adam, C.; Mati, I. K.; Cockroft, S. L., Electrostatic Modulation of Aromatic Rings via Explicit Solvation of Substituents. *J. Am. Chem. Soc.* **2013,** *135* (27), 9976 - 9979.

4. Byron, D. J.; Gray, G. W.; Wilson, R. C., The Effects of 2'-Substituents on the Ionisation Constants of Biphenyl-4-carboxylic Acid, 4-Aminobiphenyl, and 4-Biphenylylacetic acid. *J. Chem. Soc. C* **1966**, 837 - 840.

5. Mati, I. K.; Cockroft, S. L., Molecular balances for quantifying non-covalent interactions. *Chem. Soc. Rev.* **2010,** *39*, 4195 - 4205.

6. Yang, L.; Adam, C.; Nichol, G. S.; Cockroft, S. L., How much do van der Waals dispersion forces contribute to molecular recognition in solution? *Nature Chemistry* **2013,** *5*, 1006.

7. Oki, M., 1,9-disubstituted triptycenes: An excellent probe for weak molecular interactions. *Acc. Chem. Res.* **1990,** *23* (11), 351 - 356.

8. Gung, B. W.; Emenike, B. U.; Lewis, M.; Kirschbaum, K., Quantification of CH···π Interactions: Implications on How Substituent Effects Influence Aromatic Interactions. *Chem. Eur. J.* **2010,** *16* (41), 12357-12362.

9. Gung, B. W.; Xue, X.; Reich, H. J., Off-Center Oxygen−Arene Interactions in Solution: A Quantitative Study. *J. Org. Chem* **2005,** *70* (18), 7232-7237.

10. Paliwal, S.; Geib, S.; Wilcox, C. S., Molecular Torsion Balance for Weak Molecular Recognition Forces. Effects of "Tilted-T" Edge-to-Face Aromatic Interactions on Conformational Selection and Solid-State Structure. *J. Am. Chem. Soc* **1994,** *116* (10), 4497-4498.

11. Motherwell, W. B.; Moïse, J.; Aliev, A. E.; Nič, M.; Coles, S. J.; Horton, P. N.; Hursthouse, M. B.; Chessari, G.; Hunter, C. A.; Vinter, J. G., Noncovalent Functional-Group–Arene Interactions. *Angew. Chem. Int. Ed.* **2007,** *46* (41), 7823-7826.

12. Gardner, R. R.; Christianson, L. A.; Gellman, S. H., Quantitative Analysis of Hydrophobically Induced Folding in a Minimal Model System. *J. Am. Chem. Soc* **1997,** *119* (21), 5041-5042.

13. McKay, S. L.; Haptonstall, B.; Gellman, S. H., Beyond the Hydrophobic Effect: Attractions Involving Heteroaromatic Rings in Aqueous Solution1. *J. Am. Chem. Soc* **2001,** *123* (6), 1244-1245.

14. Carroll, W. R.; Pellechia, P.; Shimizu, K. D., A Rigid Molecular Balance for Measuring Face-to-Face Arene−Arene Interactions. *Org. Lett.* **2008,** *10* (16), 3547-3550.

15. Hof, F.; Scofield, D. M.; Schweizer, W. B.; Diederich, F., A Weak Attractive Interaction between Organic Fluorine and an Amide Group. *Angew. Chem. Int. Ed.* **2004,** *43* (38), 5056-5059.

16. Adam, C.; Yang, L.; Cockroft, S. L., Partitioning Solvophobic and Dispersion Forces in Alkyl and Perfluoroalkyl Cohesion. *Angew. Chem. Int. Ed.* **2015,** *54* (4), 1164-1167.

17. Yang, L.; Adam, C.; Cockroft, S. L., Quantifying Solvophobic Effects in Nonpolar Cohesive Interactions. *J. Am. Chem. Soc* **2015,** *137* (32), 10084-10087.

18. Pascoe, D. J.; Ling, K. B.; Cockroft, S. L., The Origin of Chalcogen-Bonding Interactions. *J. Am. Chem. Soc* **2017**.

19. Shimizu, K. D.; Carroll, W. R.; Zhao, C.; Smith, M. D.; Pellechia, P. J., A Molecular Balance for Measuring Aliphatic CH-Pi Interactions. *Org. Lett.* **2011,** *13* (16), 4320 - 4323.

20. Li, P.; Zhao, C.; Smith, M. D.; Shimizu, K. D., Comprehensive Experimental Study of N-Heterocyclic π-Stacking Interactions of Neutral and Cationic Pyridines. *J. Org. Chem* **2013,** *78* (11), 5303-5313.

21. Maier, J. M.; Li, P.; Hwang, J.; Smith, M. D.; Shimizu, K. D., Measurement of Silver−π Interactions in Solution Using Molecular Torsion Balances. *J. Am. Chem. Soc* **2015,** *137* (25), 8014-8017.

22. Hwang, J.; Li, P.; Carroll, W. R.; Smith, M. D.; Pellechia, P. J.; Shimizu, K. D., Additivity of Substituent Effects in Aromatic Stacking Interactions. *J. Am. Chem. Soc* **2014,** *136* (40), 14060-14067.

23. Maier, J. M.; Li, P.; Vik, E. C.; Yehl, C. J.; Strickland, S. M. S.; Shimizu, K. D., Measurement of Solvent OH−π Interactions Using a Molecular Balance. *J. Am. Chem. Soc* **2017,** *139* (19), 6550-6553.

24. Li, P.; Maier, J. M.; Vik, E. C.; Yehl, C. J.; Dial, B. E.; Rickher, A. E.; Smith, M. D.; Pellechia, P. J.; Shimizu, K. D., Stabilizing Fluorine–π Interactions. *Angew. Chem. Int. Ed.* **2017,** *56* (25), 7209-7212.

25. Hwang, J.; Li, P.; Smith, M. D.; Warden, C. E.; Sirianni, D. A.; Vik, E. C.; Maier, J. M.; Yehl, C. J.; Sherrill, C. D.; Shimizu, K. D., Tipping the Balance between S-π and O-π Interactions. *J. Am. Chem. Soc* **2018,** *140* (41), 13301-13307.

26. Maier, J. M.; Li, P.; Ritchey, J. S.; Yehl, C. J.; Shimizu, K. D., Anion-enhanced solvophobic effects in organic solvent. *Chem. Comm.* **2018,** *54* (61), 8502-8505.

27. Hwang, J.; Li, P.; Vik, E. C.; Karki, I.; Shimizu, K. D., Study of Through-Space Substituent-π Interactions Using N-Phenylimide Molecular Balances. *Organic Chemistry Frontiers* **2019**.

28. Topsom, R. D., The isolated molecule approach. Theoretical studies of the inductive effect. *J. Am. Chem. Soc* **1981,** *103* (1), 39-44.

29. Marriott, S.; Topsom, R. D., A Theoretical Scale of Substituent Field Parameters. *J. Am. Chem. Soc.* **1984,** *106* (1), 7 - 10.

30. Suresh, C. H.; Alexander, P.; Vijayalakshmi, K. P.; Saj, Use of molecular electrostatic potential for quantitative assessment of inductive effect. *Phys. Chem. Chem. Phys.* **2008,** *10* (43), 6492 - 6499.

31. Sayyed, F. B.; Suresh, C. H.; R., G. S., Appraisal of Through-Bond and Through-Space Substituent Effects via Molecular Electrostatic Potential Topography. *J. Phys. Chem. A* **2010,** *114* (42), 12330 - 12333.

32. Sayyed, F. B.; Suresh, C. H., Substituent Effects in Cation-Pi Interactions: A Unified View from Inductive, Resonance, and Through-Space Effects. *J. Phys. Chem. A* **2011,** *115* (22), 5660 - 5664.

33. Parrish, R. M.; Sherrill, C. D., Quantum-Mechanical Evaluation of π–π versus Substituent−π Interactions in π Stacking: Direct Evidence for the Wheeler–Houk Picture. *J. Am. Chem. Soc* **2014,** *136* (50), 17386-17389.

34. Sinnokrot, M. O.; Sherrill, C. D., Unexpected Substituent Effects in Face-to-Face π-Stacking Interactions. *J. Phys. Chem. A* **2003,** *107* (41), 8377-8379.

35. Sinnokrot, M. O.; Sherrill, C. D., Substituent Effects in π−π Interactions: Sandwich and T-Shaped Configurations. *J. Am. Chem. Soc* **2004,** *126* (24), 7690-7697.

36. Sinnokrot, M. O.; Sherrill, C. D., High-Accuracy Quantum Mechanical Studies of π−π Interactions in Benzene Dimers. *J. Phys. Chem. A* **2006,** *110* (37), 10656-10668.

37. Lee, E. C.; Kim, D.; Jurečka, P.; Tarakeshwar, P.; Hobza, P.; Kim, K. S., Understanding of Assembly Phenomena by Aromatic−Aromatic Interactions: Benzene Dimer and the Substituted Systems. *J. Phys. Chem. A* **2007,** *111* (18), 3446-3457.

38. Wheeler, S. E.; Houk, K. N., Through-Space Effects of Substituents Dominate Molecular Electrostatic Potentials of Substituted Arenes. *J. Chem. Theory Comput.* **2009,** *5* (9), 2301 - 2312.

39. Wheeler, S. E.; Bloom, J. W. G., Toward a More Complete Understanding of Noncovalent Interactions Involving Aromatic Rings. *J. Phys. Chem. A* **2014,** *118* (32), 6133 - 6147.

40. Wheeler, S. E., Understanding Substituent Effects in Noncovalent Interactions Involving Aromatic Rings. *Acc. Chem. Res.* **2013,** *46* (4), 1029 - 1038.

41. Wheeler, S. E.; Houk, K. N., Substituent Effects in Cation/Pi Interactions and Electrostatic Potentials above the Center of Substituted Benzenes Are Due Primarily to through-Space Effects of the Substitents. *J. Am. Chem. Soc.* **2009,** *131* (9), 3129 - 3127.

42. Wheeler, S. E.; Houk, K. N., Are Anion/Pi Interactions Actually a Case of Simple Charge-Dipole Interactions? *J. Phys. Chem.* **2010,** *114* (33), 8658 - 8664.

43. Wheeler, S. E.; Houk, K. N., Origin of substituent effects in edge-to-face aryl–aryl interactions. *Molecular Physics* **2009,** *107* (8-12), 749-760.

44. Dominelli-Whiteley, N.; Brown, J. J.; Muchowska, K. B.; Mati, I. K.; Adam, C.; Hubbard, T. A.; Elmi, A.; Brown, A. J.; Bell, I. A. W.; Cockroft, S. L., Strong

Short-Range Cooperativity in Hydrogen-Bond Chains. *Angew. Chem. Int. Ed.* **2017,** *56* (26), 7658-7662.

45. Lide, D. R., *CRC Handbook of Chemistry and Physics*. 83rd ed.; CRC Press: 2002; p 2664.

46. Roberts, J. D.; Moreland Jr, W. T., Electrical Effects of Substituent Groups in Saturated Systems. Reactivities of 2-substituted Bicyclo[2.2.2]octane-1-carboxylic Acids. *J. Am. Chem. Soc.* **1953,** *75* (9), 2167 - 2173.

47. Smith, M. B.; March, J., *March's Advanced Organic Chemistry: Reactions, Mechanisms, and Structure*. 6th ed.; John Wiley & Sons, Inc.: United States of America, 2007.

48. Miyaura, N.; Suzuki, A., Palladium-Catalyzed Cross-Coupling Reactions of Organoboron Compounds. *Chem. Rev.* **1995,** *95* (7), 2457-2483.

49. Bueno, A. B.; Carreño, M. C.; García Ruano, J.; Fischer, J., Short and efficient synthesis of (R)-4-Hydroxy-4-methyl cyclohexenone. *Tetrahedron Letters* **1995,** *36* (21), 3737-3740.

50. Hansch, C.; Leo, A.; Taft, R. W., A survey of Hammett substituent constants and resonance and field parameters. *Chem. Rev.* **1991,** *91* (2), 165-95.

51. McDaniel, D. H.; Brown, H. C., An Extended Table of Hammett Substitutent Constants Based on the Ionization of Substituted Benzoic Acids. *J. Org. Chem* **1958,** *23* (3), 420-427.

52. Hammett, L. P., Some Relations Between Reaction Rates and Equilibrium Constants. *Chem. Rev.* **1935,** *16* (2), 125 - 136.

53. Hammett, L. P., The Effect of Structure upon the Reactions of Organic Compounds. Benzene Derivatives. *J. Am. Chem. Soc.* **1937,** *59* (1), 96 - 103.

54. Hammett, L. P., Linear free energy relationships in rate and equilibrium phenomena. *Transactions of the Faraday Society* **1938,** *34* (0), 156-165.

55. Cativiela, C.; Garcia, J. I., Electronic effects of heterocyclic substituents. Spectroscopical and theoretical (AM1) study in a series of heterocyclic carboxaldehydes. *Canadian Journal of Chemistry* **1990,** *68* (9), 1477-1481.

56. Westheimer, F. H.; Kirkwood, J. G., The Electrostatic Influence of Substituents on the Dissociation Constants of Organic Acids. II. *J. Chem. Phys.* **1938,** *6* (9), 513-517.

57. Kirkwood, J. G.; Westheimer, F. H., The Electrostatic Influence of Substituents on the Dissociation Constants of Organic Acids. I. *J. Chem. Phys.* **1938,** *6* (9), 506-512.

58. Stock, L. M., The origin of the inductive effect. *J. Chem. Ed.* **1972,** *49* (6), 400.

59. Wilcox, C. F.; Leung, C., Transmission of substituent effects. Dominance of field effects. *J. Am. Chem. Soc* **1968,** *90* (2), 336-341.

60. Bowden, K.; Grubbs, E. J., Through-bond and Through-space Models for Interpreting Chemical Reactivity in Organic Reactions. *Chem. Soc. Rev.* **1996,** *25* (3), 171 - 177.

61. Wheeler, S. E.; Houk, K. N., Substituent Effects in the Benzene Dimer are Due to Direction Interactions of the Substituents with the Unsubstituted Benzene. *J. Am. Chem. Soc.* **2008,** *130* (33), 10854 - 10855.

62. Clayden, J.; Greeves, N.; Warren, S.; Wothers, P., *Organic Chemistry*. Oxford University Press: United Kingdom, 2001.

63. Struble, M. D.; Kelly, C.; Siegler, M. A.; Lectka, T., Search for a Strong, Virtually "No-Shift" Hydrogen Bond: A Cage Molecule with an Exceptional OH···F Interaction. *Angew. Chem. Int. Ed.* **2014,** *53* (34), 8924-8928.

64. Golden, R.; Stock, L. M., Dissociation constants of 8-substituted 9,10-ethanoanthracene-1-carboxylic acids and related compounds. Evidence for the field model for the polar effect. *J. Am. Chem. Soc* **1972,** *94* (9), 3080-3088.

65. Cockroft, S. L.; Hunter, C. A., Desolvation and substituent effects in edge-to-face aromatic interactions. *Chem. Comm.* **2009,** (26), 3961-3963.

Chapter 3

Transferability of Through-Space Substituent Effects: Reactivity

Abstract

Hammett substituent constants are powerful tools that aid reaction mechanism elucidation and predicting reactivity and chemical equilibria. The success of Hammett substituent constants has been their established transferability in a wide range of contexts beyond the original system in which they were defined. In **Chapter 2** new Hammett-type substituent constants ($\sigma_{p(conf)}$) were determined in situations where through-space effects dominate. Thus, this chapter seeks to determine whether the general transferability of Hammett constants is retained in such circumstances by examining the reactivity of phenyl-pyridine derivatives. The through-space effects on reaction rates are analysed using the same Hammett-type analysis and *in silico* methods as in **Chapter 2**. Ultimately, the through-space substituent effects in the pyridine compounds were not well predicted by the constant derived in **Chapter 2**. This result is understood through the sensitivity of field effects to geometrical influences and solvent properties (as uncovered in **Chapter 2**) meaning that such effects perhaps cannot be subject to universal quantification. Additionally, this study provides evidence that through-space substituent effects, and substituent effects at large, are best understood *via* simple computational modelling.

Supplementary details are given in Appendix B.

Contributions: All experimental and computational results of the pyridine derivatives in this chapter were obtained by RJB.

3.1 Introduction

Ever since the inception of Hammett's seminal constants, σ_m and σ_p, researchers have sought a universally applicable parameter with which to explain and predict substituent effects on organic molecules.[1] For such a parameter to be effective, its predictive power must be transferable to systems other than that within which it was defined. While Hammett parameters are the "go-to" method of examination of electronic substituent effects in modern-day physical organic chemistry, it is the transferable aspect of quantification that Hammett, and myriad others, have not fully achieved.[1] As such, a wide range of substituent constants exist that have been mostly defined empirically, and occasionally computationally, for which the applicability must be determined on a case-by-case basis. The lack of coherence between these constants speaks to the lack of understanding regarding the method of transmission of substituent effects on chemical reactivity and equilibria.

Recently, there has been a growing number of largely computational studies that have highlighted the importance of through-space effects on non-covalent interactions, reaction rates and chemical equilibria.[7-9, 11-14] A limited number of empirical studies have shown that through-space substituent effects pose a potentially untapped source of directing and activating reactivity in organic molecules.[15-16] In addition, **Chapter 2** of this thesis detailed the importance of through-space effects on chemical equilibria *via* specially designed molecular balances. Quantification and assessment of these effects was achieved through Hammett-type analysis of experimental equilibrium constants (to generate a new substituent constant, $\sigma_{p(conf)}$) and computational ESP values and slices. This study showed that through-space effects can override and even run concurrent to traditional through-bond effects and also highlighted their susceptibility to tuning *via* steric bulk.

It is known that through-space effects depend upon to the relative positioning of the substituent and reactive centre and were postulated to be sensitive to polar solvents owing to their intrinsic electrostatic nature.[2-4, 17-20] This too was uncovered in **Chapter 2** of this thesis using a modification of Hunters' solvation model However, the question remains whether these effects and their environmental sensitivity can be quantified in

a transferable manner. Thus, probing the general applicabilty of $\sigma_{p(conf)}$ will require assessing its ability to predict substituent effects in a new model system.

3.2 Aims of the Project

This chapter seeks to evaluate the transferability of the substituent constants that are dominated by through-space influences as determined in **Chapter 2**. First, the ability of these through-space dominated substituent effects to influence chemical reactivity will be assessed using the *N*-methylation reaction rates of a series of pyridine derivatives. Hammett analysis of these rate constants will then be used to obtain a parameter that encodes through-space substituent effects on chemical reactivity, $\sigma_{p(react)}$. The same computational techniques that proved to be successful in analysing the through-space effects observed in **Chapter 2** will be utilised here in combination with evaluation *via* empirical measurements. Finally, correlation of the $\sigma_{p(react)}$ and $\sigma_{p(conf)}$ is performed to test the transferability, and therefore utility of Hammett substituent constants that are dominated by through-space effects.

3.3 Through-Space Effects on Chemical Reactivity

3.3.1 Model Reaction and System Design

In a 2003 study that sought to quantify the effects of functional group interactions on transition states, Hunter and co-workers used supramolecular zipper complexes to assess how the rate of *N*-methylation of a pyridine group was influenced by substituent-tuned edge-to-face aromatic interactions (**Figure 3.1**).[17, 21]

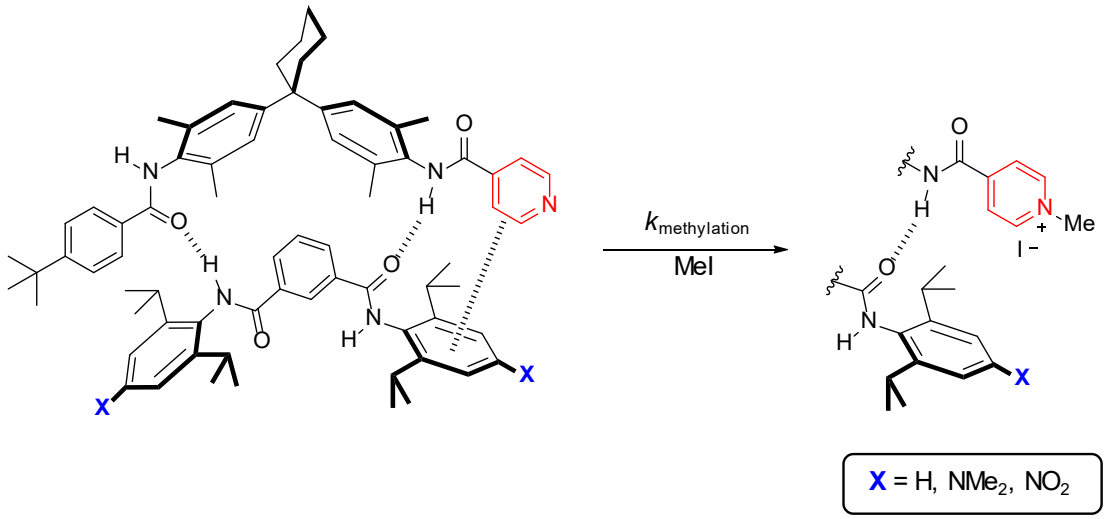

Figure 3.1: The reaction used by Hunter *et. al.* to evaluate the effect of substituent X (highlighted in blue) on the rates of *N*-methylation of pyridyl functionalities (red) *via* edge-to-face stacking interactions.[21]

The reaction used to examine substituent effects on reaction rates follows an S_N2 mechanism (**Figure 3.2**).[22] The electrophile, methyl iodide, undergoes backside nucleophilic attack *via* the lone pair of the pyridine nitrogen to give the *N*-methylated pyridine product bearing a positive charge on the nitrogen atom. The transition state in the rate-determining step of an S_N2 mechanism contains both the pyridine nucleophile and the methyl iodide electrophile. Hunter proposed that substituent effect-mediated stabilisation of this transition state might be key to modulating the reaction rate.[21]

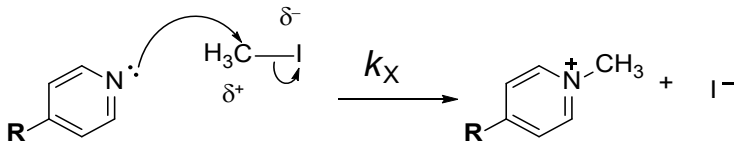

Figure 3.2: S_N2 mechanism of the *N*-methylation of a pyridine derivative.

Rate constants in Hunters study were determined by monitoring the disappearance of the pyridyl starting material using ^1H NMR spectroscopy and performed in the presence of excess methyl iodide to allow the use of *pseudo* first order kinetics.[21] This meant that there were no complications from side reactions, making this experimental set up a useful means of testing substituent effects on reaction rates. A thermodynamic

double-mutant cycle analysis of these data showed that when X = NMe_2, the edge-to-face interaction between the pyridine ring and the X-substituted ring in the transition state was favourable. This complex exhibited an enhanced reaction rate compared to when X = H or NO_2, where the latter exhibited negative catalysis.[17, 21] As such, it was proposed interactions that stabilise the developing positive charge of the pyridine nitrogen atom in the transition state will lead to faster reaction rates. However, through-space contributions were not discussed in this early work.[21]

An additional aspect of pyridine containing compounds that makes their focus in this study interesting is the prevalence of such compounds in natural products and drug molecules. Thus, understanding the influence of through-space substituent effects on their properties could aid in the understanding of pyridine containing compounds in these areas.

This study by Hunter[21] provided inspiration for the present study of through-space substituent effects on reactivity. Rather than using a supramolecular complex to assess intermolecular substituent effects on reaction rates, a simpler, intramolecular, and pyridine-based design was sought for this study. Thus, the *N*-methylation of 4-phenylpyridine derivatives (series **2–X**) and controls (series **2'–Y**) was proposed as a model system for examining through-space substituent effects on chemical reactivity (**Figure 3.3**). These phenylpyridine derivative compounds present analogous substituent positioning to the biphenyl moieties within the **1–X** and **1'–Y** series of molecular balances used in **Chapter 2** to quantify through-space substituent effects. Thus, these design similarities should enable an assessment of the transferability of the substituent constants derived in **Chapter 2**, $\sigma_{p(conf)}$.

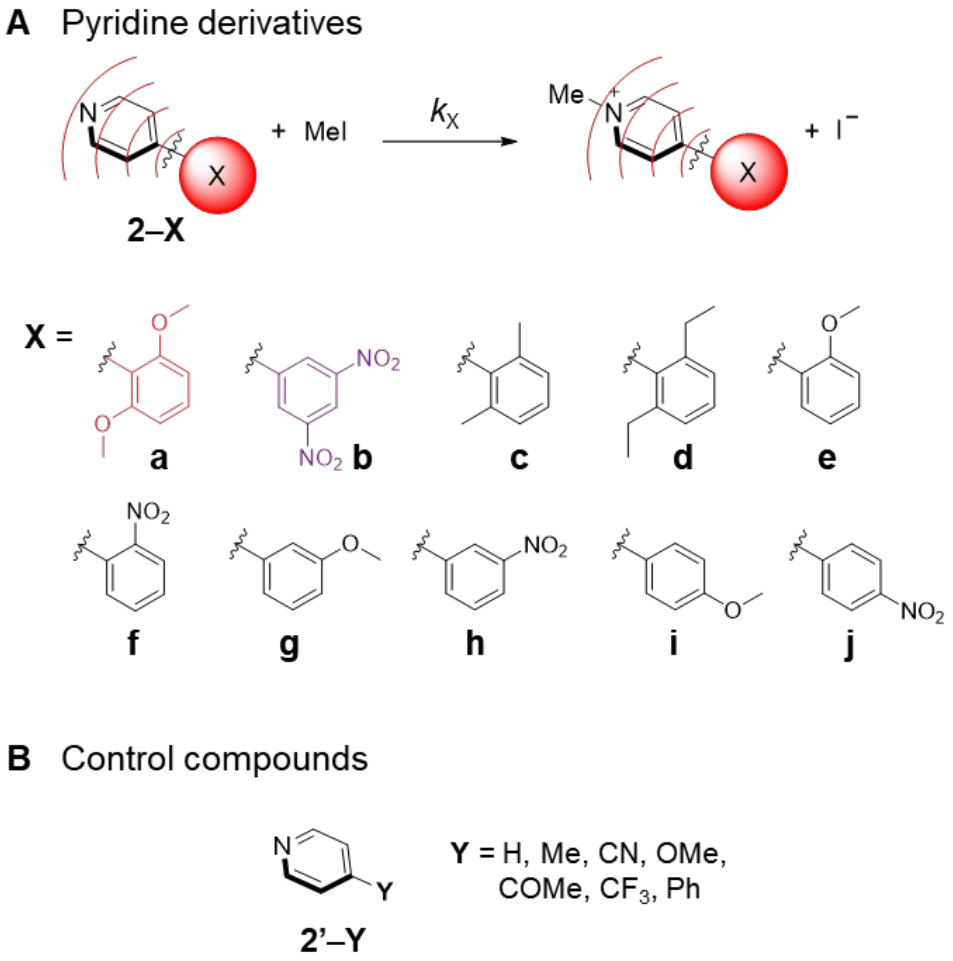

Figure 3.3: Pyridine derivatives used in this study. **(A)** 4-Phenylpyridine derivatives wherein variation of the X-substituents allows assessment of through-space field effects on chemical reactivity as represented by the red lines. All pyridine derivatives were synthesised by RJB. **(B)** 4-Substituted pyridines that serve as controls in the present study.

Like the **1'–Y** series of molecular balances, the simple, 4-substituted pyridyl series **2'–Y** act as control compounds where through-bond substituent effects are dominant. Thus, this series will calibrate the behaviour of the model reaction arising from through-bond substituent effects to allow assessment of the through-space dominated substituent effects in series **2–X**. The inductive effects of X-substituents on the pyridine ring in the **2–X** series are expected to have a minimal influence on the reactivity of these compounds.[3, 23] Akin to the molecular balances of **Chapter 2**, all of compounds in series **2–X** have a twisted geometry which should minimise resonant contributions (**Figure 3.4**).

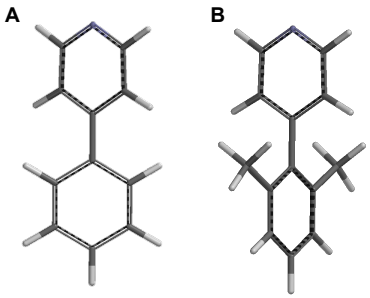

Figure 3.4: Computational models of **(A) 2'–Ph** and **(B) 2–c** showing that the equilibrium geometry of the pyridyl-phenyl bond is non-planar. Structures were minimised using DFT/B3LYP/6–31G* in Spartan '14. All calculations performed by RJB.

Preliminary experiments to monitor the *N*-methylation of pyridine (**2'–H**) and 4-phenylpyridine (**2'–Ph**) with methyl iodide under *pseudo* first order conditions showed that both the starting materials and their *N*-methylated products form very simple spectra in which the signals of the protons *ortho* to the pyridine nitrogen atom are well resolved from other ^{1}H signals. Thus, the formation of the product and the disappearance of the starting material over time could be easily monitored using ^{1}H NMR spectroscopy. Therefore, the proposed 4-phenylpyridine derivative series (**2–X**) was taken forward as the model system with which to assess through-space substituent effects on reactivity and then the transferability of the constant derived in **Chapter 2**.

3.3.2 Pyridine Derivative Synthesis

The **2'–Y** series was comprised entirely of commercially available 4-substituted pyridine compounds. The **2–X** series were all prepared in one step *via* simple Suzuki-Miyaura coupling reactions from 4-bromopyridine hydrochloride and the appropriate 4-substituted phenylboronic acid derivative (or with these reaction partners swapped). For all of these compounds, the phenylboronic acid derivatives were commercially available.

Variation of the palladium catalyst, ligand and base used in the Suzuki-Miyaura couplings provided access to the **2–X** series. Compounds **2–a**, **2–c** and **2–f** to **2–j** inclusive were prepared with tetrakis(triphenylphosphine)palladium (0) as both the

catalyst and ligand, with sodium carbonate as the base (**Figure 3.5**).[24] Compound **2–e** was prepared with potassium phosphate as the base and the catalyst was tris(dibenzylideneacetone)dipalladium (0) meaning a ligand was required. Thus, this preparation includes tricyclohexylphospine (**Figure 3.6**).[25]

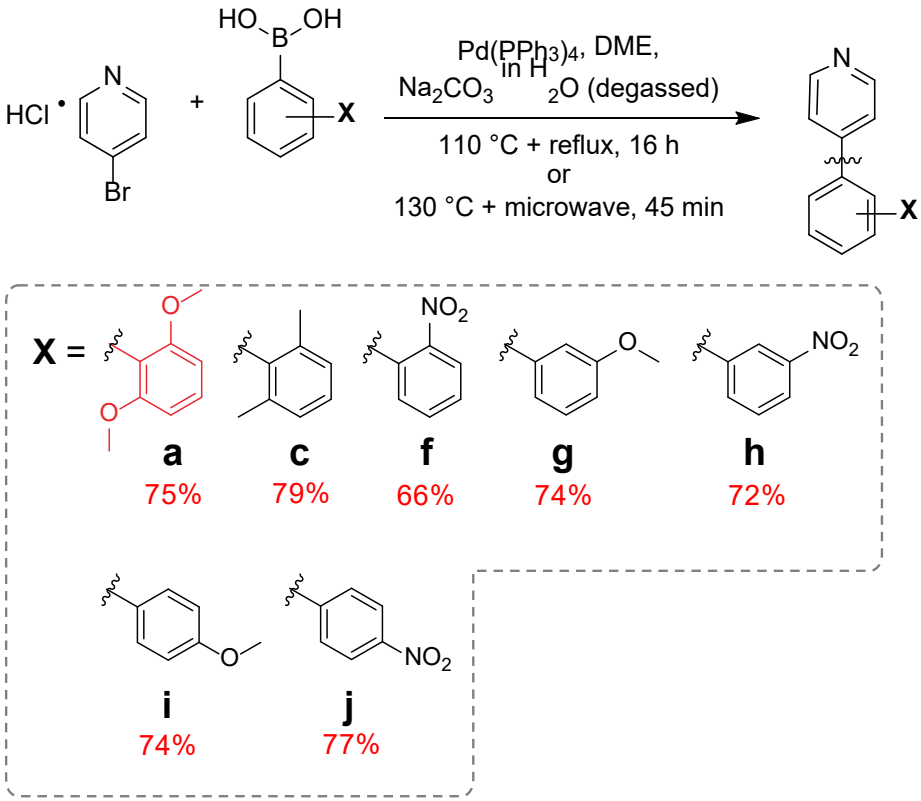

Figure 3.5: Synthesis of compounds **2–a**, **2–c** and **2–f** to **2–j** inclusive using tetrakis(triphenylphosphine)palladium (0) as the catalyst in the cross-coupling procedure.[24]

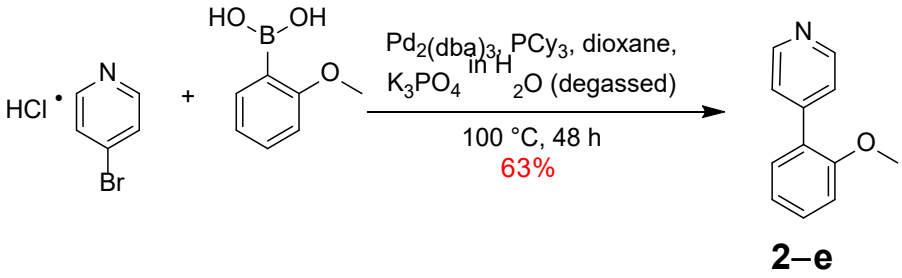

Figure 3.6: Synthesis of **2–e**, with tris(dibenzylideneacetone)dipalladium (0) as the catalyst.[25]

The synthesis of the remaining 4-phenylpyridine derivatives was performed with the coupling partners swapped with respect to the synthetic procedures for the rest of the **2–X** series. The boronic acid partner is now the pyridine component of the reaction and thus, the substituted phenyl component is the halide (**Figure 3.7**).[25]

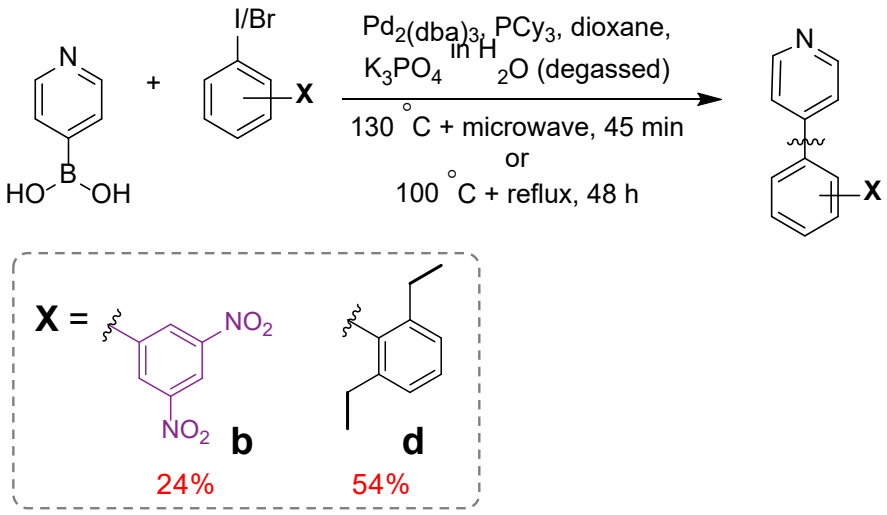

Figure 3.7: Synthesis of **2–b** and **2–d**, where the coupling partners are swapped with respect to those in the synthesis of the rest of the **2–X** series.

Since the intention is to examine the transferability of the constants defined in **Chapter 2** to the reactivity of these pyridine derivatives, it was desirable that the pyridine derivatives in the present study bore the same substituents. This requirement was largely achieved, with the exception of two compounds that could not be synthesised as 4-phenylpyridine analogues. The synthesis of the pyridine analogue of molecular balance **1–d**, which would be useful in the assessment of through-space substituent effects through comparison of **2–b**, was first attempted *via* the same cross-coupling reaction that furnished the molecular balance (**Figure 3.8**).

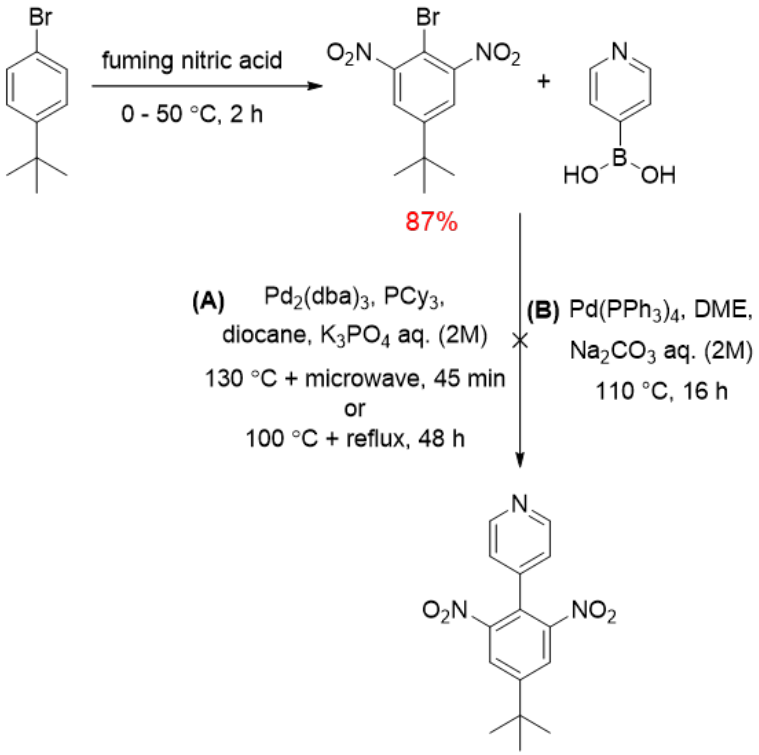

Figure 3.8: First proposed synthetic route to the pyridine analogue of molecular balances **1–d**.[24, 26]

The halide component of this proposed coupling reaction was synthesised in high yield by nitration of 4-*tert*-butylbromobenzene.[26] However, Suzuki-Miyaura cross-coupling conditions with 4-pyridylboronic acid did not yield any trace of the desired product. Suzuki-Miyaura couplings also allow the identity of the halide and boronic acid coupling partners to be swapped. Unfortunately, the attempted synthesis of the proposed boronic acid did not yield any desired product (**Figure 3.9**), and thus, the proposed coupling between it and 4-bromopyridine hydrochloride could not be performed.

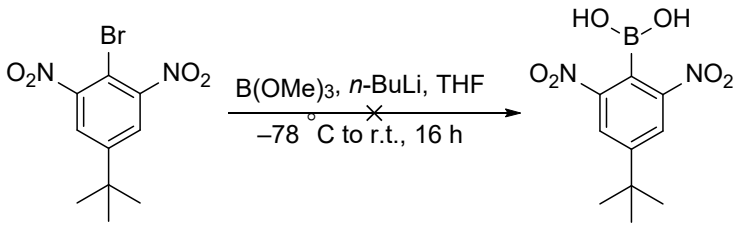

Figure 3.9: The *n*-butyl lithium mediated borylation of the parent bromine in the quest to obtain the pyridine analogue of molecular balance **1–d**.

The complementary compound to **2–a** would be the pyridine counterpart of molecular balance **1–b**. In ***Section 2.4***, balances **1–a** and **1–b** revealed the conformationally tuneable nature of through-space substituent effects *via* changes in geometry. Thus, it would have been useful to obtain the pyridine analogue of **1–b** to help assess this aspect of through-space substituent effects on reaction rates. The proposed synthetic route of this compound was similar to that of the molecular balance (**Figure 3.10**). While the installation of the *tert*-butyl groups to 1,3-dihydroxybenzene and subsequent methylation of this compound were successful, repeated attempts at borylation did not furnish the desired product meaning the coupling with 4-phenylboronic acid was not achieved.[27]

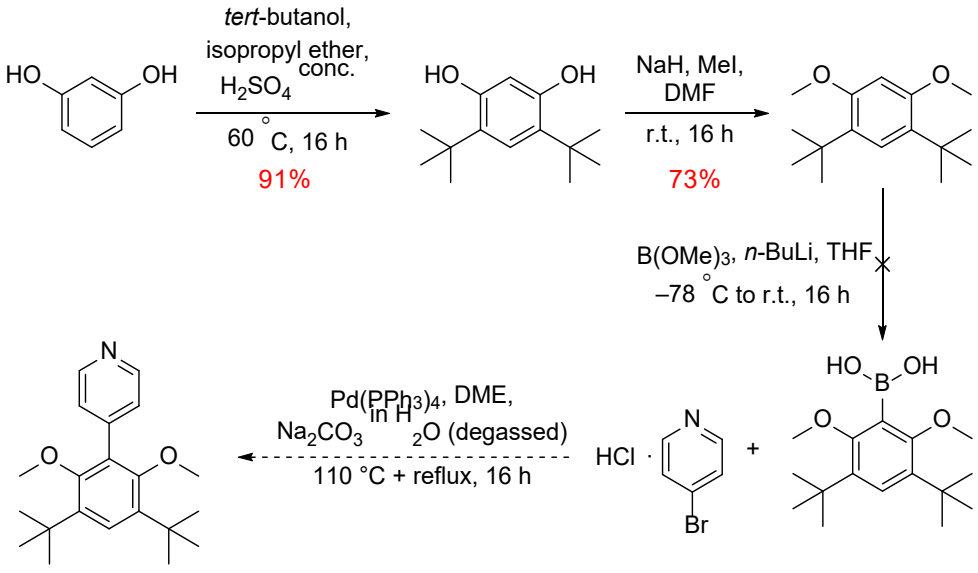

Figure 3.10: Proposed synthetic route to the pyridine analogue of molecule balance **1–b**.

N-bromosuccinimide (NBS) mediated bromination of this intermediate was also unsuccessful meaning that the desired pyridine derivative could not be accessed *via* coupling using 4-pyridylboronic acid (**Figure 3.11**).

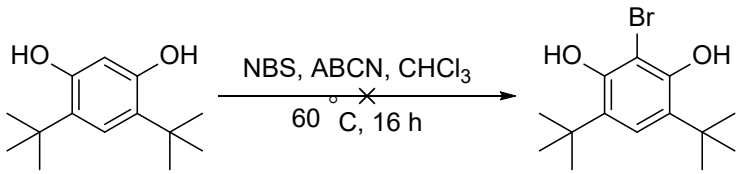

Figure 3.11: Proposed synthesis of the brominated phenyl derivative to access the pyridine analogue of molecular balance **1–b** by switching the coupling partners of the Suzuki-Miyaura coupling reaction in **Figure 3.10**.

3.3.3 Measurement of Rate Constants

The *N*-methylation rates of series **2'–Y** and **2–X** were obtained through the relative disappearance of the starting materials *via* ^{1}H NMR spectroscopy under *pseudo* first order conditions. The integrals of the signals corresponding to the protons *ortho* to the pyridine nitrogen atom of both the starting material and the *N*-methylated product (2,6 and 2',6' protons respectively) were determined at thirty minute intervals (**Figure 3.12**).

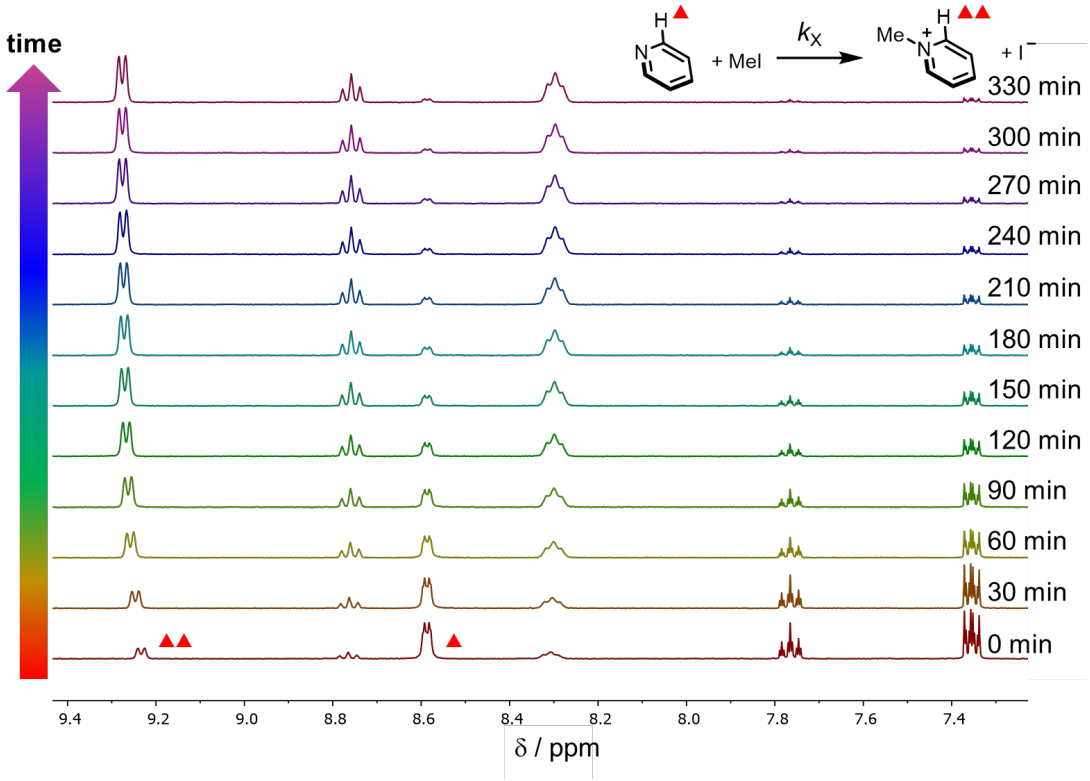

Figure 3.12: *N*-Methylation of **2'–H** was monitored by ^{1}H NMR spectra (acetone-d_6, 400 MHz, 298 K) over five hours and 30 minutes with the 2,6 and 2',6' signals denoted by one and two red triangles respectively.

Through division of the 2,6 integral with the sum of these integrals, the change in concentration of the starting material, [sm], over the time of the experiment was determined. As the reaction was under *pseudo* first order conditions, an excess of methyl iodide was used, thus allowing the experimental data to be fitted to this rate equation (**Equation 3.1**) to obtain the experimental rate constant, k_X, through linear regression (**Figure 3.13**).

$$[sm] = [sm]_0 \times e^{-k_X t} \qquad \textbf{Equation 3.1}$$

Where t is time and $[\mathrm{sm}]_0$ is the concentration of the starting material at the beginning of the experiment, i.e. when t = 0.

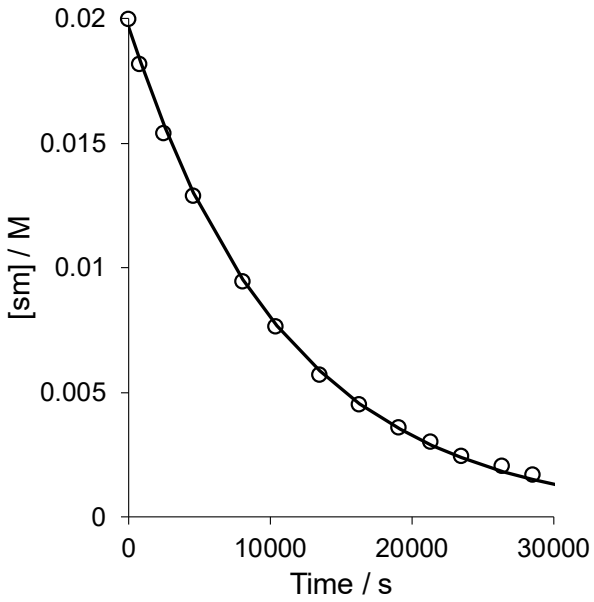

Figure 3.13: The experimental change in the starting material concentration, [sm], over time (hollow circles) with the fit of this data to the *pseudo* first order rate equation, **Equation 3.1**, (solid line) for **2'–H** (20 mM, acetone-d_6, 400 MHz, 298 K).

As rate constants were determined from the relative disappearance of the starting material to the appearance of the product using ^{1}H NMR spectroscopy, it was important that both the starting material and product were soluble in the reaction solvent. Therefore, all reactions were performed in acetone-d_6, which maintained solubility of the diverse range of pyridine derivatives and their ionic *N*-methylated products. While it is known that solvents can alter the rate of S_N2 reactions, in particular through solvation of the transition state,[28-29] all of the reactions in this study were performed in the same solvent. Therefore, as the compounds in this study were all subject to similar solvent effects, experimentally observed changes to the rate constant between compounds can be largely attributed to substituent effects.

To verify that the assumption of *pseudo* first-order conditions was correct, reaction rates were measured at various pyridine derivative concentrations. To do this, three compounds in the **2'–Y** series spanning the extremes and median experimental behaviour were reacted at 20 mM (the concentration used in the present study) to 100 mM (five times that used in the present study). Rate constants were found to be

unaffected by changes in concentrations of the pyridine derivative for all three **2'–Y** compounds (**Figure 3.14**).

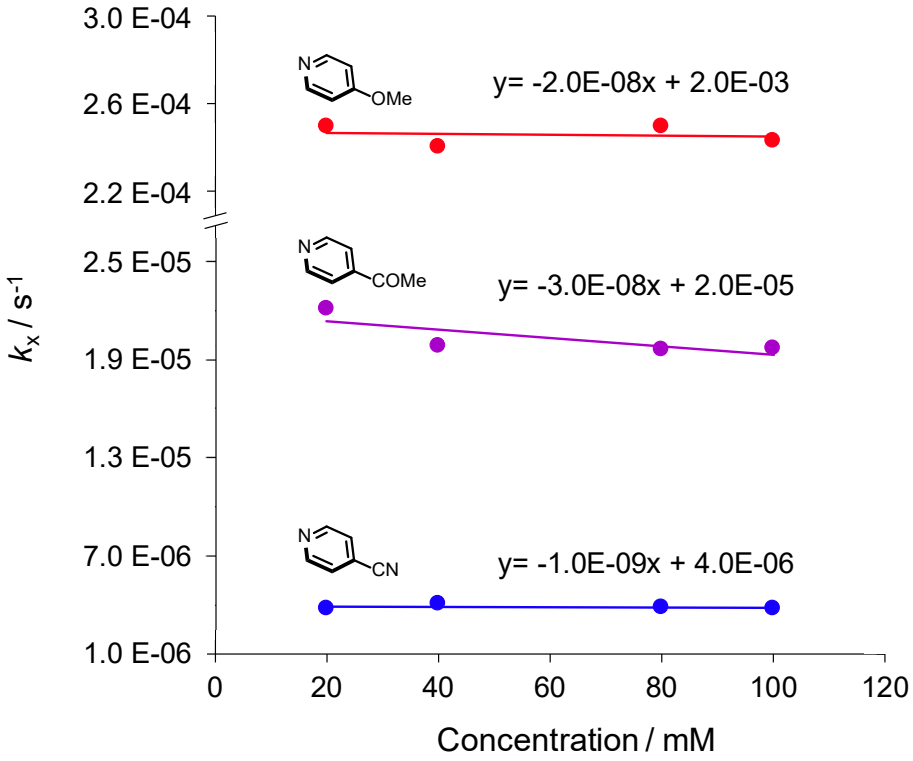

Figure 3.14: Rate constants, k_x, of **2'–OMe**, **2'–COMe** and **2'–CN** at 20 mM, 40 mM, 80 mM and 100 mM pyridine concentration. A version of this graph with error bars is given in Appendix B. Data obtained by RJB. Measured in acetone-d_6 (400 HMz, 298 K).

The choice of ^{1}H NMR spectroscopy to measure the experimental rate constants in this study was driven by the ease with which the reactions were performed and the simplicity of the spectra. There was no overlap between the signals of interest with the solvent or methyl iodide and the use of a methyl iodide in vast excess did not result in a loss of spectroscopic information of the pyridine and its *N*-methylated product as the reaction progressed. This made for easy analysis of the spectra to obtain reliable and repeatable experimental rate constants. In addition, well-resolved, high-quality spectra could be obtained at low pyridine derivative concentrations (20 mM) meaning that large quantities of the starting materials were not required.

Having verified the experimental robustness of the experimental procedure, the rate constants, k_X, for the *N*-methylation of both the **2'–Y** and **2–X** series (**Figure 3.3**) were determined (reported alongside derived substituent effects in **Table 3.1**).

3.3.4 Quantification of Substituent Effects on Reactivity

Hammett analysis using the relationship $-\log_{10}(k_X/k_H)$ was performed on the experimentally determined rate constants, k_X, of the pyridine derivatives, in an analogous manner to the treatment of the equilibrium constants, K_X, in **Chapter 2**. The negative of the logarithm is taken such that substituents that enhance the rate of the reaction with respect to **2'–H** have negative values, meaning that the sign of the substituent effects in relation to the rate constants, k_X, match the standard Hammett constant definition.

The $-\log_{10}(k_X/k_H)$ values obtained using the Hammett-style relationship were evaluated through comparison between those of the **2'–Y** series and the corresponding Hammett σ_p values (**Figure 3.15**).

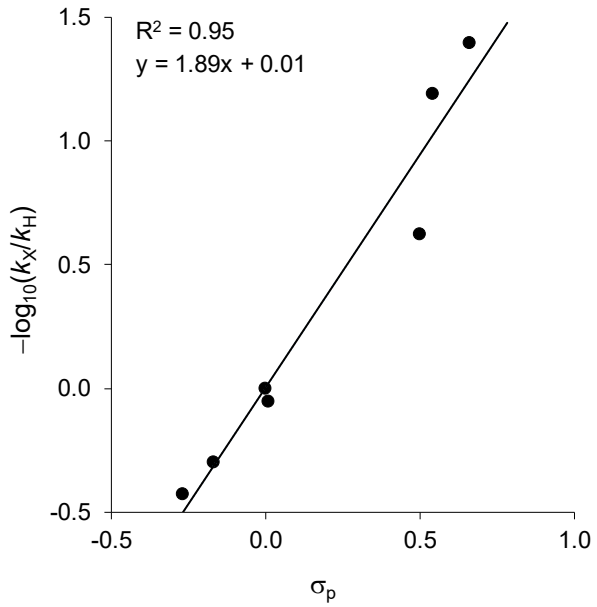

Figure 3.15: Correlation between σ_p Hammett substituent constants and the $-\log_{10}(k_X/k_H)$ values of the **2'–Y** series to transpose experimentally determined rate constants onto the

classic Hammett scale of substituent effects.[1, 30] $k_{X/H}$ values measured in acetone-d_6 (400 MHz, 298 K).

A strong correlation between the values obtained from treatment of the experimental rate constants with Hammett-style analysis, an R^2 of 0.95, confirms that this method of substituent effect quantification is applicable to the model reaction used in this study. Thus, the rate constants, k_X, describe the transferrable substituent effects previously established by Hammett.[1] The equation of the straight line ($y = mx + c$) in **Figure 3.15** (**Equation 3.2**) can be used to define a parameter, $\sigma_{p(react)}$, where the substituent constants are transposed onto the Hammett scale akin to the method used in **Chapter 2**.

$$\sigma_{p(react)} = \frac{\left(-log_{10}\left(\frac{k_X}{k_H}\right)\right) - \gamma}{\rho} \qquad \textbf{Equation 3.2}$$

Where ρ is the Hammett reaction constant and is the gradient of the best fit line in **Figure 3.15** and thus equal to 1.89. The intercept of the best fit line of **Figure 3.15** is thus, γ and equal to 0.01.

The rate constants of the pyridine derivatives in series **2'–Y** and **2–X** (**Figure 3.3**), measured in acetone-d_6 at 298 K, and the values of $-\log_{10}(k_X/k_H)$ and $\sigma_{p(react)}$ are presented in **Table 3.1**.

Table 3.1: Rate constants (k_X) of all pyridine derivatives studies measured in acetone-d_6 (400 MHz, 298 K), values averaged over two experiments and their $-\log_{10}(k_X/k_H)$ and $\sigma_{p(react)}$ values. All values of k_X and their analysis to obtain $-\log_{10}(k_X/k_H)$ and $\sigma_{p(react)}$ values was performed by RJB. Error analysis details and both experimental k_X values of all compounds can be found in Appendix B.

Compound	Average k_X / x10^{-5} s^{-1}	$-\log_{10}(k_X/k_H)$	$\sigma_{p(react)}$[a]
2'–H	9.26	0.00	0.00 (0.00)
2'–OMe	24.97	–0.43	–0.23 (–0.27)
2'–Me	18.48	–0.30	–0.16 (–0.17)
2'–Ph	10.46	–0.05	–0.03 (+0.01)
2'–CN	0.37	+1.39	+0.74 (+0.66)
2'–CF_3	0.60	+1.19	+0.63 (+0.54)
2'–$COCH_3$	2.21	+0.62	+0.33 (+0.50)
2–a	23.37	–0.40	–0.22
2–b	2.98	+0.49	+0.26
2–c	9.61	–0.02	–0.01
2–d	8.92	+0.02	0.00
2–e	15.22	–0.22	–0.12
2–f	5.29	+0.24	+0.12
2–g	10.49	–0.05	–0.03
2–h	3.37	+0.44	+0.23
2–i	15.21	–0.22	–0.12
2–j	3.39	+0.44	+0.23

[a] Hammett σ_p constant values quoted in brackets for the **2'–Y** series.[1, 30]

In the **2'–Y** series, enhancement of the experimental rate constant was achieved through stabilisation of the developing positive charge in the polar transition state afforded by through-bond electron-donating substituents. Thus, enhanced reaction rate constants, relative to the unsubstituted case (**2'–H**), were observed for traditionally through-bond electron-donating substituents (OMe, Me and Ph) and these substituents have negative values of $\sigma_{p(react)}$. Correspondingly, the through-bond

electron-withdrawing substituents (CN, CF_3 and $COCH_3$) result in lower reaction rate constants than **2'–H**, with positive $\sigma_{p(react)}$ values. The observed relative rates are in step with those of Hunter and co-worker's 2003 study (**Figure 3.1**), supporting the validity of experimental rate constant determination and quantification through Hammett-style analysis.[21]

With an understanding of how substituents of differing electronic properties effect the experimental rates, and how this is transposed onto the classic Hammett scale, evaluation of how the substituents of the 4-phenyl pyridine series, **2–X**, influence the reactivity of the pyridine ring can be performed. Such interpretation allowed the results of the **2–X** compounds to be placed in the context of the **2'–Y** series, where substituent effects are easy to understand in traditional through-bond terms and thus help to highlight interesting experimental results within the **2–X** series.

Two subsets of compounds displayed interesting experimental behaviour akin to those seen in the **1–X** series of molecular balances (**Figure 3.16**).

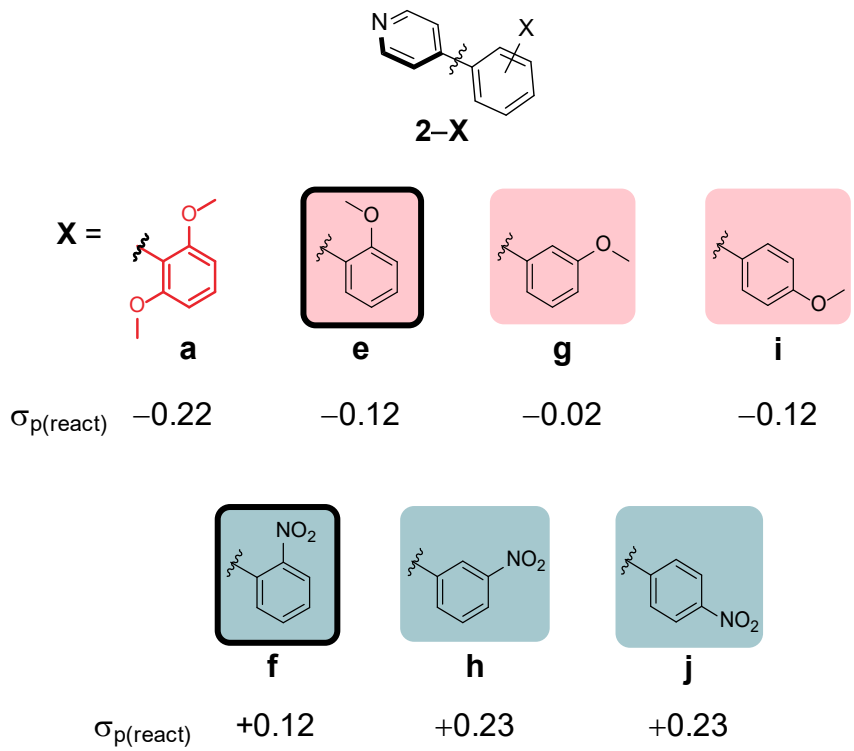

Figure 3.16: Two subsets of compounds within series **2–X** that displayed interesting experimental behaviour, shown with their $\sigma_{p(react)}$ values. Compounds wherein through-space substituent effects are possible are outlined in black.

The first of these subsets comprised of **2–a**, **2–e**, **2–g** and **2–i**, which all contained methoxy substituents in various numbers and positions around the X-substituted ring (top row, **Figure 3.16**). The other subset of **2–X** compounds with interesting results contained nitro groups in different positions around the X-substituted ring, compounds **2–f**, **2–h** and **2–i** (bottom row, **Figure 3.16**). For the compounds of both subsets where the substituent is in the *meta* or *para* position to the pyridyl-phenyl bond, the effect on the rate constant is in line with that expected from the σ_m and σ_p Hammett substituent constants. For the methoxy substituted **2–X** subset, moving the methoxy group from the *para* position to the pyridyl-phenyl bond in **2–g**, to the *meta* position relative to the pyridyl-phenyl bond in **2–i** results in a change in $\sigma_{p(react)}$ of 0.10 towards electronically neutral behaviour (akin to **2'–H**). This is accompanied by a difference in the average experimental rate constant of 4.78 s^{-1}. Such a change between these compounds is in line with what would be expect based upon their Hammett constants, where a *meta* positioned methoxy group has a σ_m of 0.12 but opposite behaviour in the

para position where σ_p −0.27. For the nitro substituted **2–X** subset, the $\sigma_{p(react)}$ values are the same when the nitro group is in the *meta* position (**2–h**) and the *para* position (**2–j**) to the pyridyl-phenyl bond and the difference in their experimental rate constants is negligible. This result is unsurprising through consultation with the Hammett parameters of a nitro group, σ_m and σ_p, which are similar, at +0.71 and +0.78 respectively.

It is substituents in the *ortho*-position to the pyridyl-phenyl bond of the X-substituted ring that display experimental results that are less explainable through traditional through-bond assessment of their behaviour. Substituents in this positon (**2–a**, **2–e** and **2–f**) resulted in faster rates than when in the *meta* or *para* positions. With a nitro group in this position, compound **2–f**, the $\sigma_{p(react)}$ value is 0.11 closer to zero than for the same group in the *meta* and *para* position meaning that it is moving towards electro-enhancing behaviour. In compound **2–e**, with a single methoxy group in this position, the $\sigma_{p(react)}$ value is the same as for **2–i** where the methoxy group is in the *para* position. In particular, the rate of **2–a**, bearing two *ortho* positioned methoxy groups, the $\sigma_{p(react)}$ value is almost twice that of **2–e**. Thus, it appears that the through-space effect of the methoxy group in this position is additive.

3.3.5 Computational Analysis

Insight into the interesting experimental rate constants as highlighted by their $\sigma_{p(react)}$ values can be gained through the use of computational modelling, in particular, calculated ESP surfaces and slices, which were invaluable in the assessment of through-space substituent effects in **Chapter 2**. In addition to visualisation of the substituent effects in series **2–X** using ESP surfaces and slices, Ionisation Energies (IE) provide a valuable metric by which to assess substituent effects in these compounds. The ionisation energy is a measure of how much energy is required to remove an electron; the smaller this energy the easier the electron removal at this site will be. Thus, as pyridine is acting as a nucleophile in the present study, a smaller value of the ionisation energy would lead to an enhanced reaction rate.

Equilibrium geometries of the pyridine compounds of both series **2'–Y** and **2–X** were obtained at the DFT/B3LYP/6–31G* level of theory using Spartan '14. From these minimised geometries, ESP and IE surfaces and ESP slices were calculated from which ESP and IE values were taken over the pyridine nitrogen atom (IE_N and ESP_N respectively). Plotting the experimentally determined $\sigma_{p(react)}$ values against IE_N and ESP_N resulted in similar correlations, with R^2 values of 0.93 and 0.92 respectively (**Figure 3.17**).

The strong correlation between IE_N and the experimental data confirms that the substituents of both **2'–Y** and **2–X** are influencing the observed rate constant through modification of the pyridine nitrogen atoms ionisation energy and thus its ability to act as a nucleophile (**Figure 3.17D**). Electrostatics were shown to be important to the *N*-methylation rate constant, k_X, through strong correlation between the ESP_N and the experimental data. Therefore, the experimentally observed substituent effects can be assessed using ESP values, surfaces and slices (**Figure 3.17B**). The IE_N and ESP_N values for all compounds are given in **Table 3.2**.

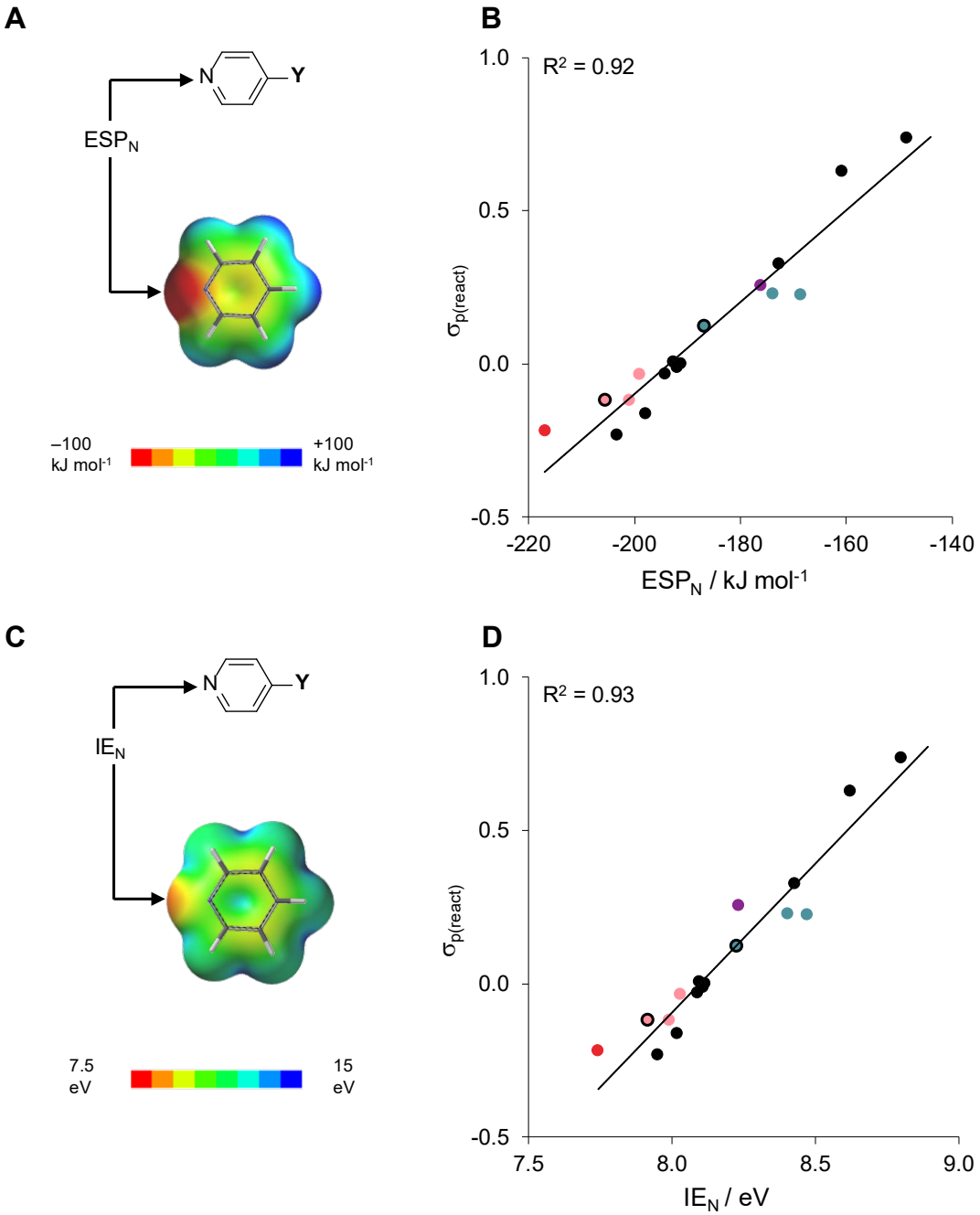

Figure 3.17: (A) Position of ESP_N calculation a shown on a ChemDraw representation of a Y-substituted pyridine compound (**TOP**) and on the ESP surface of pyridine, **2'–H** (**BOTTOM**). **(B)** Plot of ESP_N against $\sigma_{p(react)}$ for all pyridine derivatives with the interesting examples discussed in ***Section 3.3.4*** highlighted according to their colour in **Figure 3.17** or as pink (compounds **2–e**, **2–g**, **2–i**) or teal (compounds **2–f**, **2–h**, **2–j**). In particular, compounds **2–e** and **2–f** are denoted with a black outline on their respective colours. **(C)** Position of IE_N calculation on pyridine, **2'–H**. **(D)** Plot of IE_N against $\sigma_{p(react)}$ for all pyridine derivatives, with the same compounds highlighted with the same colours as in **Figure 3.18B**. All errors were omitted from these plots for clarity. A version of the graph with error bars included is included in Appendix B. Structures and surfaces were minimised using DFT/B3LYP/6–31G* in Spartan '14. All data obtained by RJB. The ESP and IE values over the pyridine nitrogen were taken at the 0.002 electron/Bohr^3 isosurface as indicated.

Table 3.2: ESP_N and IE_N values of all compounds within the **2'–Y** and **2–X** series. All structures and surfaces (from which ESP_N and IE_N values were calculated) were minimised and calculated using DFT/B3LYP/6–31G* in Spartan '14. Full details on ESP_N and IE_N calculation are given in Appendix B.

Compound	ESP_N / kJ mol^{-1}	IE_N / kJ mol^{-1}
2'–H	–191.2	8.12
2'–OMe	–203.3	7.95
2'–Me	–197.8	8.02
2'–Ph	–194.2	8.09
2'–CN	–148.6	8.80
2'–CF_3	–160.8	8.62
2'–$COCH_3$	–172.7	8.43
2–a	–216.9	7.74
2–b	–176.2	8.23
2–c	–191.9	8.11
2–d	–192.6	8.09
2–e	–205.6	7.92
2–f	–186.9	8.22
2–g	–199.0	8.03
2–h	–173.9	8.40
2–i	–200.9	7.99
2–j	–168.6	8.47

The influence of traditionally electron-withdrawing and donating groups on the ESP_N values is the same as was on the ESP_{ipso} values of the molecular balances (**Table 3.2**). Electron-donating substituents in the **2'–Y** series (OMe and Me) had more negative potentials and correspondingly red colours to the pyridine nitrogen atom on the ESP surfaces and slices. The reverse was true for the through-bond electron-withdrawing substituents of the **2'–Y** series (CF_3, CN and $COCH_3$).

Analysis of the ionisation energies in series **2'–Y** showed that traditionally electron-donating substituents resulted in lower IE_N values, with electron-withdrawing substituents giving higher values of IE_N with respect to pyridine, **2'–H** (**Table 3.2**).

Ionisation energy surfaces indicate areas where electron removal requires the most (blue) and least (red) energy meaning that electron-donating substituents had more red colour over the pyridine nitrogen atom (**Figure 3.18**). Thus, for those substituents which are electro-enhancing, the pyridine nitrogen atom is more ionisable.

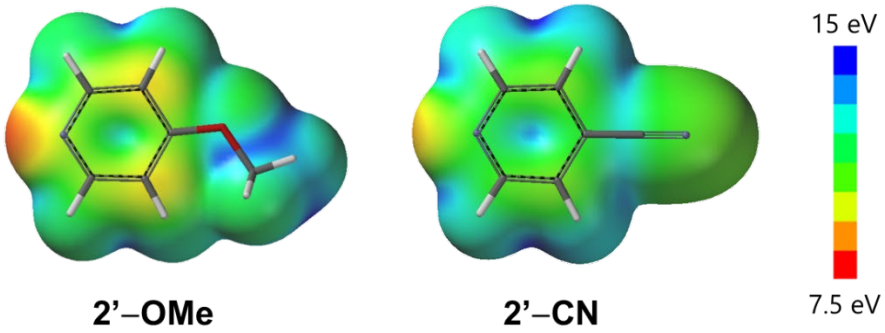

Figure 3.18: Local ionisation potential surfaces of **2'–OMe** and **2'–CN**. Structures and surfaces were minimised using DFT/B3LYP/6–31G* in Spartan '14.

Visualisation of the compounds highlighted by their $\sigma_{p(react)}$ values in the previous section through their ESP surfaces and slices unveiled similar substituent effects on the pyridine ring as on the Y-substituted rings of the **1–X** series (**Figure 3.19**).

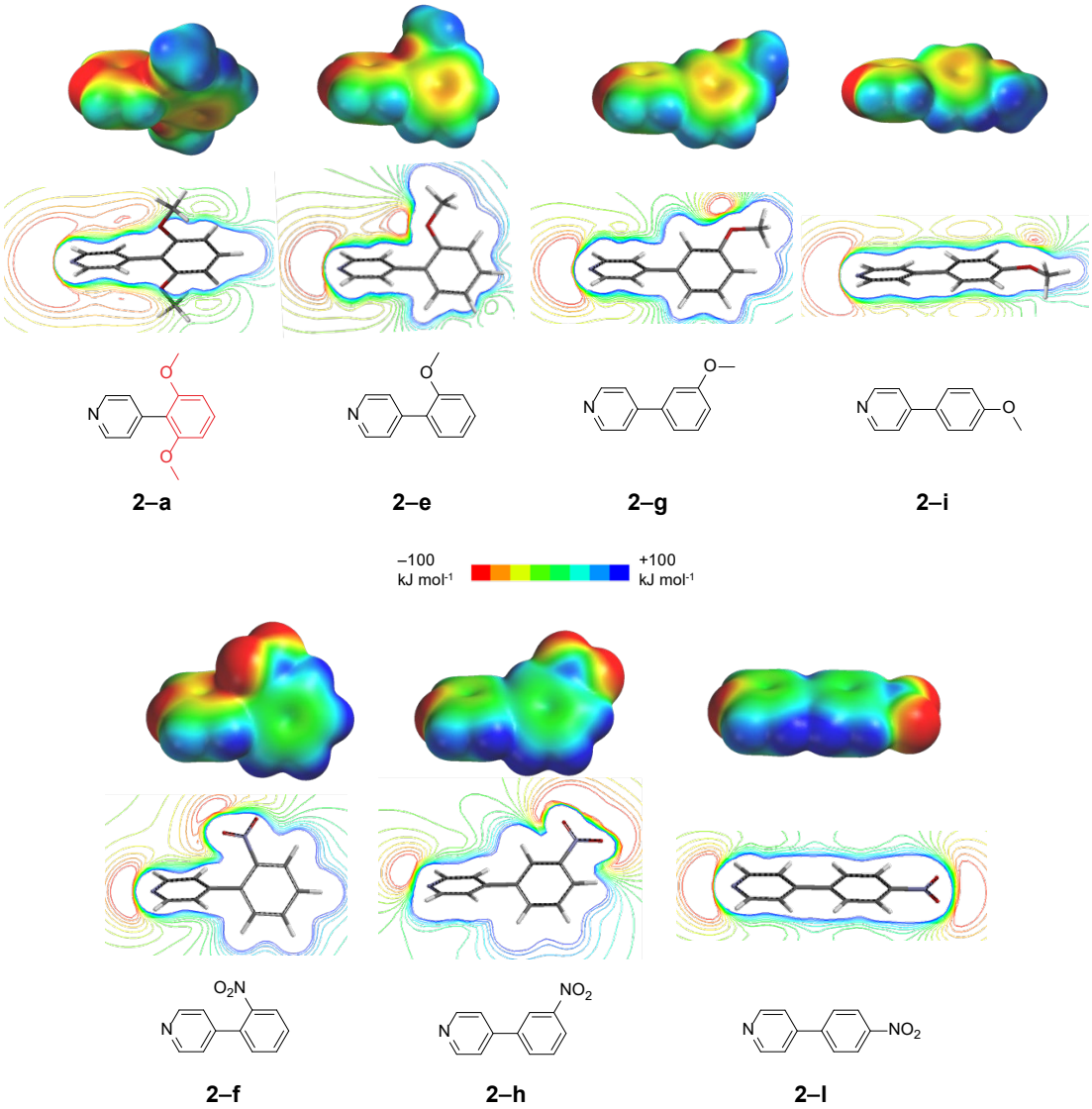

Figure 3.19: The ESP surfaces (**TOP**) and slices (**MIDDLE**) of the compounds highlighted in **Figure 3.17**. All structures and surfaces were minimised and calculated using DFT/B3LYP/6–31G* in Spartan '14. The ESP surfaces and slices of all compounds in both the **2'–Y** and **2–X** series are in Appendix B.

For those pyridine derivatives where the substituent on the X-substituted ring is *ortho* to the pyridyl-phenyl bond (**Figure 3.3**), the same through-space effect was seen as in the analogous molecular balances (**Figure 2.4**) *via* the ESP slices of these compounds. The field perturbation caused by the methoxy group(s) in **2–e**/**2–a** and the nitro group in **2–f** are geometrically capable of influencing the electrostatics of the pyridine ring and thus of the reactive centre (**Figure 3.19**) mirroring what was observed in balances **1–a** and **1–d** (**Figure 2.24**). This through-space influence is shown to modify the

reactivity of the pyridine nitrogen atom through both the computationally derived ESP values and ionisation energies of these compounds, which show more negative ESP_N values and lower IE_N values than pyridine, **2'–Y**. These computational results point to through-space electro-enhancement of the reactive centre, a conclusion which is supported by the experimentally determined rate constants.

The compound for direct comparison of substituent effects with **2–a**, which would have been the pyridine analogue of molecular balance **1–b**, was not obtained (see ***Section 3.3.2***). Despite the lack of experimental support, computationally derived ESP_N and IE_N values, the former of which have proven to be key in measuring and predicting the through space effects in the **1–X** series of molecular balances, support the importance of through-space effects in governing the reactivity of compound **2–a** (**Figure 3.20**).

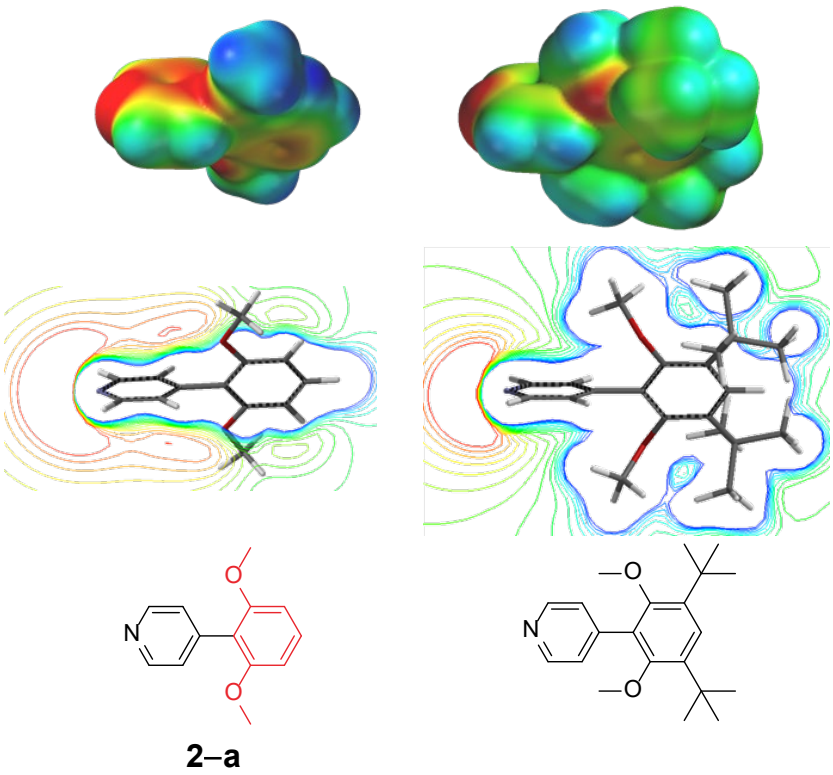

2–a

Figure 3.20: ESP surfaces (**TOP**) and slices (**MIDDLE**) of **2–a** (**LEFT**) and the pyridine analogue of molecular balance **1–b** (**RIGHT**). All structures and surfaces were minimised and

calculated using DFT/B3LYP/6–31G* in Spartan '14. The ESP surfaces and slices of all compounds in both the **2'–Y** and **2–X** series are in Appendix B.

The same twisting of the methoxy groups seen for the **1–b** was seen in the pyridine analogue and this is accompanied by a less negative ESP_N values and larger IE_N value than for **2–a**. Thus, the substituent effect of **2–a** on the rate constant can be attributed to the through-space effect of the methoxy groups.

A similar computational analysis for the pyridine analogue of **1–d**, can be performed and compared to compound **2–b** (**Figure 3.21**).

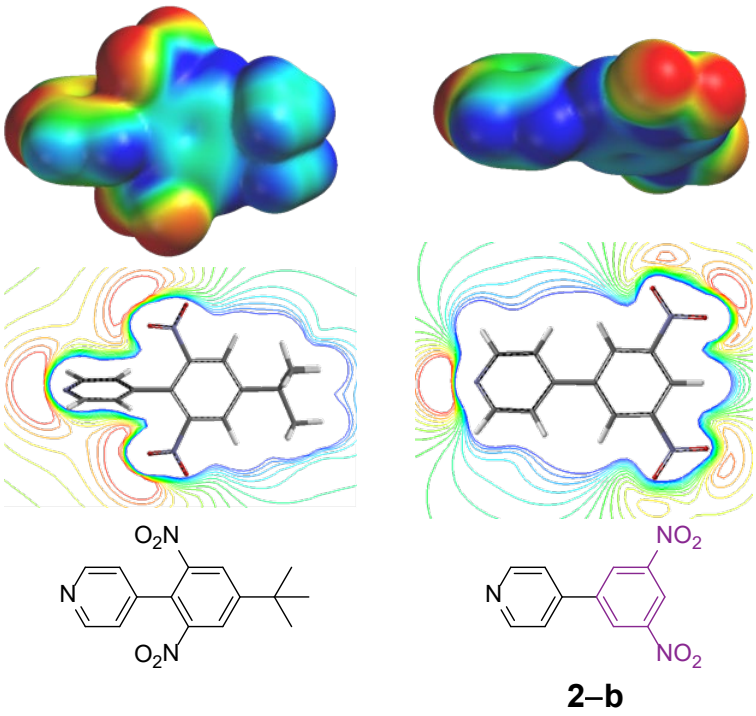

Figure 3.21: ESP surfaces (**TOP**) and slices (**MIDDLE**) of the pyridine analogue of molecular balance **1–d** (**LEFT**) and **2–b** (**RIGHT**). All structures and surfaces were minimised and calculated using DFT/B3LYP/6–31G* in Spartan '14. The ESP surfaces and slices of all compounds in both the **2'–Y** and **2–X** series are in Appendix B.

The same electro-enhancing behaviour of the substituent of **1–d** is observed for the pyridine derivative as was observed for the molecular balance. The field perturbation of the nitro groups when *ortho* to the pyridyl-phenyl bond influences the electrostatics

of the pyridine reactive centre as shown by the ESP slice. The corresponding ESP_N values of this compound is more negative and the IE_N lower than that of **2–b**, providing further indication that this compound would have enhanced reactivity *via* through-space electro-enhancement.

Much like molecular balances **1–b**, **1–c**, **1–e** and **1–k** to **1–n** inclusive, the 4-phenyl substituted pyridine derivatives bearing substituents on the X ring in the *meta* or *para* position to the pyridyl-phenyl bond are not able to influence the electrostatics of the pyridine ring (see ***Section B.1.1***). These pyridine derivatives, **2–g** to **2–j** inclusive, have less negative ESP_N values and larger IE_N values than **2–e** and **2–f**, indicating more electro-attenuating behaviour than in the *ortho* position. This is mirrored in their smaller rate constants than their *ortho* substituted analogues.

3.3.6 Conclusions on Through-Space Effects on Reactivity

A combined computational and experimental examination of whether the substituents shown to exhibit through-space effects in the molecular balance **1–X** series can affect reaction rates was presented. Experimental rate constants were used to obtain $-\log_{10}(k_X/k_H)$ values that were then used to transpose substituent effects on reactivity onto the standard Hammett substituent constant scale, giving $\sigma_{p(react)}$. This parameter was used to rank the reactivity of the pyridine derivatives at the heart of this study. This ranking, together with excellent correlations with computed ESPs and IEs, showed the compounds already established as exhibiting through-space effects (**Chapter 2**) displayed this behaviour in the present study. Furthermore, analysis of the most striking kinetic influences showed that through-space influences did indeed dominate substituent effects on chemical reactivity in these contexts.

3.5 Transferability of Through-Space Substituent Effects

With an understanding of how the molecular balances behave in solvents of differing properties (see ***Section 2.5***) and the ability of through-space effects to modulate chemical reactivity (see ***Section 3.3***), the transferability of the $\sigma_{p(conf)}$ constants derived in **Chapter 2** can be evaluated.

A transferable substituent constant to quantify through-space substituent effects would be able to predict this type of behaviour in other systems. Thus, $\sigma_{p(conf)}$ should be able to predict the through-space effects present in compounds **2–a**, **2–e** and **2–f** through correlation with the values of substituent effect quantification from the kinetic data. While the kinetic data was obtained in actone-d_6, the conformational equilibria data was obtained in a total of eleven solvents. The $\sigma_{p(conf)}$ values were determined from the experimental data obtained in benzene-d_6 due to the quality of the correlation between the Hammett σ_p and $-\log_{10}(K_X/K_H)$ values being the best in this solvent (R^2 of 0.97). However, $-\log_{10}(K_X/K_H)$ values were calculated for each solvent studied and thus allows a thorough evaluation of how the quantification of through-space substituent effects by the molecular balances can be applied to a different system. As such, this section will use the basic quantification of the substituent effects in the molecular balances in each solvent studied, $-\log_{10}(K_X/K_H)$, to correlate with the kinetic data obtained in acetone-d_6, $-\log_{10}(k_X/k_H)$ (**Figure 3.22**).

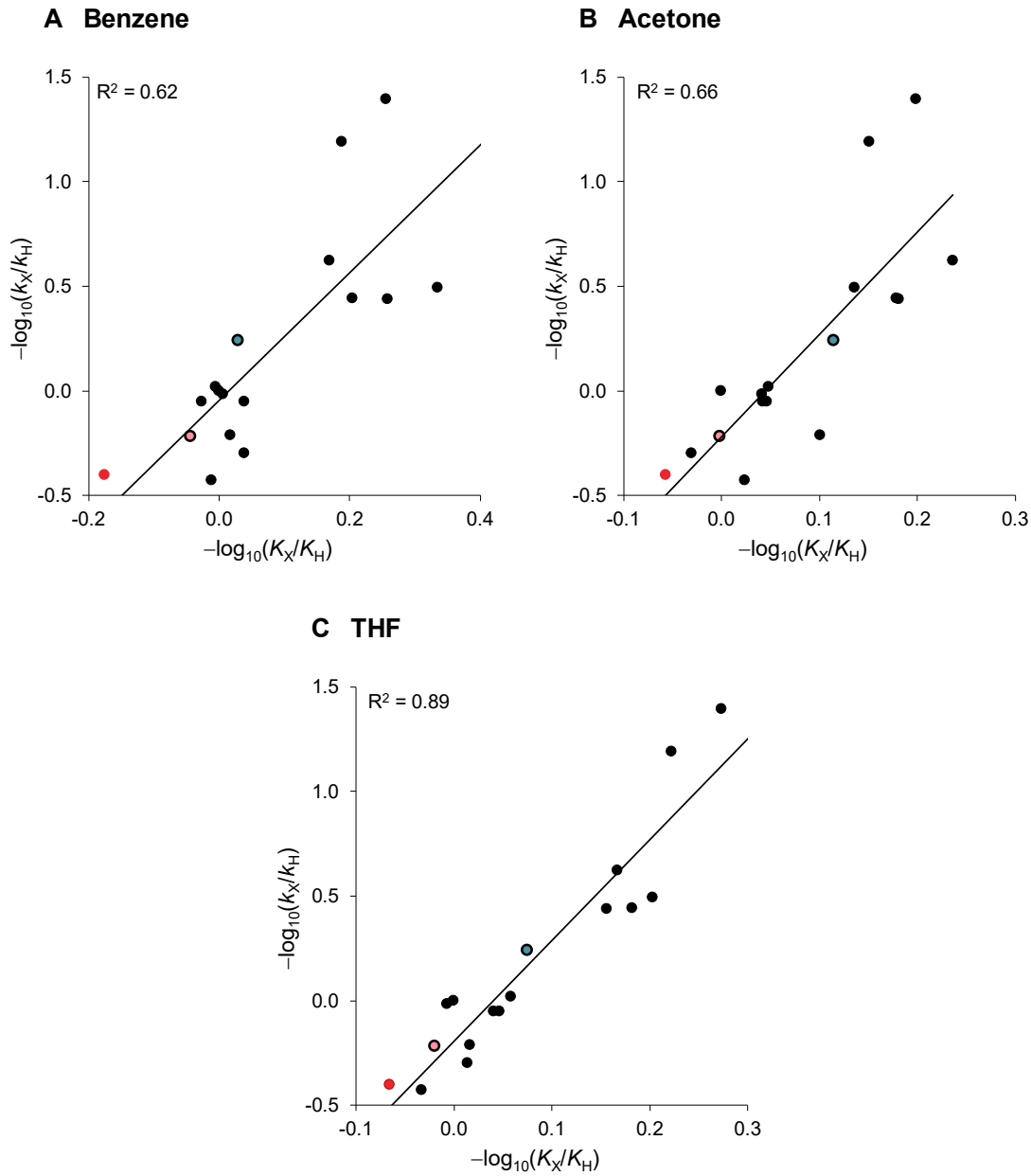

Figure 3.22: Plots of the kinetic data, $-\log_{10}(k_X/k_H)$, against the values of $-\log_{10}(K_X/K_H)$ obtained in **(A)** benzene-d_6, **(B)** acetone-d_6 and **(C)** THF-d_8. Compounds **2–a**/**1-a**, **2–b**/**1–e**, **2–e**/**1–l** and **2–f**/**1–j** highlighted according to their colours in **Figures 2.4** and **3.17**. All kinetic data obtained by RJB and the molecular balance analysed by RJB, with data collection by RJB, Ioulia K. Mati and previously reported as described in **Figure 2.4**.[31-33] Correlations between $-\log_{10}(k_X/k_H)$ and $-\log_{10}(K_X/K_H)$ in all other solvents is provided in Appendix B.

The correlation between the kinetic data and the solvent from which $\sigma_{p(conf)}$ was derived, benzene-d_6, was quite poor with an R^2 of 0.62 (**Figure 3.22A**). One could attribute such a poor correlation to the difference in the properties of these two

solvents. Solvents are known to affect the rates of S_N2 reactions through specific solvation of the transition state, which is also the rate determining step in such mechanisms.[28-29] However, surprisingly, the correlation between the $-\log_{10}(k_X/k_H)$ of the kinetic data, obtained in acetone-d_6, and the $-\log_{10}(K_X/K_H)$ values for the molecular balances in acetone-d_6 was not much better than with that in benzene (**Figure 3.22B**). Strikingly, a better correlation was found with the $-\log_{10}(K_X/K_H)$ values of the molecular balances in THF-d_8 (**Figure 3.22C**). While THF and acetone have similar polarity and cohesive energy densities,[34] the better correlation with the former solvent could be due to the specific solvation of the *N*-methylation transition state in acetone being better described by the solvent effects of THF on the molecular balance equilibria. However, such a conclusion is speculative and would require conducting the present reaction in a diverse range of solvents to obtain experimental data on how the rate is affected by solvent effects. Moreover, as noted earlier, such an experiment would require that both the reagents and products are soluble in the solvent of choice. Correlation of this data with solvent parameters would help to understand the transition state of the reaction better and thus the solvent effects upon it.[35] Nonetheless, this finding highlights the sensitivity of through-substituent effects to changes in substituent position relative to transition states and the reaction solvent. As these substituent effects dependent upon geometry and the solvent, this could result in difficulty in finding a general, widely transferable empirically derived substituent constant that can predict through-space effects.

3.6 Conclusions and Remarks

A quantitative analysis of through-space substituent effects on reactions rates and the effects of solvation on through-space effects have been provided leading to evaluation of the transferability of $\sigma_{p(conf)}$. A combined experimental and computational approach was utilised to investigate if the through-space substituent effects observed in **Chapter 2** could influence chemical reactivity. Experimental rate constants were used to obtain $-\log(k_X/k_H)$ values which were transposed onto the Hammett scale through plotting against σ_p. The equation of this straight line plot gave the value of ρ (which was 1.98)

alongside that of a constant, γ (which was 0.01). These values were then used to obtain a new substituent constant, $\sigma_{p(react)}$ of each substituent through Hammett-type analysis. Computed ionisation energy and electrostatic potential surfaces and slices provided invaluable information of the importance of field effects through comparison with the experimental $\sigma_{p(react)}$ values. Together, these techniques showed that through-space substituent effects were in operation in the pyridine derivatives studied and were thus able to influence the reaction rates of the pyridine *N*-methylation reactions.

Solvent effects on the molecular balances in **Chapter 2** were evaluated in **Chapter 2**, ***Section 2.5*** by obtaining $-\log(K_X/K_H)$ values in eleven solvents of varying degrees of polarity. This balance design is known to be sensitive to solvation effects and this is upheld within the balances studied in **Chapter 2**. The sensitivity of these effects to solvation is due to the electrostatic nature of the through-space field effects. Therefore, the extent to which through-space substituent effects can influence chemical reactivity or equilibria will be at least partially influenced by the solvent. The electrostatic nature of field effects also means that they are sensitive to the geometrical relationship of the substituent with the reaction centre. Thus, that the molecular balances studied in **Chapter 2** are sensitive to solvent effects is not unexpected, but does highlight an important aspect of through-space substituent effects that could mean universally applicable empirical quantification of these effects will be challenging to achieve. It should be noted that universal applicability is difficult even for the well-established and widely used Hammett constants (which were defined in water), of which many iterations and re-definitions have been performed to suit the widest range of circumstances.[1] Despite the issues regarding quantification of through-space effects due to their sensitivity to environmental factors, through-space effects have been shown to dominate over through-bond influences, meaning that they cannot be ignored in the quantification of electronic substituent effects.

The predictive power of ESPs in determining through-space substituent effects has been demonstrated during the empirical studies contained within **Chapters 2 and 3**, as well as the theoretical works of Wheeler, Houk and Suresh.[7-9, 36] In fact, Suresh and Galabov have defined constants with which to understand electronic substituent effects on benzene ring using ESP values. Though it should be noted that the transferability

of the constants defined in these computational studies has not been examined.[37-42] A further advantage to *in silico* studies is the ability they afford to examine substituents and systems that are harder to study empirically.[42] However, computational analysis also has drawbacks in that modelling solvation effects is both computationally expensive and error prone. This particular weakness of computational work is less challenging to the synthetic chemist. Experimentally, screening the effect of solvents on substituent effects is a relatively simple, but time-consuming process. Indeed, the parameters defined in ***Section 2.5*** were derived in a range of solvents (see ***Section A.5***). However, since data determined from empirical studies inevitably encode both induction and field effects, combined experimental and theoretical studies provide the most pragmatic means of gaining understanding of the contributions to substituent effects. Although it has been found that a single, robust parameter to encode through-space substituent effects is not feasible due to complications from solvent effects and contextual differences, it is hoped that researchers can make use of this set of parameters when analysing through-space substituent effects in their own systems.

3.7 References

1. Hansch, C.; Leo, A.; Taft, R. W., A survey of Hammett substituent constants and resonance and field parameters. *Chem. Rev.* **1991,** *91* (2), 165-95.

2. Grubbs, E. J.; Fitzgerald, R.; Phillips, R. E.; Petty, R., The transmission of substituent effects in isomeric dichloroethano-bridged anthracene derivatives. *Tetrahedron* **1971,** *27* (5), 935-944.

3. Wilcox, C. F.; Leung, C., Transmission of substituent effects. Dominance of field effects. *J. Am. Chem. Soc.* **1968,** *90* (2), 336-341.

4. Stock, L. M., The origin of the inductive effect. *J. Chem. Ed.* **1972,** *49* (6), 400.

5. Golden, R.; Stock, L. M., Dissociation constants of 8-substituted 9,10-ethanoanthracene-1-carboxylic acids and related compounds. Evidence for the field model for the polar effect. *J. Am. Chem. Soc.* **1972,** *94* (9), 3080-3088.

6. Topsom, R. D., The isolated molecule approach. Theoretical studies of the inductive effect. *J. Am. Chem. Soc.* **1981,** *103* (1), 39-44.

7. Wheeler, S. E.; Bloom, J. W. G., Toward a More Complete Understanding of Noncovalent Interactions Involving Aromatic Rings. *J. Phys. Chem. A* **2014,** *118* (32), 6133 - 6147.

8. Wheeler, S. E., Understanding Substituent Effects in Noncovalent Interactions Involving Aromatic Rings. *Acc. Chem. Res.* **2013,** *46* (4), 1029 - 1038.

9. Sayyed, F. B.; Suresh, C. H.; R., G. S., Appraisal of Through-Bond and Through-Space Substituent Effects via Molecular Electrostatic Potential Topography. *J. Phys. Chem. A* **2010,** *114* (42), 12330 - 12333.

10. Roberts, J. D.; Moreland Jr, W. T., Electrical Effects of Substituent Groups in Saturated Systems. Reactivities of 2-substituted Bicyclo[2.2.2]octane-1-carboxylic Acids. *J. Am. Chem. Soc.* **1953,** *75* (9), 2167 - 2173.

11. Chen, C.-T.; Siegel, J. S., Through-Space Polar-.pi. Effects on the Acidity and Hydrogen-Bonding Capacity of Carboxylic Acids. *J. Am. Chem. Soc.* **1994,** *116* (13), 5959-5960.

12. Padial, J. S.; de Gelder, R.; Fonseca Guerra, C.; Bickelhaupt, F. M.; Mecinović, J., Stabilisation of 2,6-Diarylpyridinium Cation by Through-Space Polar–π Interactions. *Chem. Eur. J.* **2014,** *20* (21), 6268-6271.

13. Bosmans, V.; Poater, J.; Hammink, R.; Tinnemans, P.; Bickelhaupt, F. M.; Mecinović, J., Probing Through-Space Polar−π Interactions in 2,6-Diarylphenols. *J. Org. Chem.* **2019,** *84* (6), 3632-3637.

14. Simó Padial, J.; Poater, J.; Nguyen, D. T.; Tinnemans, P.; Bickelhaupt, F. M.; Mecinović, J., Stabilization of 2,6-Diarylanilinum Cation by Through-Space Cation−π Interactions. *J. Org. Chem.* **2017,** *82* (18), 9418-9424.

15. Guan, L.; Holl, M. G.; Pitts, C. R.; Struble, M. D.; Siegler, M. A.; Lectka, T., Through-Space Activation Can Override Substituent Effects in Electrophilic Aromatic Substitution. *J. Am. Chem. Soc.* **2017**.

16. Holl, M. G.; Struble, M. D.; Singal, P.; Siegler, M. A.; Lectka, T., Positioning a Carbon-Fluorine Bond over the Pi Cloud of an Aromatic Ring: A Different Type of Arene Activation. *Angew. Chem. Int. Ed.* **2016,** *55* (29), 8266 - 8269.

17. Neel, A. J.; Hilton, M. J.; Sigman, M. S.; Toste, F. D., Exploiting non-covalent π interactions for catalyst design. *Nature* **2017,** *543*, 637.

18. Westheimer, F. H.; Kirkwood, J. G., The Electrostatic Influence of Substituents on the Dissociation Constants of Organic Acids. II. *J. Chem. Phys.* **1938,** *6* (9), 513-517.

19. Kirkwood, J. G.; Westheimer, F. H., The Electrostatic Influence of Substituents on the Dissociation Constants of Organic Acids. I. *J. Chem. Phys.* **1938,** *6* (9), 506-512.

20. Bowden, K.; Grubbs, E. J., Through-bond and Through-space Models for Interpreting Chemical Reactivity in Organic Reactions. *Chem. Soc. Rev.* **1996,** *25* (3), 171 - 177.

21. Hunter, C. A.; Low, C. M. R.; Vinter, J. G.; Zonta, C., Quantification of Functional Group Interactions in Transition States. *J. Am. Chem. Soc* **2003,** *125*, 9936 - 9937.

22. Smith, M. B.; March, J., *March's Advanced Organic Chemistry: Reactions, Mechanisms, and Structure*. 6th ed.; John Wiley & Sons, Inc.: United States of America, 2007.

23. Derick, C. G., Application of Polarity Measured in Terms of a Logarithmic Function of the Ionization Consant. III. Correlation of Chemical Structure with Ionization. *J. Am. Chem. Soc.* **1911,** *33* (7), 1181-1189.

24. Leão Lana, E. J.; Carazza, F.; Aparacida de Oliveira, R., Synthesis of 2-Aryl- and 2-Heteroaryl-3,5-dimethoxy-1,4-benzoquinones Involving Pd-Catalyzed Cross-Coupling of (2,3,4,6-Tetramethoxyphenyl)boronic Acid. *Helvetica Chimica Acta* **2004,** *87* (7), 1825-1831.

25. Kudo, N.; Perseghini, M.; Fu, G. C., A Versatile Method for Suzuki Cross-Coupling Reactions of Nitrogen Heterocycles. *Angew. Chem. Int. Ed.* **2006,** *45* (8), 1282-1284.

26. Ashton, P. R.; Harris, K. D. M.; Kariuki, B. M.; Philp, D.; Robinson, J. M. A.; Spencer, N., A borazaaromatic analogue of isophthalic acid. *Journal of the Chemical Society, Perkin Transactions 2* **2001,** (11), 2166-2173.

27. Nishimura, N.; Yoza, K.; Kobayashi, K., Guest-Encapsulation Properties of a Self-Assembled Capsule by Dynamic Boronic Ester Bonds. *J. Am. Chem. Soc.* **2010,** *132* (2), 777-790.

28. Away, K. C. W.; Lai, Z.-G., Solvent effects on SN2 transition state structure. II: The effect of ion pairing on the solvent effect on transition state structure. *Canadian Journal of Chemistry* **1989,** *67* (2), 345-349.

29. Westaway, K. C., Solvent effects on the structure of SN2 transition states. *Canadian Journal of Chemistry* **1978,** *56* (20), 2691-2699.

30. McDaniel, D. H.; Brown, H. C., An Extended Table of Hammett Substitutent Constants Based on the Ionization of Substituted Benzoic Acids. *J. Org. Chem.* **1958,** *23* (3), 420-427.

31. Mati, I. K. Molecular torsion balances for quantifying non-covalent interactions. The University of Edinburgh, 2013.

32. Mati, I. K.; Adam, C.; Cockroft, S. L., Seeing through solvent effects using molecular balances. *Chem. Sci.* **2013,** *4*, 3965 - 3972.

33. Muchowska, K. B.; Adam, C.; Mati, I. K.; Cockroft, S. L., Electrostatic Modulation of Aromatic Rings via Explicit Solvation of Substituents. *J. Am. Chem. Soc.* **2013,** *135* (27), 9976 - 9979.

34. Lide, D. R., *CRC Handbook of Chemistry and Physics*. 83rd ed.; CRC Press: 2002; p 2664.

35. Abraham, M. H., Solvent effects on reaction rates. *Pure & Appl. Chem* **1985,** *57* (8), 1055-1064.

36. Sayyed, F. B.; Suresh, C. H., Substituent Effects in Cation-Pi Interactions: A Unified View from Inductive, Resonance, and Through-Space Effects. *J. Phys. Chem. A* **2011,** *115* (22), 5660 - 5664.

37. Suresh, C. H.; Gadre, S. R., Electrostatic Potential Minimum of the Aromatic Ring as a Measure of Substituent Constant. *J. Phy. Chem. A* **2007,** *111* (4), 710-714.

38. Suresh, C. H.; Gadre, S. R., A Novel Electrostatic Approach to Substituent Constants: Doubly Substituted Benzenes. *J. Am. Chem. Soc.* **1998,** *120* (28), 7049 - 7055.

39. Suresh, C. H.; Alexander, P.; Vijayalakshmi, K. P.; Saj, Use of molecular electrostatic potential for quantitative assessment of inductive effect. *Phys. Chem. Chem. Phys.* **2008,** *10* (43), 6492 - 6499.

40. Sayyed, F. B.; Suresh, C. H., An electrostatic scale of substituent resonance effect. *Tetrahedron Lett.* **2009,** *50* (52), 7351 - 7354.

41. Galabov, B.; Nikolova, V.; Ilieva, S., Does the Molecular Electrostatic Potential Reflect the Effects of Substituents in Aromatic Systems? *Chem. Eur. J.* **2013,** *19* (16), 5149-5155.

42. Remya, G. S.; Suresh, C. H., Quantification and classification of substituent effects in organic chemistry: a theoretical molecular electrostatic potential study. *Phys. Chem. Chem. Phys.* **2016,** *18* (30), 20615-20626.

Chapter 4

Pseudo-Hydrogen Bonding

Abstract

Owing to their roles in governing DNA structure, protein-ligand binding, reactivity and supramolecular assembly, the importance of hydrogen bonding interactions within biological and chemical systems cannot be understated. When these interactions involve weak donors or acceptors they become inherently difficult to study, while solvent influences further complicate these studies. The quantification of weak hydrogen bonding has thus proven challenging. This work examines unexpected conformational preferences of molecular balances that on first appearances could have been attributed to weak intramolecular hydrogen bonds. The unexpected competitive nature of these apparent interactions were explored using the combined computational and experimental analysis approach proven to be successful in **Chapters 2** and **3**, and expanded upon through the use of SAPT energy partitioning. Using this technique to interpret the experimental conformational free energies of a series of molecular balances, an understanding of the components that contribute to apparent intramolecular hydrogen bond interactions was achieved. Surprisingly, even for the strongest hydrogen bond donor-acceptor pairing, conformational preferences were found to have major contributions from repulsive intramolecular interactions. In the most extreme examples, the attractive component of the apparent intramolecular hydrogen bonds was negligible, with the apparent hydrogen bonded contact instead being driven by steric or electrostatic destabilisation of the alternative, non-hydrogen-bonding conformation. Thus, we propose the term "*pseudo*-hydrogen bonding" to describe such hydrogen bonds.

Supplementary details are given in Appendix C.

Contributions: Series **2Y** was synthesised and analysed by RJB except **2F** and **2di-F** which were obtained by Nicholas Dominelli-Whiteley.[1] Compounds **1H**, **2H**, **3H** and series **1X** were previously reported,[2] with the exception of **1*p*-Br** which was obtained by RJB. Series **0X** was previously reported[2-4] with the exception of **0Me** which was obtained by RJB. Computational analysis (including SAPT) of series **2Y** and subsequent Boltzmann analysis was performed by RJB.

4.1 Introduction

4.1.1 Hydrogen Bonds

Hydrogen bonding is arguably the most significant non-covalent interaction, playing integral roles in the essential functions of life itself; protein structures and interactions, enzyme function, protein-ligand binding and even the secondary structure of DNA are underpinned by hydrogen bonding interactions.[5-9] Chemists have utilised the hydrogen bond in a wealth of different applications including medicinal chemistry, asymmetric catalysis and supramolecular chemistry.[10-13] It is this ubiquitous importance that has driven the vast number of studies investigating the nature of this interaction.

Despite the varied and vast number of examples of hydrogen bonds in nature and synthetic chemistry, the complexity of this interaction means the physicochemical origin of hydrogen bonding remains an active area of research as it depends upon the nature of the interacting pair, and thus the hydrogen bond strength.[14] The initial definition of a hydrogen bond is that of an attractive, directional and electrostatically driven interaction between a D–H···A pair, where D and A were N, O or F, with the lone pairs acting as the hydrogen bond acceptor.[14-17] Since this definition, experimental evidence primarily in the form of crystal structures coupled with *in silico* studies have shown that the dominant force governing a hydrogen bond is dependent upon intermolecular distances, directionality and interaction strength.[14] Thus is it difficult to attribute one single energetic facet as being solely responsible for hydrogen bonding interactions, though it is generally considered an electrostatic interaction.[15, 18]

Although the origin of hydrogen bonding is complicated, quantification of the ability of a functional group to accept and donate hydrogen bonds has been achieved within a series of studies by Abraham and Hunter.[19-21] In the 1990s and early 2000s, Abraham sought to quantify hydrogen-bond behaviour of a wide range of functionalities.[19-21] **Equation 4.1** was used to obtain a series of constants, α_2^H and β_2^H, that encode a functional group's ability to donate and accept hydrogen bonds respectively. Equilibrium association constants determined by NMR titration of 1:1 hydrogen bonding complexes provided the experimental data used in this quantification.[19-21]

$$logK = c_1\alpha_2^H\beta_2^H + c_2 \qquad \textbf{Equation 4.1}$$

Where constants c_1 and c_2 are solvent dependent and *K* is the experimental association constant of the 1:1 hydrogen bond complexation.

Correlating Abrahams α_2^H and β_2^H constants with computationally derived ESP surface maxima and minima respectively provided good linear correlations, showing that a simple electrostatic model of hydrogen bonding was sufficient to describe the thermodynamics of such interactions in solution.[22] Hunter used these plots from a 2004 study to obtain new donor and acceptor constants, α and β respectively, within an electrostatically dominated solvent competition model through implementation of **Equation 4.2**.[22]

$$\Delta G = -(\alpha - \alpha_s)(\beta - \beta_s) \qquad \textbf{Equation 4.2}$$

Where α and β are the hydrogen bond acceptor and donor parameters of the solute molecules and α_s and β_s are the hydrogen bond acceptor and donor constants of the solvent. In this model system, there is competition between solvent-solvent interactions and solvent-solute interactions leading to the establishment of an equilibrium between the 'free' state in which the solvent-solute interactions dominate and the 'bound' state where solvent-solvent/solute-solute interactions dominate (**Figure 4.1**).[22]

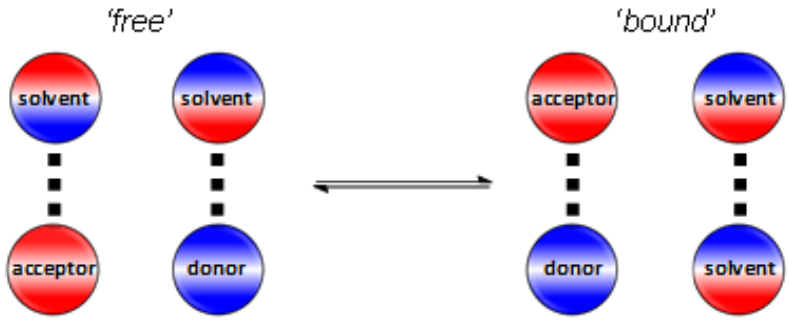

Figure 4.1: The equilibrium between 'free' and 'bound' states of a solute established as a result of competition between solute and solvent interactions which is central in Hunters 2004 study.[22]

The relative strength of a hydrogen bond can be assessed using the α and β constants derived from **Equation 4.2**; the larger the value of α or β, the better a functional group is at forming hydrogen bonds, acting as either a donor or acceptor, respectively. These constants allow the estimation of the free energy of an interaction between two functionalities of the solutes in a given solvent. Such an approach allows profiles to be drawn for a particular solvent that reveal the combinations of functional groups that have favourable (ΔG is negative, blue quadrants) and unfavourable (ΔG is positive, red quadrants) interactions (**Figure 4.2**). The strength of hydrogen bonds is known to be sensitive to their environment meaning that they can be fine-tuned by changing the functional groups involved in the interaction.[22-23] Thus, quantification of hydrogen bonds in this manner allows for the tuning of hydrogen bond strengths within a given system.

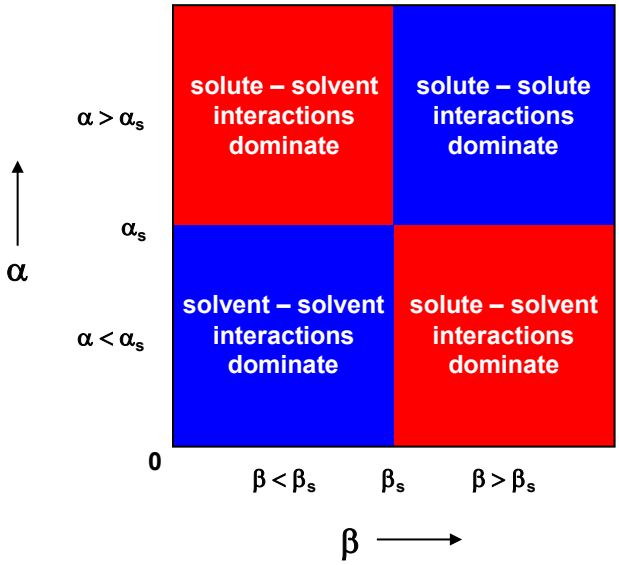

Figure 4.2: The regions of α and β values for the solute functionalities that will give rise to favourable (blue quadrants) and unfavourable (red quadrants) interactions with respect to the α_s and β_s values of the solvent.[22]

The strength of hydrogen-bonding interactions ranges from ~0.5 to 250 kJ mol^{-1}.[24] The strongest hydrogen bonds are those formed between with FH/NH/OH donors and nitrogen- or oxygen-containing acceptors, which were among the first elements classified as taking part in hydrogen bonds. However, as weaker interactions have been discovered over the past 100 years since the term "hydrogen bond" was coined, the consensus of the functional groups that can take part in such an interaction has expanded such that acceptors need not bear a lone pair. Thus, any element with a greater electronegativity than hydrogen has been found to be capable of accepting a hydrogen bond as have π-systems. In fact, interactions as exotic as 'dihydrogen bonding' fall under the umbrella of "hydrogen bonding" and involves a metal bound hydride as the hydrogen bond acceptor.[14] These weaker hydrogen bonding interactions are known to be difficult to study, but could be important within biological systems, for example within the solvent-excluded interior of a protein binding site.[24-25] Thus, numerous studies have been performed to understand the hydrogen-bond acceptor ability of these weak interactions. In particular, the ability of fluorine to accept hydrogen bonds in organic molecules has been the subject of many theoretical and experimental studies due to the important role fluorine plays in medicinal chemistry.[15]

4.1.2 Organofluorine and Other Halides as Hydrogen Bond Acceptors

Organofluorine compounds are those containing a C–F bond and though they are rare in nature,[26-28] they are prevalent motifs in medicinal, agricultural and synthetic chemistry with more than one third of agrochemicals and one fifth of all marketed drugs containing organofluorine.[15, 28-29] Carbon-bound fluorine has a van der Waals radii of 1.47 Å; between the size of hydrogen and oxygen, and smaller than methyl and hydroxyl groups.[28, 30] As a result, fluorine is routinely used in medicinal chemistry to replace hydrogen and other functional groups to alter the pharmacological properties of biologically active substrates.[29-31] Despite the important role fluorinated compounds play in a field where hydrogen bonds are ubiquitous, the ability of organofluorine to partake in hydrogen bonding interactions has been a controversial issue.

The highly polarised nature of the C–F bond caused by the high electronegativity of fluorine results in reduced fluorine lone pair donation meaning that it is a poor coordinator.[27] Thus, the ability of organofluorine to act as a hydrogen-bond acceptor would be predicted to be poor.[27] Indeed, Dunitz and co-workers performed a comprehensive study of the Brookhaven Protein Data Bank (PDB) and Cambridge Structural Database (CSD) and found that instances where CF···HX interactions fall within the remit of hydrogen bonds are rare.[32] The criterion defining a hydrogen bond was set as a CF···HX separation ≤ 2.3 Å, and less than one percent of organofluorine and HX-containing crystal structures met this. This finding echoed that of previous statistical analysis of crystallographic databases.[33] In particular, CF···HO interactions were found to be especially rare, with only two structures uncovered during Dunitz *et. al*'s database analysis and twelve within Smith and co-workers study.[32-33] Despite the rarity of such contacts within crystal structures, it was noted within both studies that organofluorine can accept hydrogen bonds, with the suggestion that it is a very weak acceptor.[27, 32-33] In fact, Taylor's 2017 analysis of the CSD showed that organofluorine only acts as a hydrogen bond acceptor when no alternative acceptor groups are present.[34]

Computational studies by various groups have shown CF···HX interactions are attractive by nature but are, in the case where X is O, half the strength of a C=O···HO

hydrogen bond interaction and generally weaker than more common acceptors such as nitrogen and other halides.[26, 29, 33-37]

Spectroscopic evidence, in the form of IR and NMR studies, provided the existence of weak organofluorine hydrogen bond acceptors in a number of systems, in agreement with the computational findings.[23, 29, 34, 36, 38-40] Takemura and co-workers performed NMR and IR spectroscopic analysis on 9-fluoro-18-hydroxy-[3.3]metacyclophane, finding that a weak CF···HO interaction was present in solution and the solid state (**Figure 4.3A**).[40] However, the same group provided conflicting crystallographic and spectroscopic evidence for the existence of a CF···HO hydrogen bond in 8-fluoro-4-methyl-1-naphthol with only NMR spectroscopy pointing towards an organofluorine hydrogen bonding interaction (**Figure 4.3B**).[38]

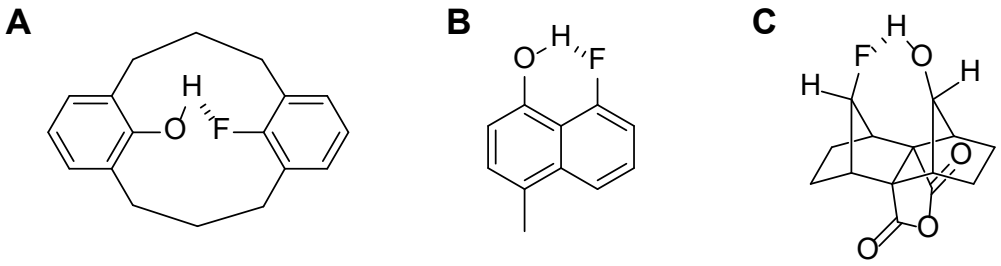

Figure 4.3: Organofluorine hydrogen bonding interactions examined by Takemura *et. al.* in 9-fluoro-18-hydroxy-[3.3]metacyclophane (**A**) and 8-fluoro-4-methyl-1-naphthol (**B**) and by Lectka *et. al.* in a rigid cage system (**C**).[37-38, 40]

A CF···HO interaction in a rigid cage system was observed as a strong hydrogen bond *via* IR and NMR spectroscopy by Lectka and co-workers.[37] However, it should be noted that the system was designed to force an interaction between the two functionalities and the hydrogen bond observed could be the result of repulsion minimisation (**Figure 4.3C**).

Linclau *et. al.* found intramolecular CF···HO hydrogen bonding interactions in flexible, acyclic saturated γ–fluorohydrins through analysis of F···HO NMR coupling constants and computational modelling.[41] Conformer populations as calculated *in silico* show a CF···HO interaction possible for all γ–fluorohydrins studied, though generally as the least populated state. However, the most stable conformer for *syn*-4-

fluoropentan-2-ol (**Figure 4.4**) contains an intramolecular CF···HO hydrogen bond that is stabilised by 2.7 kJ mol^{-1} with respect to the first secondary minimum.

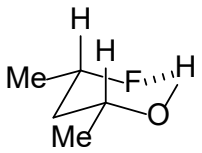

Figure 4.4: *Syn*-4-fluoropentan-2-ol, a flexible, acyclic saturated γ–fluorohydrin studied by Linclau and co-workers.[41]

^{1}H and ^{19}F decoupled ^{1}H NMR coupling constants of the hydroxyl group of this compound reveal a value of 6.6 Hz to the fluorine, confirming the dominance of this conformer within the computed conformer analysis. This study therefore provided experimental evidence that CF···HO hydrogen bonding is strong enough to enforce conformational preference within a flexible system.[41]

Linclau and co-workers have also investigated the effect of fluorination on the hydrogen-bond donor ability of alcohol functionalities within a range of systems. The high electronegativity of fluorine is expected to increase the hydrogen bond donor ability of nearby alcohol groups through an inductive effect. However, the hydrogen-bond acidity of alcohol groups in fluorohydrins was found to decrease with respect to their non-fluorinated counterparts within conformationally restricted systems *via* experimental IR complexation data with *N*-methylpyrrolidinone in CCl_4.[15] Energetic dissection through use of the electrostatic potential, $V_\alpha(r)$, showed that the attenuation of the C=O···HO interaction due to fluorination was significant, ranging from −2 to −6 kJ mol^{-1}. Such attenuation was dependent upon the relative conformations of the fluorine and hydroxyl groups.[15] This initial 2012 study was expanded upon in a comprehensive 2017 study of increasingly conformationally flexible β-fluorohydrins.[42] In depth experimental and computational analysis showed that the effects of fluorine on the hydrogen-bond donor ability of the hydroxyl group involved an interplay between electronegativity effects (increasing acidity) and an intramolecular F···HO hydrogen bond (decreasing acidity). This interplay was sensitive to the conformational relationship between fluorine and the hydroxyl group.

Overall, this work showed that fluorination effects an hydrogen-bond donor ability *via* two mechanisms: electronegative withdrawal and intramolecular hydrogen bonding.[42]

The groups of Linclau and Bernet have both shown that fluorine was capable of competing with OH···O intramolecular hydrogen bonds within levoglucosan derivatives (**Figure 4.5**).[43-44]

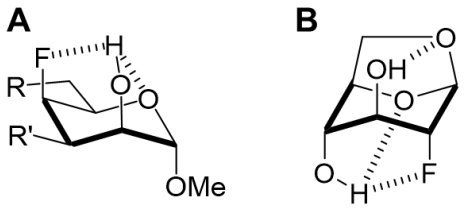

Figure 4.5: Selected levoglucosan derivatives studied by the groups of Bernet (**A**) and Linclau (**B**), showing the formation of three-centre hydrogen bonds where organofluorine participates as a hydrogen-bond acceptor within the presence of a stronger acceptor.[43-44]

Bernet and co-workers indirectly show the competition between fluorine and the ring oxygen through analysis of the dihedral angle between the alcohol group and the proton on the same carbon *via* NMR coupling constants. The position of the alcohol group is shifted from pointing directly towards the oxygen acceptor in the absence of fluorine to being further away in the presence of a fluorine substituent. This effect was attributed to the formation of a competitive CF···HO intramolecular hydrogen bonding interaction and a resulting three-centre hydrogen bond, comprising of the ring oxygen and fluorine as acceptors.[43] Expanding upon this work, Linclau *et. al.* studied the effect of a competing methoxy group as well as fluorine within levoglucosan derivatives. ^{1}H NMR coupling constants and Natural Bond Orbital (NBO) analysis confirm an intramolecular hydrogen bond with a methoxy substituent, as well as the ring oxygen, as one would expect for a good acceptor such as a methoxy group. The experimental and theoretical behaviour of the methoxy group competition for the alcohol group was also seen, though to a less extent owning its weak accepting ability, for fluorine.[45]

These studies showed that fluorination in biologically relevant compounds can sufficiently perturb stronger, more classical hydrogen-bonding interactions.

Abraham studied has also studied intramolecular hydrogen bonds within a series of *ortho* halo substituted phenols (**Figure 4.6**).[46]

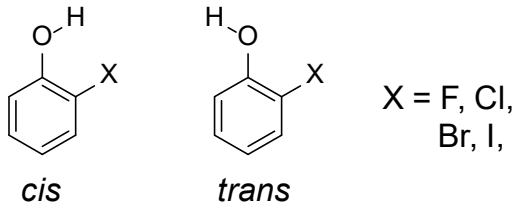

Figure 4.6: Series of 2-halophenols analysed by Abraham *et. al.* in their study of the capability of halogens to participate in hydrogen bond interactions.[46]

IR and NMR spectroscopy of this series of compounds show a preference for the *cis* isomer in non-polar solvents where X is chlorine, bromine or iodine. However, the Abraham solute hydrogen-bond acidity parameter, *A*, values of these compounds do not indicate the presence of an intramolecular hydrogen bond within these compounds despite their conformational preference. Theoretical examination of these interactions show that no intramolecular hydrogen bond is formed in 2-fluorophenol, with only very weak hydrogen bonds to the other halogens.[46] Indeed, the weak hydrogen bonding nature of halogens is well documented and was quantified *via* 1:1 complexation between a series of halogenoalkanes and 4-fluorophenol in CCl_4 by Laurence and co-workers.[47]

Vulpetti *et. al.* examined the strength of hydrogen bonds between strong and weak donors with organofluorine compounds, including CH_2F, CHF_2 and CF_3 moieties, using ^{19}F NMR.[29, 36] ^{19}F-NMR titration experiments shed light on their respective hydrogen-bonding strengths upon 1:1 complexation with a strong hydrogen-bond donor, with CH_2F being the strongest and CF_3 being the weakest acceptor.[29] This study found CF_3 to engage in such a weak hydrogen-bond interaction with the donor that it was not possible to measure, but Suryaprakash *et. al.* have shown the existence of a

CF_3···HN hydrogen bond interaction *via* NMR and *ab initio* measurements.[29, 48] Indeed, CHF was found to be a better hydrogen-bond acceptor than CF_2 in a study by Bernet.[44] In their 2016 study, solution-phase evidence of the non-competitive nature of organofluorine as a hydrogen bond acceptor was provided; where such interactions are formed primarily in environments with either no stronger acceptors or a high concentration of strong donors present owing to their weak interaction strength. This conclusion allowed the authors to suggest the presence of weak organofluorine-containing hydrogen bonds in solvent-shielded protein binding pockets.[36]

Overall, the extensive assessment of halogens, with a particular focus on fluorine, suggest that they can form weak hydrogen bonds, meaning that such interactions are expected to be of lesser importance than more traditional hydrogen-bonding partners.[26]

4.1.3 Other Functional Groups as Hydrogen Bond Acceptors

Hydrogen bonds can form between donor groups and π-systems, resulting in what are termed "π-hydrogen bonds" and are generally considered weak and attractive in nature.[25, 49] The prevalence of aromatic rings mean that such π-hydrogen bonds may play important roles within biological and chemical systems. Accordingly, many spectroscopic and physical organic studies into OH···π hydrogen bonding have been performed.[24-25, 49-50] The OH···π hydrogen bond was studied as early as the 1950s in IR studies conducted by various groups.[24, 51] Physical organic examination has been performed by Shimizu and co-workers who used their molecular balance scaffold to measure the interaction between protic solvents, specifically those containing a hydroxyl group, and an aromatic shelf (**Figure 4.7**).[52]

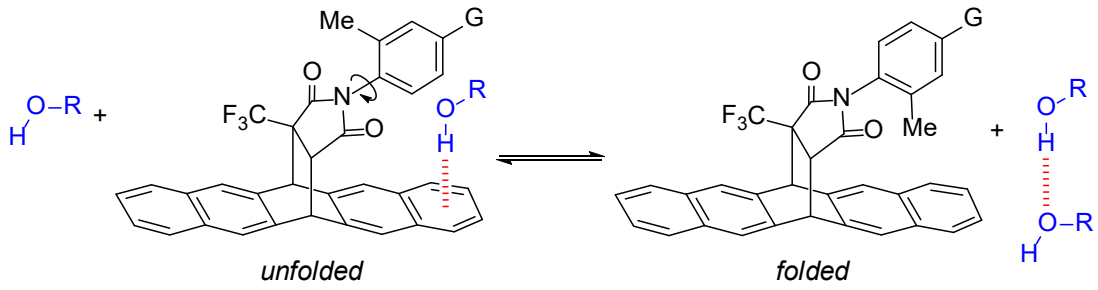

Figure 4.7: Molecular balance used by Shimizu *et. al.* to measure solvent OH···π interactions where G is either carboxylic acid or dendritic acid and were used to improve the solubility of the molecular balance in protic solvents.[52]

The aromatic shelf is exposed to the solvent in the unfolded conformation, but is obstructed by the methyl group in the folded conformation. Therefore, solvent OH···π interactions compete with the CH···π interaction in the folded conformer. The use of control compounds allowed for the dissection of the folding free energy, Δ*G*, of the molecular balance to obtain a free energy associated with the solvent OH···π interaction. The Δ*G* values of this balance were measured in protic and aprotic solvents. The solvophobic effect of protic solvents was seen to be attenuated by favourable OH···π hydrogen bonding interactions through correlations between Δ*G* and the solvents hydrogen-bond acceptor properties. Protic and aprotic solvents formed individual correlations on a plot of the Δ*G* values against the cohesive energy density (*ced*) of the solvents. The difference between these correlations were used to obtain an estimation of the OH···π with the energy for the interaction of water with the balance surface being in line with previously reported experimental and computational figures for this solvents hydrogen bond strength with benzene, 0.75 kcal mol^{-1}.[52]

Motherwell and co-workers has also utilised their dibenzobicyclo[3.2.2]nonane balance design to investigate OH···π interactions (**Figure 4.8**).[53]

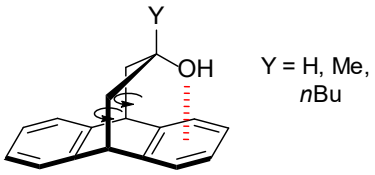

Figure 4.8: Motherwell balance used to study OH···π interactions.[53]

The folding free energy of this molecular balance was used to ascertain the relative strength of the OH···π interaction for three different Y substituents. When Y = Me or *n*Bu, the favoured conformer was that shown in **Figure 4.8**, whereas when Y = H, the conformer without the OH···π interaction was preferred. This conformational preference was attributed to the larger size of the hydroxyl group relative to the hydrogen atom, which undergoes preferential solvation.[53]

As well as arenes acting as π-hydrogen bond acceptors, nitrile groups have also been shown to be capable of accepting hydrogen bonds. Turner *et al.* used spectroscopic techniques to assess the ability of the nitrile group to accept hydrogen bonds.[54] This experimental evaluation showed that they can adopt this behaviour in donor rich environments.[54]

4.2 Project Background

Molecular balances have previously been used by the Cockroft group to evaluate cooperativity in hydrogen-bonded chains of one, two or three phenol groups (compounds **1H**, **2H** and **3H** respectively in **Figure 4.9A**).[2] Two conformations of the molecular balances are observed at room temperature; one in which an internal C=O···HO hydrogen bond can form (the 'folded' conformer) and one where such an interaction is not possible (the 'unfolded' conformer). Restricted rotation around the formamide group allows both conformers to observed *via* NMR spectroscopy, where the relative ^{19}F integrals of each balance are used to obtain the experimental equilibrium constant, K_{exp}. These values can then be used to obtain the experimental conformational free energy, ΔG_{exp}, *via* **Equation 4.3**.

$$\Delta G_{exp} = -RTlnK_{exp} \qquad \textbf{Equation 4.3}$$

It was previously established that the folding equilibria of these balances are governed primarily by the strength of the intramolecular C=O···HO interaction, which can be dissected from background electronic effects by comparison with the control series **0X** and **1X** as was performed in the previous study through Hammett analysis.[2]

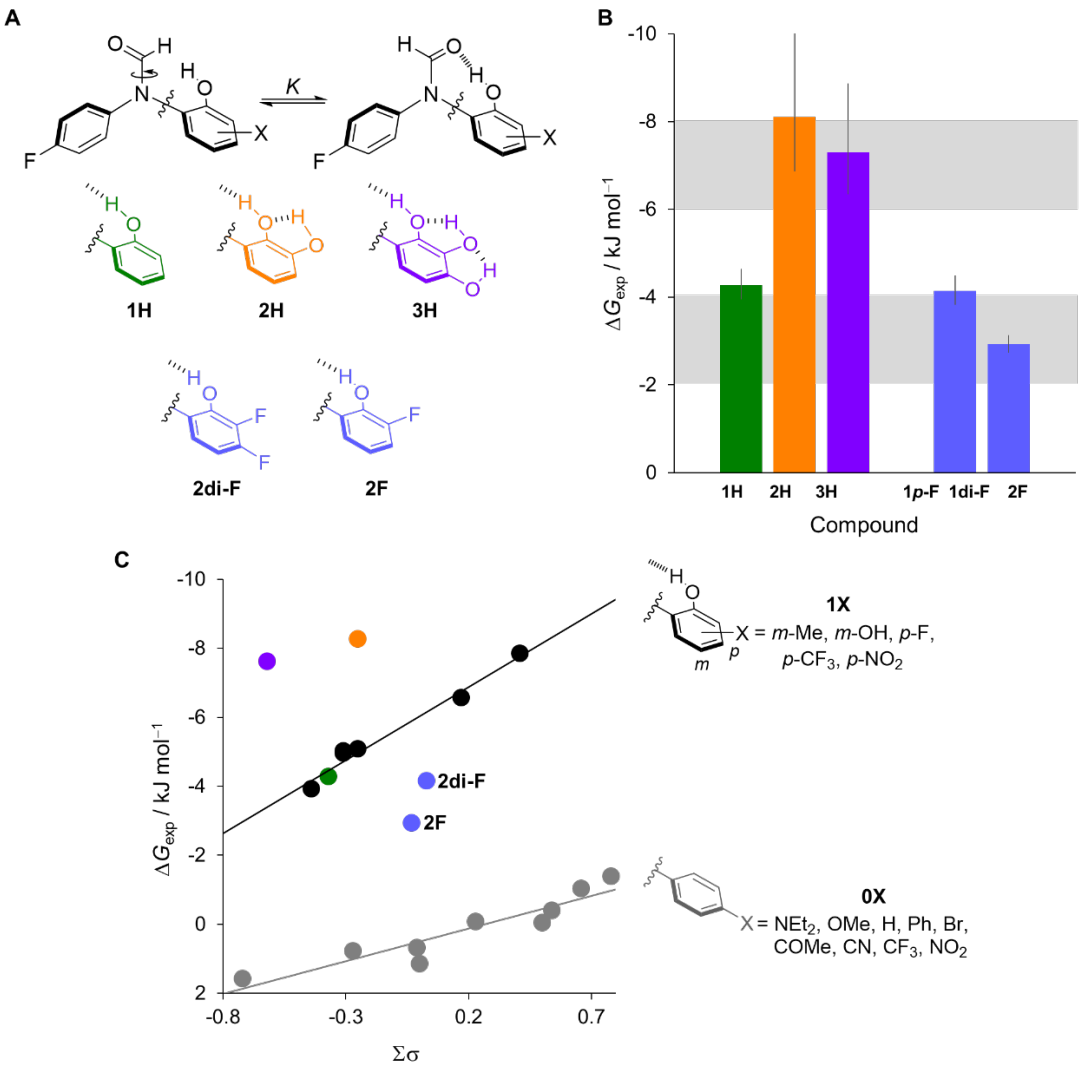

Figure 4.9: (A) Molecular balances used to study hydrogen bond cooperativity (**1H**, **2H** and **3H**) and those bearing fluorine substituents in various positions and numbers around the X-substituted ring (**1*p*-F**, **2di-F** and **2F**). **(B)** Experimental conformational free energies, ΔG_{exp}, measured in chloroform-*d* (376.5 MHz, 298 K) of **1H**, **2H**, **3H**, **1*p*-F**, **2di-F** and **2F**. **(C)** Plot of ΔG_{exp} against $\Delta\sigma$ values with the control series, **0X** and **1X** shown. Errors were conservatively estimated using an error of 0.12 kJ mol^{-1}. Error bars were omitted from **(C)** for clarity, a version

with error bars is presented in Appendix C. All data was previously reported[2-4] except that of **1*p*-F**, **2di-F** and **2F** which are unpublished work by Nicholas Dominelli-Whiteley.[1]

The folded conformer hosts a hydrogen bond between the formyl oxygen and the hydroxyl group of the X-substituted ring, and was favoured for **1H** with an experimental conformational free energy, ΔG_{exp}, value of –4.3 kJ mol^{-1}. This value was found to approximately double upon the addition of a second hydroxyl group to the hydrogen bonding network (**2H**), increasing the favourability of the folded conformer. However, a slight decrease in the preference of the folded conformation with respect to **2H** was observed upon the addition of a third hydroxyl group (**3H**). Further computational analysis and the use of experimental control compounds allowed the conclusion that the doubling of ΔG_{exp} between **1H** and **2H** was not significantly affected by through-bond substituent effects and that inductive polarisation provided a substantial contribution to this effect.

During this investigation, compounds bearing fluorine substituents were also synthesised with the intention that they would act as controls for the oxygen atom of the hydroxyl groups due to the isosteric relationship between oxygen and fluorine.[27] Thus, based on the prior work of Abraham (**Figure 4.6**)[46] it was expected that there would be little to no internal hydrogen bond formed between the hydroxyl group and fluorine substituent of **2F**. However, the experimental free energy of **2F** showed attenuation of the C=O···HO internal hydrogen bond with respect to **1H**, **2H** and **3H**, suggesting significant competition for the hydrogen bond by fluorine (**Figure 4.9B** and **C**). Similar behaviour was also identified when a second fluorine atom added to the X-substituted ring, **2di-F**. Correcting for secondary substituent effects on the position of the conformational equilibrium using a Hammett analysis was also unable to explain the significant decrease in the internal C=O···HO hydrogen bond in the *ortho*-fluorinated **2di-F** and **2F** balances (**Figure 4.9C**). Given the widely accepted weak acceptor ability of organofluorine,[15, 41-44, 46] the competitive nature of the CF···HO interaction in **2di-F** and **2F** in the presence of a stronger hydrogen-bond acceptor, C=O, was striking. Indeed, there are few examples where favourable CF···HO have been invoked.[26, 34]

4.3 Aims of the Project

The experimental behaviour of **2F** and **2di-F** pointed towards an internal F···HO hydrogen bond that was not explained by through-bond substituent effects. The aim of this study was to understand the secondary substituent effects at play by expanding the investigation to include other halides and functional groups as potential competitive hydrogen-bond acceptors (**2Y** series in **Figure 4.10**).

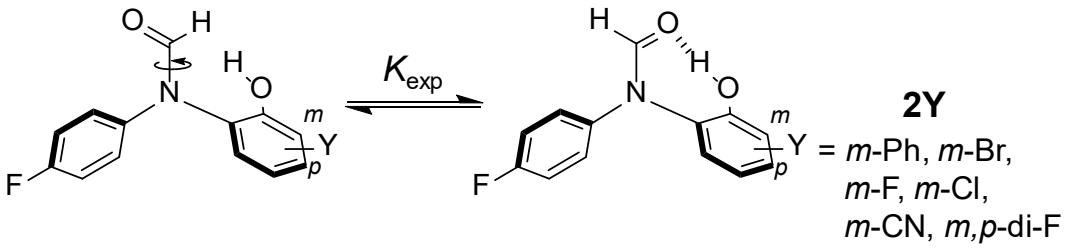

Figure 4.10: The molecular torsion balance series, **2Y**, at the heart of this study. The internal C=O···HO hydrogen bond is highlighted with a dashed line. All compounds were obtained by RJB, except **2F** and **2di-F** which were obtained by Nicholas Dominelli-Whiteley.[1]

This chapter will utilise the combined computational and experimental method of understanding substituent effects established in **Chapters 2** and **3** to meet the aim of this study. In addition, a theoretical Symmetry Adapted Perturbation Theory (SAPT) based Energy Decomposition Analysis (EDA) will be employed to understand the secondary substituent effects at play within compound **2F** and related compounds that suggest the apparent occurrence of an strongly competitive fluorine hydrogen-bond acceptor.

4.4 Molecular Balance Synthesis

Series **2Y** was synthesised *via* four or five steps that, for all but **2Br**, began with commercially available aniline or aryl halide derivatives that took part in Buchwald-Hartwig cross-coupling reactions (**Figure 4.12**). The *N*,*N*-diarylamine precursor of

2Br was obtained through Chan-Lam coupling of 4-fluorophenylboronic acid and 3-bromo-2-methoxyanimile (**Figure 4.11**) after several failed palladium-mediated coupling attempts.

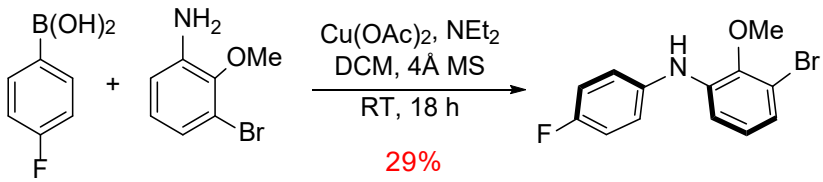

Figure 4.11: First step in the synthesis of **2Br** which is a copper catalysed Chan-Lam coupling to afford the *N*,*N*-diarylamine parent of balance **2Br**.[55]

These initial cross-couplings were followed by the formylation and subsequent deprotection of the methoxy group by boron tribromide to unveil the hydroxyl group central to the present study (**Figure 4.10**).

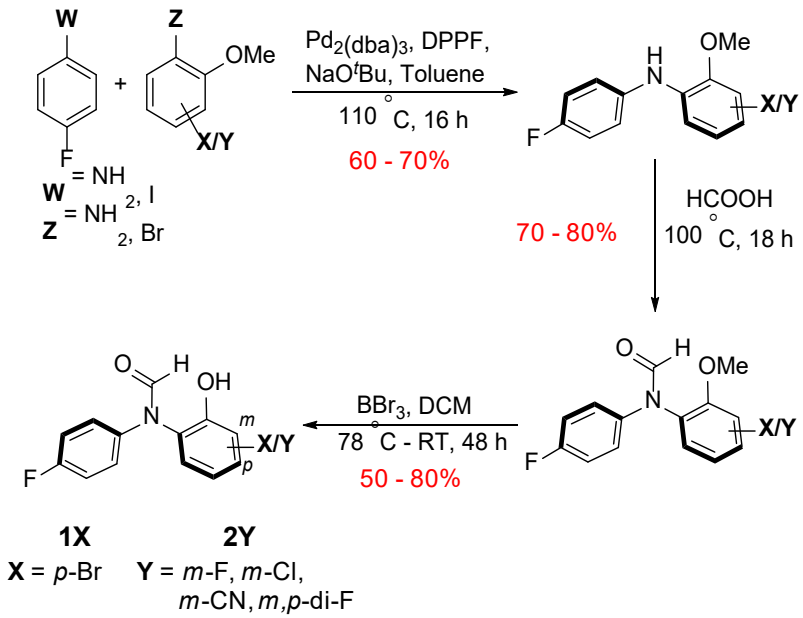

Figure 4.12: General procedure for the palladium-mediated coupling of halo-aromatics to aryl amines in preparation of molecular balances within series **2Y** (except **2Br**). All compounds obtained by RJB except **2F** and **2di-F** which were obtained by Nicholas Dominelli-Whiteley.[1] Full synthetic details given in Appendix C.

Balance **2Ph** was obtained *via* Suzuki-Miyaura coupling between phenylboronic acid and the methoxy protected precursor to the **2Cl** balance (**Figure 4.13**), with the final balance being obtained by boron tribromide-mediated deprotection of the methoxy group as outlined in the final step of **Figure 4.12**.

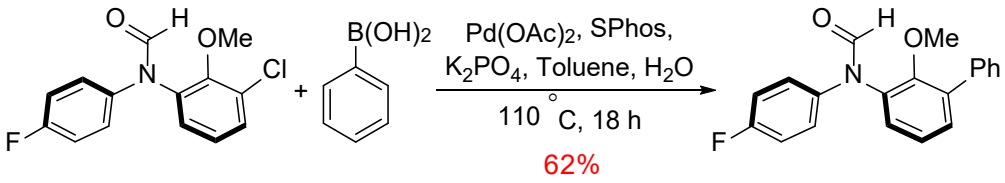

Figure 4.13: Synthesis of the methoxy protected **2Ph** balance from the methoxy protected parent of balance **2Cl** *via* palladium-mediated coupling with phenylboronic acid which is followed by deprotection of the hydroxyl group with boron tribromide to afford **2Ph**. This compound obtained by RJB.

Synthesis of **2NO$_2$** and **2CF$_3$** were attempted *via* the route outlined in **Figure 4.11** but, due to decomposition at different stages, were not obtained. The amine precursor of **2NO$_2$** decomposed readily and the final compound of **2CF$_3$** decomposed on silica gel during purification. In addition, the methoxy protected precursor of **2Me** was obtained but subsequent methoxy deprotection was unsuccessful.

4.5 Results and Discussion

4.5.1 Computational and Experimental Results

Measurement of the experimental conformational free energies of series **2Y**, ΔG_{exp}, was performed as for the molecular balances in **Chapters 2**. ^{19}F NMR was utilised to give ready access to the conformational equilibrium constants, K_{exp}, which allowed for the calculation of ΔG_{exp} *via* **Equation 4.3**. Conformer assignment was performed by the same method as described in **Chapter 2**.

When compared to balance **1H**, ΔG_{exp} values that are less negative indicate attenuation of the C=O···HO interaction (**Table 4.1**). Thus, balances **2F**, **2Br**, **2Cl** and **2Ph** all

show competition for the hydroxyl group. Balance **2Ph** shows an almost complete attenuation of the C=O···HO interaction as it is close to zero. While these balances compete for the hydroxyl group, **2CN** seems to facilitate the C=O···HO interaction with an experimental free energy that indicates the 'folded' conformer is more favourable in this balance than **1H**. It is worth noting that the solvent in which the experimental free energies were measured in was chloroform-*d* which provides an environment with relatively weak solvent competition to the hydrogen bond interactions present within the balances studied. Chloroform is a poor hydrogen bond acceptor, with a β value of 0.9 and while the donating capability of this solvent is not insignificant, α = 2.2, this effect will not strongly perturb the conformational equilibria.[4, 22]

Table 4.1: ΔG_{exp} values of series **2Y** and **1H** obtained in chloroform-*d* (376.5 MHz, 298 K). All data was obtained by RJB except **1H** which was previously reported[2] and **2F** and **2di-F** which were obtained by Nicholas Dominelli-Whiteley.[1] Error analysis is given in Appendix C.

Compound	ΔG_{exp} / kJ mol^{-1}
1H	–4.3
2Ph	–1.0
2F	–2.9
2di-F	–4.1
2Br	–2.1
2Cl	–1.9
2CN	–7.0

DFT calculations have been useful in the prediction of conformational energy differences of the Cockroft balance; providing insight into chalcogen bonding, cooperative hydrogen bonding networks and solvation effects on substituents.[2-4, 56] Therefore, examination of series **2Y** using computationally derived conformational energies was performed. While only two conformations were observed by NMR spectroscopy, rotation around the C–O bond of the hydroxyl group means that there are two conformations of both the 'folded' and 'unfolded' conformations, giving rise to four conformational states (**Figure 4.14**). However, since this rotation is rapid, only rotation around the C–N bond of the amide gives rise to the conformations that are

observed by NMR spectroscopy. Two of the four possible conformations involve an OH···Y interaction (**Figure 4.14C** and **D** *versus* **Figure 4.14A** and **B**).

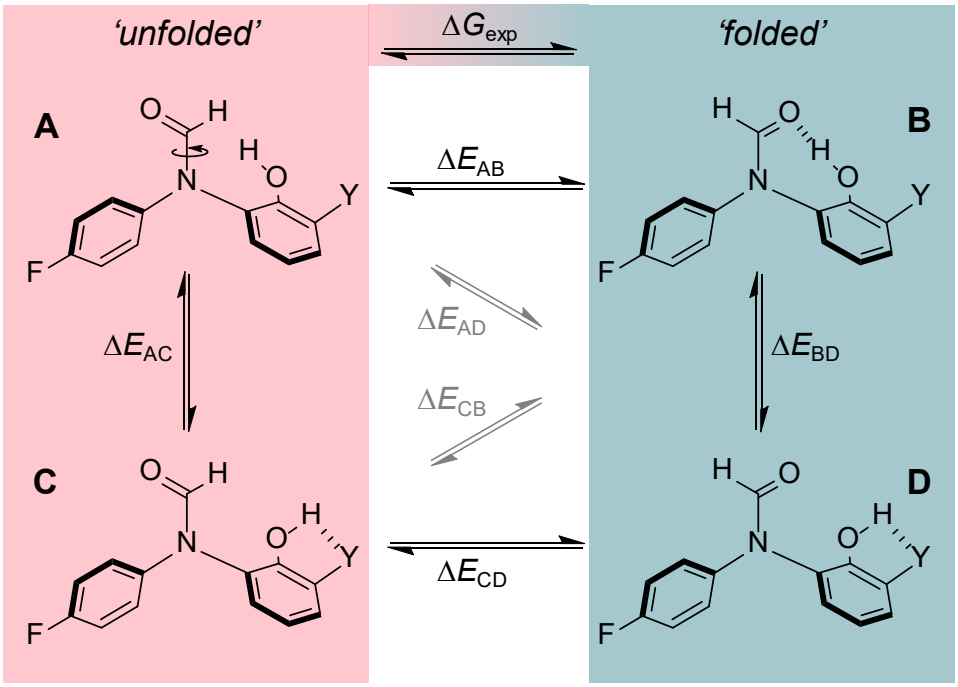

Figure 4.14: The four possible conformers of the molecular balances in this study together with the six equilibria between them and the experimentally observed free energy between the overall two state 'folded' *vs* 'unfolded' equilibrium, ΔG_{exp}. All energies, E_A to E_D and all of the ΔE values are given in Appendix C.

Thus, the experimental values of the conformational free energy will be comprised of a Boltzmann distribution of these four states. The computationally derived conformational energy differences, E, required to compare with the experimental values, ΔG_{exp}, to help understand these results was therefore subjected to Boltzmann analysis. The equilibrium geometries and energies of each local conformational minimum were obtained at the DFT/B3LYP/6–311G* level of theory using Spartan '14. By obtaining the relative populations of the two conformers which are both 'unfolded', **A** and **C** in **Figure 4.14**, and applying **Equation 4.4**, the overall energy of the 'unfolded' conformer that takes account of the distribution of these two states, $E_{unfolded}$, can be found.

$$E_{unfolded} = \left(E_A \times \frac{\%popA}{100}\right) + \left(E_C \times \frac{\%popC}{100}\right) \quad \textbf{Equation 4.4}$$

Where E_A is the energy of conformer **A** and %popA is the percentage of the Boltzmann distribution of states **A** and **C** that is conformer **A** and likewise for conformer **C**. The same analysis is performed to the 'folded' conformers, **B** and **D** in **Figure 4.14**, and from these two values a computationally derived conformational energy, ΔE_{Boltz}, according to **Equation 4.5**.

$$\Delta E_{Boltz} = E_{folded} - E_{unfolded} \quad \textbf{Equation 4.5}$$

It is worth noting that for all balances in **2Y**, the dominant 'folded' conformer was consistently **B**, occupying >98 % of the Boltzmann population of **B** and **D** across the series (**Table C.2**). While it is not surprising that the preferred 'folded' conformer is the one in which the C=O···HO interaction is present, it is surprising that conformer **C** contributes between 50 and 80% of the population of the 'unfolded' conformer for all balances except **2Me**. It is in this conformation that a OH···Y interaction is present meaning that this interaction is a significant proportion of all states in the gas phase for these balances.

The gas-phase computationally derived and Boltzmann weighted conformational energy difference, ΔE_{Boltz}, provides a good correlation with the experimentally observed free energy, ΔG_{exp} (**Figure 4.15**).

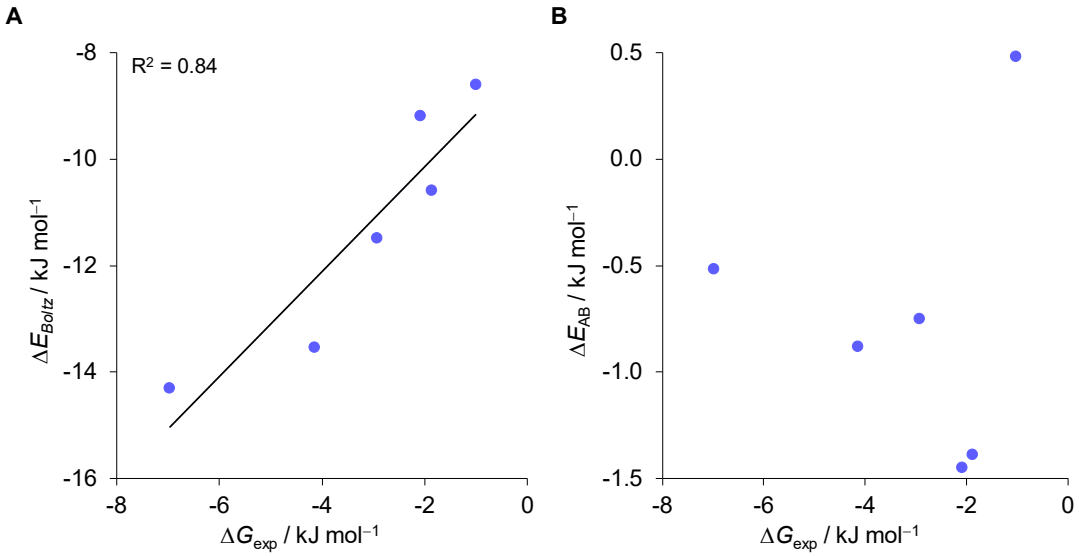

Figure 4.15: Plots of gas phase DFT conformational energy differences with the experimental observable, ΔG_{exp}. **(A)** DFT prediction from Boltzmann analysis of the four possible conformers shown in **Figure 4.14**, ΔE_{Boltz}. **(B)** Computational conformational energies were obtained from conformers A and B only, ΔE_{AB}. ΔG_{exp} values obtained in chloroform-*d* (376.5 MHz, 298K) and ΔE values obtained at the DFT/B3LYP/6–311G* level of theory using Spartan '14. All compounds were obtained by RJB except **2F** and **2di-F** which were obtained by Nicholas Dominelli-Whiteley.[1] Errors in ΔG_{exp} are omitted for clarity, but a version with these present is given in Appendix C.

This is contrasted with the lack of correlation between the computationally derived conformational energy difference determined using only conformers A and B, ΔE_{AB} (**Figure 4.15B**). This demonstrates that a weighted Boltzmann analysis, taking account of all four possible conformations of series **2Y**, is the correct approach to employ when comparing experimental and computed data in this system. However, insight into the origin of the computationally predicted and experimentally observed conformational energies of **2Y** is not provided by this simple computational approach.

4.5.2 Hammett Analysis

In addition to the C=O···HO interaction present in series **2Y**, it is known that through-bond substituent effects influence the conformational equilibrium of the Cockroft balance.[3-4] While the computational analysis described in ***Section 4.5.1*** allows some insight into the nature of the interactions at play in series **2Y**, it does not dissect out substituent effects on the experimentally observed free energies. Therefore, further

analysis is required to perform this dissection. In the initial study from which this work originated,[2] the contribution of these background through-bond substituent effects to the boost in ΔG_{exp} values seen between compounds **1H** and **2H** was examined *via* Hammett analysis. With data in hand for the full **2Y** series of balances, the earlier analysis presented in **Figure 4.9**, in which ΔG_{exp} is plotted against the sum of the Hammett constants of the Y substituents, $\Sigma\sigma$, can be expanded (**Figure 4.16**).

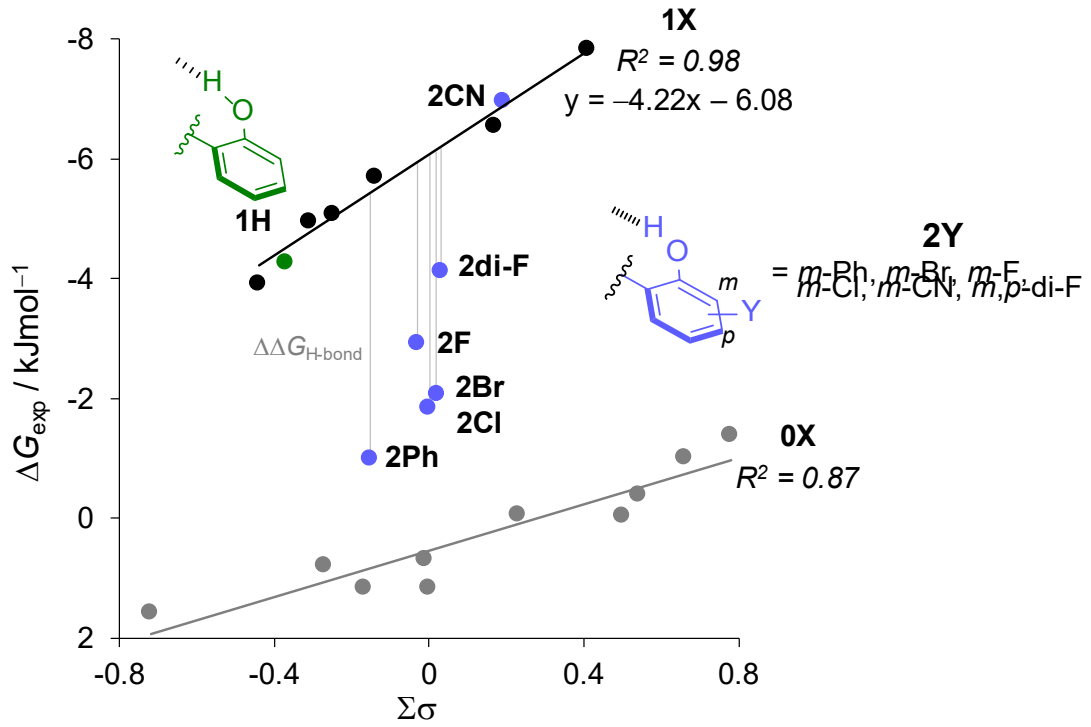

Figure 4.16: Plot of the experimental free energies, ΔG_{exp}, against the sum of the Hammett constants, $\Sigma\sigma$, of **2Y** alongside series **0X** and **1X**. Hammett constants were defined relative to the amide, where the *ortho* hydroxyl groups were approximated by σ_p. Series **0X** and **1X** previously reported,[2-4] with the exception of **1*p*-Br** and **0Me** which were obtained by RJB. **2F** and **2di-F** were obtained by Nicholas Dominelli-Whiteley.[1] $\Delta\Delta G_{H\text{-}bond}$ values are indicated by grey lines from the **1X** best fit line to **2Y** data points. Hammett analysis for series **2Y** was performed by RJB. Full details of Hammett analysis is given in Appendix C. Experimental ΔG_{exp} measured in chloroform-*d* (376.5 MHz, 298K). Error bars are omitted for clarity but a version with these shown is given in Appendix C.

The control series form independent correlations; series **1X**, where the balances bear a single hydroxyl group *ortho* to the amide, have generally more negative ΔG_{exp} values than the **0X** series with the difference between their correlations giving an

approximation of the contribution of one C=O···HO interaction to the overall free energy of folding. The best fit line of series **1X** has a steeper gradient than **0X**, indicating that the C=O···HO interaction is sensitive to electronic X substituent effects. The positive slope of the gradient of the **1X** best fit line shows that the internal C=O···HO hydrogen bond is enhanced by electron-withdrawing substituents, with ΔG_{exp} values indicating a stronger preference for the 'folded' conformer.

Balances with experimental free energies that are more negative than the **1X** series show a stronger preference for the 'folded' conformations and thus enhancement of the C=O···HO interaction. This was previously observed for balances **2H** and **3H** where the cooperative network enhanced the terminal internal hydrogen bond. It follows then, that balances that fall off the best fit line of series **1X** towards series **0X**, where no internal hydrogen bond is possible, show a reduced preference for the C=O···HO hydrogen bond. This is observed for series **2Y**, except **2CN** which sits on the **1X** best fit line. That most compounds in this series do not correlate with **1X** means that the experimentally observed attenuation of the internal hydrogen bond cannot be explained by background electronic substituent effects.

The observation that the **2Y** series spans between the **1X** and **0X** best-fit lines indicates the OH···Y interactions vary from being non-competitive (**2CN** close to the **1X** best-fit line) to strongly competitive (**2Ph**, close to the **0X** best-fit line). Strong competition for the C=O···HO interaction in **2Ph** could be explained by a favourable OH···π hydrogen bonding interaction. The possibility of such an interaction is postulated by the computational modelling which shows an intramolecular distance of < 3 Å between the hydroxyl and phenyl moieties, within the range of hydrogen bonding interactions (**Figure C.2**). However, hydrogen-bonding interactions involving π systems as acceptors are considered to be weaker than for more traditional acceptors such as oxygen.[57] Indeed, further analysis is required to establish a more complete picture of the competing interactions that contribute to the observed conformational preferences.

Indeed, the results of the Hammett analysis can be used to perform further dissection by estimating the contribution of the internal OH···Y interaction to the experimental ΔG_{exp} values calculated *via* the equation of the best fit line of series **1X** (**Figure 4.16**,

Equation 4.6). This equation can be used to calculate a value of the free energy, ΔG_{est}, that estimates the free energy of series **2Y** with no OH···Y competition.

$$\Delta G_{est} = (-4.22 \times \Sigma\sigma) - 6.08 \qquad \textbf{Equation 4.6}$$

The free energy of the internal OH···Y interaction, $\Delta\Delta G_{H\text{-}bond}$, is then obtained *via* subtraction of ΔG_{exp} from ΔG_{est} (**Table 4.2**).

Table 4.2: ΔG_{est} and $\Delta\Delta G_{H\text{-}bond}$, values of series **2Y** and **1H** using the ΔG_{exp} values listed in **Table 4.1** and measured in chloroform-*d* (376.5 MHz, 298 K). All data was obtained by RJB except **1H** which was previously reported[2] and **2F** and **2di-F** which were obtained by Nicholas Dominelli-Whiteley.[1] Hammett analysis performed by RJB. Error analysis is given in Appendix C.

Compound	ΔG_{est} / kJ mol^{-1}	$\Delta\Delta G_{H\text{-}bond}$ / kJ mol^{-1}
1H	–4.5	–0.2
2Ph	–5.4	–4.4
2F	–5.9	–3.0
2di-F	–6.2	–2.1
2Br	–6.2	–4.1
2Cl	–6.1	–4.2
2CN	–6.9	0.1

The values of $\Delta\Delta G_{H\text{-}bond}$ are visualised through the grey lines as indicated in **Figure 4.16**; larger $\Delta\Delta G_{H\text{-}bond}$ value indicate a larger deviation of the experimental behaviour of the **2Y** balance from that estimated by the **1X** best fit line. One striking example is that of **2CN**, which does not fall off of this line with a $\Delta\Delta G_{H\text{-}bond}$ value of 0.1 kJ mol^{-1}. This is the most polar Y substituent studied and this starkly different behaviour from the rest of the **2Y** series could be the result of solvation of this moiety.[4]

4.5.3 SAPT Analysis

While $\Delta\Delta G_{\text{H-bond}}$ provides insight into the free energy of the internal OH···Y interaction, this analysis does not give information as to the attractive and repulsive interactions at play within the OH···Y interactions. Thus, the secondary substituent effects at play in series **2Y** were further investigated using computational energy decomposition analysis (EDA), an approach that is increasingly used to understand molecular interactions. This type of analysis breaks down the overall molecular interaction energy into its constituent components. The particular method employed in this study was Functional group Intramolecular Symmetry Adapted Perturbation Theory (FISAPT), which is an extension to standard SAPT methodologies.[58-60] Combining F-SAPT, which allows the two-body partitioning of SAPT terms as a means to separate functional groups, and I-SAPT, which allows the calculation of SAPT interaction energies between two functional groups that are connected by a third, gives rise to the FISAPT methodology.[61-62] FISAPT decomposes intramolecular non-covalent interaction energies between functional groups into attractive electrostatic, dispersion and induction terms and a repulsive exchange term. [63]

FISAPT calculations are limited to using the SAPT(0) methodology, which is the simplest within the levels of SAPT calculations available. This methodology treats each interacting body at the Hartree-Fock level which provides the simplest estimation of electron correlation. In addition, the PSI4 programme within which SAPT computations are performed has restricted basis sets meaning that such approaches are unable to handle heavy elements.[63-64] Therefore, SAPT analysis of bromine, and therefore **2Br**, is not possible without additional parameterisation and computational benchmarking (which lies beyond the scope of this PhD thesis and the expertise of the Cockroft group).

FISAPT calculations were performed on a simplified version of the balances in **2Y**, using *ortho* (and *meta* for **2di-F**) Y-substituted phenols (**Figure 4.17**).

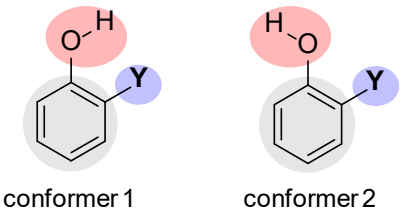

Figure 4.17: The Y-substituted phenols investigated by FISAPT analysis showing the dissections performed in the FISAPT calculation; the interacting functional groups (pink and lilac) and the third-body linker (grey).

Two conformations were subject to energetic decomposition analysis; one where a "hydrogen bonding" interaction with the Y substituent is present ('conformer 1', **Figure 4.17**) and one in which the OH group points in the opposite direction ('conformer 2', **Figure 4.17**). Both phenol derivatives were minimised at the DFT/B3LYP/6–311G* level of theory in Spartan '14, with the FISAPT calculations performed at 6–31G* within PSI4 using the coordinates of the minimised geometries. The FISAPT interaction energy was defined as being the interaction between the hydroxyl group and the Y substituent, with the aryl ring being defined as the third-body linker (**Figure 4.17**). From the electrostatic, exchange, induction and dispersion terms obtained from the FISAPT analysis of each conformer, the difference in the energy of these terms between the two conformers was obtained (**Table C.5**). These differences were correlated with $\Delta\Delta G_{\text{H-bond}}$ for all FISAPT terms (**Figure 4.18**) rather than with ΔG_{exp} as the latter include the secondary substituent effects that were dissected out during the Hammett analysis and thus provide poorer correlations with the FISAPT terms (**Figure C.10**). Included in **Figure 4.18** is balance **1H** which gives the experimental behaviour of a balance with no OH···Y interaction and the FISAPT difference between conformers 1 and 2 is zero for all components. Thus, this balance provides a useful comparison for the balances in series **2Y**. As noted in ***Section 4.5.2***, the experimental values of **2CN** are impacted by solvation effects and as such, they have not been included in the correlations in **Figure 4.18**.

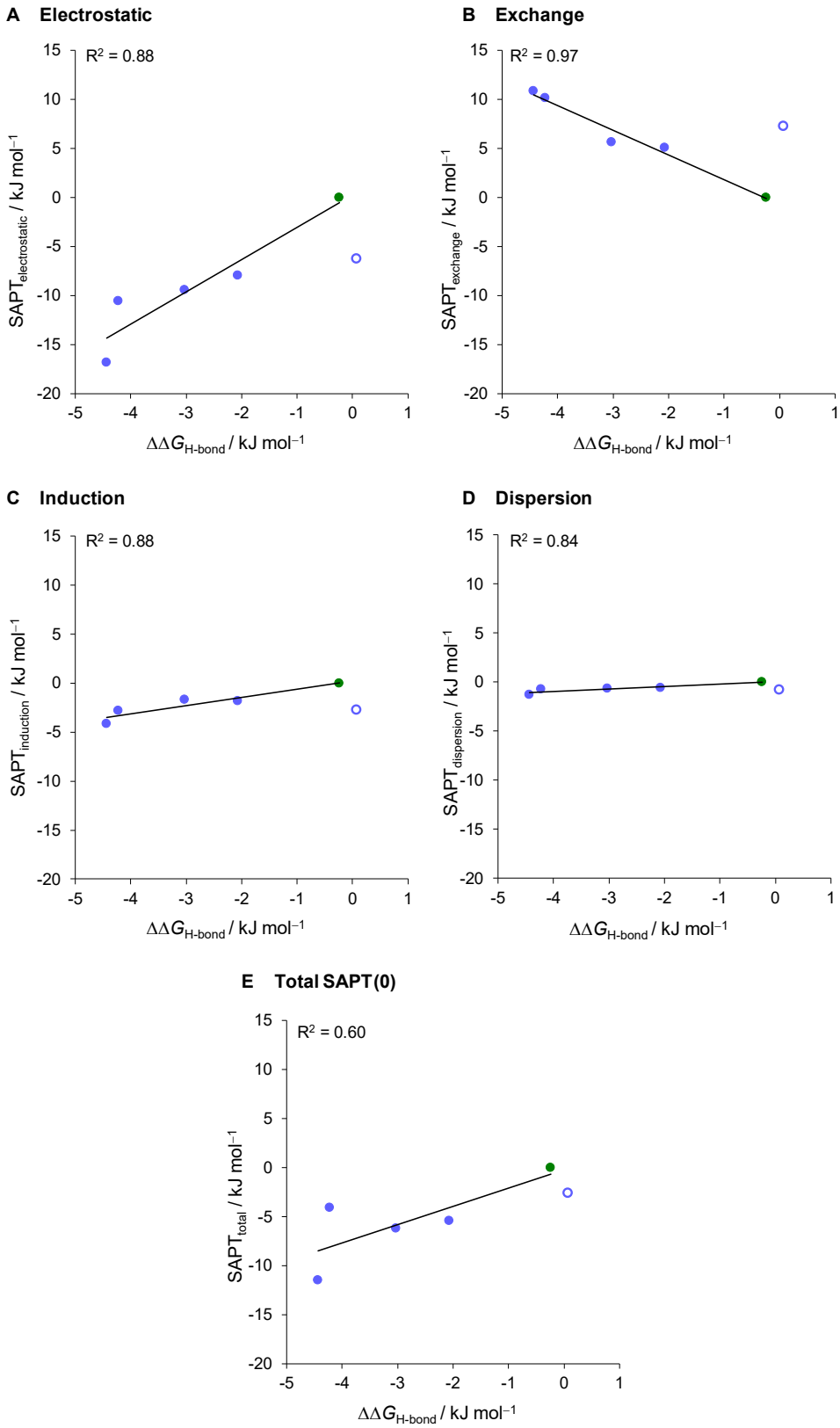

Figure 4.18: Plots of $\Delta\Delta G_{\text{H-bond}}$, with all FISAPT components of series **2Y** and **1H**. **2CN** shown as a hollow data point and not included in the correlations. Calculated using PSI4 SAPT(0)/6–31G* from DFT/B3LYP/6–311G* minimised geometries.

The less than ideal correlation between the experimental data and the total SAPT interaction energy demonstrates the limitations of the approximations made during the FISAPT dissection (**Figure 4.18E**). Nonetheless, all components were found to provide strong correlations with $\Delta\Delta G_{\text{H-bond}}$, with the electrostatic and exchange components providing the strongest (R^2 = 0.88 and 0.97 respectively, **Figure 4.18A** and **B**) and dominating the total SAPT interaction energies of series **2Y** (**Figure C.9**). The significance of the electrostatic term is unsurprising given that hydrogen bonding interactions are commonly dominated by electrostatics.[15, 18] More importantly, the FISAPT energy decomposition allows the repulsive and attractive contributions to the conformational preferences in the series **2Y** to be visualised in **Figures 4.19** and **4.20** which shows the SAPT electrostatic and exchange energies respectively of both conformers and each component.

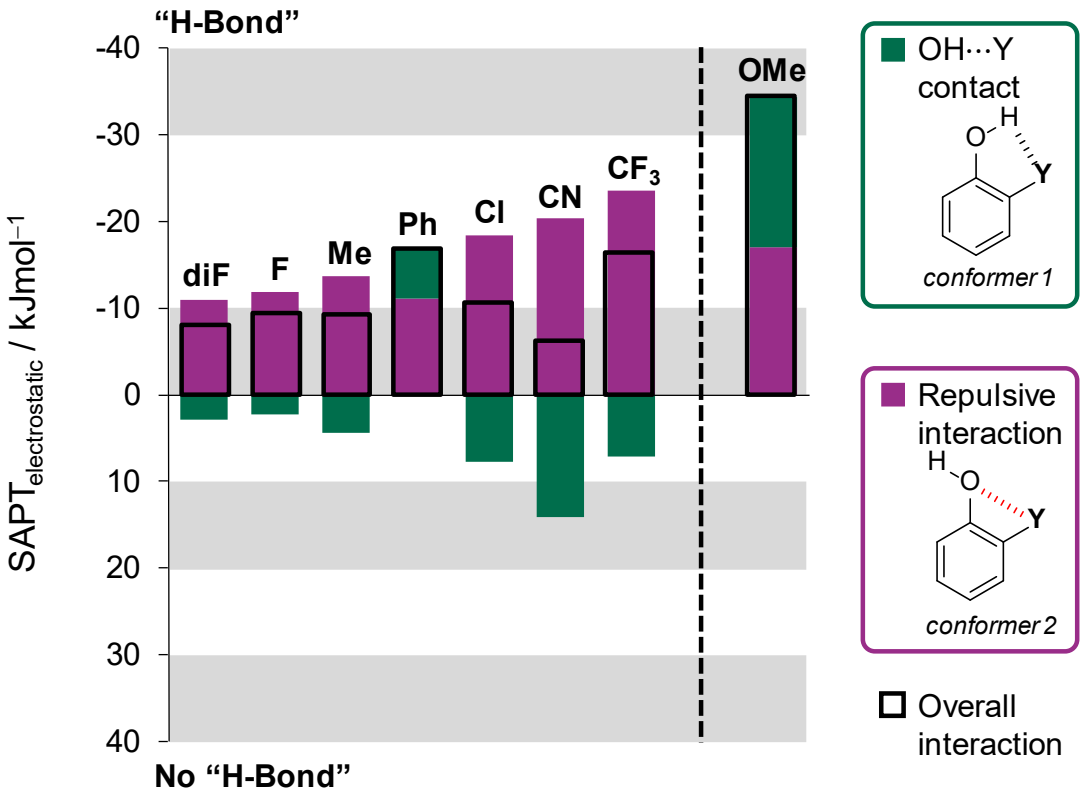

Figure 4.19: The electrostatic contribution from FISAPT calculations of the "OH···Y contact" (green bars), "repulsive interactions" (purple bars) and difference between these to give the overall interaction (hollow bars) of the simple phenolic models of the molecular balances studies in this Chapter. **2Me**, **2CF$_3$** and **2OMe** have no experimental balance counterpart.

Calculated using PSI4 SAPT(0)/6–31G* from DFT/B3LYP/6–311G* minimised geometries. All analysis performed by RJB. FISAPT energies are tabulated in Appendix C.

While no FISAPT decomposition is available for **2Br**, the experimental energy of this compound is similar to **2Cl** so one would expect, based upon the good correlation between the FISAPT and $\Delta\Delta G_{\text{H-bond}}$ values, that a similar energetic decomposition would be observed for **2Br** as **2Cl**.

Focussing on the electrostatic component of the FISAPT analysis first (**Figure 4.19**), the interaction between the oxygen atom of the hydroxyl group and the Y substituent when the O–H bond points away from Y ('conformer 2') is repulsive in the **2Y** series (purple bars in **Figure 4.19**), which promotes the conformation that contains an OH···O=C contact ('conformer 1'). The electrostatic contributions to conformer 1 (green bars in **Figure 4.189**) are also generally repulsive and thus would promote conformer 2; exceptions where Y = Ph (weak H-bond acceptor) and Y = OMe (good H-bond acceptor). However, in most cases the greater *repulsive* energetic contributions arising from HO···Y contacts (conformer 2) make a larger contribution to the preference for the OH···Y contact than any *attractive* OH···Y interaction (hollow bars in **Figure 4.19**). In other words, the experimentally observed "OH···Y hydrogen bonds" are instead the conformations containing the least repulsive interactions. One might therefore characterise such apparent "hydrogen bonds" to weak acceptors as "*pseudo*-hydrogen bonding" interactions due to the absence of an attractive force.

Another striking result is that for when Y is OMe. Fifty per cent of the total energetic contribution to the OH···OMe hydrogen bond in the electrostatic component (hollow bars in **Figure 4.19**) arises from oxygen/Y substituent repulsion, with the other fifty per cent arising from the expected electrostatically favourable OH···OMe hydrogen bond. This result, combined with those of the rest of the **2Y** series, contrast with the natural assumption that hydrogen bonding contacts between functional groups arise from favourable interactions.[34] Instead, the energetic decomposition provided by FISAPT unveils that oxygen···Y-substituent repulsion dominates the preferred conformational preferences, a finding that is mirrored in the experimental ΔG_{exp} values (**Table 4.1**).

The electrostatic component shows that the behaviour of F is similar to that of Me, underscoring the poor acceptor ability of the fluorine. Interestingly, the FISAPT decomposition predicts that the O–H···CF_3 *pseudo*-hydrogen bond is more favourable than the O–H···F *pseudo*-hydrogen bond in **2F**, due to increased O···CF_3 repulsion.

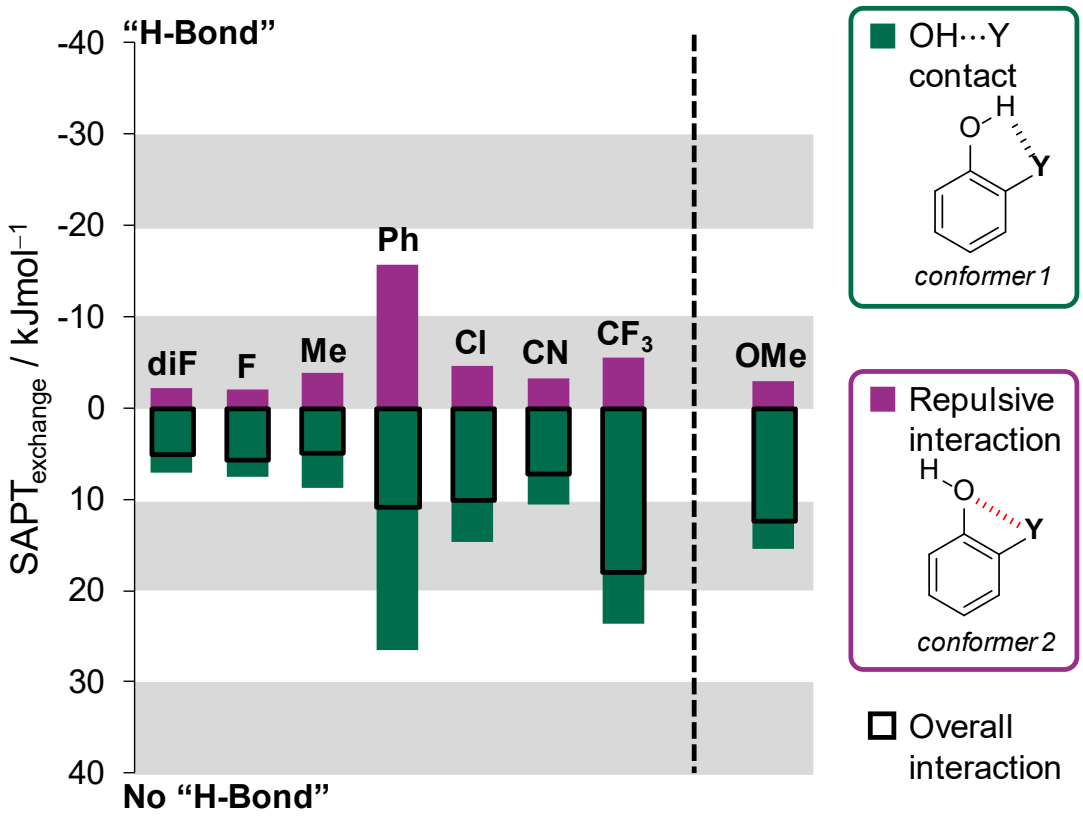

Figure 4.20: The exchange contribution from FISAPT calculations of the "OH···Y contact" (green bars), "repulsive interactions" (purple bars) and difference between these to give the overall interaction (hollow bars) of the simple phenolic models of the molecular balances studies in this Chapter. **2Me**, **2CF₃** and **2OMe** have no experimental balance counterpart. Calculated using PSI4 SAPT(0)/6–31G* from DFT/B3LYP/6–311G* minimised geometries. All analysis performed by RJB. FISAPT energies are tabulated in Appendix C.

The exchange component of FISAPT is a measure of the Pauli repulsion between the interacting functional groups and can be considered as a measure of the steric repulsion between the two units. Thus, for all compounds in **2Y** and even for **2OMe**, which is a good hydrogen bond acceptor, this value is repulsive for both conformers 1 and 2 (**Figure 4.20**) with conformer 1 having a larger magnitude than conformer 2.

Therefore, the overall exchange component energies (hollow bars, **Figure 4.19**) are also repulsive for all **2Y** compounds. Overall, exchange acts against a OH···Y contact for all phenolic models studied.

Upon summing the electrostatic and exchange components (**Figure 4.21**), a good correlation with the experimental data, $\Delta\Delta G_{\text{H-bond}}$, is observed (**Figure 4.22**) meaning that the FISAPT dissection was able to predict and explain the experimental results discussed in ***Sections 4.5.1*** and ***4.5.2***.

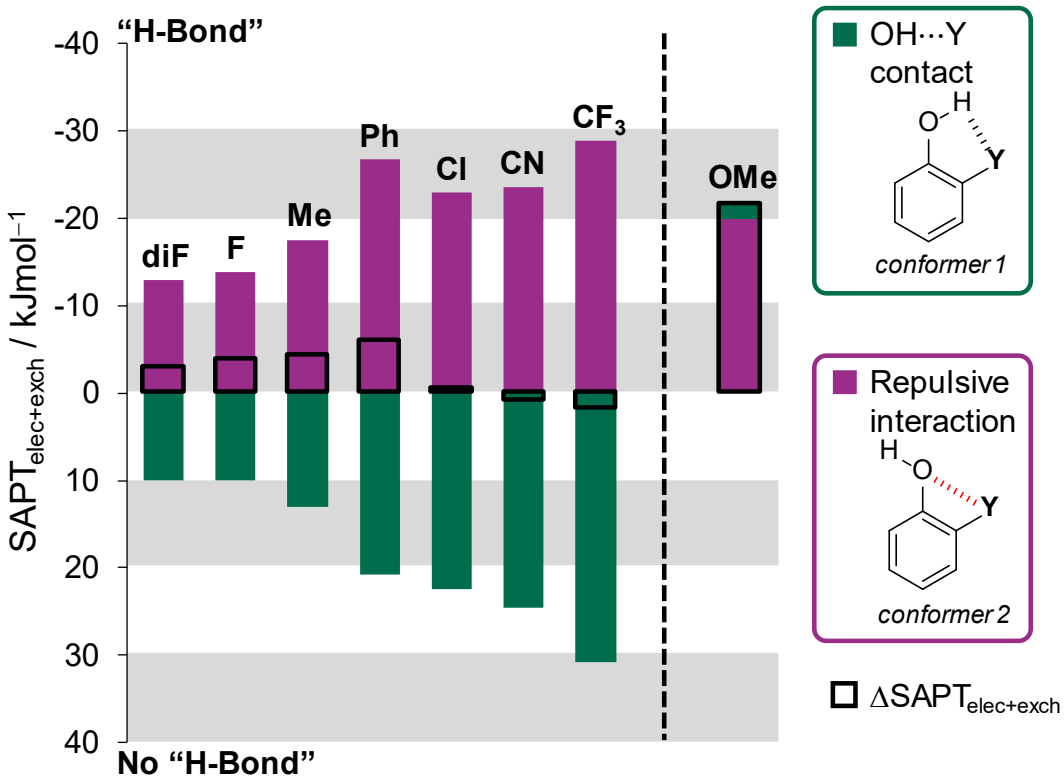

Figure 4.21: The sum of the electrostatic and exchange components from FISAPT calculations of the "OH···Y contact" (green bars), "repulsive interactions" (purple bars) and difference between these to give the overall interaction, $\Delta SAPT_{elec+exch}$, (hollow bars) of the simple phenolic models of the molecular balances studies in this Chapter. **2Me**, **2CF$_3$** and **2OMe** have no experimental balance counterpart. Calculated using PSI4 SAPT(0)/6–31G* from DFT/B3LYP/6–311G* minimised geometries. All analysis performed by RJB. FISAPT energies are tabulated in Appendix C.

Taking the difference between the two conformers to obtain $\Delta SAPT_{elec+exch}$ (hollow bars in **Figure 4.21**) and correlating this with the $\Delta\Delta G_{H\text{-}bond}$ values determined in ***Section 4.5.2*** results in an R^2 of 0.99, with chlorine being an outlier (**Figure 4.22**). This outlier could be due to the difficulty in modelling heavier elements using FISAPT.[45, 63]

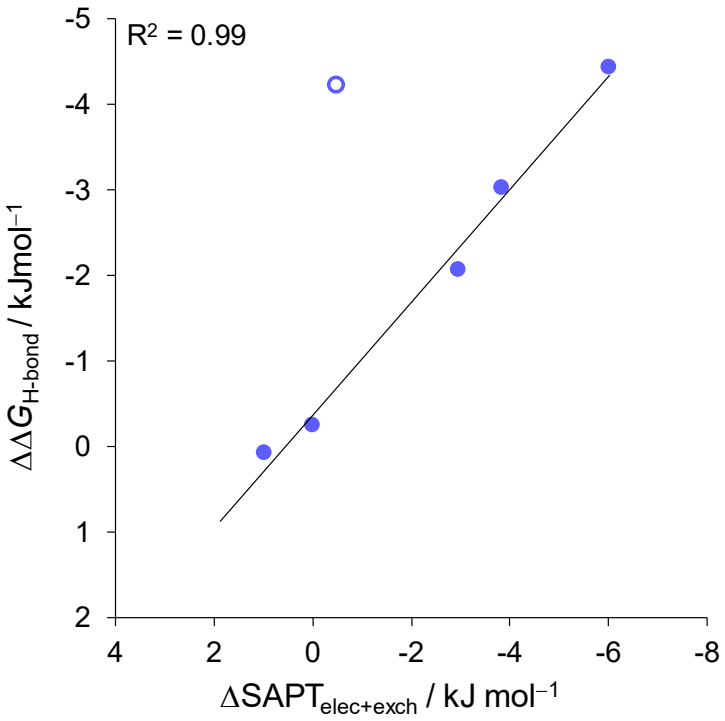

Figure 4.22: Plot of $\Delta SAPT_{elec+exch}$ against $\Delta\Delta G_{H\text{-}bond}$. Chlorine is shown as a hollow data point and is not part of the correlation of the rest of the **2Y** series. **2Me**, **2CF$_3$** and **2OMe** have no experimental balance counterpart. Calculated using PSI4 SAPT(0)/6–31G* from DFT/B3LYP/6–311G* minimised geometries. All analysis performed by RJB. FISAPT energies are tabulated in Appendix C.

4.6 Conclusions and Remarks

A thorough investigation into an unexpectedly competitive "hydrogen bond" encountered in a previous study has been performed using a combined theoretical and experimental analysis. Experimentally obtained conformational free energies, ΔG_{exp},

and computational conformational analysis show that the weak hydrogen bond acceptors within **2Y** were capable of competing for the hydroxyl donor with a strong acceptor and to a significant enough degree as to perturb the ΔG_{exp} value away from the 'folded' conformer. Energetic decomposition analysis of these OH···Y interactions *via* FISAPT calculations unveiled the rather important role that repulsive interactions may play in intramolecular hydrogen bonding interactions. The preference for OH···Y contact involving weak acceptors were found to be dominated by the minimisation of repulsive O···Y interactions, rather than favourable OH···Y interactions. Hence, it is proposed that such situations are best described as "*pseudo*-hydrogen bonds", due to the lack of the attractive characteristic of true hydrogen bonds. Strikingly, *pseudo*-hydrogen bonding characteristics also contribute to the stability of conventional intramolecular hydrogen bonds; the energetic contribution of arising from the avoidance of O···OMe repulsion was equal in energy to the electrostatically favoured OH···OMe hydrogen bond. Thus, this study affords general insight into the nature of intramolecular hydrogen bonding, contradicting the natural assumption that apparent hydrogen-bonded contacts observed within small molecules or crystal structures are dominated by attractive interactions. Indeed, these findings have implications in the understanding of hydrogen bonding interactions in other systems where weak acceptors are involved. It is possible that the previously reported intramolecular hydrogen bonds involving traditionally weak acceptors could instead have been dominated by the minimisation of repulsion as found in this study.[38, 40]

4.7 References

1. Dominelli-Whiteley, N. Hydrogen-Bonding and Halogen-Arene Interactions. University of Edinburgh, 2017.

2. Dominelli-Whiteley, N.; Brown, J. J.; Muchowska, K. B.; Mati, I. K.; Adam, C.; Hubbard, T. A.; Elmi, A.; Brown, A. J.; Bell, I. A. W.; Cockroft, S. L., Strong Short-Range Cooperativity in Hydrogen-Bond Chains. *Angew. Chem. Int. Ed.* **2017,** *56* (26), 7658-7662.

3. Mati, I. K.; Adam, C.; Cockroft, S. L., Seeing through solvent effects using molecular balances. *Chem. Sci.* **2013,** *4*, 3965 - 3972.

4. Muchowska, K. B.; Adam, C.; Mati, I. K.; Cockroft, S. L., Electrostatic Modulation of Aromatic Rings via Explicit Solvation of Substituents. *J. Am. Chem. Soc.* **2013,** *135* (27), 9976 - 9979.

5. Watson, J. D.; Crick, F. H. C., Molecular Structure of Nucleic Acids: A Structure for Deoxyribose Nucleic Acid. *Nature* **1953,** *171* (4356), 737-738.

6. Mundlapati, V. R.; Ghosh, S.; Bhattacherjee, A.; Tiwari, P.; Biswal, H. S., Critical Assessment of the Strength of Hydrogen Bonds between the Sulfur Atom of Methionine/Cysteine and Backbone Amides in Proteins. *The Journal of Physical Chemistry Letters* **2015,** *6* (8), 1385-1389.

7. Chen, D.; Oezguen, N.; Urvil, P.; Ferguson, C.; Dann, S. M.; Savidge, T. C., Regulation of protein-ligand binding affinity by hydrogen bond pairing. *Science Advances* **2016,** *2* (3), e1501240.

8. Böhm, H.-J.; Klebe, G., What Can We Learn from Molecular Recognition in Protein–Ligand Complexes for the Design of New Drugs? *Angew. Chem. Int. Ed. in English* **1996,** *35* (22), 2588-2614.

9. Shan, S.-o.; Loh, S.; Herschlag, D., The Energetics of Hydrogen Bonds in Model Systems: Implications for Enzymatic Catalysis. *Science* **1996,** *272* (5258), 97.

10. Kuhn, B.; Mohr, P.; Stahl, M., Intramolecular Hydrogen Bonding in Medicinal Chemistry. *J. Med. Chem.* **2010,** *53* (6), 2601-2611.

11. Jeffrey, J. L.; Jack, T. A.; MacMillan, D. W. C., O-H hydrogen bonding promotes H-atom transfer from a C-H bonds for C-alkylation of alcohols. *Science* **2015,** *349* (6255), 1523 - 1536.

12. Hubbard, T. A.; Brown, A. J.; Bell, I. A. W.; Cockroft, S. L., The Limit of Intramolecular H-Bonding. *J. Am. Chem. Soc.* **2016,** *138* (46), 15114-15117.

13. Jones, C. R.; Dan Pantoş, G.; Morrison, A. J.; Smith, M. D., Plagiarizing Proteins: Enhancing Efficiency in Asymmetric Hydrogen-Bonding Catalysis through Positive Cooperativity. *Angew. Chem. Int. Ed.* **2009,** *121* (40), 7527-7530.

14. E. Arunan, G. R. D., R. A. Klein, J. Sadlej, S. Scheiner, I. Alkorta, D. C. Clary, R. H. Crabtree, J. J. Dannenberg, P. Hobza, H. G. Kjaergaard, A. C. Legon, B. Mennucci, D. J. Nesbitt, Defining the hydrogen bond: An account (IUPAC Technical Report). *Pure Appl. Chem.* **2011,** *83* (8), 1619-1636.

15. Graton, J.; Wang, Z.; Brossard, A.-M.; Gonçalves Monteiro, D.; Le Questel, J.-Y.; Linclau, B., An Unexpected and Significantly Lower Hydrogen-Bond-Donating Capacity of Fluorohydrins Compared to Nonfluorinated Alcohols. *Angew. Chem. Int. Ed.* **2012,** *51* (25), 6176-6180.

16. Nekoei, A. R.; Vatanparast, M., π-Hydrogen bonding and aromaticity: a systematic interplay study. *Phys. Chem. Chem. Phys.*
2019, *21* (2), 623-630.

17. Pauling, L., The Nature of the Chemical Bond. Application of Results Obtained from the Quantum Mechanics and from a Theory of Paramagnetic Susceptibility to the Structure of Molecules. *J. Am. Chem. Soc.* **1931,** *53* (4), 1367-1400.

18. Desiraju, G. R., A Bond by Any Other Name. *Angew. Chem. Int. Ed.* **2011,** *50* (1), 52-59.

19. Abraham, M. H.; Platts, J. A., Hydrogen Bond Structural Group Constants. *J. Org. Chem.* **2001,** *66* (10), 3484-3491.

20. Abraham, M. H., Scales of solute hydrogen-bonding: their construction and application to physicochemical and biochemical processes. *Chem. Soc. Rev.* **1993,** *22* (2), 73-83.

21. H. Abraham, M.; Berthelot, M.; Laurence, C.; J. Taylor, P., Analysis of hydrogen-bond complexation constants in 1,1,1-trichloroethane: the α2Hβ2H relationship. *Journal of the Chemical Society, Perkin Transactions 2* **1998,** (1), 187-192.

22. Hunter, C. A., Quantifying Intermolecular Interactions: Guidelines for the Molecular Recognition Toolbox. *Angew. Chem. Int. Ed.* **2004,** *43* (40), 5310 - 5324.

23. Linclau, B.; Graton, J.; Le Questel, J.-Y., Influence of fluorination on alcohol hydrogen-bond donating properties. Elsevier: 2019; pp 301-324.

24. Takahashi, O.; Kohno, Y.; Nishio, M., Relevance of Weak Hydrogen Bonds in the Conformation of Organic Compounds and Bioconjugates: Evidence from Recent Experimental Data and High-Level ab Initio MO Calculations. *Chem. Rev.* **2010,** *110* (10), 6049-6076.

25. Salonen, L. M.; Ellermann, M.; Diederich, F., Aromatic Rings in Chemical and Biological Recognition: Energetics and Structures. *Angew. Chem. Int. Ed.* **2011,** *50* (21), 4808-4842.

26. Champagne, P. A.; Desroches, J.; Paquin, J.-F., Organic Fluorine as a Hydrogen-Bond Acceptor: Recent Examples and Applications. *Synthesis* **2015,** *47* (03), 306-322.

27. O'Hagan, D., Understanding organofluorine chemistry. An introduction to the C–F bond. *Chem. Soc. Rev.* **2008,** *37* (2), 308-319.

28. Müller, K.; Faeh, C.; Diederich, F., Fluorine in Pharmaceuticals: Looking Beyond Intuition. *Science* **2007,** *317* (5846), 1881.

29. Dalvit, C.; Invernizzi, C.; Vulpetti, A., Fluorine as a Hydrogen-Bond Acceptor: Experimental Evidence and Computational Calculations. *Chem. Eur. J.* **2014,** *20* (35), 11058-11068.

30. Böhm, H.-J.; Banner, D.; Bendels, S.; Kansy, M.; Kuhn, B.; Müller, K.; Obst-Sander, U.; Stahl, M., Fluorine in Medicinal Chemistry. *ChemBioChem* **2004,** *5* (5), 637-643.

31. Smart, B. E., Fluorine substituent effects (on bioactivity). *Journal of Fluorine Chemistry* **2001,** *109* (1), 3-11.

32. Dunitz, J. D.; Taylor, R., Organic Fluorine Hardly Ever Accepts Hydrogen Bonds. *Chem. Eur. J.* **1997,** *3* (1), 89-98.

33. Howard, J. A. K.; Hoy, V. J.; O'Hagan, D.; Smith, G. T., How good is fluorine as a hydrogen bond acceptor? *Tetrahedron* **1996,** *52* (38), 12613-12622.

34. Taylor, R., The hydrogen bond between N—H or O—H and organic fluorine: favourable yes, competitive no. *Acta Crystallographica Section B Structural Science, Crystal Engineering and Materials* **2017,** *73* (3), 474-488.

35. Schneider, H.-J., Hydrogen bonds with fluorine. Studies in solution, in gas phase and by computations, conflicting conclusions from crystallographic analyses. *Chemical Science* **2012,** *3* (5), 1381-1394.

36. Dalvit, C.; Vulpetti, A., Weak Intermolecular Hydrogen Bonds with Fluorine: Detection and Implications for Enzymatic/Chemical Reactions, Chemical Properties, and Ligand/Protein Fluorine NMR Screening. *Chem. Eur. J.* **2016,** *22* (22), 7592-7601.

37. Struble, M. D.; Kelly, C.; Siegler, M. A.; Lectka, T., Search for a Strong, Virtually "No-Shift" Hydrogen Bond: A Cage Molecule with an Exceptional OH···F Interaction. *Angew. Chem. Int. Ed.* **2014,** *53* (34), 8924-8928.

38. Takemura, H.; Ueda, R.; Iwanaga, T., C–F···HO hydrogen bond in 8-fluoro-4-methyl-1-naphthol. *Journal of Fluorine Chemistry* **2009,** *130* (7), 684-688.

39. Silla, J. M.; Duarte, C. J.; Rittner, R.; Freitas, M. P., Conformational analysis of 6-fluorosalicylic acid. *RSC Advances* **2013,** *3* (48), 25765-25768.

40. Takemura, H.; Kotoku, M.; Yasutake, M.; Shinmyozu, T., 9-Fluoro-18-hydroxy-[3.3]metacyclophane: Synthesis and Estimation of a C−F···H−O Hydrogen Bond. *European Journal of Organic Chemistry* **2004,** *2004* (9), 2019-2024.

41. Linclau, B.; Peron, F.; Bogdan, E.; Wells, N.; Wang, Z.; Compain, G.; Fontenelle, C. Q.; Galland, N.; Le Questel, J.-Y.; Graton, J., Intramolecular OH···Fluorine Hydrogen Bonding in Saturated, Acyclic Fluorohydrins: The γ-Fluoropropanol Motif. *Chem. Eur. J.* **2015,** *21* (49), 17808-17816.

42. Graton, J.; Compain, G.; Besseau, F.; Bogdan, E.; Watts, J. M.; Mtashobya, L.; Wang, Z.; Weymouth-Wilson, A.; Galland, N.; Le Questel, J.-Y.; Linclau, B., Influence of Alcohol β-Fluorination on Hydrogen-Bond Acidity of Conformationally Flexible Substrates. *Chem. Eur. J.* **2017,** *23* (12), 2811-2819.

43. Quiquempoix, L.; Bogdan, E.; Wells, N.; Le Questel, J.-Y.; Graton, J.; Linclau, B., A Study of Intramolecular Hydrogen Bonding in Levoglucosan Derivatives. *Molecules* **2017,** *22* (4), 518.

44. Giuffredi, G. T.; Gouverneur, V.; Bernet, B., Intramolecular OH···FC Hydrogen Bonding in Fluorinated Carbohydrates: CHF is a Better Hydrogen Bond Acceptor than CF2. *Angew. Chem. Int. Ed.* **2013,** *52* (40), 10524-10528

45. Champagne, P. A.; Benhassine, Y.; Desroches, J.; Paquin, J.-F., Friedel–Crafts Reaction of Benzyl Fluorides: Selective Activation of C□F Bonds as Enabled by Hydrogen Bonding. *Angew. Chem. Int. Ed.* **2014,** *53* (50), 13835-13839.

46. Abraham, M. H.; Abraham, R. J.; Aliev, A. E.; Tormena, C. F., Is there an intramolecular hydrogen bond in 2-halophenols? A theoretical and spectroscopic investigation. *Phys. Chem. Chem. Phys.* **2015,** *17* (38), 25151-25159.

47. Ouvrard, C.; Berthelot, M.; Laurence, C., The first basicity scale of fluoro-, chloro-, bromo- and iodo-alkanes: some cross-comparisons with simple alkyl derivatives of other elements. *Journal of the Chemical Society, Perkin Transactions 2* **1999,** (7), 1357-1362.

48. Chaudhari, S. R.; Mogurampelly, S.; Suryaprakash, N., Engagement of CF3 Group in N–H···F–C Hydrogen Bond in the Solution State: NMR Spectroscopy and MD Simulation Studies. *J. Chem. PB* **2013,** *117* (4), 1123-1129.

49. Wu, Q.; Su, H.; Wang, H.; Wang, H., Ab initio calculations, structure, NBO and NCI analyses of XH···π interactions. *Chemical Physics Letters* **2018,** *693*, 202-209.

50. Nishio, M.; Umezawa, Y.; Fantini, J.; Weiss, M. S.; Chakrabarti, P., CH–π hydrogen bonds in biological macromolecules. *Phys. Chem. Chem. Phys.* **2014,** *16* (25), 12648-12683.

51. Yoshida, Z.-i.; Osawa, E., Intermolecular Hydrogen Bond Involving a π-Base as the Proton Acceptor. II.1 Interaction between Phenol and Various π-Bases. Preliminary Infrared Study2. *J. Am. Chem. Soc.* **1965,** *87* (7), 1467-1469.

52. Maier, J. M.; Li, P.; Vik, E. C.; Yehl, C. J.; Strickland, S. M. S.; Shimizu, K. D., Measurement of Solvent OH−π Interactions Using a Molecular Balance. *J. Am. Chem. Soc.* **2017,** *139* (19), 6550-6553.

53. Motherwell, W. B.; Moïse, J.; Aliev, A. E.; Nič, M.; Coles, S. J.; Horton, P. N.; Hursthouse, M. B.; Chessari, G.; Hunter, C. A.; Vinter, J. G., Noncovalent Functional-Group–Arene Interactions. *Angew. Chem. Int. Ed.* **2007,** *119* (41), 7969-7972.

54. Turner, D. R.; Edwards, A. J.; Piltz, R. O., Nitrile groups as hydrogen-bond acceptors in a donor-rich hydrogen-bonding network. *CrystEngComm* **2012,** *14* (20), 6447-6451.

55. Vantourout, J. C.; Miras, H. N.; Isidro-Llobet, A.; Sproules, S.; Watson, A. J. B., Spectroscopic Studies of the Chan–Lam Amination: A Mechanism-Inspired Solution to Boronic Ester Reactivity. *J. Am. Chem. Soc.* **2017,** *139* (13), 4769-4779.

56. Pascoe, D. J.; Ling, K. B.; Cockroft, S. L., The Origin of Chalcogen-Bonding Interactions. *J. Am. Chem. Soc.* **2017**.

57. Meyer, E. A.; Castellano, R. K.; Diederich, F., Interactions with Aromatic Rings in Chemical and Biological Recognition. *Angew. Chem. Int. Ed.* **2003,** *42* (11), 1210-1250.

58. Jeziorski, B.; Moszynski, R.; Szalewicz, K., Perturbation Theory Approach to Intermolecular Potential Energy Surfaces of van der Waals Complexes. *Chem. Rev.* **1994,** *94* (7), 1887-1930.

59. Hohenstein, E. G.; Sherrill, C. D., Wavefunction methods for noncovalent interactions. *WIREs Computational Molecular Science* **2012,** *2* (2), 304-326.

60. Gonthier, J. F.; Sherrill, C. D., Density-fitted open-shell symmetry-adapted perturbation theory and application to π-stacking in benzene dimer cation and ionized DNA base pair steps. *The Journal of Chemical Physics* **2016,** *145* (13), 134106.

61. Parrish, R. M.; Parker, T. M.; Sherrill, C. D., Chemical Assignment of Symmetry-Adapted Perturbation Theory Interaction Energy Components: The Functional-Group SAPT Partition. *Journal of Chemical Theory and Computation* **2014,** *10* (10), 4417-4431.

62. Parrish, R. M.; Gonthier, J. F.; Corminbœuf, C.; Sherrill, C. D., Communication: Practical intramolecular symmetry adapted perturbation theory via Hartree-Fock embedding. *J. Chem.Phys.* **2015,** *143* (5), 051103.

63. Parker, T. M.; Burns, L. A.; Parrish, R. M.; Ryno, A. G.; Sherrill, C. D., Levels of symmetry adapted perturbation theory (SAPT). I. Efficiency and performance for interaction energies. *J. Chem. Phys.* **2014,** *140* (9), 094106.

64. Parrish, R. M.; Burns, L. A.; Smith, D. G. A.; Simmonett, A. C.; DePrince, A. E.; Hohenstein, E. G.; Bozkaya, U.; Sokolov, A. Y.; Di Remigio, R.; Richard, R. M.; Gonthier, J. F.; James, A. M.; McAlexander, H. R.; Kumar, A.; Saitow, M.; Wang, X.; Pritchard, B. P.; Verma, P.; Schaefer, H. F.; Patkowski, K.; King, R. A.; Valeev, E. F.; Evangelista, F. A.; Turney, J. M.; Crawford, T. D.; Sherrill, C. D., Psi4 1.1: An Open-Source Electronic Structure Program Emphasizing Automation, Advanced Libraries, and Interoperability. *Journal of Chemical Theory and Computation* **2017,** *13* (7), 3185-3197.